Jamming, glass transition, and entropy in monodisperse and polydisperse hard-sphere packings

Dissertation zur Erlangung des Doktorgrades
der Naturwissenschaften (Dr. rer. nat.)
dem Fachbereich Chemie
der Philipps-Universität Marburg

vorgelegt von

Dipl.-Phys. Vasili Baranau

aus Minsk, Weißrussland

Marburg an der Lahn 2016

Vom Fachbereich Chemie
der Philipps-Universität Marburg (Hochschulkennziffer: 1180)
als Dissertation am 14. Juli 2016 angenommen

Erstgutachter: Prof. Dr. Ulrich Tallarek
Zweitgutachter: Priv.-Doz. Dr. Matthias Schröter

Tag der mündlichen Prüfung: 29. August 2016

Abstract

This thesis is dedicated to the investigation of properties of computer-generated monodisperse and polydisperse three-dimensional hard-sphere packings, frictional and frictionless. For frictionless packings, we (i) assess their total (fluid) entropy in a wide range of packing densities (solid volume fractions), (ii) investigate the structure of their phase space, (iii) and estimate several characteristic densities (the J-point, the ideal glass transition density, and the ideal glass density). For frictional packings, we estimate the Edwards entropy in a wide range of densities. We utilize the Lubachevsky–Stillinger, Jodrey–Tory, and force-biased packing generation algorithms. We always generate packings of 10^4 particles in cubic boxes with periodic boundary conditions. For estimation of the Edwards entropy, we also use experimentally produced and reconstructed packings of fluidized beds. In polydisperse cases, we use the log-normal, Pareto, and Gaussian particle diameter distributions with polydispersities (relative radii standard deviations) from 0.05 (5%) to 0.3 (30%) in steps of 0.05. This work consists of six chapters, each corresponding to a published paper.

In the first chapter, we introduce a method to estimate the probability to insert a particle in a packing (insertion probability) through the so-called pore-size (nearest neighbour) distribution. Under certain assumptions about the structure of the phase space, we link this probability to the (total) entropy of packings. In this chapter, we use only frictionless monodisperse hard-sphere packings. We conclude that the two characteristic particle volume fractions (or densities, φ) often associated with the Random Close Packing limit, $\varphi \approx 0.64$ and $\varphi \approx 0.65$, may refer to two distinct phenomena: the J-point and the Glass Close Packing limit (the ideal glass density), respectively.

In the second chapter, we investigate the behaviour of jamming densities of frictionless polydisperse packings produced with different packing generation times. Packings produced quickly are structurally closer to Poisson packings and jam at the J-point ($\varphi \approx 0.64$ for monodisperse packings). Jamming densities (inherent structure densities) of packings with sufficient polydispersity that were produced slowly approach the glass close packing (GCP) limit. Monodisperse packings overcome the GCP limit ($\varphi \approx 0.65$) because they can incorporate crystalline regions. Their jamming densities eventually approach the face-centered cubic (FCC) / hexagonal close packing (HCP) crystal density $\varphi = \frac{\pi}{3\sqrt{2}} \approx 0.74$. These results support the premise that $\varphi \approx 0.64$ and $\varphi \approx 0.65$ in the monodisperse case may refer to the J-point and the GCP limit, respectively. Frictionless random jammed packings can be produced with any density in-between.

In the third chapter, we add one more intermediate step to the procedure from the second chapter. We take the unjammed (initial) packings in a wide range of densities from the second chapter, equilibrate them, and only then jam (search for their inherent structures). Thus, we investigate the structure of their phase space. We determine the J-point, ideal glass transition

density, and ideal glass density. We once again recover $\varphi \approx 0.64$ as the J-point and $\varphi \approx 0.65$ as the GCP limit for monodisperse packings. The ideal glass transition density for monodisperse packings is estimated at $\varphi \approx 0.585$.

In the fourth chapter, we demonstrate that the excess entropies of the polydisperse hard-sphere fluid at our estimates of the ideal glass transition densities do not significantly depend on the particle size distribution. This suggests a simple procedure to estimate the ideal glass transition density for an arbitrary particle size distribution by solving an equation, which requires that the excess fluid entropy shall equal to some universal value characteristic of the ideal glass transition density. Excess entropies for an arbitrary particle size distribution and density can be computed through equations of state, for example the Boublík–Mansoori–Carnahan–Starling–Leland (BMCSL) equation.

In the fifth chapter, we improve the procedure from the first chapter. We retain the insertion probability estimation from the pore-size distribution, but switch from the initial assumptions about the structure of the phase space to a more advanced Widom particle insertion method, which for hard spheres links the insertion probability to the excess chemical potential. With the chemical potential at hand, we can estimate the excess fluid entropy, which complies well with theoretical predictions from the BMCSL equation of state.

In the sixth chapter, we extend the Widom particle insertion method from the fifth chapter as well as the insertion probability estimation method from the first chapter to determine the upper bound on the Edwards entropy per particle in monodisperse frictional packings. The Edwards entropy counts the number of mechanically stable configurations at a given density (density interval). We demonstrate that the Edwards entropy estimate is maximum at the Random Loose Packing (RLP) limit ($\varphi \approx 0.55$) and decreases with density increase. In this chapter, we accompany computer-generated packings with experimentally produced and reconstructed ones.

Overall, this study extends the understanding of the glass transition, jamming, and the Edwards entropy behavior in the system of hard spheres. The results can help comprehend these phenomena in more complex molecular, colloidal, and granular systems.

Zusammenfassung

Die vorliegende Arbeit untersucht die Eigenschaften monodisperser und polydisperser, ungeordneter Hartkugelpackungen, die mithilfe verschiedener Computeralgorithmen (Lubachevsky–Stillinger, Jodrey–Tory und force-biased) generiert wurden. Die Packungen bestehen aus jeweils 10^4 Kugeln in einer kubischen Box mit periodischen Randbedingungen. Polydispersen Packungen wurden als Partikelgrößenverteilungen die logarithmische Normalverteilung, die Pareto-Verteilung oder die Normalverteilung mit Dispersitäten zwischen 5% und 30% (in 5%-Schritten) zugrunde gelegt. Für reibungsfreie Packungen wird (i) die Gesamtentropie über einen weiten Bereich an Packungsdichten eingeschätzt, (ii) die Struktur des Phasenraums untersucht und (iii) eine Einschätzung charakteristischer Dichten (des J-Punkts, der Dichte des idealen Glasübergangs, der Dichte des idealen Glases) durchgeführt. Für reibungsbehaftete Packungen wird die Edwards-Entropie über einen weiten Bereich an Packungsdichten geschätzt; dabei werden zusätzlich zu den computer-generierten Packungen auch rekonstruierte, experimentelle Fließbetten untersucht. Die Arbeit besteht aus sechs Kapiteln; jedes Kapitel ist bereits veröffentlicht.

Das erste Kapitel beschäftigt sich mit der Wahrscheinlichkeit, mit der eine einzelne Kugel in eine computergenerierte, monodisperse Packung aus reibungsfreien Kugeln eingefügt werden kann. Zur Abschätzung der sogenannten Einfügungswahrscheinlichkeit wird eine Methode entwickelt, die auf der Verteilung der Abstände von beliebigen Punkten im Leerraum zu den nächsten Kugelflächen in der Packung (Porengrößenverteilung) beruht. Basierend auf bestimmten Annahmen über die Struktur des Phasenraums wird die Einfügungswahrscheinlichkeit mit der Gesamtentropie verknüpft. Durch die entwickelten Methode werden zwei charakteristische, oft mit dem "Random Close Packing Limit" aßoziierte Packungsdichten, $\varphi \approx 0.64$ und $\varphi \approx 0.65$, auf unterschiedliche Phänomene zurückgeführt: den J-Punkt und das "Glaß Close Packing Limit" (die Dichte des idealen Glases).

Im zweiten Kapitel wird untersucht, wie sich die Generierungszeit mono- und polydisperser Packungen aus reibungsfreien Kugeln auf die "Jamming"-Dichten (d.h., die Dichten von inhärenten Strukturen) auswirkt. Schnell generierte Packungen haben strukturelle ähnlichkeit mit Poißon-Packungen und "jammen" sich am J-Punkt ($\varphi \approx 0.64$ für monodisperse Packungen). Die "Jamming"-Dichten langsam generierter, ausreichend polydisperser Packungen nähern sich dem Glaß Close Packing (GCP) Limit. Langsam generierte, monodisperse Packungen überwinden das GCP Limit ($\varphi \approx 0.65$) durch den Einschluß kristalliner Regionen; die "Jamming"-Dichten nähern sich der Dichte kubisch-flächenzentrierter und hexagonal-dichtester Packungen an ($\varphi = \frac{\pi}{3\sqrt{2}} \approx 0.74$). Diese Ergebniße stützen die in Kapitel 1 erarbeitete These, wonach die charakteristischen Dichten $\varphi \approx 0.64$ und $\varphi \approx 0.65$ monodisperser Packungen den J-Punkt beziehungsweise das GCP Limit repräsentieren. Ungeordnete Packungen aus reibungsfreien Kugeln

können mit jeder beliebigen Dichte zwischen diesen beiden Punkten generiert werden.

Im dritten Kapitel wird dem im zweiten Kapitel entwickelten Verfahren ein weiterer Schritt hinzugefügt. Die ursprünglichen "unjammed" Packungen aus dem zweiten Kapitel, die einen weiten Bereich an Packungsdichten repräsentieren, werden zuerst äquilibriert und dann auf inhärente Strukturen untersucht. Damit wird wird die Struktur des Phasenraums mono- und polydisperser, reibungsfreier Hartkugelpackungen untersucht und die Dichten des J-Punkts, des idealen Glasübergangs und des idealen Glases bestimmt. Erneut werden $\varphi \approx 0.64$ als der J-Punkt und $\varphi \approx 0.65$ als das GCP Limit für monodisperse Packungen bestätigt. Als Dichte des idealen Glasübergangs wird für monodisperse Packungen $\varphi \approx 0.585$ bestimmt.

Im vierten Kapitel wird gezeigt, daß die Exzeßentropien eines polydispersen Hartkugel-Fluids am idealen Glasübergang nur unwesentlich von der Partikelgrößenverteilung abhängen. Somit bietet sich ein einfaches Verfahren zur Einschätzung der Dichte des idealen Glasübergangs für beliebige Partikelgrößenverteilungen an: Das Lösen einer Gleichung, die für die Exzeßentropie einen universellen Wert, bezeichnend für den idealen Glasübergang, fordert. Exzeßentropien polydisperser Hartkugel-Fluids können für beliebige Partikelgrößenverteilungen und Packungsdichten aus Zustandsgleichungen, z.B. der Boublík–Mansoori–Carnahan–Starling–Leland (BMCSL) Gleichung, berechnet werden.

Im fünften Kapitel wird die im ersten Kapitel vorgestellte Methode zur Einschätzung der Einfügungswahrscheinlichkeit weiterentwickelt. Die Einschätzung aus der Porengrößenverteilung wird beibehalten, aber statt der ursprünglichen Annahme über die Phasenraumstruktur wird nun eine fortgeschrittene Partikeleinfügungsmethode nach Widom verwendet, die die Einfügungswahrscheinlichkeit mit dem chemischen Exzeßpotential verbindet. Aus dem chemischen Exzeßpotential kann dann die Exzeßentropie geschätzt werden. Die so erhaltenen Werte stimmen gut mit der theoretischen Vorhersage aus der BMCSL-Zustandsgleichung gemäß Kapitel 4 überein.

Im sechsten Kapitel werden die Partikeleinfügungsmethode nach Widom aus dem fünften Kapitel sowie die Methode zur Einschätzung der Einfügungswahrscheinlichkeit aus der Porengrößenverteilung aus dem ersten Kapitel dazu benutzt, die Obergrenze der Edwards-Entropie pro Partikel in monodispersen Packungen aus reibungsbehafteten Kugeln zu bestimmen. Die Edwards-Entropie zählt die mechanisch stabilen Partikelanordnungen in einem bestimmten Dichteintervall. Es wird gezeigt, daß die Edwards-Entropie am "Random Loose Packing Limit" ($\varphi \approx 0.55$) ihren maximalen Wert erreicht und dann mit zunehmender Dichte sinkt. In diesem Kapitel werden zusätzlich zu computergenerierten Packungen auch rekonstruierte, experimentelle Fließbetten untersucht.

Zusammengefaßt erweitern die Ergebniße der vorliegenden Arbeit das Verständnis von Glasübergang, Jamming und Verhalten der Edwards-Entropie in Hartkugelpackungen und tragen somit zu einem tieferen Verständnis dieser Phänomene in komplexen molekularen, kolloidalen und granularen Systeme bei.

Acknowledgments

This thesis would have never been possible without the support of numerous people. I am sincerely grateful to my supervisor Prof. Dr. Ulrich Tallarek for fruitful discussions, encouragement, and financial support. It was a great experience to work in his group due to the scientific environment and productive and friendly atmosphere he created. I appreciate the valuable input of my co-authors Dr. Siarhei Khirevich, Dr. Dzmitry Hlushkou, Dr. Song-Chuan Zhao, Dr. Mario Scheel, and Dr. Matthias Schröter. I am grateful to Dr. Siarhei Khirevich and Dr. Anton Daneyko for their help with hardware and software infrastructure that we use in the group, for sharing their experience with working with supercomputers, and for countless hours of scientific and non-scientific discussions. I am thankful to Dr. Dzmitry Hlushkou for helping with the arrival to Marburg and initial accommodation. I would like to thank my colleagues who helped me to adapt in a new country and created a pleasant working environment: Dr. Daniela Stoeckel, Dr. Kristof Hormann, Tibor Müllner, Dr. Stefan Bruns, Dr. Alexandra Höltzel, Arved Reising, and Julia Rybka. I owe my deepest gratitude to my parents and friends for their support.

List of publications

First author

1. V. Baranau, D. Hlushkou, S. Khirevich and U. Tallarek. Pore-size entropy of random hard-sphere packings. *Soft Matter*, 9.12: 3361–3372, 2013. DOI: 10.1039/C3SM27374A
2. V. Baranau and U. Tallarek. Random-close packing limits for monodisperse and polydisperse hard spheres. *Soft Matter*, 10.21: 3826–3841, 2014. DOI: 10.1039/C3SM52959B
3. V. Baranau and U. Tallarek. On the jamming phase diagram for frictionless hard-sphere packings. *Soft Matter*, 10.39: 7838–7848, 2014. DOI: 10.1039/C4SM01439A
4. V. Baranau and U. Tallarek. How to predict the ideal glass transition density in polydisperse hard-sphere packings. *The Journal of Chemical Physics*, 143.4: 044501, 2015. DOI: 10.1063/1.4927077
5. V. Baranau and U. Tallarek. Chemical potential and entropy in monodisperse and polydisperse hard-sphere packings using Widom's particle insertion method and a pore size distribution-based insertion probability. *The Journal of Chemical Physics*, 144.21: 214503, 2016. DOI: 10.1063/1.4953079
6. V. Baranau, S.-C. Zhao, M. Scheel, U. Tallarek and M. Schröter. Upper bound on the Edwards entropy in frictional monodisperse hard-sphere packings. *Soft Matter*, 12.17: 3991–4006, 2016. DOI: 10.1039/C6SM00567E

Co-author

1. A. Daneyko, D. Hlushkou, V. Baranau, S. Khirevich, A. Seidel-Morgenstern and U. Tallarek. Computational investigation of longitudinal diffusion, eddy dispersion, and trans-particle mass transfer in bulk, random packings of core–shell particles with varied shell thickness and shell diffusion coefficient. *Journal of Chromatography A*, 1407: 139–156, 2015. DOI: 10.1016/j.chroma.2015.06.047
2. K. Hormann, V. Baranau, D. Hlushkou, A. Höltzel and U. Tallarek. Topological analysis of non-granular, disordered porous media: determination of pore connectivity, pore coordination, and geometric tortuosity in physically reconstructed silica monoliths *New Journal of Chemistry*, 40.5: 4187–4199, 2016. DOI: 10.1039/C5NJ02814K

Erklärung

Ich versichere, dass ich die vorliegende Dissertation mit dem Titel

“Jamming, glass transition, and entropy in monodisperse and polydisperse hard-sphere packings”

selbständig, ohne unerlaubte Hilfe angefertigt und mich dabei keiner anderen als der von mir ausdrücklich bezeichneten Quellen und Hilfen bedient habe. Die Dissertation wurde in der jetzigen oder einer ähnlichen Form noch bei keiner anderen Hochschule oder Fachhochschule eingereicht und hat noch keinem sonstigen Prüfungszweck gedient.

Ort, Datum, Unterschrift _____

Contribution of authors

This work is a product of collective effort of several authors, whose contribution is explained below:

- Chapter 1
  Simulations, data analysis, and initial text preparation were performed by me. The manuscript was subsequently edited by Prof. Dr. Ulrich Tallarek, Dr. Siarhei Khirevich, and Dr. Dzmitry Hlushkou. The manuscript was submitted by Prof. Dr. Ulrich Tallarek.
- Chapter 2-5
  Simulations, data analysis, and initial text preparation were performed by me. The manuscripts were subsequently edited and submitted by Prof. Dr. Ulrich Tallarek.
- Chapter 6
  Simulations, data analysis, and initial text preparation were performed by me. Dr. Mario Scheel performed experimental packing reconstruction and read and edited the manuscript. Dr. Song-Chuan Zhao performed processing of reconstructed images and detection of particles from these images. He read and edited the manuscript and provided the pair-correlation function figure. Prof. Dr. Ulrich Tallarek read and edited the manuscript. Dr. Matthias Schröter contributed extensively to the text and figures; he also submitted the manuscript.

Place, Date, Signature of Author _____

Place, Date, Signature of First Supervisor _____

Contents

Introduction

Hard spheres have been a favourite model for several generations of physicists in a few related areas of science: granular matter, glass physics, and colloidal science.[1–3] Even much prior to being intensively investigated in physics, hard spheres attracted a significant attention from mathematicians: as early as in 1611 Johannes Kepler posed his famous conjecture stating that the face-centered cubic (FCC) and hexagonal close packing (HCP) arrangements are the densest possible configurations of hard spherical objects. The proof of the conjecture was published as recently as in 2005,[4] with the formal verification of the proof completed only in 2015.[5] Hard-sphere systems and questions related to them also naturally appear in certain application. For example, they can also be used as a model media in simulations of diffusion, flow, and hydrodynamic dispersion.[6–8]

Hard spheres are a popular model due to their simplicity and at the same time ability to capture characteristics important in corresponding areas of science. Indeed, each hard sphere possesses only three degrees of freedom, a minimal number, alternatively achieved only by an infinitesimal point. If a hard sphere surface is interpreted in terms of a potential, it corresponds to an infinitely high spherically symmetric potential wall, which is a remarkably simple potential. But contrary to the ideal gas, high number density of a hard-sphere system implies high volume density (solid volume fraction) φ. The fraction of configurations without particle intersections in the phase space decreases rapidly with the volume density,[9] so that hard spheres at high number densities exhibit non-trivial properties.

Problem statement

In 1960, Bernal and Mason reported that monodisperse spheres poured into a container eventually occupy a volume fraction φ up to $\sim 64\%$, while structures in which they assemble look random.[10] This density of ~ 0.64 and the phenomenon itself were termed the "Random Close Packing" (RCP) limit. Similar values for the "maximum density of random packings" were re-

[1] C. Song, P. Wang, and H. A. Makse. *Nature*, 453, 629–632, 2008.
[2] G. Parisi and F. Zamponi. *Rev. Mod. Phys.*, 82, 789–845, 2010.
[3] S. Torquato and F. H. Stillinger. *Rev. Mod. Phys.*, 82, 2633–2672, 2010.
[4] T. C. Hales. *Ann. Math.*, 162, 1065–1185, 2005.
[5] T. C. Hales et al. *arXiv e-prints*, 1501, arXiv:1501.02155, 2015.
[6] S. Khirevich, A. Höltzel, and U. Tallarek. *Commun. Comput. Phys.*, 13, 801–822, 2013.
[7] U. M. Scheven et al. *Phys. Rev. E*, 89, 053023, 2014.
[8] H. Liasneuski et al. *J. Appl. Phys.*, 116, 034904, 2014.
[9] Z. W. Salsburg and W. W. Wood. *J. Chem. Phys.*, 37, 798–804, 1962.
[10] J. D. Bernal and J. Mason. *Nature*, 188, 910–911, 1960.

ported in other experiments and computer simulations,[1,11–13] though there is a systematic spread in the results ($0.634 - 0.652$), and the entire concept remains controversial.[14] This range of densities is typical for particles with zero or low friction. Frictional particles can assemble themselves in packings of lower density, while still maintaining mechanical stability, up to $0.54 - 0.55$ for infinite friction.[1] This density ~ 0.55 is termed the "Random Loose Packing" (RLP) limit.[15,16]

The motivation for the present research came from a rather unrelated area of high-performance liquid chromatography. It is a technique in analytical chemistry that allows separating mixtures of chemical substances. The idea is to push a solution of substances through a chromatographic column, which is often a tube packed with rigid spherical particles with adsorbing surfaces.[17] Different substances are adsorbed by sphere surfaces for different times and thus eventually leave the tube at different times (*i.e.*, they have different average retention times). Packings are typically produced as random and dense sphere arrangements to generate as little as possible packing heterogeneity and thus improve hydrodynamic transport through the packing. In other words, it is believed that packing density shall be as close to the "RCP limit" as possible. The actual density of the column interior is usually lower, in particular due to friction between particles and surface roughness, which matter during packing preparation. Also, particles in chromatographic columns are not monodisperse and may have a decently broad radii distribution, with relative radii standard deviations (polydispersities) $\delta = \sqrt{\langle \Delta r^2 \rangle}/\langle r \rangle$ up to 0.25.[18] Here, r is the particle radius. The RCP limit depends on polydispersity,[19,20] so the main question that motivated the research in the present thesis was: What are the RCP limits for certain particle size distributions?

Now we briefly cover the strategies that we tried to tackle this problem. In doing so, we will present the areas of physics that were involved in this endeavour. Most of the definitions are presented in an informal way. The remaining sections of the introduction give a more profound overview of the involved areas. Only the final chapter of the thesis uses experimentally reconstructed packings, otherwise we used only computer-generated three-dimensional packings with periodic boundary conditions containing 10^4 particles.

Approaches we tried

At first, we hoped to determine the RCP limit of polydisperse packings by studying their entropies, because many authors observe changes like local extrema or kinks in the behaviour of entropy

[11] G. D. Scott and D. M. Kilgour. *J. Phys. D: Appl. Phys.*, 2, 863–866, 1969.
[12] C. S. O'Hern et al. *Phys. Rev. E*, 68, 011306, 2003.
[13] S. C. Kapfer et al. *Phys. Rev. E*, 85, 030301, 2012.
[14] S. Torquato, T. M. Truskett, and P. G. Debenedetti. *Phys. Rev. Lett.*, 84, 2064–2067, 2000.
[15] G. Y. Onoda and E. G. Liniger. *Phys. Rev. Lett.*, 64, 2727–2730, 1990.
[16] M. Jerkins et al. *Phys. Rev. Lett.*, 101, 018301, 2008.
[17] J. C. Giddings. *Dynamics of chromatography: Principles and theory*. New York: Marcel Dekker, 1965.
[18] A. Daneyko et al. *Anal. Chem.*, 83, 3903–3910, 2011.
[19] M. Clusel et al. *Nature*, 460, 611–615, 2009.
[20] I. Biazzo et al. *Phys. Rev. Lett.*, 102, 195701, 2009.

and structural descriptors of monodisperse packings at $\varphi \approx 0.646 - 0.652$.[13,21–24] An example of a structural descriptor is the standard deviation of Voronoi cell volumes. Many papers report the emergence of crystalline regions in this range of densities.[13,24–27] Thus, we started from the entropy of monodisperse packings. Our results suggested that what is usually termed the RCP limit may actually correspond to two distinct phenomena: $\varphi \approx 0.64$ may correspond to the so-called J-point,[12] while $\varphi \approx 0.65$ may correspond to the ideal glass density also known as the Glass Close Packing (GCP) limit.[2,28,29] A frictionless packing is called jammed, if it contains at least a subset of particles that touch and block each other in such a way that they cannot be rearranged, even collectively.[3,30,31] When a packing is not jammed, we can always rearrange particles and contract the box where the particles reside (thus increasing φ) to make the packing jammed. If during rearrangement we also ensure that particles are displaced as little as possible, we produce the "closest jammed configuration" with the corresponding *closest jamming density*. The J-point is the *closest jamming density* of Poisson packings (collections of independently and uniformly distributed infinitesimal spheres). The GCP limit, on the other hand, is defined as the highest density (and the corresponding configuration) that can be produced for a given particle size distribution if arrangement of particles into crystal-like regions is suppressed.

The entropy approach turned out to be not so fruitful in the case of polydisperse packings, because sufficiently polydisperse packings cannot crystallize[32–34] and thus cannot cross the GCP limit at all, so that the entropy or structural descriptors just monotonously change and expected local extrema or kinks at the GCP limit cannot be observed. Therefore, we switched to another approach. We generated packings in a wide range of densities and searched for their closest jammed configurations. This procedure also confirmed that for monodisperse packings $\varphi \approx 0.64$ is the J-point and $\varphi \approx 0.65$ can correspond to the GCP limit, while random jammed packings can be produced anywhere in-between.[35] This approach was even more suitable for sufficiently polydisperse packings, because they cannot crystallize and thus crystallization does not interfere with the results. The interpretation of $\varphi \approx 0.65$ as the GCP limit explains why crystalline inclusions are inevitably observed after this density: It is impossible to produce packings otherwise. The drawback of this approach is that the results in the intermediate range of jamming densities (between the J-point and the GCP limit) are dependent on the preparation protocol of initial

[21] A. V. Anikeenko and N. N. Medvedev. *Phys. Rev. Lett.*, 98, 235504, 2007.
[22] A. V. Anikeenko, N. N. Medvedev, and T. Aste. *Phys. Rev. E*, 77, 031101, 2008.
[23] T. Aste and T. Di Matteo. *Eur. Phys. J. B*, 64, 511–517, 2008.
[24] B. A. Klumov, S. A. Khrapak, and G. E. Morfill. *Phys. Rev. B*, 83, 184105, 2011.
[25] M. Bargieł and E. M. Tory. *Adv. Powder Technol.*, 12, 533–557, 2001.
[26] K. Lochmann et al. *Eur. Phys. J. B*, 53, 67–76, 2006.
[27] B. A. Klumov, Y. Jin, and H. A. Makse. *J. Phys. Chem. B*, 118, 10761–10766, 2014.
[28] G. Parisi and F. Zamponi. *J. Chem. Phys.*, 123, 144501, 2005.
[29] L. Berthier and T. A. Witten. *Phys. Rev. E*, 80, 021502, 2009.
[30] A. Donev. *J. Appl. Phys.*, 95, 989–999, 2004.
[31] A. Donev et al. *J. Comput. Phys.*, 197, 139–166, 2004.
[32] E. Sanz et al. *Phys. Rev. Lett.*, 106, 215701, 2011.
[33] E. Zaccarelli et al. *Phys. Rev. Lett.*, 103, 135704, 2009.
[34] C. Valeriani et al. *J. Phys.: Condens. Matter*, 23, 194117, 2011.
[35] P. Chaudhuri, L. Berthier, and S. Sastry. *Phys. Rev. Lett.*, 104, 165701, 2010.

packings.

To get rid of protocol-dependence, we switched to a protocol-independent procedure, *i.e.*, tried to erase the memory about the initial generation algorithm before searching for the closest jammed configurations. To do this, we equilibrated the initially generated packings and only then searched for their closest jamming densities. This means that we were searching for jammed configurations that dominate the phase space, *i.e.*, dominant jammed configurations. It allowed us to build a map "dominant jamming density φ_{DJ} *vs.* initial density φ" and in such way provide a certain description of the phase space of hard spheres. We observed that at low and moderate densities the phase space is dominated by the J-point, but starting from a certain density ($\varphi \approx 0.52$ for monodisperse spheres) φ_{DJ} grows and at a certain density ($\varphi \approx 0.585$ for monodisperse spheres) reaches its maximum, $\varphi_{\mathrm{DJ}} = \varphi_{\mathrm{GCP}}$. In the monodisperse case these processes are actually hindered by spontaneous crystallization in the range $\varphi = 0.545 - 0.61$ (different from the crystallization at $\varphi = 0.65$ observed during packing generation);[36] and the values provided here are extrapolations from polydisperse cases. Our observations are most naturally explained in terms of the so-called many glassy states model,[2,29,37] which is related to the vast and active study of glass transition and supercooled liquids.[38–43]

While these approaches more or less tackled the initial question about the RCP limit of polydisperse packings, we made one step further into the direction of granular physics, which studies granular media.[1,44–47] Granular materials are in general dissipative collections of grains that are athermal, *i.e.*, large enough to allow neglecting thermal fluctuations. So far, spheres were assumed frictionless. When friction is introduced, hard spheres become the simplest example of a granular medium. Sand is a more complicated example. An especially interesting case of granular matter are systems of mechanically stable grains and in particular of mechanically stable frictional hard spheres. As we already mentioned, adding friction lets packings reach densities much lower than the J-point, as low as $\varphi \approx 0.55$, still maintaining mechanical stability.[1,15,16] One of the questions in granular physics is what is the number of mechanically stable configurations at a given volume fraction (or, more precisely, in an interval of volume fractions around any given φ). This number of states (more precisely, the density of states) is termed the Edwards entropy.[44,45,48] It is not well known how the Edwards entropy behaves in the available range from the RLP limit to the GCP limit (partially crystallized packings excluded). We extended

[36] L. Filion et al. *J. Chem. Phys.*, 133, 4115, 2010.
[37] R. J. Speedy. *Mol. Phys.*, 95, 169–178, 1998.
[38] C. A. Angell. *J. Phys. Chem. Solids*, 49, 863–871, 1988.
[39] F. H. Stillinger. *Science*, 267, 1935–1939, 1995.
[40] P. G. Debenedetti and F. H. Stillinger. *Nature*, 410, 259–267, 2001.
[41] V. Lubchenko and P. G. Wolynes. *Annu. Rev. Phys. Chem.*, 58, 235–266, 2007.
[42] A. Cavagna. *Phys. Rep.*, 476, 51–124, 2009.
[43] L. Berthier and G. Biroli. *Rev. Mod. Phys.*, 83, 587–645, 2011.
[44] S. F. Edwards and R. B. S. Oakeshott. *Physica A*, 157, 1080–1090, 1989.
[45] S. F. Edwards. *Physica A*, 353, 114–118, 2005.
[46] M. Pica Ciamarra et al. *Soft Matter*, 8, 9731–9737, 2012.
[47] D. Bi et al. *Annu. Rev. Condens. Matter Phys.*, 6, 63–83, 2015.
[48] P. Wang et al. *Physica A*, 390, 427–455, 2011.

the techniques from our entropy approach for studying the RCP limit onto the case of frictional packings and estimated the upper bound on the Edwards entropy in monodisperse hard sphere packings.

In the remainder of the introduction, we give a brief overview of the areas of jamming, glass transition, and granular media from the perspective of hard-sphere systems, thus providing context for individual chapters of the thesis.

Jamming

As mentioned, the investigation of jamming phenomena, starting from the experiments of Bernal, demonstrated reproducibility of the RCP limit for monodisperse packings with low or zero friction at a density $\varphi = 0.634 - 0.652$. Related phenomena, also mentioned, are structural changes at $\varphi = 0.646 - 0.652$ and in particular the onset of crystallization in monodisperse packings in this range of densities.

Packings that result from pouring particles into a container are mechanically stable in the sense that they do not collapse under gravity, though they can be unstable under shaking and shear. In general, a set of particles will be mechanically stable if the number of unknown frictional and normal force components is not larger than the number of force and torque balance equations.[1,48] A set of particles where the equality holds is called isostatic.[1,48] In case of frictionless spheres, usually studied in the context of jamming, this condition leads to the restriction on the average number of contacts per particle (coordination number): it cannot be lower than six. Jamming is equivalent to mechanical stability of frictionless packings (though mechanically stable frictional packings are also sometimes called jammed). A stable packing usually consists of a mechanically stable "backbone" and a small set of particles (around $2 - 3\%$) that can still move and do not contribute to mechanical stability.[3] They are called rattlers.

An important feature of jamming is that jammed states possess infinite kinematic pressure (calculated through the momentum transferred between particles per unit of time through collisions, if particles are allowed to fly and undergo elastic collisions in the absence of external force fields).[2,9,49] The infinity of pressure can be interpreted through the phase space depiction of hard sphere systems,[2,3,9,50] which is very fruitful in general. Each packing can be described as a point in the corresponding phase space. If a packing contains N particles, the phase space is $3N$-dimensional. If the boundary conditions are periodic and we want to exclude translational degrees of freedom, we can fix one of the particles so that the phase space will become $(3N-3)$-dimensional.[9] During experimental preparation of polydisperse packings, particle diameters are fixed, but the containing box is contracted. In computer simulations, on the other hand, it is easier to keep the box size fixed, but specify diameters up to a constant. This constant is controlled by the current packing density. When we specify a point in the phase space (particle coordinates), we can optionally specify the packing density, which would determine actual particle radii. Alternatively, we can determine packing density as some function of particle coordinates.

[49] M. Skoge et al. *Phys. Rev. E*, 74, 041127, 2006.
[50] F. H. Stillinger and Z. W. Salsburg. *J. Stat. Phys.*, 1, 179–225, 1969.

If packing density is specified, certain portions of the phase space, which correspond to particle intersections, are unavailable. Possible intersections of any pair of particles exclude a hypercylinder from the phase space.[9] The higher the density, the larger are the excluded hypercylinders. At high densities, the available phase space splits into relatively disjoint regions[2] and for even higher densities the regions become closed. With the density increase, closed available regions of the phase space can be approximated by polytopes.[3,9,50] With further density increase, these polytopes converge to infinitesimal volumes, which represent jammed states. When a polytope is infinitely small, the hyper-point in the phase space that represents a packing will collide during equilibration infinitely frequently with the boundary of the polytope. This means that particles in the packing collide infinitely frequently, which implies infinite kinematic pressure at jammed states. From this polytope picture, Salsburg and Wood[9] derived an equation of state for configurations close to being jammed.[37,49] An asymptotically equal equation of state was also derived from the free-volume theory.[9,51–53] Salsburg and Wood also showed that from purely geometrical arguments the average coordination number in a jammed packing cannot be lower than six, a fact derived independently from the force-torque balance requirements.

Glass transition

Glass physics, when dealing with hard spheres, is also interested in frictionless particles. In real molecular and atomic systems, the following observation was pivotal in defining the research area of the glass transition: when liquids are quickly cooled so that crystallization is avoided, their viscosity starts to rapidly increase with the temperature decrease.[38,42] When the viscosity reaches a conventional high value (10^{13} Poise), the liquid is proclaimed to be a glass.[42] The phenomenology of such supercooled liquids is very diverse and is a subject of active and sometimes controversial research.[38–43]

A very simplified picture of glass formation is the following.[39,40] During a fast temperature decrease (quench, or in case of an infinitely fast decrease, Stillinger quench), the system has not enough time to crystallize and ends up in a basin of attraction of a local potential energy minimum (termed also "inherent structure"[39,54]), not in a basin of attraction of a crystalline configuration. Low temperature ensures that it is very hard for a system to jump over potential energy barriers between basins of attraction, which leads to high viscosity, low diffusivity, high relaxation time, etc.[42]

Though there is no continuous potential interaction between spheres and thus no direct potential energy minima and basins of attraction associated with these minima, it is possible to introduce them into our system. At each packing configuration specified by particle positions, we can proportionally increase particle diameters from zero until at least one pair of particles touches each other. This will define a certain maximum density for each packing configuration and thus

[51] J. G. Kirkwood. *J. Chem. Phys.*, 18, 380–382, 1950.
[52] R. J. Buehler et al. *J. Chem. Phys.*, 19, 61–71, 1951.
[53] W. W. Wood. *J. Chem. Phys.*, 20, 1334–1334, 1952.
[54] S. Torquato and Y. Jiao. *Phys. Rev. E*, 82, 061302, 2010.

the maximum density landscape in the phase space. This maximum density landscape, taken with the minus sign, will form an equivalent of the potential energy landscape. The landscape will contain characteristic minima, and we can associate corresponding basins of attraction with these minima.

As mentioned, the higher the density, the larger is the part of the phase space that is occupied by unavailable regions, formed by unavailable hypercylinders. At high densities, a significant part of the phase space will be unavailable, and movement between basins of attraction (more precisely, between their available parts) will be hindered.[2] It correlates with the observation that the self-diffusion coefficient and the so-called alpha-relaxation time τ_α[42] increase rapidly after a certain density and eventually seem to diverge, though the exact density of divergence depends on the model employed for extrapolation of these lines.[29,55] The density of their divergence is termed the ideal glass transition density φ_g[2,29,43] and it is believed that the phase space becomes non-ergodic at this density.[33] The two typical fits that are used for the plots like τ_α *vs.* φ are the Mode-Coupling Theory (MCT) fit, $\tau_\alpha = \tau_0/(\varphi_g - \varphi)^\gamma$, and the Vogel-Fulcher-Tammann (VFT) fit, $\tau_\alpha = \tau_0 \exp[A/(\varphi_g - \varphi)^\delta]$.[29,55] For the system of 50:50 (by number) bidisperse spheres with radii ratio 1.4, the VFT fit produced $\varphi_g = 0.637$ (with $\delta = 2$).[55] The MCT fit could not fit the data in the entire range of φ, but when applied to $\varphi < 0.585$ it produced $\varphi_g = 0.59$. The inapplicability of the MCT fit in the entire range of densities can be regarded from a certain point of view as an expected result, because there is another interpretation of the MCT fit divergence: It marks the onset of the so-called activated dynamics, which implies that the MCT fit actually shall diverge before φ_g.[42]

It was believed that φ_g in the monodisperse case is related to the phenomenon of spontaneous crystallization.[56] Spontaneous crystallization happens when monodisperse sphere packings are allowed to equilibrate. In the range of densities $0.545 - 0.61$ their equilibrium state resembles a crystal,[57] though obviously spheres do not form a mechanically stable crystal packing. Crystal-like configurations dominate the phase space because the decrease in the entropy stemming from the restriction of "angular" degrees of freedom is compensated by the increase of the entropy from positional degrees of freedom (spheres have more options to vibrate around centers of the crystal lattice).[58] So it was initially believed that for monodisperse spheres the upper boundary of the interval of spontaneous crystallization, $\varphi \approx 0.61$, corresponds to φ_g. Recent careful simulations that track the self-diffusion coefficient at different densities suggest that these are unrelated phenomena and the divergence of relaxation times may happen at a slightly lower density than $\varphi \approx 0.61$.[32–34]

It can be shown that local minima in our pseudo-"potential energy landscape" correspond to jammed configurations. Indeed, if particles are assigned coordinates from such a local minimum and particle radii are proportionally increased to ensure the maximum density of this configura-

[55] G. Brambilla et al. *Phys. Rev. Lett.*, 102, 085703, 2009.
[56] W. van Megen and S. M. Underwood. *Phys. Rev. E*, 49, 4206–4220, 1994.
[57] W. G. Hoover and F. H. Ree. *J. Chem. Phys.*, 49, 3609–3617, 1968.
[58] D. Frenkel. "Order through disorder: Entropy-driven phase transitions" in: *Complex Fluids* ed. by Luis Garrido. Springer Berlin Heidelberg, 1993.

tion, any possible displacement of non-rattler particles (including collective rearrangements), will correspond to a lower maximally achievable density or in other words to particle intersections, if particles retain their radii from the initial locally optimal configuration. Thus, all displacements from the initial locally optimal configuration are forbidden and this configuration is jammed by definition. Thus, jammed configurations are the attractors of basins of attraction in the energy landscape. Minima in the potential energy landscape are also called inherent structures. Because an infinitely fast quench (Stillinger quench) by definition follows the path of the steepest descent in the potential energy landscape, such a quench ends up in the jammed configuration closest to the initial configuration. Thus, inherent structures are the closest jammed configurations for configurations in corresponding basins of attraction. This reveals a deep connection between the problems of jamming and glass transition in hard spheres.

Many glassy states

The phenomena of jamming and glass transition can be unified for hard spheres in the so-called "many glassy states" model.[2,29] This model was used for hard spheres as early as in 1998 by Speedy.[37] Another line of research that led to a very similar model was the mean-field description of glasses.[2,28]

As mentioned, if equilibrated hard spheres undergo infinitely fast compressions, they will get jammed at states with certain densities. These jamming densities of equilibrated hard spheres depend on the initial packing density, at which equilibration was performed.[29] In other words, equilibration at a given φ reaches basins of attraction that dominate the phase space at this φ. At different packing densities φ different basins of attraction dominate the phase space and thus their jamming densities (dominant jamming densities) φ_{DJ} are distinct. Thus, one can build a map φ_{DJ} *vs*. φ. An explanation of the fact why only one jamming density will dominate the phase space at a given φ can be found in Ref.[37]

If crystallization is suppressed, the largest possible jamming density is termed the glass close packing (GCP) limit φ_{GCP}.[2,29,59] It is of course automatically the largest possible density in general (including unjammed states), because otherwise we could perform a Stillinger quench from the corresponding unjammed configuration and reach the closest jammed configuration with density higher than φ_{GCP}. The initial density where the phase space is dominated by the GCP density ($\varphi_{\mathrm{DJ}} = \varphi_{\mathrm{GCP}}$) is believed to be exactly the ideal glass transition density φ_g, at which the alpha-relaxation time diverges and the phase space becomes non-ergodic. For $\varphi < \varphi_g$, φ_{DJ} is lower.[29] As we mentioned, an independent investigation from O'Hern suggested[12] that Poisson packings of hard spheres with $\varphi = 0$ jam after Stillinger quenches at a density ~ 0.64. This density was termed the "J-point" φ_J and was associated with the RCP limit. This interpretation of the RCP limit actually goes back to 1964 to Stillinger[60] (the concepts of inherent structures and their basins of attraction were also introduced in this paper, though the name "inherent structure" was coined later). At $\varphi = 0$, Poisson packings are the equilibrium ones, and thus we conclude that

[59] L. Berthier, H. Jacquin, and F. Zamponi. *Phys. Rev. E*, 84, 051103, 2011.
[60] F. H. Stillinger, E. A. DiMarzio, and R. L. Kornegay. *J. Chem. Phys.*, 40, 1564–1576, 1964.

$\varphi_{\text{DJ}}(\varphi = 0) = \varphi_J$. In the intermediate regime, $0 < \varphi < \varphi_g$, φ_{DJ} was reported to change at first slowly with φ and at a certain density (termed φ_{onset}) to start to increase rapidly.[29] This density φ_{onset} is associated with another density at which the phase space becomes "disjoint", but still remains ergodic. It is termed φ_d.[2] For the system of 50:50 (by number) bidisperse spheres with radii ratio 1.4, φ_d is estimated at 0.56, φ_J at 0.642, and the lower boundary for φ_{GCP} is 0.662.[29] For monodisperse packings, we obtained $\varphi_d \approx 0.52$, $\varphi_J \approx 0.64$, $\varphi_{\text{GCP}} \approx 0.65$, and $\varphi_g \approx 0.586$. To get some monodisperse values, we had to extrapolate the results from our polydisperse simulations onto a monodisperse case. Association of $\varphi \approx 0.65$ with the GCP limit unites the many glassy states model with the observation of structural changes and the onset of crystallization for monodisperse packings at $\varphi = 0.646 - 0.652$.

Granular matter

As mentioned, adding friction and focusing on mechanically stable frictional packings introduces a range of distinctive phenomena like the RLP limit and makes hard spheres a simple but important model in granular physics. An interplay between friction, average coordination number, and the possible range of densities for mechanically stable packings is summarized by Song *et al.*[1] We note though that this paper does not differentiate between the J-point and the GCP limit and merges the range between them into the RCP limit. Frictionless random packings can obtain densities in the range from the J-point to the GCP limit (and higher, if crystallization is allowed). In the picture from Ref.[1], packings at the "RCP limit" have the average coordination number of six. Packings with infinite friction can reach densities as low as the RLP limit and will have the average coordination number of four in the entire range from the RLP to the GCP limit. Packings with intermediate friction will have an intermediate coordination number and the lowest possible density of mechanically stable packings will be somewhere between the RLP limit and the J-point; both the average coordination number and the lowest possible density change monotonously with friction. We also note that Song *et al.*[1] report the density for the RCP limit (for monodisperse particles) as 0.634, which is lower than other estimates. What we observed in our simulations is that for finite packings the J-point splits into a range of densities, $0.636 - 0.64$ for 10^4 particles (a similar effect also reported by O'Hern and co-workers[12]). So we presume that $\varphi_{\text{RCP}} = 0.634$ observed by Song *et al.*[1] can be attributed to finite-size effects. Up until now we were not mentioning the spreading of the J-point into a segment for finite packings for simplicity.

A natural question that can be asked about the range of densities available for mechanically stable packings with a given friction coefficient (from φ_{RLP} to φ_{GCP} for infinite friction) is how many mechanically stable configurations exist at each density in this range (possibly excluding partially crystallized configurations). In 1989, Edwards conjectured that the volume of the mechanically stable packing is an analogue of energy in thermal systems.[44] This means that the analogue of entropy in granular matter is the number of mechanically stable packing configurations with the given volume or, equivalently, at a given packing density.[44,47,48,61] This quantity is

[61] D. Asenjo, F. Paillusson, and D. Frenkel. *Phys. Rev. Lett.*, 112, 098002, 2014.

termed the Edwards or granular entropy.[44,45,47,61,62] As in the "usual" statistical physics, system parameters in the microcanonical ensemble define actually not the number of states, but the density of states. In case of hard-sphere packings, the system parameters are only the number of particles and system volume (or the packing density φ). To switch from the density of states to the number of states we need to switch from the microcanonical to the canonical ensemble. The canonical ensemble means that we prepare an ensemble of large mechanically stable packings with a certain exact φ and examine the volume of a small subpacking inside. The average φ of the subpacking will be of course equal to the global φ, but it will fluctuate around this value. If Edwards' conjecture about replacing energy with volume is indeed true, the volume of the subpacking V shall comply with the Boltzmann distribution $\frac{1}{Z}\exp(-V/\chi)$, where χ is the analogue of the classical temperature and is termed compactivity (and Z is as usual the partition function).[44,46–48,63] We note here that there is a body of work that suggests that another state variable shall be included along with the compactivity to describe granular systems. It is termed angoricity and uses the force-moment tensor of a granular system as the energy.[45,47,64,65] Some reports[47,66] suggest that if the friction coefficient of a subpacking is different from the one of the "bath", compactivity does not equilibrate between the subsystem and the bath, while the angoricity does.

The concept of the Edwards entropy is widely used, but there are still very few methods for its estimation. Direct enumeration of mechanically stable states is possible only in small[67–70] or simplified model systems[71,72]. A group of methods attempts to estimate the Edwards entropy in the canonical ensemble through volume fluctuations of a repeatedly driven granular packing.[63,73,74] However, the results from these methods do not agree. The density of mechanically stable states and thus also the Edwards entropy in the canonical ensemble are presumed to be zero at the left vicinity of the RLP limit and also zero at the GCP limit (if partially crystalline configurations are excluded from the phase space). If the entropy is finite at the RLP limit itself, there is a discontinuity in the entropy at the RLP limit, so that the entropy jumps from zero to a finite value. A finite value of entropy at the RLP limit (in the canonical ensemble) is indeed sometimes reported.[63,73] Refs.[63,73] report that the entropy in the canonical ensemble decreases monotonously from the RLP to the GCP limit, while Ref.[74] reports a maximum of the entropy in-between. We investigate the behaviour of the Edwards entropy (in the microcanonical ensemble) in Chapter

[62] R. K. Bowles and S. S. Ashwin. *Phys. Rev. E*, 83, 031302, 2011.
[63] S. Zhao and M. Schröter. *Soft Matter*, 10, 4208–4216, 2014.
[64] S. Henkes, C. S. O'Hern, and B. Chakraborty. *Phys. Rev. Lett.*, 99, 038002, 2007.
[65] S. Henkes and B. Chakraborty. *Phys. Rev. E*, 79, 061301, 2009.
[66] J. G. Puckett and K. E. Daniels. *Phys. Rev. Lett.*, 110, 058001, 2013.
[67] M. Pica Ciamarra and A. Coniglio. *Phys. Rev. Lett.*, 101, 128001, 2008.
[68] G. Gao et al. *Phys. Rev. E*, 80, 061304, 2009.
[69] N. Xu, D. Frenkel, and A. J. Liu. *Phys. Rev. Lett.*, 106, 245502, 2011.
[70] S. S. Ashwin et al. *Phys. Rev. E*, 85, 061307, 2012.
[71] R. Monasson and O. Pouliquen. *Physica A*, 236, 395–410, 1997.
[72] R. K. Bowles and S. S. Ashwin. *Phys. Rev. E*, 83, 031302, 2011.
[73] C. Briscoe et al. *Phys. Rev. Lett.*, 101, 188001, 2008.
[74] S. McNamara et al. *Phys. Rev. E*, 80, 031301, 2009.

6 of this thesis.

Each chapter of this thesis corresponds to a published paper and has its own introduction and conclusion sections that present the motivation and implications of the individual studies. A concise description of the work done can be found in the “Summary and conclusions” section (p. 149).

Chapter 1

Pore-size entropy of random hard-sphere packings

Authors:

Vasili Baranau, Dzmitry Hlushkou, Siarhei Khirevich and Ulrich Tallarek*

State of publication:

Published on February 27, 2013 in Soft Matter, Vol. 9.12, pp 3361–3372
DOI: 10.1039/C3SM27374A

Abstract

We introduce a method for calculating the entropy of random hard-sphere packings, also referred to as pore-size entropy. The method is applicable to packings of monodisperse or polydisperse spheres as well as non-spherical particles. Pore-size entropy allows us to analyze packing microstructure and provides deep insight into the traditional concept of pore-size distribution. Specifically, the logarithm of the pore-size distribution's tail area is equal to the packing entropy. We reveal a local minimum in the plot of pore-size entropy *vs.* packing density (φ) for monodisperse frictionless sphere packings at a critical density $\varphi_C \approx 0.65$, independent of the employed packing generation protocol (Lubachevsky–Stillinger, Jodrey–Tory, and force-biased algorithms), which is a density with minimal number of available packing configurations. This entropy minimum is followed by an entropy increase as φ increases up to ~ 0.68, corresponding to the emergence of crystalline structures in the coexistence region; beyond this packing density the entropy decreases again. In a complementary study we modify the Lubachevsky–Stillinger protocol and reproduce the random-close packing limit at $\varphi_{\mathrm{RCP}} \approx 0.64$. We conclude that $\varphi_{\mathrm{RCP}} \approx 0.64$ is the jamming point of the glassy states with the lowest density, whereas $\varphi_C \approx 0.65$ is the jamming point of the densest glassy state (the ideal glass state).

1.1 Introduction

Numerous authors demonstrate structural changes in random packings of monosized frictionless hard spheres (*e.g.*, the onset of crystallization) for solid volume fractions φ ranging from 0.646 to 0.65, which is sometimes believed to indicate the random-close packing (RCP) limit or even used as a definition of the latter.[13,21–25] The fact that packings of monosized spheres are random up to a density of $\varphi \approx 0.65$ and start arranging into crystalline structures for higher densities suggests that an entropic measure could be helpful in defining, detecting, and understanding the properties of this transition. Numerous papers have introduced and utilized entropy for hard-sphere systems.[1,22,44,48,64,73,75–82] On the other hand, one of the tools for description and investigation of packing properties is the pore-size distribution, also called the nearest-surface distance distribution or void-size distribution; introduced, examined, and applied to hard-sphere packings in many publications.[83–91]

The main intention of this paper is to link the packing entropy to the nearest-surface distance distribution, providing a better understanding of the latter. The entropic measure that we derive is numerically robust and can easily be applied to monodisperse and polydisperse sphere packings, as well as to non-spherical[92,93] particles; further, it does not depend on *a priori* parameters (*e.g.*, Debye length,[22,80] Planck length,[1,48,73,76] or others), presenting a convenient and powerful tool for

[13] S. C. Kapfer et al. *Phys. Rev. E*, 85, 030301, 2012.
[21] A. V. Anikeenko and N. N. Medvedev. *Phys. Rev. Lett.*, 98, 235504, 2007.
[22] A. V. Anikeenko, N. N. Medvedev, and T. Aste. *Phys. Rev. E*, 77, 031101, 2008.
[23] T. Aste and T. Di Matteo. *Eur. Phys. J. B*, 64, 511–517, 2008.
[24] B. A. Klumov, S. A. Khrapak, and G. E. Morfill. *Phys. Rev. B*, 83, 184105, 2011.
[25] M. Bargieł and E. M. Tory. *Adv. Powder Technol.*, 12, 533–557, 2001.
[1] C. Song, P. Wang, and H. A. Makse. *Nature*, 453, 629–632, 2008.
[44] S. F. Edwards and R. B. S. Oakeshott. *Physica A*, 157, 1080–1090, 1989.
[48] P. Wang et al. *Physica A*, 390, 427–455, 2011.
[64] S. Henkes, C. S. O'Hern, and B. Chakraborty. *Phys. Rev. Lett.*, 99, 038002, 2007.
[73] C. Briscoe et al. *Phys. Rev. Lett.*, 101, 188001, 2008.
[75] Y. Jin and H. A. Makse. *Physica A*, 389, 5362–5379, 2010.
[76] C. Briscoe et al. *Physica A*, 389, 3978–3999, 2010.
[77] A. Donev, F. H. Stillinger, and S. Torquato. *J. Chem. Phys.*, 127, 124509, 2007.
[78] V. S. Kumar and V. Kumaran. *J. Chem. Phys.*, 123, 114501, 2005.
[79] R. Blumenfeld and S. F. Edwards. *Phys. Rev. Lett.*, 90, 114303, 2003.
[80] T. Aste and T. Di Matteo. *Phys. Rev. E*, 77, 021309, 2008.
[81] S. S. Ashwin and R. K. Bowles. *Phys. Rev. Lett.*, 102, 235701, 2009.
[82] P. Giaquinta and G. Giunta. *Physica A*, 187, 145–158, 1992.
[83] S. Torquato, B. Lu, and J. Rubinstein. *Phys. Rev. A*, 41, 2059–2075, 1990.
[84] B. Lu and S. Torquato. *Phys. Rev. A*, 45, 5530–5544, 1992.
[85] S. Torquato. *Phys. Rev. E*, 51, 3170–3182, 1995.
[86] M. Alonso et al. *Chem. Eng. Sci.*, 50, 1983–1988, 1995.
[87] M. Alonso, M. Satoh, and K. Miyanami. *Can. J. Chem. Eng.*, 70, 28–32, 1992.
[88] I. Schenker et al. *Phys. Rev. E*, 80, 021302, 2009.
[89] I. Schenker et al. *Granul. Matter*, 14, 333–340, 2012.
[90] S. Torquato. *Annu. Rev. Mater. Res.*, 32, 77–111, 2002.
[91] D. Stoyan et al. *J. Non-Cryst. Solids*, 357, 1508–1515, 2011.
[92] A. Donev, S. Torquato, and F. H. Stillinger. *J. Comput. Phys.*, 202, 765–793, 2005.
[93] A. V. Kyrylyuk et al. *Soft Matter*, 7, 1671–1674, 2011.

a detailed analysis of packing properties, including preparation protocol-specific disorder and structural transitions upon compaction.

In the assumption of equiprobable microstates at a given packing density[44,80,94] the entropy of a packing is the logarithm of the total number of valid packing configurations described by particle coordinates and radii, which is proportional to the probability of finding a valid packing (*i.e.*, without particle intersections) among all packing configurations. We assume that the probability of a successful insertion of a particle into a valid packing is equal to the probability of finding a valid packing among all packing configurations. We subsequently estimate the probability of a successful particle insertion by building a pore-size distribution for a packing, fitting it with a Gaussian curve[88] and calculating the area under the tail of this distribution, starting from the mean particle radius. Therefore, pore-size entropy also suggests deep insight into the traditional concept of the pore-size distribution; specifically, the logarithm of its tail area equals the entropy of a packing.

To test the validity of this approach we apply the entropy measure in a wide range of packing densities ($\varphi = 0.6 - 0.7$) to computer-generated monodisperse frictionless sphere packings, each containing 10000 spheres residing in a cubic box with periodic boundary conditions in all directions. Packings were generated with (i) the Lubachevsky–Stillinger (LS) algorithm,[95] (ii) the Jodrey–Tory (JT) algorithm,[96,97] and (iii) a force-biased algorithm (FBA).[98,99]

The pore-size entropy reveals a pronounced minimum at a critical density of $\varphi_C = 0.647 - 0.651$, in agreement with structural transition densities reported previously (we will also refer to this minimum as a "structural transition density"). There still remains an open question on how this structural transition density is related to the generally accepted RCP limit ($\varphi_{\mathrm{RCP}} \approx 0.64$) obtained experimentally and by the direct generation of jammed configurations.[1,10–12,75,100–102] In this paper, by the RCP limit we will understand the infinite-pressure limit of the least dense glassy states,[2] which can be obtained by the generation of mechanically stable packings in the infinitely large compression-rate limit (which indeed produces packings at $\varphi_{\mathrm{RCP}} \approx 0.64$).[2,103,104] By jamming

[94] K. Wang et al. *Phys. Rev. E*, 86, 011305, 2012.
[95] B. D. Lubachevsky and F. H. Stillinger. *J. Stat. Phys.*, 60, 561–583, 1990.
[96] W. S. Jodrey and E. M. Tory. *Phys. Rev. A*, 32, 2347–2351, 1985.
[97] M. Bargieł and J. Mościński. *Comput. Phys. Commun.*, 64, 183–192, 1991.
[98] J. Mościński et al. *Mol. Simul.*, 3, 201–212, 1989.
[99] A. Bezrukov, M. Bargieł, and D. Stoyan. *Part. Part. Syst. Char.*, 19, 111–118, 2002.
[10] J. D. Bernal and J. Mason. *Nature*, 188, 910–911, 1960.
[11] G. D. Scott and D. M. Kilgour. *J. Phys. D: Appl. Phys.*, 2, 863–866, 1969.
[12] C. S. O'Hern et al. *Phys. Rev. E*, 68, 011306, 2003.
[100] J. D. Bernal. *Nature*, 185, 68–70, 1960.
[101] C. S. O'Hern et al. *Phys. Rev. Lett.*, 88, 075507, 2002.
[102] N. Xu, J. Blawzdziewicz, and C. S. O'Hern. *Phys. Rev. E*, 71, 061306, 2005.
[2] G. Parisi and F. Zamponi. *Rev. Mod. Phys.*, 82, 789–845, 2010.
[103] G. Gao, J. Bławzdziewicz, and C. S. O'Hern. *Phys. Rev. E*, 74, 061304, 2006.
[104] C. F. Schreck, C. S. O'Hern, and L. E. Silbert. *Phys. Rev. E*, 84, 011305, 2011.

we understand collective jamming in packings of frictionless particles[3,14,30,31] (equivalent to mechanical stability,[1] isostaticity,[3,12,20,35,48,101,102,105–113] and infinite pressure in systems of particles supplied with velocity[9]).

We will discuss the relation between the structural transition density (φ_C) and the RCP limit (φ_{RCP}) in Sections 1.4.3 and 1.4.4. To resolve the issue of the two density estimates (φ_C and φ_{RCP}) we amend the Lubachevsky–Stillinger generation protocol to completely equilibrate sphere packings (*i.e.*, conduct molecular dynamics simulations with zero compression rate until pressure is stationary) after each 2×10^4 collisions with compression. This amendment allows systematic reproduction of the RCP limit at $\varphi_{\text{RCP}} \approx 0.64$ with fast compressions. We are not aware of any work that recovers both characteristic packing densities (~ 0.64 and ~ 0.65) with the same packing generation protocol.

The last result suggests that the structural transition observed at $\varphi_C = 0.647 - 0.651$ and the RCP limit at $\varphi_{\text{RCP}} \approx 0.64$ are distinct phenomena, which cannot be justified by a difference in the preparation protocols. We explain this observation on the basis of a picture proposed in a review by Parisi and Zamponi.[2] While $\varphi_{\text{RCP}} \approx 0.64$ corresponds to the jammed configurations of the least dense glassy states (φ_{th} in this review), $\varphi_C = 0.647 - 0.651$ corresponds to the jammed configuration of the densest glassy state (φ_{GCP} in this review).

We provide an overview of the employed packing generation methods in Section 1.2; the pore-size entropy measure is derived and its connection to the pore-size distribution explained in Section 1.3; results, a discussion, and conclusions are provided in Sections 1.4 and 1.5.

1.2 Packing generation methods

In this paper, we analyze computer-generated packings, each containing 10000 spheres residing in a cubic box with periodic boundary conditions in all directions. Packings of monodisperse frictionless spheres were generated with (i) the Lubachevsky–Stillinger (LS) algorithm[95] using codes from Skoge *et al.*[49] and Donev *et al.*,[92] (ii) the Jodrey–Tory (JT) algorithm,[96,97] and (iii) a

[3] S. Torquato and F. H. Stillinger. *Rev. Mod. Phys.*, 82, 2633–2672, 2010.
[14] S. Torquato, T. M. Truskett, and P. G. Debenedetti. *Phys. Rev. Lett.*, 84, 2064–2067, 2000.
[30] A. Donev. *J. Appl. Phys.*, 95, 989–999, 2004.
[31] A. Donev et al. *J. Comput. Phys.*, 197, 139–166, 2004.
[20] I. Biazzo et al. *Phys. Rev. Lett.*, 102, 195701, 2009.
[35] P. Chaudhuri, L. Berthier, and S. Sastry. *Phys. Rev. Lett.*, 104, 165701, 2010.
[105] S. Alexander. *Phys. Rep.*, 296, 65–236, 1998.
[106] N. Xu and E. S. C. Ching. *Soft Matter*, 6, 2944–2948, 2010.
[107] H. A. Makse, D. L. Johnson, and L. M. Schwartz. *Phys. Rev. Lett.*, 84, 4160–4163, 2000.
[108] P. Wang et al. *J. Stat. Mech.*, P12005, 2010.
[109] C. F. Moukarzel. *Phys. Rev. Lett.*, 81, 1634–1637, 1998.
[110] A. Donev, S. Torquato, and F. H. Stillinger. *Phys. Rev. E*, 71, 011105, 2005.
[111] L. E. Silbert. *Soft Matter*, 6, 2918–2924, 2010.
[112] A. Mehta. *Soft Matter*, 6, 2875–2883, 2010.
[113] C. B. O'Donovan and M. E. Möbius. *Phys. Rev. E*, 84, 020302, 2011.
[9] Z. W. Salsburg and W. W. Wood. *J. Chem. Phys.*, 37, 798–804, 1962.
[49] M. Skoge et al. *Phys. Rev. E*, 74, 041127, 2006.

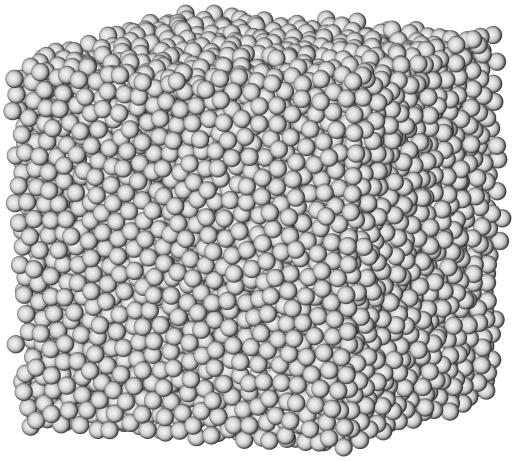

Figure 1.1: A random packing of 10000 monosized spheres at a solid volume fraction of $\varphi = 0.64$, generated with the force-biased algorithm.

force-biased algorithm (FBA),[98,99] which is a modification of the JT algorithm also used by several other authors.[22,25,26,75]

The LS algorithm is, in principle, a molecular dynamics simulation aiming at absolutely elastic hard sphere movement modeling, which starts from a random distribution of spheres in a given simulation box of radii sufficiently small to avoid sphere intersections. In the course of event-driven molecular dynamics simulation the particle radii are gradually increased with a certain expansion rate until pressure, produced by particle momentum, reaches a predefined large enough value. The lower the expansion rate, the denser will be the final configuration. For monodisperse particles, the LS algorithm can easily produce almost perfectly crystalline packings. The maximal reduced pressure in a packing was 10^{12} and the spheres' growth rate varied from 10^{-5} to 0.2. The total number of packings generated with the LS algorithm was 230.

The JT algorithm also starts from a random distribution of sphere (particle) centers in a simulation box. Each sphere is supplied with an inner diameter chosen to be proportional to the desired sphere diameter and to make the particles in the closest pair touch each other with their inner diameter shells, and consequently to avoid any particle intersections in a packing. Alternatively, a single inner diameter ratio can be specified for the entire packing as the ratio of inner diameters to the desired particle diameters. Similarly, a packing is supplied with an outer diameter ratio, initially larger than unity (so that each sphere has an outer diameter proportional to and larger than the desired one). A common approach for the outer diameter ratio initialization is to ensure that the total volume of the particles is equal to the box volume. At each iteration, the following steps are performed: (i) the pair of particles with the largest outer diameter intersection is found; (ii) particles of this pair are spread along their intersection line so that the intersection of outer shells is completely removed (but new intersections with other

[26] K. Lochmann et al. *Eur. Phys. J. B*, 53, 67–76, 2006.

particles may occur); (iii) the outer diameter ratio is decreased according to some contraction rate; and (iv) the inner diameter ratio is updated to make particles in the closest pair touch each other with their inner diameter shells.

In its classical version the JT algorithm terminates when the outer diameter ratio is equal to the inner diameter ratio; the lower the outer diameter ratio contraction rate, the denser becomes the final configuration. In the current paper we use a modified termination condition for JT packings and stop the generation when the inner diameter ratio is equal to unity, which allows to achieve the exact required density. We chose the contraction rate (k in the original paper[96]) as 10^{-5}. The algorithm can easily produce monodisperse packings up to the structural transition density φ_C. To overcome this limit we restarted the generation several (up to 20) times using the particle positions from the previous run as starting configuration.

The FBA is a modification of the JT algorithm, which can be classified as a "collective rearrangement" method. The initial distribution of particles is also random and particles are supplied with inner and outer diameters of the same meaning. Particles are also supplied with elastic potential (usually of the third order by overlap distance),[99] which is cut-off at the outer particle shell. Therefore, it is possible to compute particle forces (of the second order by overlap distance) between each particle pair with intersecting outer shells, as well as net forces for each particle. The iteration proceeds as follows: (i) all the particle forces and net forces for each particle are determined; (ii) all particles are displaced by distances proportional to their net forces and in the direction of net forces; (iii) the outer diameter ratio is decreased according to some contraction rate; and (iv) the inner diameter ratio is updated so that inner diameter shells of the particles in the closest pair touch each other. In this paper, we modify a standard termination condition for the algorithm and stop the generation when one of the two criteria is satisfied: (i) the outer diameter ratio is equal to the inner diameter ratio; or (ii) the inner diameter ratio is equal to unity (if the first condition has not yet been met). The lower the outer diameter ratio contraction rate, the denser the final configuration: In contrast to the JT algorithm this algorithm can easily overcome the structural transition density φ_C of monodisperse sphere packings.

The parameters of the FBA were the following (notation taken from Bezrukov *et al.*[99]): force scaling factor, $\rho = 0.5$; values of τ control the final density and span from 4×10^3 to 7×10^6. The total number of packings generated with the FBA was 230. An exemplary sphere packing at a packing density of $\varphi = 0.64$ is presented in Fig. 1.1.

Here, we point out a connection between the FBA and energy minimization protocols used in many papers.[12,35,101,102,106] In these protocols, the particles are supplied with elastic potential and are initially placed randomly in a simulation box. The following steps are performed on each iteration of the algorithm: (i) particles are displaced to find local minima of elastic energy associated with intersections employing a standard optimization method, and (ii) the box is expanded to decrease particle overlaps.

A decrease of the outer diameter ratio in the FBA is equivalent to a box expansion in energy minimization protocols. Further, the displacement of particles in the direction of net forces in

the FBA can be interpreted as the simplest version of a potential energy minimization through the steepest descent method. Therefore, the FBA corresponds to simultaneous box expansion and intersection energy minimization and, in principle, is very similar to energy minimization protocols.

1.3 Pore-size entropy

In this section a new method for calculation of granular matter entropy (called pore-size entropy) is introduced. It can be easily applied to monodisperse and polydisperse hard-sphere packings as well as to packings of non-spherical[92,93] particles. Further, it does not depend on *a priori* parameters (*e.g.*, Debye length;[22,80] Planck length;[1,48,73,76] or others) and allows us to directly analyze packing properties like structural transition and packing protocol-specific disorder.

We now provide an overview of the derivation of the entropic measure. In the assumption of equiprobable microstates at a given packing density[44,80,94] the entropy of a packing is the logarithm of the total number of valid packing configurations described by particle coordinates and radii, which is proportional to the probability of finding a valid packing (*i.e.*, without particle intersections) among all packing configurations. We assume that the probability of a successful insertion of a particle into a valid packing is equal to the probability of finding a valid packing among all packing configurations. We subsequently estimate the probability of a successful particle insertion by building a pore-size distribution for a packing, fitting it with a Gaussian curve[88] and calculating the area under the tail of this distribution, starting from the mean particle radius. Thus, this measure also suggests deep insight into the traditional concept of pore-size distribution; specifically, the logarithm of its tail area equals the entropy of a packing. We start the derivation from monosized packings and extend the idea to polydisperse packings.

1.3.1 Phase space description

Each packing configuration of N monosized particles can be represented as a point in a $3N$-dimensional packing phase space (3 coordinates per particle center). For packing box sides L_x,L_y, and L_z, respectively, the total phase space volume equals $V_{\text{tot}} = (L_x L_y L_z)^N$. If a given point in the phase space corresponds to at least one physical overlap between particles, it is unavailable. The true Gibbs entropy of an N-particle packing ensemble with a given density is determined by the volume of the phase space available to the packings. The structure of basins of attraction for available states in small packings of hard particles has been studied in several recent papers.[69,70]

To construct the entropy, we uniformly discretize the entire phase space by M points, for example, through discretization of each of the packing box dimensions by M_x, M_y, and M_z points, respectively, in which case $M = (M_x M_y M_z)^N$. With the assumption of equiprobable

[69] N. Xu, D. Frenkel, and A. J. Liu. *Phys. Rev. Lett.*, 106, 245502, 2011.
[70] S. S. Ashwin et al. *Phys. Rev. E*, 85, 061307, 2012.

system microstates,[44,80,94] the entropy S of the packing ensemble is calculated by

$$S = \ln(M_{\text{avail}}) = \ln(M \cdot p_{\text{avail}}) = \ln(M) + \ln(p_{\text{avail}}), \tag{1.1}$$

where M_{avail} is the total number of valid phase space points and p_{avail} is the probability to encounter an available state in the phase space (the density of available states).

To assess relative entropy values we do not need the constant term $\ln(M)$ in the computation, as it does not depend on packing protocol, packing volume fraction, particle size distribution, etc., which leads to

$$S_{\text{avail}} = \ln(p_{\text{avail}}), \tag{1.2}$$

thus allowing infinitely precise discretization. We add a subscript "avail" to the entropy to emphasize that it is a contribution to the entropy and will bear negative values.

This formula can be treated without the notion of entropy as follows: The phase space region for a packing of a given size is characterized by the probability to encounter an available hyperpoint in that region, which we assess through the logarithm in Eq. (1.2).

We point out a distinction between a "strong" form of the equiprobability assumption and a "weak" one. The strong form implies that valid packing configurations in the entire range of densities are equally probable (*i.e.*, the phase space has an additional dimension of packing density or particle diameter); the weak form implies that packing configurations are equiprobable for any given density, though configuration (microstate) probabilities for different densities may not be equal. The discussion in the present paper relies on the weak form of the equiprobability assumption, whereas configurations for distinct densities may have drastically different probabilities.

We note that different protocols may yield distinct entropy values even if the equiprobability assumption holds for each of the protocols. This may happen if the protocols sample different subregions of the phase space and can reach different numbers of valid configurations, though valid reachable configurations for each of the protocols are equiprobable.

1.3.2 Slicing assumption

Each packing of N monosized particles can be percepted as a 3-dimensional slice of a $3(N+1)$-dimensional packing phase space of $N+1$ particles; with 3 coordinates of the last particle left unconstrained.

This slice may be viewed as a $3(N+1)$-dimensional thin layer in a phase space, given that the first N particles are allowed to change their coordinates slightly by the discretization length. The volume of this layer is $V_{\text{layer}} = L_x L_y L_z (L_x L_y L_z / M_x M_y M_z)^N$.

As far as the packings are random and uniform, we predict that the probability p_{avail} to encounter an available hyperstate in this thin hyperlayer is very close to the one computed from the entire phase space (if the number of particles in the packings is sufficiently large). In

other words, the density of available states in the hyperlayer is equal to the density in the entire packing. As far as the first N particles have no intersections and their coordinates are fixed, and just the last particle can be moved, each available hyperstate actually corresponds to the successful insertion of the $(N+1)$th particle in the packing of N particles.

Thus, one can estimate p_{avail} by taking a computer-generated packing and trying to insert a test particle in the voxels of the discrete mesh of $M_x M_y M_z$ points (equivalent to the successful estimation of the insertion probability, p_{insert}), which yields

$$p_{\text{insert}} = p_{\text{avail}}. \tag{1.3}$$

This procedure is still numerically challenging and depends on the discretization. The slicing assumption reflects a traditional approach in statistical physics, when properties of the system ensemble are determined from a single large enough system.

If it turns out that the weak form of the equiprobability assumption does not hold in the thermodynamic limit, the entropy computed by a single packing will be distinct from the true entropy computed as $S = -\sum p_i \cdot \ln(p_i)$, where the sum is taken over all the packing states and p_i is the state probability. Instead, the entropy will reflect the value for the phase space, as if it were constructed from the equiprobable configurations which are very similar in structure to the current packing (so the current packing is a typical one). The discrepancy between actual and estimated entropies will depend on the probability distribution. Even in this case the measure that we will derive may serve as a convenient tool for investigation of packing microstructure.

We are unable to restrict packing configurations accounted for in the entropy values only to jammed configurations due to the slicing assumption; therefore, the entropy will be comprised of configurational and vibrational contributions, *i.e.*, mechanically stable and unstable, but still valid, configurations will be counted to give the entropy value.

1.3.3 Insertion probability

The following method for estimating the insertion probability was derived. We randomly generate a sufficient number of points uniformly inside the packing and determine the maximum radius of a sphere to be inserted at a given point by the distance from the nearest particle surface. If a point resides inside an initially generated particle, the insertion radius is still equal to the distance from the surface, but it carries a negative sign.

If the coordinates of such a random point are $\vec{r}$, the nearest neighbor center coordinates are $\vec{r}_{\text{neigh}}$, and the nearest neighbor radius is R, the insertion radius is $r_{\text{insert}} = ||\vec{r} - \vec{r}_{\text{neigh}}|| - R$. Then we build an insertion radii distribution for the entire packing and estimate the probability density function $f_{\text{pore}}(r)$ of a successful insertion of a sphere with a given radius. This distribution is described in many papers as pore-size distribution.[83–91]

The probability of successful insertion of a sphere with radius r_{insert} is given by the tail area

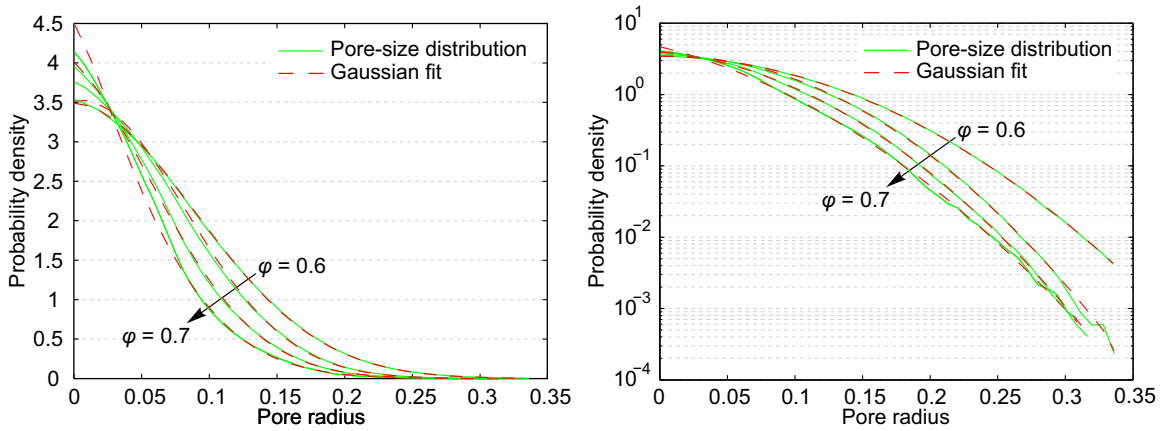

Figure 1.2: Probability density functions for pore radii distributions (solid green lines) and their best fits with Gaussian curves (dashed red lines). Left panel: linear scale, right panel: log-linear scale. Packing densities φ along the direction of the arrow: 0.6, 0.6303, 0.6658, 0.7. The packings were generated with the Lubachevsky–Stillinger algorithm. Pore radii were normalized with respect to the particle diameter.

of the pore-size distribution, starting from r_{insert}:

$$p_{\text{insert}}\left(r_{\text{insert}}\right) = \int_{r_{\text{insert}}}^{\infty} f_{\text{pore}}\left(r'\right) \mathrm{d}r'. \tag{1.4}$$

We follow the work of Schenker *et al.*[88] and approximate the pore-size distribution with a standard Gaussian curve

$$f_{\text{pore}}\left(r\right) \approx C \frac{1}{\sigma\sqrt{2\pi}} \exp\left(-\frac{\left(r-\mu\right)^2}{2\sigma^2}\right), \quad r > 0, \tag{1.5}$$

$$p_{\text{insert}}\left(r\right) \approx C \frac{1}{2}\left(1 - \operatorname{erf}\left(\frac{r-\mu}{\sigma\sqrt{2}}\right)\right), \quad r > 0, \tag{1.6}$$

where μ and σ are parameters determined from the fitting of the pore-size distribution (obtained numerically). Standard distribution fitting techniques are inapplicable, as normal distribution is not exposed for the entire range of radii, just for pores with positive radius. Thus, one can use maximum likelihood fitting for normal distribution truncated above zero.[114] Another possibility is to use a quadratic least-squares fit over the logarithm of the experimentally measured pore-size distribution. Polynomial coefficients can easily be converted into Gaussian distribution parameters afterwards.

The normalization constant C in Eqs. (1.5) and (1.6) originates in the fact that some pore centers will be generated inside existing particles. As far as the probability to generate a random point in the interparticle void space, *i.e.*, between particles, is equal to the packing porosity

[114] A. C. Cohen. *Ann. Math. Stat.*, 21, 557–569, 1950.

(interparticle void volume fraction), $\varepsilon = 1 - \varphi$, the normalization factor satisfies the equation

$$\int_0^\infty f_{\text{pore}}(r)\,\mathrm{d}r = C\int_0^\infty \frac{1}{\sigma\sqrt{2\pi}}\exp\left(-\frac{(r-\mu)^2}{2\sigma^2}\right)\mathrm{d}r = \varepsilon. \tag{1.7}$$

The insertion probability estimate p_{insert} can be applied to both monodisperse and polydisperse packings.

Fig. 1.2 shows pore-size distributions for LS-generated random packings of monodisperse particles at different packing densities (φas indicated), alongside with their Gaussian fits (the particle radius for all packings is 0.5 a.u.). The fit quality is very good, but decreases at increasing φ; coefficients of determination R^2 for the fits in Fig. 1.2 (computed for distribution tails with pore radii larger than 0.2 a.u.) are 0.9999, 0.9988, 0.9980, and 0.9797 in the order of increasing φ. The reason underlying this trend is that the pore-size distributions are not perfectly Gaussian (Eq. (1.5)); this deviation increases with the packing density. We note in advance that the slight deviations of radii distributions from a perfect bell shape explain the noise in the pore-size entropy plots for packings denser than $\varphi_C = 0.647 - 0.651$ in Fig. 1.3.

1.3.4 Packing entropy

Finally, for monodisperse sphere packings with particle radius r_0 the entropy is computed by combining Eqs. (1.2), (1.3), and (1.6)

$$S_{\text{avail}} = \ln\left(p_{\text{avail}}\right) = \ln\left(p_{\text{insert}}\left(r_0\right)\right) = \ln\left(C\frac{1}{2}\left(1 - \operatorname{erf}\left(\frac{r_0-\mu}{\sigma\sqrt{2}}\right)\right)\right). \tag{1.8}$$

Eq. (1.8) shows that the entropy of a packing is the logarithm of the pore-size distribution's tail area (starting from the particle radius) and thereby relates the pore-size distribution to packing entropy.

One can estimate the entropy easily even without fitting of the pore-size distribution as follows. The probability to insert a particle in a dense packing is extremely low. Therefore, we may substitute the complementary error function from Eq. (1.6) with the first term of its asymptotic expansion:[115]

$$1 - \operatorname{erf}(x) \approx \frac{e^{-x^2}}{x\sqrt{\pi}}. \tag{1.9}$$

Consequently,

$$S_{\text{avail}} = \ln\left(p_{\text{insert}}\left(r_0\right)\right) \approx \ln\left(\frac{1}{2\sqrt{\pi}}\right) + \ln(C) - \ln\left(\frac{r_0-\mu}{\sigma\sqrt{2}}\right) - \frac{1}{2}\left(\frac{r_0-\mu}{\sigma}\right)^2. \tag{1.10}$$

[115] M. Abramowitz and I. A. Stegun. *Handbook of mathematical functions: With formulas, graphs, and mathematical tables*. New York: Dover Publications, 1965.

Typical values for the fitting parameters (measured in particle diameters, so that $r_0 = 0.5$) are $\mu = -0.057$ and $\sigma = 0.085$, and a typical value for the normalization constant is $C = 2$, while a typical entropy value is $S_{\text{avail}} = -25$. Therefore, the last term in Eq. (1.10) is by an order of magnitude larger than the other ones, so we can approximate the entropy as

$$S_{\text{avail}} = \ln\left(p_{\text{insert}}\left(r_0\right)\right) \approx -\frac{1}{2}\left(\frac{r_0}{\sigma}\right)^2. \tag{1.11}$$

Subsequently, we try to compute the insertion probability for particles with smaller radius and to link it to the entropy. Let the smaller radius r be different from the initial particle radius r_0 by the factor α, $r_0 = \alpha r$, then

$$\begin{aligned} S_{\text{avail}} &= \ln\left(p_{\text{insert}}\left(r_0\right)\right) \approx -\frac{1}{2}\left(\frac{r_0}{\sigma}\right)^2 = -\frac{1}{2}\left(\frac{\alpha r}{\sigma}\right)^2 = \\ &= -\alpha^2\frac{1}{2}\left(\frac{r}{\sigma}\right)^2 \approx \alpha^2 \ln\left(p_{\text{insert}}\left(\frac{r_0}{\alpha}\right)\right). \end{aligned} \tag{1.12}$$

If there are enough generated pores with a radius larger than r_0/α, we can estimate the insertion probability directly from dividing the number of large-enough pores by the total number of pores and substitute it into Eq. (1.12). This approach benefits from the absence of a distribution fitting, which affects entropy values significantly, as far as $p_{\text{insert}}(r_0)$ is very low. In our simulations we have found that $\alpha = 2$ is sufficient and provides the best trade-off between the required number of large pores and the deviation from Eq. (1.8).

It is straightforward to extend the above formalism to packings of polydisperse particles by using four dimensions per particle in the phase space: three for the particle center coordinates and one for the particle radius. The dimensionality of the phase space of N-particle-packing ensembles is therefore $4N$ and the total phase space volume for the packings is $V_{\text{tot}} = (L_x L_y L_z R_{\text{max}})^N$, where R_{max} is the largest particle radius supported by the particle size distribution. Eq. (1.2) still holds, as well as the slicing assumption, although each packing of N polydisperse particles now represents a four-dimensional slice of the phase space, and to estimate the available states density we should try to insert particles of random radii (according to their size distribution) in each point inside the packing. The insertion probability can be approximated with the pore-size distribution as follows

$$p_{\text{insert}} = \int_0^\infty p_{\text{insert}}\left(r\right) \cdot f_{\text{size}}\left(r\right) \mathrm{d}r, \tag{1.13}$$

where $p_{\text{insert}}(r)$ is determined by Eqs. (1.4) and (1.5), and $f_{\text{size}}(r)$ is the probability density function of the particle radii distribution. The entropy of polydisperse packings is thus equal to

$$S_{\text{avail}} = \ln \int_0^\infty C\frac{1}{2}\left(1 - \operatorname{erf}\left(\frac{r-\mu}{\sigma\sqrt{2}}\right)\right) f_{\text{size}}\left(r\right) \mathrm{d}r. \tag{1.14}$$

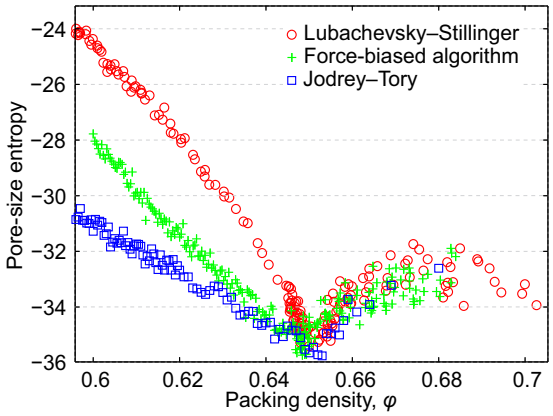

Figure 1.3: Pore-size entropy (Eq. (1.12)) *vs.* packing density for monodisperse sphere packings generated with the Lubachevsky–Stillinger algorithm (◯), force-biased algorithm (+), and the Jodrey–Tory algorithm (□).

It is also feasible to estimate the probability p_{avail} of available packing configurations by trying to insert a particle with number-mean radius into a polydisperse packing, *i.e.*, to calculate the entropy of polydisperse packings by Eq. (1.8) or (1.12), with r_0 as the number-mean particle radius.

1.4 Results and discussion

1.4.1 Pore-size entropy

We now apply the pore-size entropy measure to several types of monodisperse sphere packings (generated as described in Section 1.2) covering a wide range of packing volume fractions φ (Fig. 1.3). Pore-size entropy is computed by Eq. (1.12) with $\alpha = 2$. The total number of randomly inserted points used for the construction of the pore-size distribution was 10^7 for each packing. We did not remove rattler particles[95] from jammed configurations, though we verified that recursive removal (without updating the packing density[110,113]) of rattler particles with less than four contacts,[49,113,116] which is a minimum number required for mechanical stability, influences the results insignificantly and we therefore do not present separate plots.

Expectedly, the pore-size entropy in Fig. 1.3 initially decreases at increasing φ, as the amount of available packing configurations decreases due to the higher probability of particle intersections. The entropy reaches a profound local minimum for all packing types at a critical density of $\varphi_C = 0.647 - 0.651$. This density is associated with the minimal number of available states that can be reached in the course of a physical packing preparation protocol. Indeed, a packing preparation process can be interpreted as moving a point of the complete packing description in a multidimensional phase space. It is tempting to attribute this density φ_C to the RCP limit, but we postpone a discussion until Section 1.4.3.

The local minimum at $\varphi_C = 0.647 - 0.651$ in Fig. 1.3 is followed by a strong entropy

[116] G. Gao et al. *Phys. Rev. E*, 80, 061304, 2009.

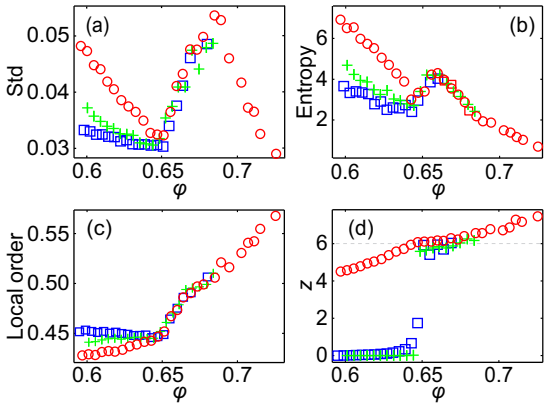

Figure 1.4: Complementary packing measures *vs.* packing density φ applied to the same monodisperse sphere packings as in Fig. 1.3 generated with the Lubachevsky–Stillinger algorithm (◯), force-biased algorithm (+), and the Jodrey–Tory algorithm (□). (a) Standard deviation of Voronoi volumes; (b) entropy of Voronoi volumes; (c) local bond-orientational order; and (d) geometrical coordination number.

increase upon further compaction of the packings, which is usually explained by the emergence of crystalline regions and releasing portions of the phase space available for new packing configurations.[22] This is due to at least two mechanisms: (i) there is a certain freedom in shifting the particles in crystalline configurations (which is sometimes called vibrational entropy;[2] it is well known that vibrational entropy for crystals is higher than for random structures, *e.g.*, liquids); (ii) the existence of crystalline subregions of higher density allows other packing subregions to form random microstructures. That is why packings are considered to be in a coexistence region for densities above φ_C.[2,75]

Finally, the pore-size entropy in Fig. 1.3 starts decreasing again at higher packing densities (beyond $\varphi \approx 0.68$). It corresponds to the exhaustion of available packing configurations, which were released after the onset of the crystallization process. Indeed, if a particle resides in a dilute crystalline packing, it can be shifted slightly, thus exploring phase space. After packing contraction the given particle can be shifted only by a smaller distance, which indicates a lower number of available states.

1.4.2 Comparison with other measures

For a better interpretation of the results in Fig. 1.3, we present in Fig. 1.4 several other well-known measures that were computed for the same packings. First, we construct Voronoi volumes around particle centers and record their standard deviation (Fig. 1.4a).[1,117] The structural transition is determined by the local minimum of the density-measure plot. Second, entropy is computed over the given Voronoi volumes according to the hard spheres' statistical mechanics formalism[22,23,80] (Fig. 1.4b). Similarly, the local minimum of the function exposes the structural transition. Third, we analyze a local bond-orientational order measure Q_6^{local} (Fig. 1.4c),[118] used

[117] S. Khirevich et al. *J. Chromatogr. A*, 1217, 4713–4722, 2010.
[118] P. J. Steinhardt, D. R. Nelson, and M. Ronchetti. *Phys. Rev. B*, 28, 784–805, 1983.

in several papers.[3,26,75,119] A steep increase of order indicates the structural transition. Finally, we utilize the geometrical coordination number metric z (Fig. 1.4d),[75] also employed and investigated in several publications.[108,110,120] To estimate the number of geometrical contacts in a packing we contract the packing uniformly with a linear strain rate equal to 10^{-3} and count particle intersections introduced during contraction. For the coordination numbers the structural transition should be tracked from the start of the plateau, when z approaches 6 (the coordination number for isostatic packings of frictionless particles), which indicates the frictionless jamming transition.

All of the complementary measures (Fig. 1.4) demonstrate good coincidence with the results from the original papers and also expose the structural transition at critical packing densities of $\varphi_C = 0.647 - 0.651$, with the exact value depending on the actual measure, the packing type, and some uncertainty resulting from noise.

We point out a very similar behavior of all the entropy-like measures: of pore-size entropy in Fig. 1.3, of the Voronoi volumes standard deviation in Fig. 1.4a, and of the Voronoi volumes entropy in Fig. 1.4b. The measures decrease as φ is increased up to φ_C, increase in the coexistence region, and thereafter start decreasing again. The reasons for this behavior were analyzed above for the pore-size entropy. The similarity between pore-size entropy and the Voronoi volumes entropy may explain the interdependence between the Voronoi volumes' distribution shape parameter "k" and the pore-size distribution's standard deviation.[88]

The different packing types we used (LS, JT, and force-biased algorithms) demonstrate significantly different values for most of the measures below φ_C (Fig. 1.3 and Fig. 1.4). All entropy-like measures and the local bond-orientational order measure show that LS packings are the most disordered ones among the studied packing types (*i.e.*, the entropies and Voronoi volumes standard deviations are the highest; local bond-orientational order is the lowest); JT packings are the least disordered packings, and FBA packings have intermediate disorder. It means that the different packing generation protocols result in different microstructures. This is very important, because the packing microstructure affects flow and mass transport in the packings, as visualized in the effective diffusivity (or diffusive tortuosity) and hydrodynamic dispersion, as well as the elastic (and other bulk) properties of the packings.[6,88,89,117,121–125] Moreover, the differences in the pore-size entropy values for monodisperse packings at identical packing density demonstrate that the pore-size distribution depends on packing microstructure (thus, on packing generation protocol) and cannot be approximated with a function that depends only on packing density, *e.g.*, using Carnahan–Starling or Percus–Yevick equations of state.[83–85]

[119] K. Lochmann, L. Oger, and D. Stoyan. *Solid State Sci.*, 8, 1397–1413, 2006.
[120] G. W. Delaney, T. D. Matteo, and T. Aste. *Soft Matter*, 6, 2992–3006, 2010.
[6] S. Khirevich, A. Höltzel, and U. Tallarek. *Commun. Comput. Phys.*, 13, 801–822, 2013.
[121] S. Khirevich et al. *J. Chromatogr. A*, 1218, 6489–6497, 2011.
[122] D. Hlushkou et al. *Anal. Chem.*, 79, 113–121, 2007.
[123] A. Daneyko et al. *J. Chromatogr. A*, 1218, 8231–8248, 2011.
[124] V. Buryachenko et al. *Int. J. Solids Struct.*, 40, 47–72, 2003.
[125] S. Khirevich et al. *J. Chromatogr. A*, 1262, 77–91, 2012.

Another remarkable feature of these sphere packings, which were generated with different packing protocols, is the similarity of measure values at densities above φ_C (Fig. 1.3 and Fig. 1.4). This supports the idea that the behavior of the packing properties becomes indistinguishable at this critical density and beyond.[35] Unsurprisingly, the origin of a packing regarding its generation protocol ultimately disappears.

The differences in pore-size entropy observed for the different packing types at identical packing densities below φ_C in Fig. 1.3 can be explained in terms of the geometrical coordination number. The slope of the density-entropy plot indicates the depletion rate at increasing packing density of the phase space volume available for the packings. The more near-neighbors the particles have in a packing, the more restrictions on the particle movement are imposed, and the less possibilities exist for contracting the packing of a given density to reach a slightly higher density, *i.e.*, the less phase space paths emanate from the current packing hyperstate in the phase space. Thus, packings with higher geometrical coordination number should exhibit a more negative slope of their density-entropy plot. As far as the pore-size entropy plots converge to the same value at φ_C for all packing types in Fig. 1.3, we conclude that packings with higher geometrical coordination number should have higher entropy values (and any other disorder measures) for densities below φ_C. This behavior is indeed reported for Fig. 1.3 and Fig. 1.4.

An important consequence of the applicability of the pore-size entropy is the justification of the slicing assumption explained in Section 1.3. As long as the pore-size distribution approach reproduces the expected entropy behavior, we may conclude that each packing of N particles represents a slice in the phase space of the $N + 1$ particles, and the available states density of this slice is equal to the available states density of the whole packing phase space (Eq. (1.3)).

Of course, sphere packings in the entire range of densities can also be constructed from a perfectly crystalline configuration just by an appropriate decrease of the particle diameter. In this case, pore-size entropy will be monotonically decreasing. The observed non-monotonic behavior in Fig. 1.3 is explained in the following way: Up to φ_C the phase space is dominated by the basins of attraction of random configurations and any algorithm, starting its operation from a random particle distribution, will hardly encounter an ordered packing. Above φ_C, the coexistence region starts and the basins of attraction of crystalline configurations occupy a significant amount of the phase space (compared to the random configurations). As a consequence, sufficiently large packings will be composed of both ordered and disordered subregions, representing the coexistence phenomenon. The calculated total entropy value will be comprised of entropies from ordered and disordered regions weighted by their relative volumes.[126]

One can consider an entire packing as a large number of smaller sub-packings, each of them probing a phase space with lower dimensionality. We can roughly estimate the number of independent smaller packings in a large one by employing a pair-correlation function.[2,75,127] If we assume that the correlations disappear at a distance of three particle diameters, the volume of an independent sub-packing is $4/3 \cdot \pi \cdot (6r_0)^3$. The total volume of a packing of 10000 particles

[126] C. Radin. *J. Stat. Phys.*, 131, 567–573, 2008.
[127] T. Aste, M. Saadatfar, and T. J. Senden. *Phys. Rev. E*, 71, 061302, 2005.

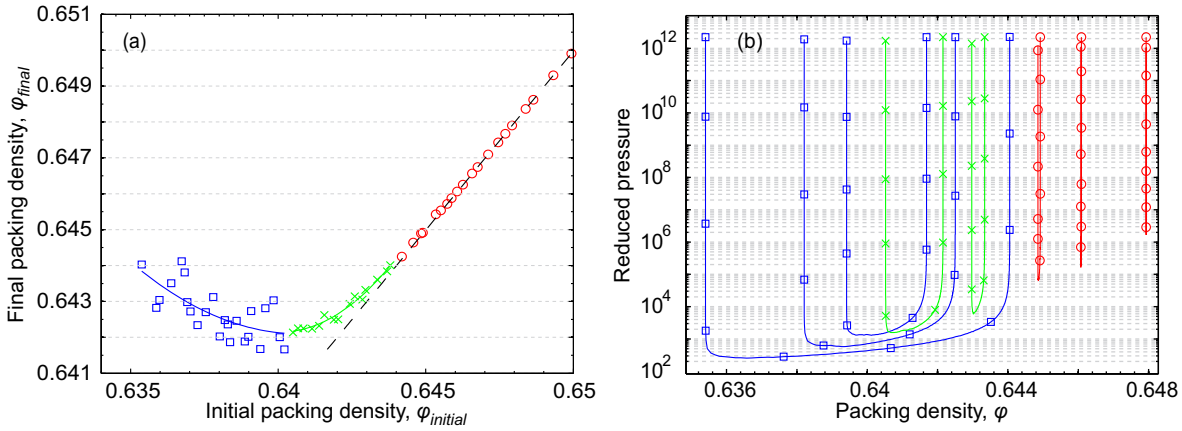

Figure 1.5: Lubachevsky–Stillinger algorithm applied with slow compression to packings initially generated with the same algorithm, but under faster compressions. (a) Final *vs.* initial packing densities: unjammed packings below the RCP limit (blue squares), jammed packings above the RCP limit (red circles), and intermediate regime (green crosses); $\varphi_{\text{final}} = \varphi_{\text{initial}}$ reference line (dashed black line). Solid lines are least-square quadratic fits for data of corresponding color. (b) Pressure *vs.* packing density for selected packings in the course of slow compression with the Lubachevsky–Stillinger algorithm. Colors and symbols correspond to panel (a).

with $\varphi = 0.64$ is $10000 \cdot 4/3 \cdot \pi \cdot r_0^3/0.64$. Therefore, the number of independent sub-packings is 72, which provides a sufficient statistics for probing both crystalline and random phase space regions.

1.4.3 Random-close packing limit

It is tempting to attribute the critical density $\varphi_C = 0.647 - 0.651$ to the RCP limit, as the pore-size entropy has a profound minimum in this interval, indicating a minimal amount of available states (Fig. 1.3). Yet, these densities differ somewhat from the generally accepted RCP limit $\varphi_{\text{RCP}} \approx 0.64$ obtained in experiments and by direct generation of jammed configurations,[1,10–12,75,100–102] but they are close to the claimed RCP limit $\varphi = 0.646 - 0.65$ detected by structural changes in packings (*e.g.*, as analyzed from the local entropy minimum or onset of crystallization),[13,21–25] which is also supported theoretically.[128] The density for mechanically stable packings of almost frictionless particles in Briscoe *et al.*[76] (*cf.* Fig. 1.2 in that paper) is also larger than $\varphi_{\text{RCP}} \approx 0.64$ and actually equal to 0.645. However, it may happen that a structural transition in a packing, *e.g.*, as indicated by the local entropy minimum in Fig. 1.3, reflects a phenomenon that is unrelated to the RCP limit and occurs at a density slightly above φ_{RCP}.[13]

In pursuit of a better understanding of these observations we examine the LS packings under fast compressions. It is argued that monosized packings in the course of fast compressions (or fast quenching in energy minimization protocols) should avoid crystallization and jam at φ_{RCP}.[12] Still, LS packings seem to jam in a wide range of densities even for fast compressions.[49] Another problem with jamming of LS packings is that these packings at low densities have coordination numbers as low as 4, meaning that they are not yet jammed (*cf.* Fig. 1.4d), though Salsburg and

[128] T. Aste and A. Coniglio. *EPL*, 67, 165–171, 2004.

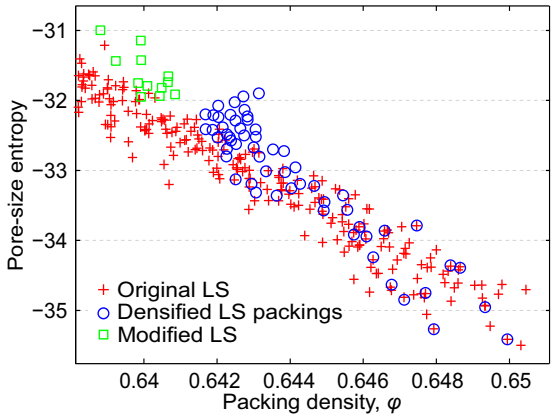

Figure 1.6: Pore-size entropy *vs.* packing density for three types of Lubachevsky–Stillinger (LS) packings: original data from Fig. 1.3 (+); packings densified with slow compression (◯); and packings used to estimate the RCP limit with the modified LS algorithm (□).

Wood[9] showed analytically that isostaticity of a subset of particles in a packing (excluding rattler particles) is a necessary condition for infinite pressure. To address these points we follow the idea of Skoge *et al.*[49] and additionally densify packings obtained with the LS protocol in a density range $\varphi_{\text{initial}} = 0.635 - 0.65$ (compression rates span from 1.2×10^{-2} to 2.5×10^{-4}, respectively). The densification is accomplished by applying the LS protocol to these packings again, but now with a low compression rate (10^{-5}), which would lead to crystalline configurations if used from the very beginning of the packing generation. The dependence of the final packing densities on the initial ones is shown in Fig. 1.5a (different symbols represent different regimes discussed below). It demonstrates that packings with $\varphi_{\text{initial}} < 0.64$ (below the usually accepted RCP limit) can be compressed further to reach densities in the interval $\varphi_{\text{final}} = 0.641 - 0.644$, which is indeed very close to φ_{RCP}.

To understand the densification process better, we plot the reduced pressure in several packings in the course of the slow compression in Fig. 1.5b. All the lines should be tracked from left to right, and the leftmost point of each line represents the initial density and pressure. We notice that the pressure rapidly drops in all cases, then recovers and finally reaches the termination value (10^{12}) again. The pressure drop happens due to the packing equilibration during slow compression, meaning that packing structures after fast compressions are out of equilibrium. During equilibration particles collide and fill the packing space more evenly to increase the average cage size per particle and reduce the number of collisions per unit time. The slower the compression during the generation of the initial LS packings (and the higher φ_{initial}), the smaller is the pressure drop, because slower compressions produce better equilibrated packings.

The presented picture resolves an apparent controversy with the LS algorithm: a necessary and sufficient condition for infinite pressure in hard-sphere packings is isostaticity,[9] though for low densities the LS packings expose coordination numbers as low as 4 and still possess very high pressure at the algorithm termination (Fig. 1.4d). We have shown in Fig. 1.5b that this pressure

represents non-equilibrium and should not be used either for the tracking of jamming or for the estimation of jamming densities, as done in several papers.[49,77,129] Instead, the packings should be preliminary equilibrated at zero (or a very low) compression rate. We also verified that the average number of contacts per sphere computed at a strain rate of 10^{-4} is $5.9 < z < 6$ for all the densified packings, if rattler particles with less than four contacts were recursively removed. The pressure drop also explains the ability to further compress packings with $\varphi_{\text{initial}} < 0.64$, which initially seemed to be jammed and kinetically arrested.

We notice that the lower φ_{initial} (if it is below 0.6405), the higher φ_{final}, *i.e.*, the blue-squares data in Fig. 1.5a have a negative slope (the least-squares quadratic fit is shown as a solid blue line). The blue-colored pressure plots shown in Fig. 1.5b also demonstrate this tendency. It can easily be explained assuming that trapping of a packing in the least dense glassy states (φ_d in the review by Parisi and Zamponi,[2] Fig. 4) happens at a density of $\varphi \approx 0.64$. Packings that start the slow compression at lower densities have more time for structural rearrangement (before they reach φ_d) and can longer avoid trapping in the glassy states above φ_d.

Data in Fig. 1.5a for $\varphi_{\text{initial}} \geq 0.644$ (red circles) almost coincide with the $\varphi_{\text{final}} = \varphi_{\text{initial}}$ reference (dashed black line). It means that packings are already kinetically arrested in glassy states, though pressure drops still take place due to non-equilibrium structure of the packings (red lines in Fig. 1.5b). We also verified that the lowest pressure value for quasistatic compressions of all packings in Fig. 1.5 is equal to the stationary reduced pressure. To determine the latter, we equilibrated packings by performing sets of 2×10^4 collisions with zero compression rate in a loop until the relative difference of reduced pressures in the last two sets is less than 10^{-4}. Therefore, packings with $\varphi_{\text{initial}} \geq 0.644$ are nearly jammed also by pressure criteria (as we mentioned, according to Salsburg and Wood[9] packings close to jamming should exhibit very high stationary reduced pressure; the lowest pressure for $\varphi_{\text{initial}} \geq 0.644$ in Fig. 1.5 is larger than 10^4, which we consider as sufficiently high). The proximity to jamming can be verified by the equation of state for hard spheres of Salsburg and Wood,[9] $p = d/(1 - \varphi/\varphi_J)$, where p is stationary reduced pressure, φ is the current packing density, φ_J is the closest jamming density achievable from the given packing configuration (which we would like to estimate), and d is the dimensionality of the system. We obtain $\varphi_J = \varphi/(1 - d/p) \approx \varphi(1 + d/p)$. φ_J for $\varphi_{\text{initial}} = 0.644$ is ~ 0.6442. We note that the method for testing mechanical stability by pressure is equivalent to the dynamical matrix test[102] or linear programming methods[31] due to the results of Salsburg and Wood.[9] The benefit of the pressure test is in our ability to explicitly estimate the quality of the threshold by assessing the difference between expected jamming densities and actual densities of the packings we consider as jammed (through the equation of state by a given threshold, as just done for $\varphi = 0.644$).

The remaining part of the plot in Fig. 1.5a (green crosses) lies in the density range $[0.6405, 0.644)$. This plot does not coincide with the $\varphi_{\text{final}} = \varphi_{\text{initial}}$ line (packings are not yet kinetically arrested), but has a positive slope smaller than unity (the least-squares quadratic fit is depicted by a solid green line). The lower φ_{initial}, the larger the difference between φ_{final} and φ_{initial} (see

[129] M. Hermes and M. Dijkstra. *EPL*, 89, 38005, 2010.

also the green lines in Fig. 1.5b). At least one of the following two scenarios is possible, or both are taking place: (i) The packings are initially trapped in glassy states and slightly rearrange due to equilibration to fill the space more evenly, which provides opportunities for a further densification and kinetic arrest; and (ii) packings do not initially reside in glassy states and become trapped in the course of the densification. Packings of higher φ_{initial} are trapped earlier, which may happen because the higher the density, the closer is the packing structure to glassy states, and the density of glassy states in the phase space increases with the packing density. To determine the actual scenario it is necessary to compare the packing structures before and after densification by, *e.g.*, Delaunay network graph isomorphism[76] or the distance between packing configurations in the phase space (normalized to a single density). However, this is beyond the scope of the present paper.

Our analysis suggests that φ_d as well as φ_{RCP} (infinite-pressure limit of φ_d) are close to 0.64. The problem with the traditional LS algorithm is that fast compressions terminate too early due to the non-equilibrium pressure excess and slow compressions are able to reach densities above the RCP limit due to crystallization. To improve our φ_{RCP} estimate, we modified the LS generation procedure and after each 2×10^4 collisions with compression we completely equilibrate the packings. The equilibration is done by performing sets of 2×10^4 collisions with zero compression rate in a loop until the relative difference of reduced pressures in the last two sets is less than 1%, so the pressure is stationary. When a packing is equilibrated we perform collisions with compression again. We terminate the generation process when the stationary reduced pressure is high enough (10^{12}).

Two sets of data were generated with this modification: Six packings with a compression rate of 0.04 and six packings with a compression rate of 0.1; previously generated LS packings in the density range $\varphi = 0.62 - 0.623$ were used as starting configurations. All of the packings jam in the density range $\varphi = 0.639 - 0.641$ and are indeed nearly isostatic (*i.e.*, the average number of contacts per sphere computed at a strain rate of 10^{-4} is $5.98 < z < 6$, if rattler particles with less than four contacts are recursively removed). This clearly corresponds to the usually accepted estimate of the RCP limit and is also consistent with our previous discussion. The RCP limit estimates for the two data sets with 5% confidence intervals are respectively $\varphi_{\text{RCP}} = 0.6401 \pm 0.0008$ and $\varphi_{\text{RCP}} = 0.64 \pm 0.0005$. Both data sets are found to belong to the same distribution and we estimate the RCP limit by the combined data as $\varphi_{\text{RCP}} = 0.6401 \pm 0.0004$. We are not aware of such a precise RCP limit estimation for the LS protocol. Our approach also benefits greatly from the ability to recover both characteristic densities (~ 0.64 and ~ 0.65) for the same protocol (Lubachevsky–Stillinger), which has not yet been done, to our knowledge. We conjecture, that in the thermodynamic limit any single packing generation with the modified LS algorithm will terminate at φ_{RCP}.[12] We have also already shown an explicit way to produce jammed packings above φ_{RCP} (though the LS algorithm by itself produces jammed packings only for $\varphi \geq 0.644$): one needs to further densify packings of lower densities by slow compression (as in Fig. 1.5).

To complete the discussion of these additionally generated packings, we plot pore-size

entropy *vs.* packing density in Fig. 1.6 for LS packings densified with the slow compression ("Densified LS packings", see also Fig. 1.5), as well as for the packings used to estimate the RCP limit by employing the modified LS algorithm ("Modified LS"). We also depict entropies for the packings from the original LS algorithm (see Fig. 1.3) for a better interpretation. Unsurprisingly, densified packings for $\varphi \geq 0.644$ (*cf.* red circles in Fig. 1.5) have their entropy unchanged in comparison to the original LS packings, as their density and structure are retained. Densified packings with final density below 0.644 (blue squares and green crosses in Fig. 1.5) and packings from the modified algorithm have entropies slightly above those for the original LS packings (Fig. 1.6). This agrees with our prediction from Section 1.4.2, where it was stated that "packings with higher geometrical coordination number should have higher entropy values for densities below φ_C". Indeed, the densified LS packings and modified LS packings are truly isostatic, whereas the original LS packings with $\varphi < 0.644$ are not isostatic.

The results in Fig. 1.6 also show that the RCP limit conforms to the "maximally random jammed state" definition.[14] Indeed, random packings (*i.e.*, without crystalline regions) have densities below $\varphi_C \approx 0.65$, and random jammed packings occupy the density range from φ_{RCP} to φ_C. The maximally random state of these random jammed states has a density $\varphi_{\text{RCP}} \approx 0.64$, because entropy decreases in this density range, as depicted in Fig. 1.6. Therefore, the definition of the RCP limit we use in this paper is equivalent to the maximally random jammed state definition.

1.4.4 Structural transition

We conclude that the critical density of the structural transition $\varphi_C = 0.647 - 0.651$, as determined by the pore-size entropy (Fig. 1.3) and the complementary measures (Fig. 1.4), does not represent the density of the RCP limit defined *via* the infinite-pressure limit of the least dense glassy states.[2]

We conjecture that $\varphi_C = 0.647 - 0.651$ represents φ_{GCP},[2] the infinite-pressure limit of the densest glassy state (the ideal glass state). This last glassy state itself is encountered at finite pressure at the Kauzmann density φ_K, which is lower than φ_{GCP}.

On the other hand, it is believed that configurational entropy for jammed packings becomes zero at φ_{GCP}, whereas pore-size entropy should tend to minus infinity (when p_{avail} in Eq. (1.2) tends to zero). For LS packings (as the most jammed of all the studied packing types, Fig. 1.4d) the pore-size entropy plot in Fig. 1.3 and the Voronoi volumes entropy plot in Fig. 1.4b can be extrapolated at φ_C (toward higher density) to minus-infinity and zero, respectively, which leads to $\varphi_{\text{GCP}} \approx 0.66$ (it is also called a Kauzmann density in the original paper for the Voronoi volumes entropy[22]).

Therefore, the above conjecture $\varphi_C = \varphi_{\text{GCP}}$ has the following inconsistencies: (i) both entropies (pore-size entropy and Voronoi volumes entropy) do not reach the expected minimum values at φ_C, they can only be inferred by extrapolation; (ii) replica theory estimates φ_K at 0.62 and φ_{GCP} at 0.68.[2] Still, replica theory may be imprecise and there is an analytical theory

which predicts the configurational entropy to disappear at $\varphi = 0.65$ (*cf.* Fig. 1.2 in Aste and Coniglio[128]). Further, finite-size effects are believed to shift φ_K and φ_{GCP} to lower values. Finally, too high entropy values at $\varphi_C = \varphi_{\text{GCP}}$ in Fig. 1.3 and Fig. 1.4b can be justified with the following arguments: (i) the entropies also account for unjammed packings with the same density; (ii) rattler particles and their flexibility in position also contribute to the entropies; and (iii) both entropies involve some approximations, which may lead to overestimated entropy values.

Another possibility is that the density φ_C simply represents the last achievable jammed state, after which crystalline regions are unavoidable, but φ_{GCP} is still not reached. The location of φ_K is also arguable; it may be at $\varphi = 0.66$ as well. We reject this conjecture ($\varphi_C < \varphi_{\text{GCP}}$) by the following arguments: (i) we once again refer to the analytical prediction for the configurational entropy to vanish at $\varphi = 0.65$;[128] (ii) the density $\varphi_C \approx 0.65$, which we obtained by different measures for different packing protocols (Fig. 1.3 and Fig. 1.4), has a universal character; and (iii) $\varphi_C \approx 0.65$ fits very well into the plot for maximal packing densities of polydisperse particles in Hermes and Dijkstra[129] (their Fig. 1.4b, compression rate 10^{-5}). It means that crystalline configurations are not only more probable for $\varphi > 0.65$, but that amorphous jammed states cannot be reached for higher φ (even if we could suppress crystallization). Therefore, we conjecture that $\varphi_C = 0.647 - 0.651$ represents φ_{GCP}, the infinite-pressure limit of the densest glassy state (the ideal glass state).

1.5 Summary and conclusions

We have introduced and analyzed a pore-size entropy measure for random packings of hard spheres. It reproduces the structural transition of monodisperse sphere packings, has a clear physical background, is numerically efficient, does not require *a priori* parameters, *e.g.*, a characteristic length, and can easily be applied also to polydisperse sphere packings. In addition, this measure provides important insight into the pore-size distribution of the packings; specifically, the logarithm of its tail area is equal to the packing entropy.

The applied pore-size entropy measure indicates a structural transition of monodisperse packings of frictionless spheres at a critical density $\varphi_C \approx 0.65$, corresponding to a minimal number of available packing states, *i.e.*, to the local entropy minimum. This minimum is followed by an entropy increase in the coexistence region up to $\varphi \approx 0.68$; above this packing density entropy starts decreasing again.

We amended the Lubachevsky–Stillinger packing generation protocol to systematically reproduce the RCP limit at $\varphi_{\text{RCP}} \approx 0.64$ for fast compressions. We are not aware of reports that recover both characteristic densities (~ 0.64 and ~ 0.65) by using the same protocol. This result suggests that the structural transition at $\varphi_C \approx 0.65$ and the RCP limit at $\varphi_{\text{RCP}} \approx 0.64$ are unrelated phenomena and cannot be justified by a difference in preparation protocols. We explain this observation on the basis of a picture proposed in a review by Parisi and Zamponi.[2] While $\varphi_{\text{RCP}} \approx 0.64$ corresponds to the jammed configurations of the least dense glassy states (φ_{th} in this review), $\varphi_C \approx 0.65$ corresponds to the jammed configuration of the densest glassy state (φ_{GCP} in

this review).

The significantly different pore-size entropy plots at packing densities below the structural transition density observed for the different protocols (Lubachevsky–Stillinger, Jodrey–Tory, force-biased algorithms) prove that packing microstructure and pore-size distribution at a given φ depend intrinsically on the packing generation protocol. The pore-size entropy is a powerful measure to detect and quantify protocol-specific packing disorder, which is known to impact key bulk and transport properties of random sphere packings encountered in materials science and industrial engineering, *e.g.*, in the processing of ceramics or the operation of fixed-bed chemical reactors and chromatographic columns. In the future we will apply the presented approach to particle size distributions (and polydisperse packings) relevant to these applications.

Acknowledgements

This work was supported by the Deutsche Forschungsgemein-schaft DFG (Bonn, Germany) under grant TA 268/5-1. We are grateful to the John von Neumann Institute for Computing (NIC) and the Jülich Supercomputing Center (JSC) for the allocation of special CPU-time grants (NIC project numbers: 4717 and 5658, JSC project ID: HMR10). We also thank the reviewers for their extremely helpful and stimulating comments.

Chapter 2

Random-close packing limits for monodisperse and polydisperse hard spheres

Authors:

Vasili Baranau and Ulrich Tallarek*

State of publication:

Published on March 03, 2014 in Soft Matter, Vol. 10.21, pp 3826–3841
DOI: 10.1039/C3SM52959B

Abstract

We investigate how the densities of inherent structures, which we refer to as the closest jammed configurations, are distributed for packings of 10^4 frictionless hard spheres. A computational algorithm is introduced to generate closest jammed configurations and determine corresponding densities. Closest jamming densities for monodisperse packings generated with high compression rates using Lubachevsky–Stillinger and force-biased algorithms are distributed in a narrow density range from $\varphi = 0.634 - 0.636$ to $\varphi \approx 0.64$; closest jamming densities for monodisperse packings generated with low compression rates converge to $\varphi \approx 0.65$ and grow rapidly when crystallization starts with very low compression rates. We interpret $\varphi \approx 0.64$ as the random-close packing (RCP) limit and $\varphi \approx 0.65$ as a lower bound of the glass close packing (GCP) limit, whereas $\varphi = 0.634 - 0.636$ is attributed to another characteristic (lowest typical, LT) density φ_{LT}. The three characteristic densities φ_{LT}, φ_{RCP}, and φ_{GCP} are determined for polydisperse packings with log-normal sphere radii distributions.

2.1 Introduction

The definition and determination of the random-close packing (RCP) limit for frictionless hard-sphere particles is a long-standing problem. For monodisperse particles, there exist at least

three estimates for the RCP limit, with distinct densities φ: (i) $\varphi = 0.634 - 0.636$;[1,6,11,130] (ii) $\varphi \approx 0.64$;[10,12,75,131] and (iii) $\varphi \approx 0.65$.[13,21–26,128] The values of 0.634 and 0.65 are supported theoretically.[1,128] In our previous work[132] we showed that $\varphi \approx 0.64$ and $\varphi \approx 0.65$ refer to different phenomena and represent the RCP limit and a lower bound of the glass close packing (GCP) limit.[2]

The RCP limit is sometimes interpreted as a special density at which almost every Poisson packing will jam in the process of infinitely fast compressions and is also referred to as the J-point.[12] For finite packings, this point is expanded into a J-segment.[12,133] The behaviour of the J-segment in the thermodynamic limit is yet unresolved; it may converge to a single J-point[12] or preserve a finite width.[133] Here we do not investigate this issue, but study finite packings of 10^4 particles and observe indeed a finite width of the J-segment for our packings. We find that $\varphi = 0.634 - 0.636$ is the lower bound of this segment, whereas $\varphi_{\mathrm{RCP}} \approx 0.64$ is the upper bound. We also reproduce the density $\varphi_{\mathrm{GCP}} \approx 0.65$ in our simulations. In addition, we determine the RCP limits and lower bounds of the GCP limits for polydisperse packings.

By *jamming* we understand in this paper collective jamming in packings of frictionless particles,[3,14,30,31] equivalent to mechanical stability[1] and infinite pressure in systems of particles supplied with velocity.[9] The equivalence of isostaticity and jamming is supported experimen-

[1] C. Song, P. Wang, and H. A. Makse. *Nature*, 453, 629–632, 2008.
[6] S. Khirevich, A. Höltzel, and U. Tallarek. *Commun. Comput. Phys.*, 13, 801–822, 2013.
[11] G. D. Scott and D. M. Kilgour. *J. Phys. D: Appl. Phys.*, 2, 863–866, 1969.
[130] A. Zinchenko. *J. Comput. Phys.*, 114, 298–307, 1994.
[10] J. D. Bernal and J. Mason. *Nature*, 188, 910–911, 1960.
[12] C. S. O'Hern et al. *Phys. Rev. E*, 68, 011306, 2003.
[75] Y. Jin and H. A. Makse. *Physica A*, 389, 5362–5379, 2010.
[131] J. G. Berryman. *Phys. Rev. A*, 27, 1053–1061, 1983.
[13] S. C. Kapfer et al. *Phys. Rev. E*, 85, 030301, 2012.
[21] A. V. Anikeenko and N. N. Medvedev. *Phys. Rev. Lett.*, 98, 235504, 2007.
[22] A. V. Anikeenko, N. N. Medvedev, and T. Aste. *Phys. Rev. E*, 77, 031101, 2008.
[23] T. Aste and T. Di Matteo. *Eur. Phys. J. B*, 64, 511–517, 2008.
[24] B. A. Klumov, S. A. Khrapak, and G. E. Morfill. *Phys. Rev. B*, 83, 184105, 2011.
[25] M. Bargieł and E. M. Tory. *Adv. Powder Technol.*, 12, 533–557, 2001.
[26] K. Lochmann et al. *Eur. Phys. J. B*, 53, 67–76, 2006.
[128] T. Aste and A. Coniglio. *EPL*, 67, 165–171, 2004.
[132] V. Baranau et al. *Soft Matter*, 9, 3361–3372, 2013.
[2] G. Parisi and F. Zamponi. *Rev. Mod. Phys.*, 82, 789–845, 2010.
[133] M. Pica Ciamarra, M. Nicodemi, and A. Coniglio. *Soft Matter*, 6, 2871–2874, 2010.
[3] S. Torquato and F. H. Stillinger. *Rev. Mod. Phys.*, 82, 2633–2672, 2010.
[14] S. Torquato, T. M. Truskett, and P. G. Debenedetti. *Phys. Rev. Lett.*, 84, 2064–2067, 2000.
[30] A. Donev. *J. Appl. Phys.*, 95, 989–999, 2004.
[31] A. Donev et al. *J. Comput. Phys.*, 197, 139–166, 2004.
[9] Z. W. Salsburg and W. W. Wood. *J. Chem. Phys.*, 37, 798–804, 1962.

tally;[3,12,35,48,101,102,106–108,110] while Salsburg and Wood proved[9] that isostaticity is a necessary condition for infinite pressure and jamming. A packing is referred to as *jammed* if there is at least a subset of particles that is jammed (other particles are rattlers). We do not exclude rattler particles from the packings when computing packing densities.

For polydisperse packings the GCP limit φ_{GCP} is defined[2] as the infinite-pressure limit for the densest glassy state (the ideal glass state), whereas for monodisperse packings it is the density above the RCP limit with minimal number of jammed packing configurations (as revealed by an entropy minimum).[22,132] We will follow these definitions.

In our previous work[132] we noticed that the pressure reported during packing generation using the Lubachevsky–Stillinger (LS) algorithm is non-stationary, because any packing generation is a non-equilibrium process. Therefore, infinite non-equilibrium pressure cannot be used as indicator for jamming. Instead, the packings should be allowed to equilibrate. Indeed, monodisperse LS packings expose an average coordination number below the isostatic value of six for densities lower than 0.644 and can be densified further using low compression rates.[132]

Research has been conducted recently to describe the pressure relaxation process for monodisperse and polydisperse packings.[134] It also shows that LS packings are not always jammed despite very high non-equilibrium pressure. We have suggested[132] that stationary pressure after relaxation may be substituted into the equation of state (EOS) of Salsburg and Wood[9] to estimate the jamming densities. Some results[134] show that the process of pressure relaxation has time scales comparable with the process of macroscopic packing rearrangement. In a certain interval of densities the particles start to form crystalline regions and the estimated jamming density for these packings may be as high as the crystalline packing density (φ_{FCC} or φ_{HCP}) for monodisperse packings, or as high as the GCP limit φ_{GCP} for polydisperse packings.[33] Thus, these density estimates do not represent the jamming densities closest to the initial packing configurations and will not assist us in defining the RCP limit φ_{RCP}. Here, we modified the LS packing generation algorithm to search for the jammed packing configurations closest to the initial ones (instead of simply estimating their densities by equilibration) and will base our definition of the RCP limit on the results produced with this modification.

The paper is structured as follows. Before we present any experimental results, we use Section 2.2 to start with definitions that become relevant for our subsequent discussion. These are *inherent structure*;[39] *basin of attraction* of an inherent structure, *bounding region, bounding surface,*

[35] P. Chaudhuri, L. Berthier, and S. Sastry. *Phys. Rev. Lett.*, 104, 165701, 2010.
[48] P. Wang et al. *Physica A*, 390, 427–455, 2011.
[101] C. S. O'Hern et al. *Phys. Rev. Lett.*, 88, 075507, 2002.
[102] N. Xu, J. Blawzdziewicz, and C. S. O'Hern. *Phys. Rev. E*, 71, 061306, 2005.
[106] N. Xu and E. S. C. Ching. *Soft Matter*, 6, 2944–2948, 2010.
[107] H. A. Makse, D. L. Johnson, and L. M. Schwartz. *Phys. Rev. Lett.*, 84, 4160–4163, 2000.
[108] P. Wang et al. *J. Stat. Mech.*, P12005, 2010.
[110] A. Donev, S. Torquato, and F. H. Stillinger. *Phys. Rev. E*, 71, 011105, 2005.
[134] M. C. Vargas and G. Pérez-Ángel. *Phys. Rev. E*, 87, 042313, 2013.
[33] E. Zaccarelli et al. *Phys. Rev. Lett.*, 103, 135704, 2009.
[39] F. H. Stillinger. *Science*, 267, 1935–1939, 1995.

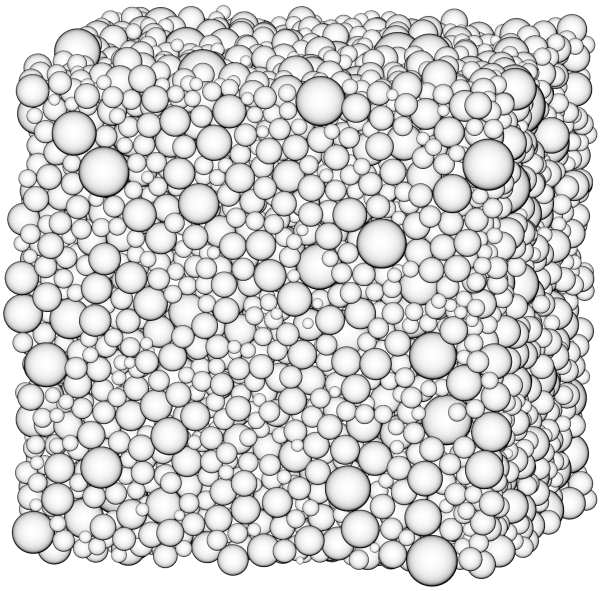

Figure 2.1: Closest jammed configuration at a density $\varphi = 0.662$ for a random packing of 10000 polydisperse spheres. The sphere radii distribution is log-normal and has a relative standard deviation $\sigma = 0.3$. The initial unjammed packing was generated with the force-biased algorithm at a density $\varphi = 0.613$.

and *closed bounding region*. We will show that an inherent structure for an arbitrary configuration of hard spheres is a jammed configuration that is the closest one to the initial configuration. To emphasize that we are investigating hard particles, not particles with soft potential, we will use throughout this paper the term "*closest jammed configuration*" instead of "inherent structure" and also refer to the "*closest jamming density*" instead of the "density of the inherent structure". In Section 2.3 we describe the modification of the LS packing generation algorithm to produce the closest jammed configurations. The subsequent application of this modification to monodisperse and polydisperse packings produced with the LS algorithm[95,135] and force-biased (FB) algorithm[98,99] is presented in Section 2.4. It reveals that the closest jamming densities for our finite packings produced with fast compressions are located in narrow density bands depending on the particle size distribution, from $\varphi = 0.634 - 0.636$ to $\varphi \approx 0.64$ for monodisperse packings. We attribute $\varphi \approx 0.64$ to the RCP limit φ_{RCP} and interpret $\varphi = 0.634 - 0.636$ as well as similar densities for polydisperse packings as another characteristic density φ_{LT}, the lowest typical (LT) jamming density. The definitions of φ_{RCP} and φ_{LT} are also provided. In addition, we estimate lower bounds of the GCP limits from the results in Section 2.4 by extrapolating packing densities to infinite generation time. We furthermore demonstrate how these three characteristic densities φ_{LT}, φ_{RCP}, and φ_{GCP} depend on the polydispersity for finite hard-sphere packings. Section 2.5 presents a summary and conclusions.

[95] B. D. Lubachevsky and F. H. Stillinger. *J. Stat. Phys.*, 60, 561–583, 1990.
[135] B. D. Lubachevsky. *J. Comput. Phys.*, 94, 255–283, 1991.
[98] J. Mościński et al. *Mol. Simul.*, 3, 201–212, 1989.
[99] A. Bezrukov, M. Bargieł, and D. Stoyan. *Part. Part. Syst. Char.*, 19, 111–118, 2002.

Table 2.1: Important symbols used in this chapter.

Symbol	Short description	Key figures and tables	Values for $\sigma = 0$
σ	Relative standard deviation (polydispersity) of the log-normal particle radii distributions		
γ	Compression rate for initial packing generation	X-axis in Fig. 2.2	
φ	Initial packing density after LS or FB generation	Y-axis in Fig. 2.2a and Fig. 2.2c	
φ_J	Closest jamming density of a packing	Y-axis in Fig. 2.2b and Fig. 2.2d	
$\varphi_{\text{min}}^{\text{fast}}$	Minimum closest jamming density for packings produced with fast compressions	Fig. 2.4; Table 2.3	~ 0.635 (for packings in this study)
$\varphi_{\text{max}}^{\text{fast}}$	Maximum closest jamming density for packings produced with fast compressions	Fig. 2.4; Table 2.3	~ 0.64
φ_{LT}	Lowest typical jamming density or its estimate, $\varphi_{\text{LT}} = \varphi_{\text{min}}^{\text{fast}}$	Fig. 2.5; Table 2.4	~ 0.635 (for packings in this study)
φ_{RCP}	Random-close packing limit or its estimate, $\varphi_{\text{RCP}} = \varphi_{\text{max}}^{\text{fast}}$	Left sides of Fig. 2.2b and Fig. 2.2d; Fig. 2.5; Table 2.4	~ 0.64
φ_{GCP}	Glass close packing limit or its estimate	Right sides of Fig. 2.2; Fig. 2.5; Table 2.2 and Table 2.4	~ 0.65
φ_{HCP}	Crystalline packing density for monodisperse packings (FCC or HCP crystals)		~ 0.74
φ_{max}	Highest packing density: φ_{HCP} for monodisperse packings, φ_{GCP} for sufficiently polydisperse packings		~ 0.74
φ_L	Lowest possible jamming density, at least $2/3 \cdot \varphi_{\text{HCP}}$ for monodisperse packings (density of tunnelled crystals[137])		~ 0.49

The particles in our polydisperse packings have log-normal radii distributions with relative standard deviations (polydispersities) σ from 0.05 to 0.3 in steps of 0.05 (particle mean diameter is normalized to unity). All sphere packings were prepared in a fully periodic cubic box (*cf.* Fig. 2.1) and consist of 10^4 particles. Polydisperse packings are generated in a wide range of compression rates using the LS and FB protocols. Each packing is created from an individual Poisson configuration of points (independent random uniform selection of sphere centre coordinates). The applied source code is available under the MIT free software license.[136]

We rely on the phase space packing description[9] and use the terms “limiting polytope”, “hypersurface”, and “hypercylinder” from that paper.

2.2 Definitions

In this section we present definitions that will be needed for our discussion of hard-sphere packing problems.

Each sphere packing configuration of N monodisperse or polydisperse particles (with predefined nominal radii) can be represented as a point in a $3N$-dimensional packing phase space (3 coordinates per particle center). For the packing box sides $L_x L_y L_z$, respectively, the total phase space volume equals $V_{\text{tot}} = (L_x L_y L_z)^N$. The actual particle radii are proportional to the nominal ones and thus are determined only by the proportionality ratio or by the actual packing density.

In our discussion we will rely on the concept of *inherent structures*. Stillinger introduced it for systems of particles with soft potential.[39] The earliest description of this concept can be found

[136] V. Baranau https://code.google.com/p/packing-generation/

in Stillinger *et al.*[60] (Eq. (23), Section IV in that paper), though this term is actually not used. A qualitative description is also given in Torquato and Jiao[54] (Section IV B in that paper). Inherent structures for systems of particles with soft potential are local potential energy minima in the phase space. The minimum that is reached by a steepest descent energy minimization for an arbitrary system configuration is an inherent structure for this configuration. Potential energy in hard-sphere packings is replaced by the maximum packing density that can be associated with this configuration (*i.e.*, when there are still no intersecting particles), taken with the minus sign.

Inherent structures for hard-sphere packings correspond to jammed configurations. Indeed, if a packing resides in an inherent structure, there are no infinitesimal changes in the configuration that will allow preserving the density; instead, any change will always require decreasing the particle radii (decreasing the density, increasing the energy). Thus, the packing configuration resides in an infinitesimal limiting polytope and is jammed. Because such an inherent structure is reached from an initial configuration through a steepest descent, it is the closest one to the initial configuration.

To emphasize that we are investigating hard particles, not particles with soft potential, we will use throughout this paper the term "*closest jammed configuration*" instead of "inherent structure". We are unaware of precise mathematical definitions of the closest jammed configuration, especially of those accounting for rattler particles, so we provide a mathematical definition in the Appendix (Section 2.6.3). We will not use precise definitions to implement searching for the closest jammed configurations. Instead, we modify the LS algorithm in Section 2.3. The closest jammed configuration is defined uniquely for any unjammed packing configuration, except for saddle points in the potential energy landscape. The precise definition in Section 2.6.3 of the Appendix defines the closest jammed configuration uniquely even for saddle points.

An initial packing configuration belongs to a *basin of attraction* of a given jammed configuration if this jammed configuration is the *closest* one for the initial packing. Any phase space point belongs to one and only one basin of attraction, because the closest jammed configuration is defined uniquely for any configuration.

Similarly, let us define a *bounding region* of a given jammed configuration at a given density as the intersection of this configuration's basin of attraction with available phase space (contact hypercylinders for that density excluded). All available phase space is uniquely split into bounding regions. When the particle radii are large enough, bounding regions become closed and are then transformed into limiting polytopes.

We can also define *bounding surfaces*, *i.e.*, the surfaces of these bounding regions (comprised of hypercylinder surfaces and "wormholes" between bounding regions). The bounding region is *closed* if the bounding surface is fully formed by hypercylinder surfaces. Any configuration in a closed bounding region is called a *glassy state*.[2] The *glass transition* occurs when the bounding region becomes closed.

[60] F. H. Stillinger, E. A. DiMarzio, and R. L. Kornegay. *J. Chem. Phys.*, 40, 1564–1576, 1964.
[54] S. Torquato and Y. Jiao. *Phys. Rev. E*, 82, 061302, 2010.

The definitions from this section together with the pressure criterion for jamming[9] allow us to transform the conventional definition of the GCP limit for polydisperse particles[2] ("the infinite-pressure limit for the densest glassy state") into a "jammed configuration with the highest density". Precise definitions for these concepts can also be found in Section 2.6.4 of the Appendix.

2.3 Algorithm used to search for the closest jammed configurations

In this section, we present a modification to the LS packing generation algorithm. This modified LS (MLS) algorithm was used to search for the closest jamming densities.

2.3.1 General idea

The LS algorithm in its conventional form cannot be used to search for the closest jammed configurations. This algorithm terminates too early for fast compressions because of the non-equilibrium pressure excess. Limiting polytopes have not yet collapsed into single points. If we apply slow compressions to unjammed packings, they will terminate in almost jammed configurations, but the latter will not correspond to the initial bounding regions and will have higher densities than the closest jammed configurations.[132]

Therefore, one way of searching for the closest jammed configuration is to use fast compressions at the beginning of the packing generation (to preserve the configuration point in an initial bounding region) and to use slow compressions at the end of the generation (to arrive at a truly jammed configuration). In order to merge these two regimes, we should gradually reduce the compression rate during the packing generation. We run the LS packing generation with a high compression rate, until the non-equilibrium reduced pressure is high (reaches a conventional value of 10^{12}), then decrease the compression rate and run the LS generation again, until the pressure is high enough again, and repeat this procedure until the compression rate is low enough. High compression rates at the initial stages will lead to a very fast movement of the bounding surfaces and to the closing of most of the wormholes between the bounding regions. Low compression rates at the end of the generation will ensure that the pressure is almost stationary, and the high pressure is a sign of the proximity to jamming. Slow compressions will also allow the configuration point to explore the bounding region and to exit the dead ends formed by concave boundaries and follow the movement of the bounding surfaces.

2.3.2 Details of the modified Lubachevsky–Stillinger (MLS) algorithm

We use the following packing generation parameters: the root mean square particle velocity is $\sqrt{3 \cdot 0.2}$, which corresponds to a packing temperature of 0.2, because we set the mass of all the particles and the Boltzmann constant to unity. The initial compression rate is 10, the termination compression rate is $\leq 10^{-4}$; we decrease the compression rate by a factor of two each time the reduced pressure (computed from 20 collisions per particle, 2×10^5 collisions for our packings comprised of 10^4 particles) reaches a value of 10^{12}. This factor of two is referred to

as the "compression rate decrease factor". To avoid the immediate termination of the packing generation after the compression rate is updated (as far as the reduced pressure remains high) we perform equilibration with zero compression rate until the reduced pressure is below 10^{12} (also computed from 2×10^5 collisions). If the reduced pressure is still above 10^{12} after 50 cycles of 2×10^5 collisions, we assume that the packing is close to jamming and terminate the generation completely. The procedure above always terminates in nearly jammed configurations. We refer to this modification as the MLS algorithm.

The code for this modification is available online.[136] The MLS algorithm is validated in Section 2.4.2, after we provide an overview of the results that we obtained by applying this algorithm with the current parameters (Section 2.4.1).

The idea of decreasing the compression rate has already been applied to the LS algorithm in order to produce nearly jammed configurations, as can be found in Torquato and Jiao[54] (Section V A), Skoge *et al.*[49] (Section II), Jiao *et al.*[138] (Section II A), and Biazzo *et al.*[20] These papers do not, in general, contain the requirement to start packing generation from fast compressions. To our knowledge, packing generation which starts from fast compressions has never been interpreted as searching for the closest jammed configuration.

2.4 Results and discussion

Here, we present our packing generation results and the results of searching for the closest jammed configurations of the generated packings. We estimate the GCP limits φ_{GCP} for monodisperse and polydisperse packings on the basis of their densities obtained after slow compressions. We analyze packing densities for fast compressions, define the RCP limits φ_{RCP} and the lowest typical (LT) jamming densities φ_{LT}, and determine these densities for monodisperse and polydisperse packings. We provide an overview of our data in Section 2.4.1. In Section 2.4.2 we validate the MLS algorithm; this validation relies on the data overview and therefore cannot be presented earlier. We analyze the data in Section 2.4.3. This analysis leads us to definitions of the RCP limits, which we introduce in Section 2.4.4. Section 2.4.5 presents concepts of typical and untypical basins of attraction, defined through the RCP limits. We discuss our results in Section 2.4.6. Our findings are summarized in Fig. 2.5 and Fig. 2.6. To ease the reading of this section, we provide with Table 2.1 an overview of the symbols used below. Some of them have already been introduced, some will be introduced later.

2.4.1 Data overview

The dependence of the packing densities φ on the inverse compression rates γ^{-1} for packings produced with the LS and FB algorithms is shown in Fig. 2.2a and Fig. 2.2c, respectively. The closest jamming densities φ_J obtained with the MLS algorithm *vs.* the inverse compression rates

[49] M. Skoge et al. *Phys. Rev. E*, 74, 041127, 2006.
[138] Y. Jiao, F. H. Stillinger, and S. Torquato. *J. Appl. Phys.*, 109, 013508, 2011.
[20] I. Biazzo et al. *Phys. Rev. Lett.*, 102, 195701, 2009.

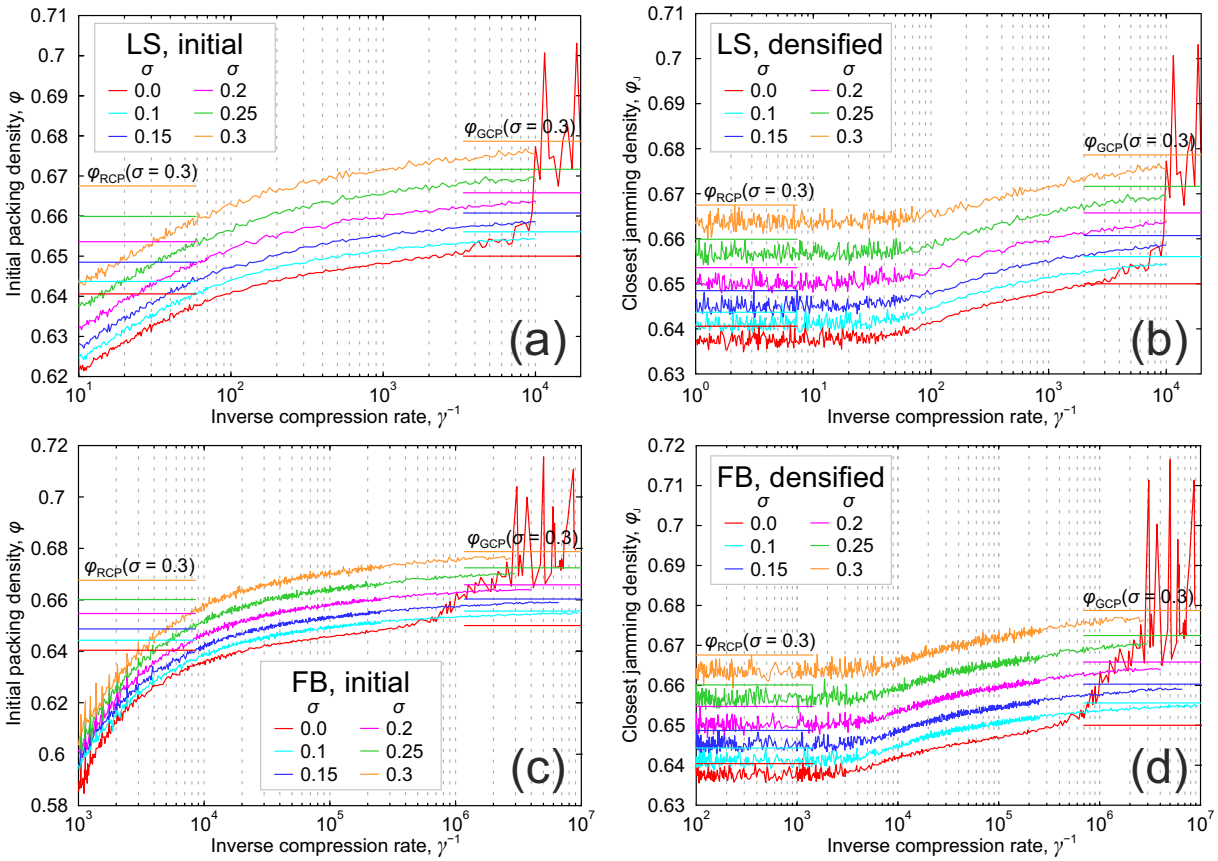

Figure 2.2: Packing density *vs.* inverse compression rate γ^{-1}. (a) Densities φ of sphere packings generated with the Lubachevsky–Stillinger (LS) algorithm. (b) Closest jamming densities φ_J for the packings in panel a. (c) Densities φ of sphere packings generated with the force-biased (FB) algorithm. (d) Closest jamming densities φ_J for the packings in panel c. The meaning of colour for the different relative standard deviations σ of the log-normal sphere radii distributions is explained in the legends. Horizontal lines with corresponding colours to the left and to the right of the figures represent the RCP limits (φ_{RCP}) and the GCP limits (φ_{GCP}), respectively.

γ^{-1} for the same LS and FB packings are shown in Fig. 2.2b and Fig. 2.2d, respectively. All packings in Fig. 2.2b and Fig. 2.2d are nearly isostatic and have very high equilibrium reduced pressure (10^{12}).

We did not average the data in Fig. 2.2; each point in these figures corresponds to a single packing. To guide the eye, points have been connected by straight lines. Averaging assumes that fluctuations in the data will disappear in the thermodynamic limit. This question is still unresolved and we do not discuss it here.[12,133] Additionally, averaging would remove the information about the exact boundaries of jamming intervals for finite packings.

We distinguish between two packing generation regimes in Fig. 2.2: slow compressions (*i.e.*, high inverse compression rates, long generation times) and fast compressions (*i.e.*, low inverse compression rates, short generation times). We consider the generation as slow for the FB packings with $\gamma^{-1} > 0.2 \times 10^4$ and for LS packings with $\gamma^{-1} > 0.6 \times 10^2$. We consider the

Table 2.2: Estimates of the GCP limit (φ_{GCP}) along with 95% confidence intervals obtained by different methods. (i) "LS/FB, initial": asymptotic expansion of actual sphere packing densities, see Fig. 2.2a and Fig. 2.2c. (ii) "LS/FB, densified": asymptotic expansion of the closest jamming densities, see Fig. 2.2b and Fig. 2.2d. Data are provided for different relative standard deviations σ of the log-normal sphere radii distributions.

σ	0.05	0.1	0.15	0.2	0.25	0.3
LS, initial	$0.653 \pm 1.849 \times 10^{-4}$	$0.656 \pm 1.955 \times 10^{-4}$	$0.660 \pm 2.282 \times 10^{-4}$	$0.665 \pm 2.889 \times 10^{-4}$	$0.671 \pm 3.486 \times 10^{-4}$	$0.678 \pm 4.549 \times 10^{-4}$
FB, initial	$0.653 \pm 1.452 \times 10^{-3}$	$0.654 \pm 1.958 \times 10^{-3}$	$0.661 \pm 1.900 \times 10^{-3}$	$0.665 \pm 1.783 \times 10^{-3}$	$0.671 \pm 3.019 \times 10^{-3}$	$0.679 \pm 3.899 \times 10^{-3}$
LS, densified	$0.653 \pm 3.572 \times 10^{-4}$	$0.656 \pm 3.447 \times 10^{-4}$	$0.661 \pm 3.853 \times 10^{-4}$	$0.666 \pm 5.234 \times 10^{-4}$	$0.672 \pm 6.517 \times 10^{-4}$	$0.679 \pm 9.441 \times 10^{-4}$
FB, densified	$0.652 \pm 1.577 \times 10^{-4}$	$0.656 \pm 1.966 \times 10^{-4}$	$0.660 \pm 2.427 \times 10^{-4}$	$0.666 \pm 3.098 \times 10^{-4}$	$0.673 \pm 4.242 \times 10^{-4}$	$0.679 \pm 5.080 \times 10^{-4}$

generation as fast for the FB packings with $\gamma^{-1} < 10^3$ and for LS packings with $\gamma^{-1} < 5$.

For slow compressions, the jamming densities in Fig. 2.2b and Fig. 2.2d remain close to the initial densities for all the packing types. This occurs because the packings are already trapped in closed or nearly closed bounding regions and are almost jammed. The search for the closest jammed configuration only slightly increases their densities. Though the plots for the LS and FB algorithms look similar, the inverse compression rates for the FB packings are shifted by two orders of magnitude with respect to the LS packings.

The obtained narrow horizontal bands for jamming densities after the fast initial compressions in Fig. 2.2b and Fig. 2.2d can be explained as follows. Fast generations do not allow the packings (with Poisson distribution of points as starting configuration) to leave the initial bounding regions, though the packings are not jammed at the end of the fast compressions. The search for the closest jamming density will also retain packings in their initial bounding regions, but will compress the regions into polytopes and finally into jammed configurations, slightly increasing the packing density. Therefore, the jamming density distribution for fast compressions should correspond to the closest jamming density distribution for Poisson packings, *i.e.*, to the uniform sampling of the phase space.

2.4.2 Validation of the modified Lubachevsky–Stillinger (MLS) algorithm

Prior to a detailed discussion of the data in Fig. 2.2, we analyze how the estimated closest jamming densities depend on algorithm parameters. For this purpose, we selected several LS packings with $\sigma = 0$ (monodisperse packings) and $\sigma = 0.3$ (widest particle size distribution in this work) and searched for their closest jamming densities with varied search parameters. We changed the compression rate decrease factor (*i.e.*, the number we used to divide the compression rate as the pressure becomes high enough), the initial compression rate, and the final compression rate. For the compression rate decrease factor we used the values 1.5, 2, 2.5, 3, and 4; for the initial compression rate—1, 10, and 20; and for the final compression rate—10^{-4} and 10^{-5}. This results in a total of 30 combinations.

Fig. 2.3a shows how the final jamming densities depend on the compression rate decrease

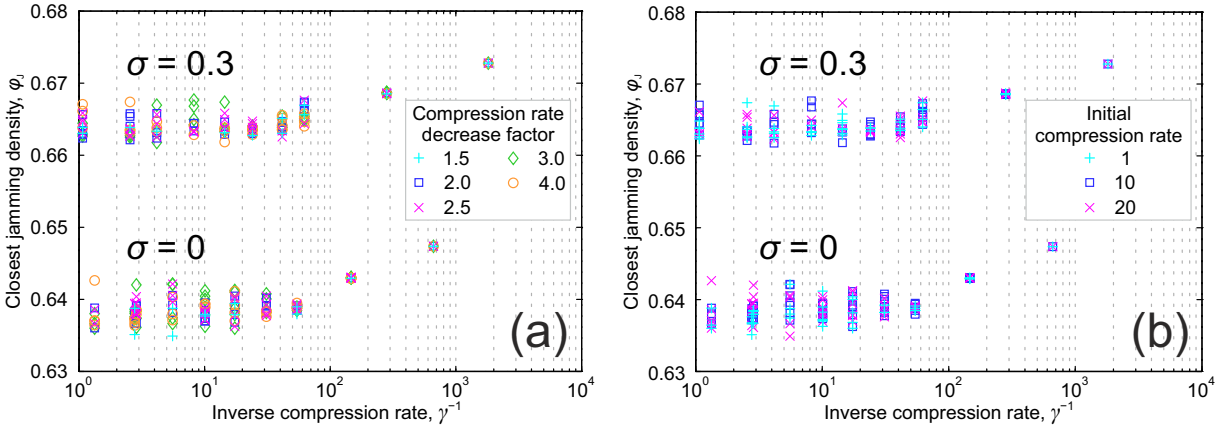

Figure 2.3: Estimated closest jamming density φ_J *vs.* inverse compression rate γ^{-1}, when search parameters for the closest jammed configurations are varied. (a) Dependence on the compression rate decrease factor. (b) Dependence on the initial compression rate. Initial sphere packings were obtained with the Lubachevsky–Stillinger (LS) algorithm and have sphere radii relative standard deviations $\sigma = 0$ and $\sigma = 0.3$.

factor. The dependence on the initial compression rate is depicted in Fig. 2.3b. All 30 combinations are represented in each figure, but are coloured according to one of the varied parameters.

Fast compressions

Packings obtained with fast compressions ($\gamma^{-1} < 5$ in Fig. 2.3b) jam at slightly different, but very close configurations. There is no apparent correlation between the chosen parameters and the final jamming densities, *i.e.*, the final jamming density varies randomly with the algorithm parameters. There are no visible correlations for the final compression rate as well (data not shown). We explain this as follows: For packings obtained with fast compressions, the available phase space is highly connected[2] and there are many achievable jammed configurations in the vicinity of the true closest jammed configuration. With changing parameters, the algorithm may randomly switch between one of these configurations. The interval of densities where the packings jam is the same as with the fast compressions in Fig. 2.2b and Fig. 2.2d (for the corresponding sphere radii distributions with $\sigma = 0$ and $\sigma = 0.3$). Further in this paper, we are only interested in the lower and upper bounds of the closest jamming density intervals for fast compressions. Thus, results below for fast compressions do not depend on the exact algorithm parameters. If the initial compression rate is 0.01, the interval of jamming densities is shifted upward and is $[0.637, 0.647]$ for monodisperse particles[54] (Table I in that paper). It means that this initial compression rate is already too low to correctly search for the closest jammed configurations.

We found that with a compression rate decrease factor of 10 the jamming densities for fast compressions are systematically shifted upward. It means that the compression rate decreases too quickly. After several decreases it is so low that the packings have enough time (until pressure becomes high again) to leave the initial bounding region and travel to bounding regions with higher jamming densities.

Slow compressions

For slow compressions ($\gamma^{-1} > 0.6 \times 10^2$ in Fig. 2.3b) fluctuations in jamming densities quickly disappear. This happens because the bounding regions where the packings initially reside after slow compressions have less "wormholes" to neighbouring regions; the available phase space is less connected. Thus, the algorithm does not switch randomly between jammed configurations in the vicinity of the true closest jammed configuration and always terminates at the latter. It shows that the results for slow compressions below also do not depend on the exact algorithm parameters.

2.4.3 Data analysis

Slow compressions, estimation of the GCP limits φ_{GCP}

Extrapolation of the $\varphi_J(\gamma^{-1})$ plots for polydisperse packings in Fig. 2.2b and Fig. 2.2d to zero compression rate (infinite generation time) provides the highest densities that can be obtained with these algorithms. We interpret these densities as the GCP limits φ_{GCP}: (i) the LS and FB algorithms are able to reach and overcome the structural transition density of $\varphi \approx 0.65$ for monodisperse packings ($\sigma = 0$), which we also interpreted as the GCP limit;[132] (ii) both algorithms are able to generate almost crystalline configurations for monodisperse packings. These densities may be regarded as lower bounds of the GCP limits, as it is sometimes argued that the GCP limits are unreachable (see, *e.g.*, Subsection II B 2 in Parisi and Zamponi[2]). Resolving the question whether they can be reached or not is beyond the scope of the present paper.

We approximate the $\varphi_J(\gamma^{-1})$ plots by the least-squares method with an asymptotic expansion $\varphi_J = \sum_{i=0}^{3} c_i \left(\sqrt{\gamma}\right)^i$ and extrapolate it to zero compression rate (infinite generation time). Estimates of the GCP limits are then found as $\varphi_{\text{GCP}} = c_0$. We took the 80 last data points to the right in Fig. 2.2b to fit the LS data and 300 points to fit the FB data (Fig. 2.2d). Both numbers were selected to exclude points from the horizontal plateaus at short generation times. Estimates of φ_{GCP} along with 95% confidence intervals for the LS and FB packings are reported in Table 2.2 in the rows "LS, densified" and "FB, densified". These estimates are displayed as horizontal lines to the right in Fig. 2.2b and Fig. 2.2d, respectively.

As the packings generated by sufficiently slow compressions are almost jammed, we may use the densities of initially created packings for the same asymptotic expansion to estimate the GCP limits. We used 125 data points to the right in Fig. 2.2a to fit the LS data and 300 points to the right in Fig. 2.2c to fit the FB data. The GCP limit estimates along with 95% confidence intervals for the LS and FB packings are reported in Table 2.2 in the rows "LS, initial" and "FB, initial". These estimates are displayed as horizontal lines to the right in Fig. 2.2a and Fig. 2.2c, respectively. Plots from Fig. 2.2 built *vs.* $\sqrt{\gamma}$, along with their polynomial fits, can be found in Section 2.6.7 of the Appendix (Asymptotic expansion of packing densities to the GCP limits).

We do not estimate the GCP limit for monodisperse packings by asymptotic expansion, because the $\varphi(\gamma^{-1})$ and $\varphi_J(\gamma^{-1})$ plots do not exhibit asymptotes for low compression rates.

Table 2.3: Minimum ($\varphi_{\text{min}}^{\text{fast}}$) and maximum ($\varphi_{\text{max}}^{\text{fast}}$) closest jamming densities for sphere packings generated with fast compressions using the Lubachevsky–Stillinger (LS) and force-biased (FB) algorithms. Data are provided for different relative standard deviations σ of the log-normal sphere radii distributions. $\varphi_{\text{min}}^{\text{fast}}$ and $\varphi_{\text{max}}^{\text{fast}}$ are the leftmost and the rightmost points, respectively, of the corresponding distributions in Fig. 2.4.

σ	0.0	0.05	0.1	0.15	0.2	0.25	0.3
$\varphi_{\text{min}}^{\text{fast}}$, LS	0.6349	0.6367	0.6391	0.6425	0.6480	0.6542	0.6601
$\varphi_{\text{min}}^{\text{fast}}$, FB	0.6356	0.6364	0.6388	0.6428	0.6469	0.6540	0.6593
$\varphi_{\text{max}}^{\text{fast}}$, LS	0.6406	0.6414	0.6437	0.6485	0.6536	0.6599	0.6675
$\varphi_{\text{max}}^{\text{fast}}$, FB	0.6404	0.6428	0.6443	0.6487	0.6547	0.6601	0.6676

Instead, they start to grow rapidly as densities $\varphi \approx \varphi_J \approx 0.65$ are reached. It is known that monodisperse packings demonstrate an entropy minimum and the onset of crystallization at $\varphi \approx 0.647 - 0.651$.[13,21–26,128,132] In our previous paper,[132] we reproduced these features at $\varphi \approx 0.647 - 0.651$ for the monodisperse FB packings shown in Fig. 2.2c (as well as for LS packings created with the code of Skoge *et al.*;[49] not used in the present paper). We analyzed the Voronoi volumes standard deviation,[1,117,125] Voronoi volumes entropy,[22,23] pore-size entropy,[132] and the local bond-orientational order Q_{local}^6.[118] Here, we also applied these measures to the monodisperse LS packings (Fig. 2.2a) and to the monodisperse densified LS and FB packings (Fig. 2.2b and Fig. 2.2d). We confirm that the behaviour of the measures remains unchanged: entropy-like measures have a local minimum at $\varphi \approx \varphi_J \approx 0.647 - 0.651$ and local order starts to increase rapidly at the same density (data not shown). Thus, we associate the growth in the $\varphi(\gamma^{-1})$ and $\varphi_J(\gamma^{-1})$ plots at $\varphi \approx \varphi_J \approx 0.65$ with the onset of crystallization; and interpret the entropy minimum for monodisperse packings as the GCP limit, $\varphi_{\text{GCP}} \approx 0.65$. It is easy to show why the GCP limit implies the onset of crystallization. If $\varphi_{\text{GCP}} \approx 0.65$ is the highest achievable density for monodisperse packings with suppressed crystallization (*e.g.*, by pinning a certain fraction of particles[139]), the only way to reach still higher densities – for generation protocols that try to avoid crystallization as long as possible – is to prepare crystalline inclusions in the packings at φ_{GCP}. We assume that, if crystallization is artificially suppressed in monodisperse packings, the $\varphi(\gamma^{-1})$ and $\varphi_J(\gamma^{-1})$ plots look similar to those for polydisperse packings, reaching asymptotes $\varphi = \varphi_{\text{GCP}}$ or $\varphi_J = \varphi_{\text{GCP}}$ at $\gamma^{-1} = \infty$, with $\varphi_{\text{GCP}} \approx 0.65$.

Fast compressions, determination of $\varphi_{\text{max}}^{\text{fast}}$

Let φ_{HCP} be the crystalline packing density for monodisperse packings (FCC or HCP crystals); let also φ_{max} be the highest possible packing density: it is φ_{HCP} for monodisperse packings and φ_{GCP} for sufficiently polydisperse packings. φ_{GCP} and φ_{max} depend on the particle radii distribution.

Closest jamming densities for fast compressions (horizontal density bands) have clear lower and upper bounds in Fig. 2.2b and Fig. 2.2d. We determine the horizontal parts of the plots visually, *i.e.*, consider the plots of packing density *vs.* inverse compression rate for the LS and FB

[117] S. Khirevich et al. *J. Chromatogr. A*, 1217, 4713–4722, 2010.
[125] S. Khirevich et al. *J. Chromatogr. A*, 1262, 77–91, 2012.
[118] P. J. Steinhardt, D. R. Nelson, and M. Ronchetti. *Phys. Rev. B*, 28, 784–805, 1983.
[139] R. L. Jack and L. Berthier. *Phys. Rev. E*, 85, 021120, 2012.

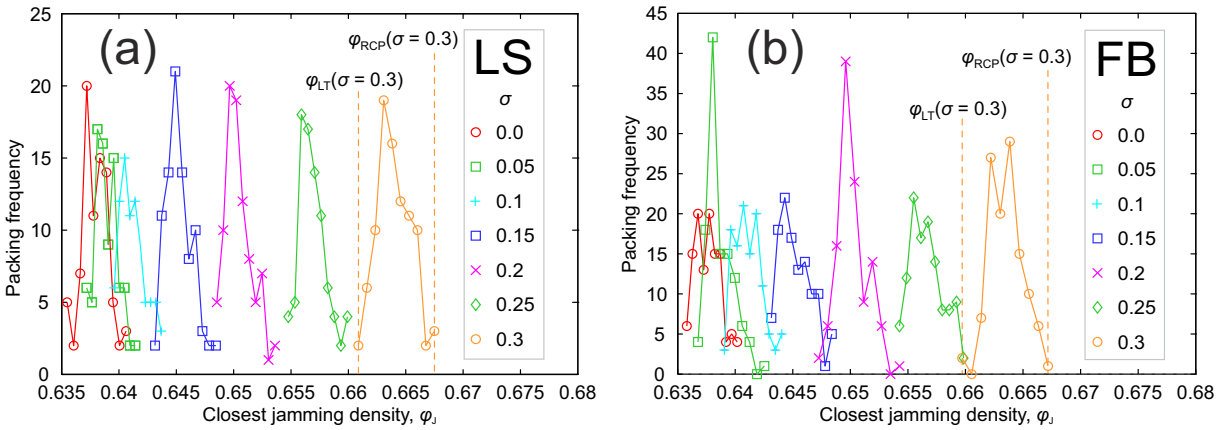

Figure 2.4: Closest jamming density distributions for sphere packings created with fast compressions. (a) Packings generated with the Lubachevsky–Stillinger (LS) algorithm. (b) Packings generated with the force-biased (FB) algorithm. The meaning of symbols for the different relative standard deviations σ of the log-normal sphere radii distributions is explained in the legends. $\varphi_{\text{max}}^{\text{fast}}$ and φ_{RCP} are determined for each σ as the rightmost points of the distributions, $\varphi_{\text{min}}^{\text{fast}}$ and φ_{LT} are determined for each σ as the leftmost points of the distributions. These values are summarized in Table 2.3.

algorithms as horizontal for $\gamma^{-1} < 5$ (Fig. 2.2b) and for $\gamma^{-1} < 10^3$ (Fig. 2.2d), respectively. The number distributions of the closest jamming densities for fast compressions by the LS and FB algorithms are presented in Fig. 2.4. These distributions are localized in narrow density bands. The maximum and minimum densities for LS and FB packings in these bands are provided in Table 2.3. The maximum achievable density for monodisperse packings is ~ 0.64 for both algorithms.

We denote these maximum and minimum densities from Table 2.3 as $\varphi_{\text{max}}^{\text{fast}}$ and $\varphi_{\text{min}}^{\text{fast}}$, respectively. They depend on the particle radii distribution.

We assume that our results for the GCP limits and further discussion for the RCP limits are protocol-independent. We base our assumption on the following points: (i) the behaviour of $\varphi_J(\gamma^{-1})$ plots is qualitatively the same for both the FB and LS protocols; (ii) the differences between the corresponding values of $\varphi_{\text{min}}^{\text{fast}}$ for different protocols are $\leq 10^{-3}$; (iii) the differences between the corresponding values of $\varphi_{\text{max}}^{\text{fast}}$ for different protocols are $\leq 10^{-3}$; (iv) the differences between the corresponding φ_{GCP} estimates from Table 2.2 are $\leq 2 \times 10^{-3}$.

2.4.4 Definition of the RCP limits φ_{RCP} through $\varphi_{\text{max}}^{\text{fast}}$

Fig. 2.4 and Table 2.3 show that $\varphi_{\text{max}}^{\text{fast}}$ is the highest practically obtained closest jamming density for sufficiently large Poisson packings or packings created with fast compressions. It implies that basins of attraction with jamming densities $\varphi_J > \varphi_{\text{max}}^{\text{fast}}$ are practically impossible to sample for sufficiently large packings; in other words, basins of attraction with $\varphi_J \leq \varphi_{\text{max}}^{\text{fast}}$ cover for such packings the fraction of the phase space that is close to unity. We associate $\varphi_{\text{max}}^{\text{fast}}$ with the random close packing limit φ_{RCP}. We assume that in the thermodynamic limit the lowest density φ_0, for which the basins of attraction with $\varphi_J \leq \varphi_0$ still cover the *almost entire* phase space,

Table 2.4: Characteristic densities for hard-sphere packings: lowest typical jamming densities (φ_{LT}), RCP limits (φ_{RCP}), and GCP limits (φ_{GCP}). Data are provided for different relative standard deviations σ of the log-normal sphere radii distributions. φ_{GCP} is obtained by averaging columns in Table 2.2. φ_{LT} and φ_{RCP} are estimated by averaging $\varphi_{\text{min}}^{\text{fast}}$ and $\varphi_{\text{max}}^{\text{fast}}$ from Table 2.3, respectively. φ_{LT}, φ_{RCP}, and φ_{GCP} are plotted *vs.* σ in Fig. 2.5.

σ	0.0	0.05	0.1	0.15	0.2	0.25	0.3
φ_{LT}	0.6353	0.6366	0.6390	0.6426	0.6475	0.6541	0.6597
φ_{RCP}	0.6405	0.6421	0.6440	0.6486	0.6542	0.6600	0.6676
φ_{GCP}	0.65	0.6526	0.6554	0.6606	0.6651	0.6716	0.6787

is also close to $\varphi_{\text{max}}^{\text{fast}}$. Under this assumption, we define *the random close packing limit* φ_{RCP} for infinite packings as the minimum density for which basins of attraction with jamming densities $\leq \varphi_{\text{RCP}}$ cover the *almost entire* phase space. The RCP limit for sufficiently large packings is thus the highest practically obtained closest jamming density for Poisson configurations or packings created with fast compressions. When packings are relatively small and all basins of attraction can in practice be sampled by Poisson configurations, we have to select an arbitrary fraction α, *e.g.*, $\alpha = 0.95$, and define the RCP limit as the density for which basins of attraction with $\varphi_J \leq \varphi_{\text{RCP}}$ cover the selected fraction α of the phase space.

In the same manner we define for infinite packings another characteristic density φ_{LT} as the maximum density for which basins of attraction with jamming densities $\geq \varphi_{\text{LT}}$ cover the *almost entire* phase space. The LT limit for sufficiently large packings is the lowest practically obtained closest jamming density for Poisson configurations or packings created with fast compressions. Thus, for the packings under study $\varphi_{\text{LT}} = \varphi_{\text{min}}^{\text{fast}}$. Mathematical formulations for both finite and infinite packings are given in the Section 2.6.6 of the Appendix.

We do not investigate the dependence of φ_{LT}, φ_{RCP}, and φ_{GCP} on the number of particles in the packings, but add the following remarks. As mentioned, monodisperse packings exhibit a structural transition and the onset of crystallization at $\varphi_{\text{GCP}} \approx 0.65$.[13,21–26,128,132] This density is reported even for packings of 10^5 particles,[13] which suggests that φ_{GCP} is preserved in the thermodynamic limit. φ_{LT} and φ_{RCP} depend on the number of particles in a packing;[12] φ_{LT} increases and φ_{RCP} slightly decreases as the number of particles increases. There are two possible scenarios for their behaviour for infinite packings: they converge to a single J-point (at $\varphi \approx 0.64$ for monodisperse packings),[12] or φ_{LT} reaches an asymptote below φ_{RCP}.[133] In both cases φ_{GCP} is different from φ_{LT} and φ_{RCP} in the thermodynamic limit.

Further below, under φ_{LT} and φ_{RCP} we will understand the corresponding densities for finite packings of 10^4 particles. It follows from Fig. 2.4 that $\varphi_{\text{RCP}} = \varphi_{\text{max}}^{\text{fast}}$ and $\varphi_{\text{LT}} = \varphi_{\text{min}}^{\text{fast}}$. Now, we join all the characteristic points obtained so far for the different particle radii distributions in a single table and in a single plot (Table 2.4 and Fig. 2.5). φ_{LT} was estimated by averaging the minimum closest jamming densities after fast compressions $\varphi_{\text{min}}^{\text{fast}}$ from Table 2.3 for both LS and FB packings; φ_{RCP} was estimated by averaging the maximum closest jamming densities after fast compressions $\varphi_{\text{max}}^{\text{fast}}$ from Table 2.3 for both LS and FB packings; φ_{GCP} was estimated by averaging the columns in Table 2.2; and φ_{GCP} for monodisperse packings was taken at a conventional value of $\varphi = 0.65$.[132] For monodisperse packings $\varphi_{\text{LT}} \approx 0.635$ and $\varphi_{\text{RCP}} \approx 0.64$.

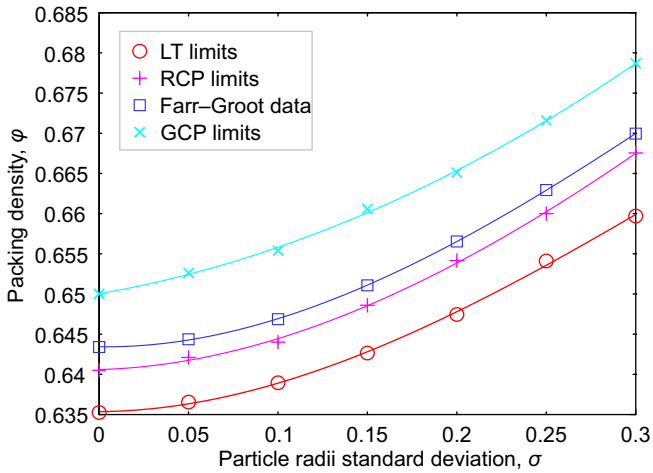

Figure 2.5: Characteristic densities for finite packings of 10^4 spheres with log-normal sphere diameter distribution: red circles (◯) are lowest typical (LT) jamming densities φ_{LT}; magenta crosses (+) are RCP limits φ_{RCP}; blue squares (□) are φ_{RCP} estimates obtained by Farr and Groot;[140] and cyan crosses (×) are GCP limits φ_{GCP}. All values (except the Farr–Groot data) can be found in Table 2.4.

The plots in Fig. 2.5 demonstrate that all of the characteristic densities increase with the width of the particle size distribution. The increase of φ_{GCP} is natural, as far as polydisperse packings have more degrees of freedom (not only three coordinates per particle, but also a radius), and there are more possibilities to arrange the packings in order to achieve a desired density. The increase of φ_{RCP} can be explained in a similar way. While φ_{LT}, φ_{RCP}, and φ_{GCP} vary with the particle radii relative standard deviation, the differences between them do not change much, *e.g.*, $\varphi_{\mathrm{GCP}} - \varphi_{\mathrm{RCP}} \approx 0.01$ for all relative standard deviations. Such a small difference explains why it is hard to discern φ_{RCP} and φ_{GCP} experimentally. We also provide in Fig. 2.5 a plot for the semi-theoretical RCP limit estimates obtained by Farr and Groot.[140] This plot has a very similar shape and is shifted slightly upward compared with our φ_{RCP} estimates.

2.4.5 Typical and untypical basins of attraction

We distinguish between *typical* basins of attraction and *untypical* ones. Basins of attraction with jamming densities in the range $[\varphi_{\mathrm{LT}}, \varphi_{\mathrm{RCP}}]$ are *typical* by definition; the others are *untypical*. The probability to sample an untypical basin of attraction with Poisson packings or with packings produced by fast compressions tends to zero in the thermodynamic limit. It is close to zero already for packings of 10^4 particles. This happens because the phase space is dominated by typical basins; their total volume is almost equal to the total phase space volume in the thermodynamic limit.

If there is a way to distinguish typical from untypical basins of attraction without relying on their jamming densities, it will be possible to provide another definition for φ_{RCP}: it is the highest jamming density for typical basins of attraction or the highest typical closest jamming density of Poisson packings. In the same manner we can define φ_{LT}: it is the lowest jamming density

[140] R. S. Farr and R. D. Groot. *J. Chem. Phys.*, 131, 244104, 2009.

for typical basins of attraction or the lowest typical closest jamming density of Poisson packings. This is the reason for using LT (lowest typical) as subscript for φ_{LT}.

It was suggested that the RCP limit is a special density at which almost every infinite Poisson packing will jam in the process of infinitely fast compressions and was referred to as the J-point.[12] In other words, it is the closest jamming density for almost every Poisson packing. We confirmed that this point is rather a segment $[\varphi_{\mathrm{LT}}, \varphi_{\mathrm{RCP}}]$ for finite packings.[12,133] It is sometimes argued that even in the thermodynamic limit this segment does not collapse to a single J-point.[133] The estimate for φ_{LT} for monodisperse packings by Pica Ciamarra *et al.*[133] ($\varphi = 0.635 - 0.636$) is in good agreement with our result ($\varphi_{\mathrm{LT}} \approx 0.635$). We note that φ_{LT} is referred to as the random-loose packing (RLP) density in these papers. We use a separate term, the "lowest typical" density, to avoid confusion with another definition and estimate for the RLP limit at $\varphi_{\mathrm{RLP}} = 0.536 - 0.55$;[1,16,141] as well as to emphasize that we are investigating frictionless particles.

Here we observed untypical jammed configurations only in the range $(\varphi_{\mathrm{RCP}}, \varphi_{\mathrm{max}}]$. There should be another set of untypical jammed configurations with densities below φ_{LT}. Examples of such configurations for monodisperse particles are tunnelled crystals, discovered by Torquato and Stillinger.[137] These tunnelled crystals form an uncountable set of untypical jammed configurations at $\varphi_J = 2/3 \cdot \varphi_{\mathrm{HCP}} = \sqrt{2}\pi/9 \approx 0.49365$. Another special procedure has been proposed to systematically create untypical jammed configurations with jamming densities in the range $[0.6, \varphi_{\mathrm{LT}})$ for monodisperse packings.[54,138] One has to select a typical jammed packing, remove a certain fraction of particles and apply a special sequential linear programming generation algorithm,[54] which is also believed to produce the closest jammed configurations. The untypical jamming densities below φ_{LT} should also have a lower limit, which we denote as φ_L, the lowest density of jammed configurations. Thus, for monodisperse packings φ_L is at least $\sqrt{2}\pi/9 \approx 0.49365$. The existence of untypical jammed configurations below φ_{LT} and a lower bound for their densities has been proposed by Pica Ciamarra *et al.*[46,67] along with a special algorithm to generate jammed untypical two-dimensional packings below φ_{LT}. This lower bound is called the "random very loose packing" density in these papers. Since we want to avoid the mixing of "lowest typical" jamming density and "random loose packing" density, we use the term "lowest" jamming density in this paper.

2.4.6 Discussion

The definition of the RCP limit for monodisperse packings shows excellent agreement with the recurring experimental value of $\varphi_{\mathrm{RCP}} \approx 0.64$.[10,12,75,131] We suggest that the two common φ_{RCP} estimates for monodisperse packings (*i.e.*, 0.64 and 0.65) actually correspond to two distinct characteristic points:

[16] M. Jerkins et al. *Phys. Rev. Lett.*, 101, 018301, 2008.
[141] G. E. Schröder-Turk et al. *EPL*, 90, 34001, 2010.
[137] S. Torquato and F. H. Stillinger. *J. Appl. Phys.*, 102, 093511, 2007.
[46] M. Pica Ciamarra et al. *Soft Matter*, 8, 9731–9737, 2012.
[67] M. Pica Ciamarra and A. Coniglio. *Phys. Rev. Lett.*, 101, 128001, 2008.

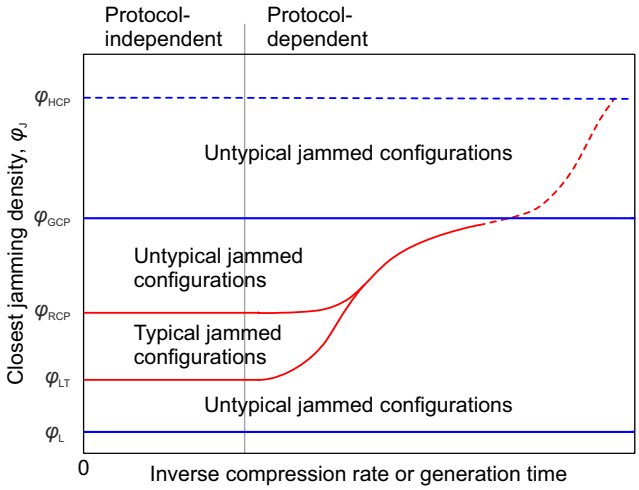

Figure 2.6: Schematic jamming phase diagram for finite packings. Dashed lines refer only to monodisperse packings. Red lines denote boundaries for typical configurations. φ_{HCP} is the highest jamming density for monodisperse packings, φ_{GCP} is the glass close packing limit, φ_{RCP} is the random close packing limit (or the highest typical jamming density), φ_{LT} is the lowest typical jamming density, and φ_L is the lowest jamming density.

1. $\varphi \approx 0.64$.[10,12,75,131] We interpret it as the RCP limit φ_{RCP}, the highest jamming density for typical basins of attraction.
2. $\varphi \approx 0.65$.[13,21–26,128,132] We interpret it as the GCP limit φ_{GCP}, the highest jamming density for polydisperse packings and the density above the RCP limit with a minimum number of jammed configurations for monodisperse packings.

For finite packings, even infinitely fast compressions of Poisson configurations produce jamming densities in the range $[\varphi_{LT}, \varphi_{RCP}]$. The lowest jamming density φ_{LT} for monodisperse packings of 10^4 particles under study is ~ 0.635.

Chaudhury *et al.*[35] demonstrated that the jamming densities depend on preparation history and should exist in a certain range. This discovery complies very naturally with the picture we present. Indeed, the jamming densities should depend on the employed generation protocol and can be found at any density in the range $[\varphi_L, \varphi_{max}]$; but searching for the closest jammed configuration for Poisson packings for sufficiently large packings will in practice always produce a density in the range $[\varphi_{LT}, \varphi_{RCP}]$.

Kamien and Liu[142] showed that there may be an uncertainty in the range of densities where the reduced pressure reaches infinity during packing densification. We showed that the pressure can reach infinity during a single packing densification in the entire range of densities $[\varphi_L, \varphi_{max}]$; again, searching for the closest jammed configuration for Poisson packings for sufficiently large packings will in practice always produce a density in the range $[\varphi_{LT}, \varphi_{RCP}]$. Our definition of the RCP limit as the highest typical jamming density is also consistent with experimental observations, which state that φ_{RCP} is the jamming density maximally achievable in experiments.[10]

[142] R. D. Kamien and A. J. Liu. *Phys. Rev. Lett.*, 99, 155501, 2007.

In Fig. 2.6 we schematically display how the closest jamming densities depend on the generation time for finite packings. We assume that algorithms start from Poisson packings and update the configuration continuously with generation time. The typical closest jamming densities were previously defined only for Poisson packings or for zero initial packing density. Under typical closest jamming densities for non-zero initial packing densities we understand the closest jamming densities that will be almost always found for packings created at a given density using a given algorithm. The right part of the plot (*cf.* vertical gray dividing line) depends on packing generation protocol, and we depict it for protocols capable of approaching the GCP limit for polydisperse packings and reaching crystalline configurations for monodisperse packings. Other protocols may converge to lower densities instead, as low as φ_{LT} or even φ_L. Indeed, the protocol of Khirevich *et al*[6] produces packings with densities close to φ_{LT} for infinite generation times. The form of the plot $\varphi_J(\gamma^{-1})$ in Fig. 2.6, as well as in Fig. 2.2b and Fig. 2.2d, was conjectured by Parisi and Zamponi[2] (see Fig. 2a in that paper). The major difference is the presence of the plateau at φ_{GCP} in the conjectured plot for monodisperse packings.

In the future we like to measure the characteristic densities φ_{LT}, φ_{RCP}, and φ_{GCP} for other particle radii distributions, *e.g.*, Gaussian and bidisperse,[119] and compare the results to predictions from other models.[19,143] Our methodology provides a framework for investigating these densities for hard particles of arbitrary shape and dimensionality.

2.5 Summary and conclusions

We introduced a modification to the LS packing generation algorithm to directly produce the closest jammed configurations (inherent structures of hard spheres) for arbitrary packings. The application of this protocol to LS and FB packings consisting of 10^4 particles yields the following conclusions, independent from the employed packing generation protocol: Closest jamming densities for Poisson packings and packings produced with fast compressions are located in narrow density bands depending on particle size distribution, from $\varphi = 0.634 - 0.636$ to $\varphi \approx 0.64$ for monodisperse particles; closest jamming densities for packings created with slow compressions converge to certain asymptotic values ($\varphi \approx 0.65$ for monodisperse particles).

We attribute the asymptotic packing densities for infinitely slow compressions to lower bounds of the GCP limits.[2] We attribute $\varphi \approx 0.64$ (monodisperse packings) to the RCP limit and interpret $\varphi = 0.634 - 0.636$ and similar densities for polydisperse packings as another characteristic density φ_{LT}. Thus, we define the RCP limit φ_{RCP} for sufficiently large finite packings as the highest practically achievable closest jamming density of Poisson configurations. Similarly, φ_{LT} is the lowest practically achievable closest jamming density of Poisson configurations. In the thermodynamic limit, φ_{RCP} and φ_{LT} may coincide and thus form a J-point, but they are different for finite packings.

[119] K. Lochmann, L. Oger, and D. Stoyan. *Solid State Sci.*, 8, 1397–1413, 2006.
[19] M. Clusel et al. *Nature*, 460, 611–615, 2009.
[143] K. A. Newhall et al. *Soft Matter*, 7, 11518–11525, 2011.

These definitions led us to the distinction between *typical* jammed configurations and corresponding basins of attraction, which have jamming densities in the range $[\varphi_{\mathrm{LT}}, \varphi_{\mathrm{RCP}}]$ and in the thermodynamic limit occupy the almost entire phase space, and *untypical* ones, whose jamming densities reside in the ranges $[\varphi_L, \varphi_{\mathrm{LT}})$ and $(\varphi_{\mathrm{RCP}}, \varphi_{\max}]$ and which in the thermodynamic limit occupy a portion of the phase space with zero probability measure. The RCP limit is thus the highest typical closest jamming density of Poisson packings and packings produced with sufficiently fast compressions; φ_{LT} is the lowest typical closest jamming density of Poisson packings and packings produced with sufficiently fast compressions.

The characteristic densities φ_{LT}, φ_{RCP}, and φ_{GCP} depend on the relative standard deviation of the employed log-normal particle radii distributions, but differences between them do not change much, *e.g.*, $\varphi_{\mathrm{GCP}} - \varphi_{\mathrm{RCP}} \approx 0.01$ for all relative standard deviations. This small difference explains why it is challenging to differentiate between φ_{RCP} and φ_{GCP} experimentally.

Acknowledgements

We are grateful to the John von Neumann Institute for Computing (NIC) and the Jülich Supercomputing Center (JSC), Forschungszentrum Jülich (FZJ, Jülich, Germany), for the allocation of special CPU-time grants (NIC project numbers: 5658 and 6550, JSC project ID: HMR10).

2.6 Appendix

Here we present precise definitions for the closest jammed configuration (inherent structure of hard spheres), basin of attraction, and bounding region. We also give mathematical definitions for the random-close packing limit φ_{RCP} and the lowest typical density φ_{LT}.

2.6.1 Mathematical difficulty with the definition in the main text

In the definition for the closest jammed configuration below (Section 2.6.3) we will use an approach slightly different from that in the main text, but will show their equivalence. At first, we explain the mathematical difficulty with the definition in the main text.

We defined the artificial potential energy for hard-sphere packings as the maximum density that can be specified for a given packing configuration (to avoid particle intersections) taken with the minus sign. This potential energy is a non-smooth function over particle coordinates. Indeed, this maximum density is controlled by the closest pair of particles. The potential energy is a smooth function in a certain range of coordinates of one of the particles in the closest pair (around its initial position). But for a sufficiently large displacement of this particle some other particle will form the closest pair with it. The potential energy will not be smooth at the position of the first particle where the closest pair changes. The gradient of the potential energy is undefined at this point.

The closest jammed configuration is specified in the main text as the local minimum in the potential energy that is reached through the gradient descent (steepest descent) in the potential energy landscape from the initial packing configuration. The steepest descent is undefined at the

points with undefined gradient. Thus, we have to use a different approach.

2.6.2 Closest jammed configuration, general idea

Each packing configuration of N monodisperse or polydisperse particles (with predefined nominal radii) can be represented as a point in a $3N$-dimensional packing phase space (3 coordinates per particle center). For packing box sides $L_x L_y L_z$, respectively, the total phase space volume equals $V_{\text{tot}} = (L_x L_y L_z)^N$. The actual particle radii are proportional to the nominal ones and thus are determined only by the proportionality ratio or by the actual packing density. If there is a particle pair in contact in a packing, the configuration point resides on the corresponding hypercylinder surface. If there are multiple pairs in contact, the configuration point resides on the intersection of the corresponding hypersurfaces.

Packing contraction is equivalent to simultaneous particle radii growth so that all radii remain equally proportional to their nominal values. It is equivalent to hypercylinder radii growth in the phase space. We proportionally increase the particle radii and simultaneously drag the configuration point so that no particle intersections appear. At the same time we require that the configuration point *moves as little as possible* in the sense of Euclidean distance. This condition ensures that the configuration point always remains on the initial hypercylinder surfaces, *i.e.*, all the particle contacts are preserved and no intersections between particles in contact appear. Indeed, if one of the contacts is broken (a particle pair is split), it means that the configuration point has moved too far away from the corresponding hypersurface, which is not the minimal possible movement of the configuration. The minimal possible movement would be to preserve the point on the given hypersurface. If there is a single particle pair in contact, it will correspond to moving the point along the normal of the contact hypercylinder. If the packing is also monodisperse, it implies symmetric particle-pair spreading.

While growing, more hypersurfaces will approach the configuration point and some will cross it. The hypersurfaces will form a disjoint phase space region and finally collapse into a single infinitesimal point, a jammed configuration. As far as we required minimization of configuration displacement, we define this very jammed configuration as the *closest* (to the initial one) *jammed configuration*.

Until the configuration point resides in the infinitesimal limiting polytope (or a hyperinterval), it is always possible to contract a packing (increase particle radii) and update the configuration to avoid intersections. Thus, the closest jammed configuration is defined for any unjammed configuration. As far as we require minimization of configuration displacement, it is also defined uniquely.

We cannot simply define the closest jammed configuration as the jammed configuration with the minimum Euclidean distance to the current configuration, because this jammed configuration may be separated by regions of the phase space that correspond to particle intersections. In other words, this jammed configuration may be unreachable for any physical compression algorithm. Our definition automatically conforms to the requirement of physical accessibility for the closest

jammed configuration.

This definition is equivalent to the definition from the main text (searching for a potential energy minimum with the steepest descent, where the potential energy is the maximum density at a given configuration taken with a minus sign). Indeed, (i) displacement minimization during the increase of particle radii is equivalent to the gradient descent in the landscape of our artificial potential energy at points where the gradient is defined; (ii) both definitions terminate at jammed configurations.

If a jammed packing contains rattler particles, there is only a subset of particles that is jammed; in other words, there is a subspace of the total phase space that has collapsed into a single point. Rattler particles are allowed to move and thus transform this point into a hyperline in the entire phase space. As far as rattler particles are usually trapped in cages formed by other particles, this hyperline is usually a hyperinterval. Such hyperlines (hyperintervals) have zero volume as their projection on the subspace of jammed particles has zero volume. Though Salsburg and Wood[9] do not explicitly mention rattlers, their discussion can be amended to incorporate rattler particles. For example, predictions of the coordination number shall be formulated for a subset of jammed particles (for a subspace that collapses into a point). When we talk about limiting polytopes and infinitesimal points into which they collapse, we keep in mind that they are defined for jammed subsets of particles and should be expanded into hyperintervals if rattlers are taken into account.

If rattlers are considered, the closest jammed configuration is not a single point, but a hyperinterval of zero volume with the same density for each configuration. We combine all these configurations into a single equivalence class.

In the next subsection we provide a precise mathematical definition for the closest jammed configuration. We will not use this definition directly to search for such configurations; instead, we modify the LS algorithm.

2.6.3 Closest jammed configuration, definition

We introduce the following notations. $\vec{x}_i$ is a coordinate of the ith particle, $\vec{x} = \{\vec{x}_1, \vec{x}_2, ..., \vec{x}_N\}$ is the packing configuration vector in the phase space, $\vec{x}_{ij}$ is the vector from the ith to the jth particle (accounting for boundary conditions, if necessary; $\vec{x}_{ii}$ may thus be non-zero), andD_i is the nominal diameter of the ith particle (its absolute value is unimportant, relative values matter in the current definition). $D_{ij} = (D_i + D_j)/2$ is the nominal distance between particles in contact. We also introduce time t and specify that the actual particle radii grow as $D_i(t) = tD_i$; the initial time is selected to avoid intersections (initially, there may be no contacts at all). The actual distance between particles in contact grows as $D_{ij}(t) = tD_{ij}$. Let us also introduce particle velocities $\vec{v}_i = d\vec{x}_i/dt$ and a $3N$-dimensional velocity vector for the configuration point $\vec{v} = \{\vec{v}_1, \vec{v}_2, ..., \vec{v}_N\}$. We further introduce the concept of bonds, *i.e.*, pairs of particles in contact. At each time there is a finite number of bonds K, which corresponds to a coordination number $c = 2K/N$. We enumerate bonds by the index $k = \overline{1, K}$. We define $\vec{x}_{i_k j_k}$ as the vector between

particles in the kth bond and $D_{i_k j_k}(t)$ as the actual distance between these particles.

While contracting the packing (increasing particle radii) between new bond formations, we (i) avoid intersections between particles; and (ii) minimize particle velocities. As we have already found out, it is equivalent to (i) ensuring that the configuration point always resides at the initial hypercylinder surfaces; and (ii) minimizing $\vec{v}$. The mathematical formulation is:

$\left(\vec{x}_{i_k j_k}\right)^2 = \left(D_{i_k j_k} t\right)^2,\ k = \overline{1, K}$, and $\|\vec{v}\| = min$.

After differentiating the restrictions for bonds with respect to time we obtain a system of linear equations, which we supply in the complete definition:

$$\vec{x}_{i_k j_k} \cdot \left(\vec{v}_{j_k} - \vec{v}_{i_k}\right) = D^2_{i_k j_k} t,\ k = \overline{1, K}, \tag{2.1}$$

$$\sum_{i=1}^{N} \vec{v}_i^2 = \min, \tag{2.2}$$

$$\mathrm{d}\vec{x}_i / \mathrm{d}t = \vec{v}_i. \tag{2.3}$$

The search for the *closest jammed configuration* is defined as the integration of Eq. (2.3) in time, with velocities determined from Eqs. (2.1) and (2.2), until the system is jammed. A general way to determine jamming is through the infinite stationary pressure produced by particles supplied with velocities.[9]

The definition by Eqs. (2.1)–(2.3) does not require that at least one pair of particles is initially in contact. If no particles are in contact, the trivial solution to the system is zero velocities for all particles, so that they grow without movement until the first contact is formed. Therefore, integration can always be formally started from zero time.

Eqs. (2.1) and (2.2) form an operator acting on the hypervectors of the phase space, which we denote as C; it produces hypervelocity for a packing configuration, $\vec{v} = C\vec{x}$. Thus, the *closest jammed configuration* $\vec{x}_J$ is defined mathematically for an arbitrary initial configuration $\vec{x}_0$ as

$$\vec{x}_J(\vec{x}_0) = \int_0^{t_{\text{jam}}} C\vec{x}(t)\mathrm{d}t, \tag{2.4}$$

where $\vec{x}(0) = \vec{x}_0$, and t_{jam} denotes the time at which the packing jams.

Eqs. (2.1) and (2.2) pose a well-known problem of a minimum-norm solution to a linear system. Here, the particle velocities are unknown variables, and Eq. (2.1) can be rewritten as $A\vec{v} = \vec{b}$. It is known that if a linear system has at least one solution, then $\vec{v} = A^+\vec{b}$ is one of its minimum-norm solutions. Here, A^+ is a Moore–Penrose matrix pseudoinverse for A. To search for the closest jamming density, we select this solution by definition. As far as particle radii can always be increased for unjammed configurations, there is at least one solution to the system (2.1). It makes the closest jammed configuration uniquely defined for any unjammed packing.

Because the probability to encounter linearly dependent rows in the matrix A tends to zero

for packings in the thermodynamic limit, we assume that for such packings the linear system (2.1) will be of full rank. For such systems $\vec{v} = A^+\vec{b}$ is the only minimum-norm solution, and A^+ can be found explicitly as $A^T\left(AA^T\right)^{-1}$. It means that in the thermodynamic limit the choice of $\vec{v} = A^+\vec{b}$ as a solution to (2.1) is unambiguous.

If rattler particles are present in the final jammed packing, the closest jammed configuration is still defined uniquely. But we would like to join all the configurations from the limiting hyperinterval into an equivalence class; *i.e.*, consider this very packing with arbitrary positions of rattlers as the same jammed configuration. Mathematically, we define a projection operator J that selects coordinates of jammed particles from the entire configuration vector. Two jammed configurations $\vec{x}$ and $\vec{y}$ belong to the same equivalence class, if

$$J\vec{x} = J\vec{y}. \tag{2.5}$$

Each packing will jam at one and only one equivalence class of the closest jammed configurations.

The system (2.1)–(2.3) is a modified formulation of the packing generation algorithm by Zinchenko.[130] The algorithm did not contain the requirement of the hypervelocity minimization, and the solution for the system (2.1), underdetermined at the initial stage, was searched for with the conjugate gradient algorithm using previous or random velocities as an initial conjugate gradient state.

2.6.4 Further definitions

Let Ω be the entire phase space, $\Omega_P(t)$ be the phase space occupied at a given time by hypercylinders of particle contacts,

$$\Omega_P(t) = \left\{\vec{x} \in \Omega \mid \exists i, j, \|\vec{x}_{ij}\| < D_{ij}(t)\right\}, \tag{2.6}$$

and $\Omega_A(t)$ be the part of the phase space available for packing configurations at a given time,

$$\Omega_A(t) = \Omega \setminus \Omega_P(t). \tag{2.7}$$

The *basin of attraction* $\Omega(\vec{x}_0)$ of the jammed configuration $\vec{x}_0$ can then be defined as

$$\Omega(\vec{x}_0) = \left\{\vec{x} \in \Omega \mid J\vec{x}_J(\vec{x}) = J\vec{x}_0\right\}. \tag{2.8}$$

A *bounding region* for the given jammed configuration $\vec{x}_0$ at a given time (equivalently, for a given density) is defined as

$$\mathrm{B}(\vec{x}_0 t) = \Omega(\vec{x}_0) \cap \Omega_A(t). \tag{2.9}$$

Let Γ be an operator that produces a surface of a set. Then the *bounding surface* for the given *bounding region* is $\Gamma\mathrm{B}(\vec{x}_0 t)$, and the bounding region is *closed* if the bounding surface is fully

formed by hypercylinder surfaces:

$$\Gamma\mathrm{B}(\vec{x}_0 t) \subset \Gamma\Omega_P(t). \tag{2.10}$$

A state $\vec{x}$ at a given density is called a *glassy state*,[2] if it resides in a closed bounding region:

$$\Gamma\mathrm{B}(\vec{x}_J(\vec{x}), t) \subset \Gamma\Omega_P(t). \tag{2.11}$$

2.6.5 Additional properties of the closest jammed configurations

Here we investigate some additional properties of the closest jammed configurations.

Total zero velocity

Eqs. (2.1) and (2.2) automatically imply zero total velocity for a packing:

$$\sum_{i=1}^{N} \vec{v}_i = \vec{0}. \tag{2.12}$$

Let us assume that the solution to the system (2.1) and (2.2) has a non-zero total velocity, which gives an additional velocity per particle $\vec{v}_0 = \frac{1}{N}\sum_{i=1}^{N} \vec{v}_i$. We examine the solution $\vec{v}_i' = \vec{v}_i - \vec{v}_0$. It corresponds to changing the reference system and automatically complies with (2.1), which can be checked directly. The sum in Eq. (2.2) will then be transformed into

$$\sum_{i=1}^{N} \vec{v}_i'^2 = \sum_{i=1}^{N} \vec{v}_i^2 - 2\vec{v}_0 \cdot \sum_{i=1}^{N} \vec{v}_i + N\vec{v}_0^2 = \sum_{i=1}^{N} \vec{v}_i^2 - 2N\vec{v}_0 \cdot \vec{v}_0 + N\vec{v}_0^2 =$$
$$= \sum_{i=1}^{N} \vec{v}_i^2 - N\vec{v}_0^2 < \sum_{i=1}^{N} \vec{v}_i^2,$$

which means that the initial set of velocities cannot be a minimum-norm solution for (2.1). As Eq. (2.12) automatically decreases the number of degrees of freedom by three, we do not follow the convention from Salsburg and Wood[9] and do not fix one of the particles at the origin of the coordinates to get rid of three redundant degrees of freedom.

Isostaticity of random jammed packings

As proved by Salsburg and Wood,[9] the lowest estimate for the maximum number of bonds in a jammed subset of particles, excluding rattlers, for a fully periodic packing is $K_0(N') = 3(N' - 1) + 1$ (a necessary condition for polytope enclosure; N' is the number of non-rattlers). If the limiting polytope for a jammed subset of particles has $K_0(N')$ hyperplanes and the number of bonds reaches this value, it means that the configuration point lies in the vicinity of each of the polytope hyperplanes (as hyperplanes correspond to contacts), which implies that the polytope has collapsed into a single point, a jammed configuration. Some polytopes may have more than

$K_0(N')$ hyperplanes, the corresponding jammed packings are hyperstatic.

There is always a simple solution to the system (2.1) for a fully periodic packing: $\vec{v}_i = \vec{x}_i/t$ with simultaneous periodic box expansion (which can almost immediately be verified directly). If the number of bonds for any subset of N' particles equals $K_0(N')$, Eq. (2.12) together with (2.1) form a linear system of $3N'+1$equations for $3N'$ unknown velocity components and an unknown box expansion rate. As far as the matrix for the linear system (2.1) will be of full rank for random packings in the thermodynamic limit, the solution $\vec{v}_i = \vec{x}_i/t$ for this subset of particles will be unique and this subset of particles is jammed. Other particles (rattlers) may also be assigned velocities $\vec{v}_i = \vec{x}_i/t$. This proves why K_0 is not only the minimum number of bonds for non-rattlers to jam a packing, but also the only possible one in random packings, and thus would explain numerous experiments reproducing the coordination number ~ 6 for non-rattler particles in jammed packings. This also leads to a convenient termination condition for the system (2.1)–(2.3): the integration in (2.4) should be stopped when the number of bonds for non-rattler particles is equal to $K_0 = 3(N'-1)+1$.

2.6.6 Definition of the RCP limit

We recall that by V_{tot} we understand the total volume of the phase space Ω and by N the number of particles, $\vec{x}_i$ is a coordinate of the ith particle, $\vec{x} = \{\vec{x}_1, \vec{x}_2, ..., \vec{x}_N\}$ is the packing configuration vector in the phase space. Let us denote by $\varphi_J(\vec{x})$ a function that produces a density for the closest jammed configuration if the packing generation is started at a configuration $\vec{x}$. Let us denote by $V_{\text{pack}} = L_x L_y L_z$ the packing box volume. Then

$$\varphi_J(\vec{x}) = \left[\sum_{i=1}^{N} \frac{\pi}{6} D_i^3(t_{\text{jam}})\right] / V_{\text{pack}}, \tag{2.13}$$

where t_{jam} is taken from (2.4). For jammed configurations, it simply returns jamming densities. That is, as the integration in (2.4) starts from zero particle radii, particles grow without movement until the first contact appears; for jammed configurations, all the contacts appear simultaneously and the packing becomes jammed at once. Let us also introduce an indicator function Ip dependent on a logical predicate p. I is equal to unity if the predicate is true; otherwise, it is zero. Let us introduce Pp as a probability to sample a basin of attraction which conforms to a certain logical predicate. Let us also define a probability $P_{\leq}(\varphi_0)$ for Poisson packings to encounter a basin of attraction with a jamming density below φ_0:

$$P_{\leq}(\varphi_0) = P\left\{\varphi_J\left(\vec{x}\right) \leq \varphi_0\right\} = \frac{1}{V_{\text{tot}}} \int_{\Omega} I\left\{\varphi_J\left(\vec{x}\right) \leq \varphi_0\right\} \mathrm{d}\vec{x}. \tag{2.14}$$

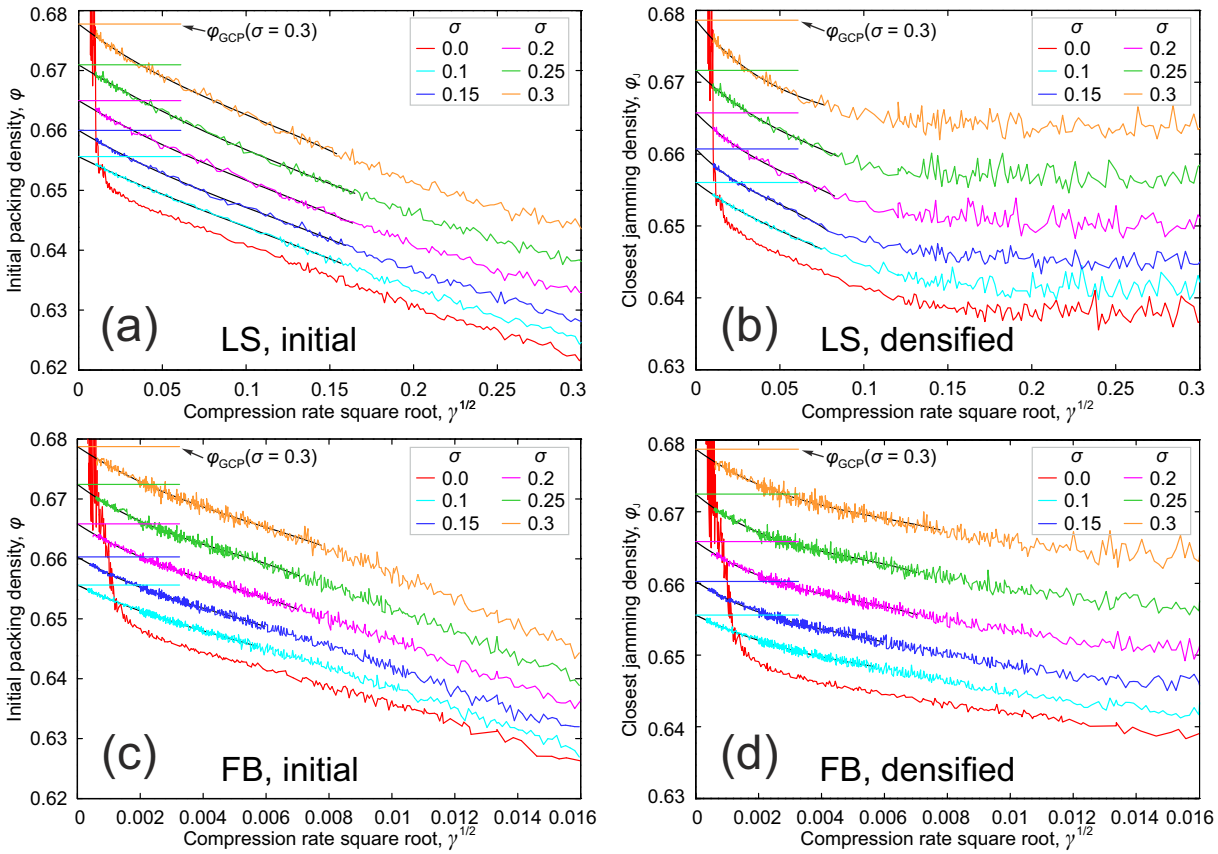

Figure 2.7: Packing density *vs.* square root of the compression rate $\sqrt{\gamma}$. (a) Densities φ of sphere packings generated with the Lubachevsky–Stillinger (LS) algorithm. (b) Closest jamming densities φ_J for the packings generated with the LS algorithm. (c) Densities φ of sphere packings generated with the force-biased (FB) algorithm. (d) Closest jamming densities φ_J for the packings generated with the FB algorithm. The meaning of colour for the different relative standard deviations σ of the log-normal sphere radii distributions is explained in the legends. Black lines are third-order least-square polynomial fits. Horizontal lines to the left are the estimated GCP limits.

Now we can mathematically define *the random close packing limit* as

$$\varphi_{\mathrm{RCP}} = \inf\left\{\varphi_0 \mid P_{\leq}(\varphi_0) = 1\right\} = \inf\left\{\varphi_0 \;\middle|\; \frac{1}{V_{\mathrm{tot}}}\int_{\Omega} I\left\{\varphi_J\left(\vec{x}\right) \leq \varphi_0\right\} \mathrm{d}\vec{x} = 1\right\}, \tag{2.15}$$

where $\inf\{x \mid p(x)\}$ is the infimum of the values x for which the predicate $p(x)$ is true. In the same manner we can define the density φ_{LT} as

$$\varphi_{\mathrm{LT}} = \sup\left\{\varphi_0 \mid P_{\geq}(\varphi_0) = 1\right\} = \sup\left\{\varphi_0 \;\middle|\; \frac{1}{V_{\mathrm{tot}}}\int_{\Omega} I\left\{\varphi_J\left(\vec{x}\right) \geq \varphi_0\right\} \mathrm{d}\vec{x} = 1\right\}, \tag{2.16}$$

where $\sup\{x \mid p(x)\}$ is the supremum of the values x for which the predicate $p(x)$ is true.

Now we transform these definitions for finite-size packings. For sufficiently large finite packings, untypical basins of attraction are still practically impossible to sample. Thus, we transform Eq. (2.15) into

$$\varphi_{\text{RCP}} = \inf \left\{ \varphi_0 \;\middle|\; \frac{1}{V_{\text{tot}}} \int\limits_{\Omega} I\left\{\varphi_J\left(\vec{x}\right) \geq \varphi_0\right\} \mathrm{d}\vec{x} \approx 1 \right\} \tag{2.17}$$

Eq. (2.16) can be transformed similarly. When packings are relatively small and all basins of attraction can in practice be sampled by Poisson packings, we have to select an arbitrary probability threshold α, *e.g.*, $\alpha = 0.95$, and define the RCP limit as

$$\varphi_{\text{RCP}} = \left\{ \frac{1}{V_{\text{tot}}} \int\limits_{\Omega} I\left\{\varphi_J\left(\vec{x}\right) \geq \varphi_0\right\} \mathrm{d}\vec{x} = \alpha \right\} \tag{2.18}$$

Eq. (2.16) can be transformed similarly. Eqs. (2.17) and (2.18) can be regarded as definitions of the RCP limit for finite packings, or as estimates for the RCP limit of infinite packings.

2.6.7 Asymptotic expansion of packing densities to the GCP limits

In this subsection of the Appendix we present the plots from Fig. 2.2 built against $\sqrt{\gamma}$ (Fig. 2.7). We fit the plots $\varphi_J(\sqrt{\gamma})$ and $\varphi(\sqrt{\gamma})$ in the main text with third-degree polynomials and expand to $\gamma = 0$ (infinite generation time) to obtain GCP limit estimates. Polynomial fits are depicted as black lines under the actual data. The GCP limits estimates (fit values at $\gamma = 0$) are depicted as horizontal lines of corresponding colour to the left of the images. The plots for data from computer simulations have no drastic changes in behavior and are fitted well, except for monodisperse packings, where crystallization starts for very slow compressions. It suggests that our estimates of the highest jamming densities are close to the real GCP limits.

Chapter 3

On the jamming phase diagram for frictionless hard-sphere packings

Authors:

Vasili Baranau and Ulrich Tallarek*

State of publication:

Published on August 05, 2014 in Soft Matter, Vol. 10.39, pp 7838–7848
DOI: 10.1039/C4SM01439A

Abstract

We computer-generated monodisperse and polydisperse frictionless hard-sphere packings of 10^4 particles with log-normal particle diameter distributions in a wide range of packing densities φ (for monodisperse packings $\varphi = 0.46 - 0.72$). We equilibrated these packings and searched for their inherent structures, which for hard spheres we refer to as closest jammed configurations. We found that the closest jamming densities φ_J for equilibrated packings with initial densities $\varphi \leq 0.52$ are located near the random close packing limit φ_{RCP}; the available phase space is dominated by basins of attraction that we associate with liquid. φ_{RCP} depends on the polydispersity and is ~ 0.64 for monodisperse packings. For $\varphi > 0.52$, φ_J increases with φ; the available phase space is dominated by basins of attraction that we associate with glass. When φ reaches the ideal glass transition density φ_g, φ_J reaches the ideal glass density (the glass close packing limit) φ_{GCP}, so that the available phase space is dominated at φ_g by the basin of attraction of the ideal glass. For packings with sphere diameter relative standard deviation $\sigma = 0.1$, $\varphi_{\text{GCP}} \approx 0.655$ and $\varphi_g \approx 0.59$. For monodisperse and slightly polydisperse packings, crystallization is superimposed on these processes: it starts at the melting transition density φ_m and ends at the crystallization offset density φ_{off}. For monodisperse packings, $\varphi_m \approx 0.54$ and $\varphi_{\text{off}} \approx 0.61$. We verified that the results for polydisperse packings are independent from the generation protocol for $\varphi \leq \varphi_g$.

3.1 Introduction

Frictionless hard-sphere packings represent a useful model for atomic systems, liquids, glasses, and crystals,[2] aside from being a system directly utilized in materials science and chemical engineering.[6,121] This simple yet powerful model exhibits a range of diverse phenomena, including melting and freezing transitions,[2,32–34,36,49,57] the ideal glass transition,[2,29,33,55,144,145] the ideal glass or the glass close packing (GCP) limit,[2,146] as well as the random close packing (RCP) limit.[1,2,12,146]

There are several attempts to merge the multitude of these effects into a single picture.[2,29] It is a difficult task, as significant debate on some of the concepts above is underway. The first big challenge is the definition and determination of the RCP limit. For monodisperse particles, there exist at least three estimates for the RCP limit, with distinct densities φ: (i) $\varphi = 0.634 - 0.636$;[1,6,11,130] (ii) $\varphi \approx 0.64$;[10,12,75,131] and (iii) $\varphi \approx 0.65$.[13,21–26,128] In our previous works,[132,146] we suggested that $\varphi \approx 0.64$ and $\varphi \approx 0.65$ refer to different phenomena and represent the RCP limit φ_{RCP} (in the sense of the J-point[146]) and a lower bound of the GCP limit φ_{GCP},[2] respectively. It implies that random jammed packings can systematically be produced at any density in the range $[\varphi_{\mathrm{RCP}}, \varphi_{\mathrm{GCP}}]$.[2,29,35] The definition and determination of the GCP limit and the corresponding ideal

[2] G. Parisi and F. Zamponi. *Rev. Mod. Phys.*, 82, 789–845, 2010.
[6] S. Khirevich, A. Höltzel, and U. Tallarek. *Commun. Comput. Phys.*, 13, 801–822, 2013.
[121] S. Khirevich et al. *J. Chromatogr. A*, 1218, 6489–6497, 2011.
[32] E. Sanz et al. *Phys. Rev. Lett.*, 106, 215701, 2011.
[33] E. Zaccarelli et al. *Phys. Rev. Lett.*, 103, 135704, 2009.
[34] C. Valeriani et al. *J. Phys.: Condens. Matter*, 23, 194117, 2011.
[36] L. Filion et al. *J. Chem. Phys.*, 133, 4115, 2010.
[49] M. Skoge et al. *Phys. Rev. E*, 74, 041127, 2006.
[57] W. G. Hoover and F. H. Ree. *J. Chem. Phys.*, 49, 3609–3617, 1968.
[29] L. Berthier and T. A. Witten. *Phys. Rev. E*, 80, 021502, 2009.
[55] G. Brambilla et al. *Phys. Rev. Lett.*, 102, 085703, 2009.
[144] G. Pérez-Ángel et al. *Phys. Rev. E*, 83, 060501, 2011.
[145] T. Voigtmann, A. M. Puertas, and M. Fuchs. *Phys. Rev. E*, 70, 061506, 2004.
[146] V. Baranau and U. Tallarek. *Soft Matter*, 10, 3826–3841, 2014.
[1] C. Song, P. Wang, and H. A. Makse. *Nature*, 453, 629–632, 2008.
[12] C. S. O'Hern et al. *Phys. Rev. E*, 68, 011306, 2003.
[11] G. D. Scott and D. M. Kilgour. *J. Phys. D: Appl. Phys.*, 2, 863–866, 1969.
[130] A. Zinchenko. *J. Comput. Phys.*, 114, 298–307, 1994.
[10] J. D. Bernal and J. Mason. *Nature*, 188, 910–911, 1960.
[75] Y. Jin and H. A. Makse. *Physica A*, 389, 5362–5379, 2010.
[131] J. G. Berryman. *Phys. Rev. A*, 27, 1053–1061, 1983.
[13] S. C. Kapfer et al. *Phys. Rev. E*, 85, 030301, 2012.
[21] A. V. Anikeenko and N. N. Medvedev. *Phys. Rev. Lett.*, 98, 235504, 2007.
[22] A. V. Anikeenko, N. N. Medvedev, and T. Aste. *Phys. Rev. E*, 77, 031101, 2008.
[23] T. Aste and T. Di Matteo. *Eur. Phys. J. B*, 64, 511–517, 2008.
[24] B. A. Klumov, S. A. Khrapak, and G. E. Morfill. *Phys. Rev. B*, 83, 184105, 2011.
[25] M. Bargieł and E. M. Tory. *Adv. Powder Technol.*, 12, 533–557, 2001.
[26] K. Lochmann et al. *Eur. Phys. J. B*, 53, 67–76, 2006.
[128] T. Aste and A. Coniglio. *EPL*, 67, 165–171, 2004.
[132] V. Baranau et al. *Soft Matter*, 9, 3361–3372, 2013.
[35] P. Chaudhuri, L. Berthier, and S. Sastry. *Phys. Rev. Lett.*, 104, 165701, 2010.

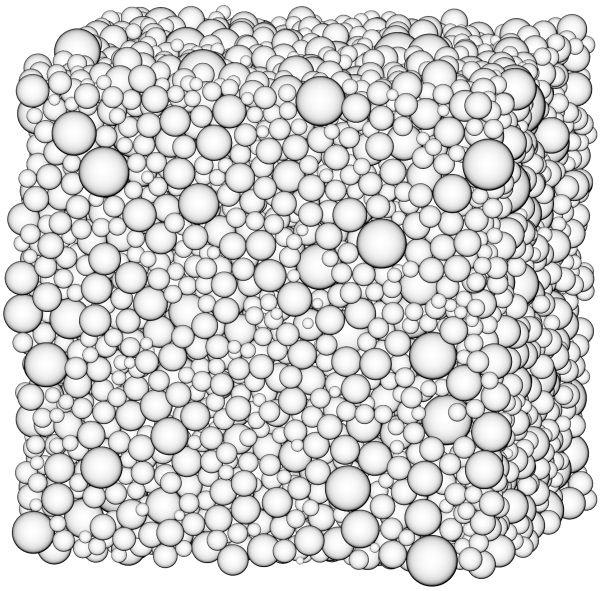

Figure 3.1: Closest jammed configuration at a density $\varphi = 0.662$ for a random packing of 10^4 polydisperse spheres. The sphere radii distribution is log-normal and has a relative standard deviation $\sigma = 0.3$. The initial unjammed packing was generated with the force-biased algorithm at a density $\varphi = 0.613$.

glass transition represent the second actively discussed topic,[2,29,43] stemming from research on glasses and colloids. It is debated whether the ideal glass exists and if so, what is the density of the ideal glass transition. It is unclear if there are multiple glassy states and what is the lowest glass transition density.

We believe that the RCP and GCP limits shall be studied together, as a part of the systematic investigation of the phase space structure for hard spheres. At each packing density φ, the phase space has areas corresponding to valid packing configurations. These areas are comprised of basins of attractions of jammed configurations.[39,54,60] Some of these basins dominate the available phase space. Thus, one of the characteristics of the phase space at a given φ is the jamming density of these dominant basins of attraction, φ_J. The main objective of this paper is to build a mapping from φ to φ_J for a wide range of initial densities φ.

With this intention to study the structure of the phase space for hard spheres from first principles, we computer-generated monodisperse and polydisperse frictionless hard-sphere packings of 10^4 particles (*cf.* Fig. 3.1) over a wide range of densities φ (for monodisperse packings $\varphi = 0.46 - 0.72$). Polydisperse particles have log-normal diameter distribution with diameter relative standard deviation (polydispersity) σ from 0.05 to 0.3 in steps of 0.05. Then, we equilibrated these packings to let packing configurations arrive at the basins of attraction of inherent structures[39,54,60] that dominate the phase space at given densities. Finally, we searched for the

[43] L. Berthier and G. Biroli. *Rev. Mod. Phys.*, 83, 587–645, 2011.
[39] F. H. Stillinger. *Science*, 267, 1935–1939, 1995.
[54] S. Torquato and Y. Jiao. *Phys. Rev. E*, 82, 061302, 2010.
[60] F. H. Stillinger, E. A. DiMarzio, and R. L. Kornegay. *J. Chem. Phys.*, 40, 1564–1576, 1964.

Table 3.1: Important symbols used in this chapter.

Symbol	Brief description	Key figures and tables	Values for $\sigma = 0$
σ	Relative standard deviation (polydispersity) of the log-normal particle radii distributions		
γ	Compression rate for initial packing generation	X-axis in Fig. 3.2a and Fig. 3.7	
φ	Initial packing density after force-biased generation	Y-axis in Fig. 3.2a, X-axis in Fig. 3.2b-d	
φ_{CJ}	Closest jamming density of a packing	Y-axis in Fig. 3.2b	
φ_J	Dominant jamming density of a packing	Y-axis in Fig. 3.2d	
φ_{LT}	Lowest typical jamming density		
φ_{RCP}	Random-close packing limit (J-point[146])	Left sides of Fig. 3.2b-d	~ 0.64
φ_{GCP}	Glass close packing limit	Right sides of Fig. 3.2b-d; Table 3.2	~ 0.65
φ_{HCP}	Crystalline packing density for monodisperse packings (FCC or HCP crystals)		~ 0.74
φ_{max}	Highest packing density: φ_{HCP} for monodisperse packings, φ_{GCP} for sufficiently polydisperse packings		~ 0.74
φ_L	Lowest possible jamming density, at least $2/3 \cdot \varphi_{\text{HCP}}$ for monodisperse packings (density of tunnelled crystals[137])		~ 0.49
φ_m	Melting transition density (onset of crystallization)	Fig. 3.2c and d	~ 0.545
φ_{off}	Offset of crystallization	Fig. 3.2c and d	~ 0.61
φ_f	Freezing transition density	Fig. 3.4	~ 0.494
φ_g	Ideal glass transition density. $\varphi_J(\varphi_g) = \varphi_{\text{GCP}}$	Fig. 3.2c and d; Table 3.2	~ 0.585
φ_{MCT}	Density at which available phase space becomes relatively disjoint. $\varphi_J\,(\varphi < \varphi_{\text{MCT}}) = \varphi_{\text{RCP}}$	Fig. 3.2c and d	~ 0.52

inherent structures of these equilibrated configurations. In this paper, we use for hard spheres the term “closest jammed configurations” instead of “inherent structures”.

The paper is structured as follows. Before we present any experimental results, we use Section 3.2 to start with definitions that are relevant for the subsequent discussion. These include closest jammed configuration, basin of attraction of a closest jammed configuration, bounding region, bounding surface, and others. An inherent structure for an arbitrary configuration of hard spheres is a jammed configuration that is the closest one to the initial configuration, hence the term closest jammed configuration.[146] We describe the methods that we use to generate packings, to conduct equilibration, and to search for the closest jammed configurations in Section 3.3. Section 3.4 contains the results of packing generation, subsequent equilibration, and searching for the closest jammed configurations. We discuss these results in the same section. Section 3.5 presents a summary and conclusions.

3.2 Definitions

In this section, we briefly provide definitions needed for the rest of the paper. A more elaborate discussion and precise mathematical definitions of most of them can be found in our previous paper.[146]

We rely on the phase space packing description introduced by Salsburg and Wood[9] and therefore use the terms “limiting polytope”, “hypersurface”, and “hypercylinder” from their

[9] Z. W. Salsburg and W. W. Wood. *J. Chem. Phys.*, 37, 798–804, 1962.

paper. Particle velocities are not included in the phase space. Under jamming, we understand collective jamming in packings of frictionless particles.[3,14,30,31] A packing is called jammed if at least a subset of its particles is jammed; other particles are referred to as rattlers. In this paper, we do not exclude rattler particles from packings, when calculating packing densities.

We utilize the concept of inherent structures, initially introduced by Stillinger for packings of particles with soft potential.[39,54,60] Inherent structures for such systems are local potential energy minima in the phase space. Potential energy in hard-sphere packings is replaced by the maximum density that a packing can have at a given phase space point, taken with the minus sign. Maximum density is calculated by fixing particle coordinates and inflating particle radii until the first contact between particles occurs. Inherent structures for hard-sphere packings correspond to jammed configurations.[146] To emphasize that we are investigating hard particles, not particles with soft potential, we use below in this paper the term "closest jammed configuration" instead of "inherent structure".

Each potential energy minimum can be associated with a corresponding basin of attraction. *I.e.*, the energy minimum of a given basin of attraction is the termination point of energy minimization—the steepest descent procedure—for any configuration in this basin of attraction. Bounding region of a given jammed configuration at a given density is by definition the intersection of this configuration's basin of attraction with the available phase space (when contact hypercylinders for the given density are excluded from the phase space). We define bounding surfaces as surfaces of bounding regions. A bounding region is closed if the bounding surface is fully formed by hypercylinder surfaces.

We define the GCP limit (φ_{GCP}) for sufficiently polydisperse packings as the highest possible jamming density of these packings.[146] For monodisperse and slightly polydisperse packings, it is the highest jamming density that can be achieved if crystallization is artificially suppressed.[146] If crystallization is allowed, the GCP limit is revealed by an entropy minimum.[22,132] We define the RCP limit φ_{RCP} as the upper bound of the J-segment.[12,133,147] Similarly, the lowest typical (LT) jamming density φ_{LT} is the lower bound of the J-segment.

We distinguish between typical basins of attraction and untypical ones. Basins of attraction with jamming densities in the range $[\varphi_{\mathrm{LT}}, \varphi_{\mathrm{RCP}}]$ are typical by definition; the others are untypical. With increasing number of particles in the packings, φ_{RCP} is almost unchanged and φ_{LT} increases.[12] Thus, we may estimate φ_{RCP} in the thermodynamic limit by the upper boundary of the J-segment for sufficiently large finite packings. In the present paper, we assume that the J-segment converges in the thermodynamic limit to a single value φ_{RCP},[12] though this question is still discussed.[133] Let $\varphi_{\max}$ be the highest possible packing density for a given sphere diameter distribution: it is the crystalline density (~ 0.74) for monodisperse packings and φ_{GCP} for sufficiently polydisperse

[3] S. Torquato and F. H. Stillinger. *Rev. Mod. Phys.*, 82, 2633–2672, 2010.
[14] S. Torquato, T. M. Truskett, and P. G. Debenedetti. *Phys. Rev. Lett.*, 84, 2064–2067, 2000.
[30] A. Donev. *J. Appl. Phys.*, 95, 989–999, 2004.
[31] A. Donev et al. *J. Comput. Phys.*, 197, 139–166, 2004.
[133] M. Pica Ciamarra, M. Nicodemi, and A. Coniglio. *Soft Matter*, 6, 2871–2874, 2010.
[147] R. Ni, M. A. Cohen-Stuart, and M. Dijkstra. *Nat. Commun.*, 4, 2704, 2013.

packings. Then, untypical basins of attraction have jamming densities in the range $[\varphi_L, \varphi_{\text{LT}}) \cup (\varphi_{\text{RCP}}, \varphi_{\max}]$, where φ_L is the lowest jamming density, which for monodisperse packings equals at least $\sqrt{2}\pi/9 \approx 0.49365$ (the density of tunneled crystals).[46,54,67,137,138]

Typical and untypical basins of attraction have just been defined for Poisson packings, *i.e.*, when the entire phase space is available or, in other words, when initial packing densities are zero. Under typical closest jamming densities for non-zero initial packing densities we understand the closest jamming densities that will be almost always found for packings created at a given density using a given algorithm, if it starts generation at a Poisson configuration. If the jamming density of a bounding region lies in the range $[\varphi_{\text{LT}}, \varphi_{\text{RCP}}]$, we refer to this region and all the configurations in this region as liquid. Earlier, we talked about the part of the phase space that is available at a given density. Parts of the available phase space may be completely separated with contact hypercylinders and may have different properties. Thus, it is important to talk about the part of the phase space that is achievable from a given type of configurations. If a bounding region covers the almost entire part of the phase space that is achievable from a given type of configurations (at a given density), we call this region dominant. Liquid, typical, and dominant basins of attraction coincide for zero initial packing density.

3.3 Methods

3.3.1 Packing generation

Particles in our polydisperse packings have log-normal radii distributions with relative standard deviations σ from 0.05 to 0.3 in steps of 0.05 (the particle mean diameter is normalized to unity). All packings are generated in a fully periodic cubic box and contain 10^4 particles (*cf.* Fig. 3.1). Packings are created in a wide range of compression rates using the force-biased (FB) protocol.[98,99] This protocol is a modification of the Jodrey–Tory algorithm.[96,97] The FB algorithm starts from a random distribution of particle centers in a simulation box. Each particle is supplied with an inner diameter chosen to be proportional to the desired particle diameter and to make particles in the closest pair touch each other with their inner diameter shells. Alternatively, a single inner diameter ratio can be specified for the entire packing as the ratio of inner diameters to the desired particle diameters. Similarly, a packing is supplied with an outer diameter ratio, initially larger than unity. The initial outer diameter ratio is chosen to ensure that the total volume of the particles equals the box volume. Particles are also supplied with elastic potential of the third order by overlap distance,[99] which is cut-off at the outer particle shell. It is now possible to compute the forces between each pair of particles, as well as the net forces for each particle. The algorithm is

[46] M. Pica Ciamarra et al. *Soft Matter*, 8, 9731–9737, 2012.
[67] M. Pica Ciamarra and A. Coniglio. *Phys. Rev. Lett.*, 101, 128001, 2008.
[137] S. Torquato and F. H. Stillinger. *J. Appl. Phys.*, 102, 093511, 2007.
[138] Y. Jiao, F. H. Stillinger, and S. Torquato. *J. Appl. Phys.*, 109, 013508, 2011.
[98] J. Mościński et al. *Mol. Simul.*, 3, 201–212, 1989.
[99] A. Bezrukov, M. Bargieł, and D. Stoyan. *Part. Part. Syst. Char.*, 19, 111–118, 2002.
[96] W. S. Jodrey and E. M. Tory. *Phys. Rev. A*, 32, 2347–2351, 1985.
[97] M. Bargieł and J. Mościński. *Comput. Phys. Commun.*, 64, 183–192, 1991.

iterative and each iteration proceeds as follows: (i) determine a net force for each particle; (ii) displace all the particles by distances proportional to the particles' net forces and in the direction of the net forces; (iii) decrease the outer diameter ratio according to a specified contraction rate; and (iv) update the inner diameter ratio so that the inner diameter shells for the pair of closest particles touch each other. Though the inner diameter ratio may decrease through the iterations, its value has an increasing trend. The algorithm terminates when the outer diameter ratio is equal to the inner diameter ratio. The lower the outer diameter ratio contraction rate, the denser is the final configuration. The source code used in this paper is available under the MIT free software license.[136]

3.3.2 Packing equilibration

Salsburg and Wood[9] derived an equation of state for hard spheres, $p = 1 + 1 \Big/ \left[\left(\varphi_{\mathrm{CJ}} / \varphi_{\mathrm{CJ}} \right)^{1/d} - 1 \right]$, where p is the estimated reduced pressure, φ is the current packing density, φ_{CJ} is the (closest) jamming density for the polytope where the given packing configuration resides, and d is the dimensionality of the system.[49] The derivation of Salsburg and Wood[9] assumes that the pressure is stationary and packings are in equilibrium. But all the packings produced in computer simulations or experiments are intrinsically out of equilibrium,[132,134] because the generation process is non-stationary by definition, especially for fast compressions. The pressure measured in the course of a packing generation should therefore not be used for the estimation of φ_{CJ} or for the tracking of jamming; instead, packings should be equilibrated preliminary, *i.e.*, exposed to molecular dynamics simulation with zero compression rate until the pressure is stationary. Equilibration moves the packing to bounding regions that dominate the part of the phase space achievable from an initial configuration.

We equilibrate the packings by performing sets of 2×10^7 collisions with zero compression rate in a loop until the relative difference of reduced pressures in the last two sets is less than 10^{-4}, so the pressure can be regarded as stationary. More precisely, to measure the pressure during 2×10^7 collisions, we average pressures for 100 sub-sets of 2×10^5 collisions, which amounts to 20 collisions in a sub-set per particle. We use our own implementation[136] of the Lubachevsky–Stillinger (LS) packing generation algorithm[95,135] to carry out the equilibration.

3.3.3 Searching for the closest jammed configurations

To search for the closest jammed configurations, we do not follow the definition of these configurations through the steepest descent energy minimization, but modify the LS algorithm instead. We run the LS algorithm with a high compression rate of 10, until the non-equilibrium reduced pressure reaches a conventional high value of 10^{12}, then decrease the compression rate by a

[136] V. Baranau https://code.google.com/p/packing-generation/
[134] M. C. Vargas and G. Pérez-Ángel. *Phys. Rev. E*, 87, 042313, 2013.
[95] B. D. Lubachevsky and F. H. Stillinger. *J. Stat. Phys.*, 60, 561–583, 1990.
[135] B. D. Lubachevsky. *J. Comput. Phys.*, 94, 255–283, 1991.

factor of two and run the LS algorithm again, until the pressure is high enough again (10^{12}). We repeat this procedure until the compression rate is $\leq 10^{-4}$. The Boltzmann constant and masses of all particles are set to unity; the temperature is set to 0.2. Fast compressions at the beginning of the search make the initial bounding region collapse as much as possible and at the same time retain the configuration point in this bounding region. Slow compressions at the end of the search allow arriving at a truly jammed configuration. The details and validation of this algorithm are provided in our previous paper.[146] There we ensured that the distribution of closest jamming densities for packings before equilibration is independent of a particular set of algorithm parameters in a wide range of the latter. We did not repeat this validation for equilibrated packings, as packings before equilibration in the previous paper covered the entire range of polydispersities as well as the entire range of initial and final packing densities considered in the present paper. Searching for the closest jammed configurations after equilibration produces dominant jamming densities.

3.4 Results and discussion

In this section, we present the results of the packing equilibration and of searching for the closest jammed configurations of the equilibrated packings. We give an overview of the data in Subsection 3.4.1 (Data overview), analyze the data in Subsection 3.4.2 (Data analysis), test our conclusions for independence from the packing generation protocol in Subsection 3.4.3 (Protocol independence), and finally provide a schematic diagram with the phase space structure in Subsection 3.4.4 (Schematic phase space structure). At the end of the section, in Subsection 3.4.5 (Applicability of liquid equations of state), we check if it is possible to recover the properties of the phase space through comparison of the reduced pressure to predictions from liquid equations of state. To ease the reading of this section, we provide with Table 3.1 an overview of the symbols used below. Some of them have already been introduced, others will be defined later.

3.4.1 Data overview

The dependence of initial packing densities φ on the inverse compression rate γ^{-1} for packings produced with the FB algorithm is shown in Fig. 3.2a. Even before equilibration, we searched for the closest jamming densities φ_{CJ} for these packings, as described in Section 3.3.3; Fig. 3.2b depicts for these packings the closest jamming densities φ_{CJ} *vs.* initial packing densities φ. Then, we equilibrated the initial packings in Fig. 3.2a and calculated closest jamming density estimates φ_{JE} from the equation of state by Salsburg and Wood, as described in Section 3.3.2. Closest jamming density estimates after equilibration φ_{JE} *vs.* initial packing densities φ are shown in Fig. 3.2c. Finally, we searched for the actual closest jammed configurations of the equilibrated packings (dominant jammed configurations). Dominant jamming densities φ_J *vs.* initial packing densities φ are shown in Fig. 3.2d. The same four plots, built *vs.* γ^{-1}, can be found in the Appendix (Section 3.6.1).

We did not average the data in Fig. 3.2; each point in these figures corresponds to a single

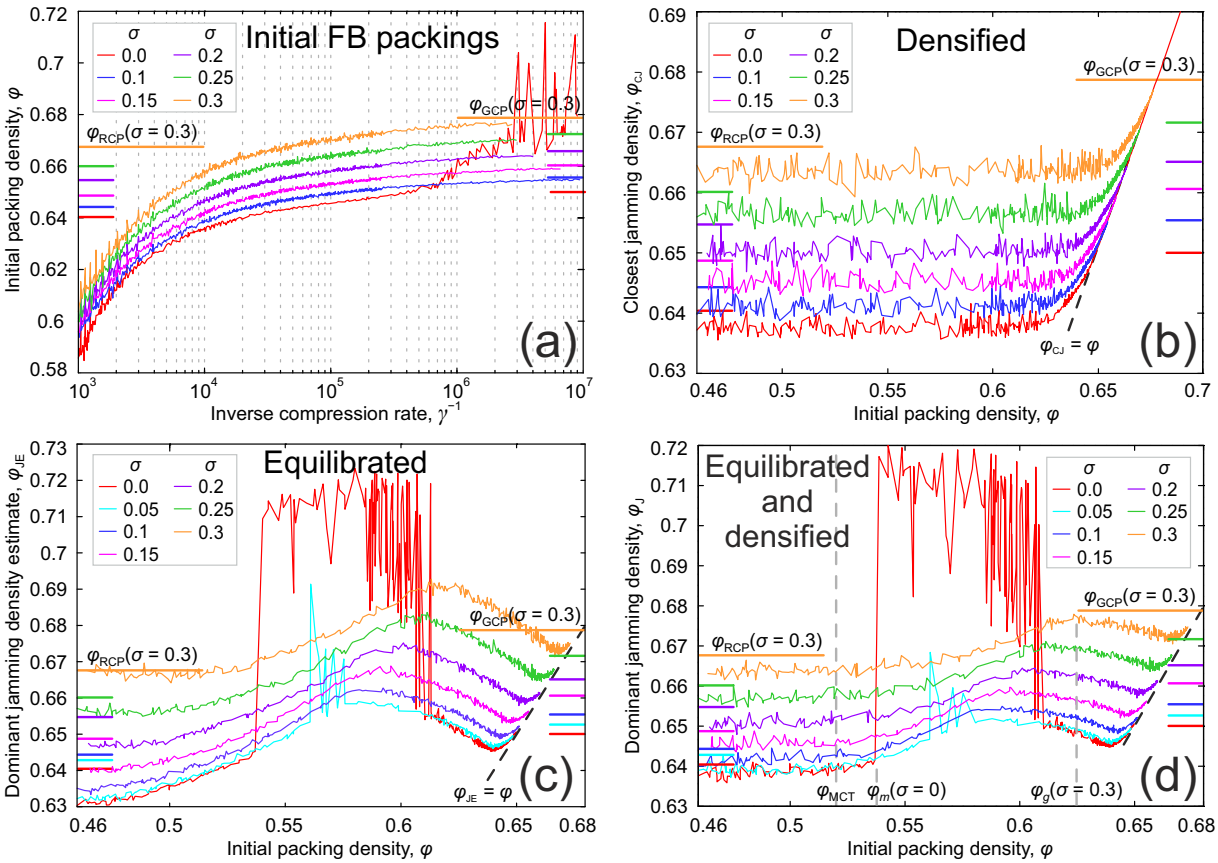

Figure 3.2: (a) Initial packing density φ *vs.* inverse compression rate γ^{-1}. (b) Closest jamming density before equilibration φ_{CJ} *vs.* initial packing density φ. (c) Closest jamming density estimate after equilibration φ_{JE} *vs.* initial packing density φ. (d) Closest jamming density after equilibration φ_J *vs.* initial packing density φ. All the packings were generated with the force-biased (FB) algorithm. Colours for the different relative standard deviations σ of the log-normal particle radii distributions are depicted in the legends.

packing. To guide the eye, points have been connected by straight lines. Averaging assumes that fluctuations in the data will disappear in the thermodynamic limit. This question is still unresolved.[12,133] If fluctuations disappear for infinite packings, averaging also assumes that the noise stemming from finite-size effects is symmetrical around the true value. This is not the case for the closest jamming densities of Poisson packings: the J-segment decreases with the increase of the number of particles, but its upper boundary φ_{RCP} is almost unchanged, only the lower boundary φ_{LT} is moving upwards.[12] Thus, averaging would not produce meaningful results; taking the upper boundary of the J-segment instead will give a better estimate of φ_{RCP} in the thermodynamic limit. Additionally, averaging would remove the information about the exact boundaries of jamming intervals for finite packings.

The RCP densities φ_{RCP} are included as horizontal lines on the left side of the plots in Fig. 3.2. Similarly, the GCP densities φ_{GCP} are shown as horizontal lines on the right side of these plots. We determined the RCP limits as the upper boundaries of the horizontal parts of the plots in Fig.

3.2b, because the horizontal parts of the plots correspond to the closest jamming densities of Poisson packings.[146] We determined the GCP limits for $\sigma \geq 0.05$ by asymptotically expanding the plots $\varphi(\gamma^{-1})$ (Fig. 3.2a) and $\varphi_{\text{CJ}}(\gamma^{-1})$ (Fig. 3.7b in Section 3.6.1 of the Appendix) into infinite generation time or zero compression rate. φ_{GCP} for monodisperse packings was taken at the value of a structural transition $\varphi \approx 0.65$.[13,21–26,128,132,146] More details on the determination of φ_{RCP} and φ_{GCP} can be found in our previous paper.[146]

3.4.2 Data analysis

The closest jamming densities of initial packings (without preliminary equilibration), Fig. 3.2b, belong to the interval $[\varphi_{\text{LT}}, \varphi_{\text{RCP}}]$ for $\varphi \leq 0.61$ in the case of monodisperse packings and for $\varphi \leq 0.63$ for packings with $\sigma = 0.3$. We may say that for these initial densities liquid bounding regions are typical for the FB algorithm. When we talk about available phase space below in this section, we will always mean available and achievable from the configurations typical for the FB algorithm (which are liquid for $\varphi < [0.61, 0.63]$, the exact value depending on σ). In the remainder of the paper, we focus on Fig. 3.2d.

Spontaneous crystallization, estimation of φ_m and φ_{off}

For monodisperse packings, bounding regions of configurations with crystalline inclusions dominate the available phase space in the density range $\varphi \approx 0.54 - 0.61$ ($\sigma = 0$, red line in Fig. 3.2d). It is manifested by a sudden departure of the $\varphi_J(\varphi)$ plot up to almost crystalline densities. This interval conforms to other studies of spontaneous crystallization and crystal nucleation.[32–34,36] These studies show that the crystal nucleation rate in monodisperse hard sphere packings is negligible for $\varphi < 0.54$, then grows rapidly at $\varphi \approx 0.54$ and reaches a plateau, and then rapidly decreases at $\varphi \approx 0.61$.[36] The density ~ 0.54 is interpreted as the melting transition density φ_m (dedicated studies produce the value $\varphi_m \approx 0.545$[2,49,57] for monodisperse packings). The density $\varphi \approx 0.61$ was earlier interpreted as the (ideal) glass transition density φ_g for monodisperse hard spheres,[56] which is usually detected by a rapid decrease of compressibility or self-diffusivity. Recent accurate studies show that the ideal glass transition happens at $\varphi_g \approx 0.585$, while at the same time crystallization is prevented after $\varphi \approx 0.61$.[32–34] Thus, we refer to $\varphi \approx 0.61$ as the density of the offset of crystallization φ_{off}. The interval of densities where bounding regions of configurations with crystalline inclusions dominate the phase space of packings with $\sigma = 0.05$ is $\varphi \approx 0.56 - 0.58$, which can be seen in a sudden departure of the dominant jamming densities in the plot $\varphi_J(\varphi)$ (cyan line in Fig. 3.2d). This range is also consistent with other results ($\varphi = 0.56 - 0.59$).[33,148] Our data report that crystallization becomes impossible for a certain σ in the range $(0.05, 0.1)$. Nucleation studies determine that crystallization in packings with Gaussian diameter distribution becomes impossible for $\sigma \approx 0.07$;[33,148] which conforms to our results (though we investigate log-normal sphere diameter distributions, for such a small polydispersity the two distributions almost coincide).

[56] W. van Megen and S. M. Underwood. *Phys. Rev. E*, 49, 4206–4220, 1994.
[148] P. N. Pusey et al. *Phil. Trans. R. Soc. A*, 367, 4993–5011, 2009.

Table 3.2: Ideal glass transition densities φ_g and corresponding ideal glass densities φ_{GCP} for packings of hard frictionless spheres with log-normal sphere diameter distributions having different diameter relative standard deviations σ (as indicated). φ_g *vs.* σ is plotted in Fig. 3.3.

σ	0.0	0.05	0.1	0.15	0.2	0.25	0.3
φ_g	0.585	0.586	0.59	0.595	0.602	0.61	0.622
φ_{GCP}	0.65	0.6518	0.6549	0.6596	0.6645	0.6711	0.6779

Change in the phase space structure at $\varphi_{\text{MCT}} \approx 0.52$

For $\varphi \leq 0.52$, the available phase space is strongly connected and dominated by liquid bounding regions for all the packing types. Thus, the closest jamming densities after equilibration are always obtained in the range of liquid jamming densities, $\varphi_J \in [\varphi_{\text{LT}}, \varphi_{\text{RCP}}]$. Starting from a certain density $\varphi \approx 0.52$, the interval of dominant jamming densities moves upward, and starting from a slightly higher characteristic density the dominant jamming density φ_J is always higher than φ_{RCP}. It means that none of the liquid bounding regions participates in dominating the available phase space any longer. Packings with slight polydispersity $\sigma = 0.05$ clearly demonstrate that the onset of crystallization does not coincide in general with this characteristic density associated with the changes in the structure of the phase space. Changes in the phase space at $\varphi \approx 0.52$, independent of the particle size distribution, are predicted under certain assumptions by the mode-coupling theory;[33,145] thus, we denote this transition density with φ_{MCT}. We assume that bounding regions become relatively disjoint at this density (*i.e.*, the fraction of the "wormholes" in bounding surfaces becomes low).[2] We show later, in Section 3.4.3, that the available phase space truly splits into disconnected portions and becomes non-ergodic only at the ideal glass transition density φ_g, which for monodisperse packings equals ~ 0.585.

Glass close packing limit, estimation of φ_{GCP}

For packings with $\sigma \geq 0.1$ and $\varphi \geq \varphi_{\text{MCT}}$, the jamming density of the dominant bounding regions increases and reaches maxima at certain densities depending on σ. We associate these maxima in Fig. 3.2d with the GCP limits φ_{GCP} (and corresponding packing configurations with the ideal glass), as the GCP limits for packings where crystallization is impossible are by definition the highest jamming densities of these packings. For packings with $\sigma = 0$ and $\sigma = 0.05$ crystallization effects are superimposed on the $\varphi_J(\varphi)$ plots in Fig. 3.2d. For monodisperse packings crystallization is no longer possible at $\varphi_{\text{off}} \approx 0.61$. To the right of this density the dominant jamming density φ_J is ~ 0.65, which also conforms to the density of the onset of crystalline inclusions in jammed packings and the density where the entropy is minimal $\varphi_{\text{GCP}} \approx 0.65$.[13,21–26,128,132,146] For polydisperse packings with $\sigma = 0.05$, crystallization is superimposed on the $\varphi_J(\varphi)$ plot in the range $\varphi \approx 0.56 - 0.58$, but it does not cover the local maximum $\varphi_J \approx 0.652$ at $\varphi \approx 0.586$; so we attribute $\varphi_J \approx 0.652$ to the GCP limit of particles with $\sigma = 0.05$. The estimates of the GCP limits compare very well to the GCP limit estimates from our previous paper,[146] where we extrapolated the closest jamming densities of computer-generated packings with $\sigma \geq 0.05$ to infinite generation time. The values from our previous paper[146] are displayed as the lines of corresponding color to the right of Fig. 3.2d. The differences between the two estimates are

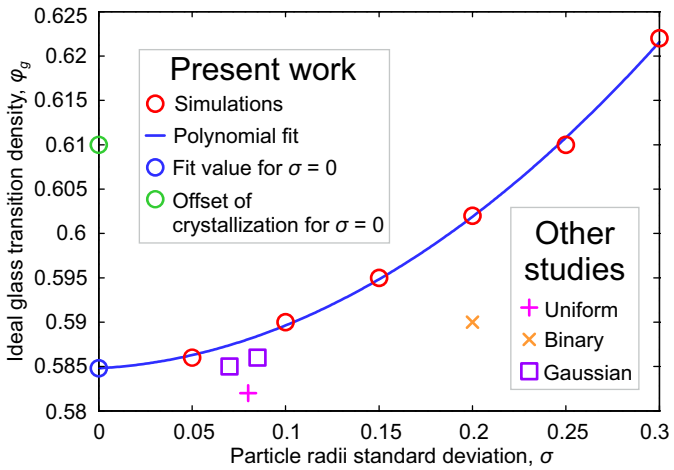

Figure 3.3: Ideal glass transition density φ_g *vs.* sphere radii relative standard deviation σ of the log-normal radii distributions (◯). Values of φ_g are summarized in Table 3.2. Estimates for φ_g from other works are also presented: 10^3 particles with uniform distribution (+);[144] binary 50:50 mixture of 10^3 particles with diameter ratio 1.4 (×);[55] and 2×10^3 particles with Gaussian distribution (□).[33]

$< 10^{-3}$ for all the packing types.

Ideal glass transition, estimation of φ_g

The initial packing density φ for which the dominant jamming density reaches its maximum is called the density of the ideal glass transition φ_g. It is usually measured through the jump in compressibility and divergent alpha-relaxation time.[2,29,33,49] We estimated φ_g from Fig. 3.2d in the following way: (i) first, we took the data points $\varphi_J(\varphi)$ from Fig. 3.2d in the vicinity of the expected ideal glass transitions (*i.e.*, in the interval ± 0.02 around the global maxima of the $\varphi_J(\varphi)$ plots); (ii) then, we selected local maxima from these data points (because local maxima represent upper boundaries of jamming intervals at each φ); and (iii) fitted these local maxima with third-order polynomials and found the positions of maxima for these polynomials. We consider these positions of maxima as the estimates for φ_g, which are depicted in Fig. 3.3. We fitted φ_g for $\sigma \geq 0.05$ with the third-order polynomial and display it in Fig. 3.3 as well. The extrapolation of this polynomial to monodisperse packings gives a value $\varphi_g = 0.585$. We assume that if crystallization is artificially suppressed in monodisperse packings (*e.g.*, by pinning a certain fraction of particles[139]), the $\varphi_J(\varphi)$ plot will look similar to those for polydisperse packings with $\sigma \geq 0.1$, reaching its maximum value at $\varphi = \varphi_g \approx 0.585$ with $\varphi_J(\varphi_g) = \varphi_{\text{GCP}} \approx 0.65$. It would explain why crystalline inclusions appear in generated packings (prior to equilibration) only at the initial density $\varphi = \varphi_{\text{GCP}} \approx 0.65$:[13,21–26,128,132,146] If $\varphi_{\text{GCP}} \approx 0.65$ is the highest (jamming) density for monodisperse packings with suppressed crystallization, the only way to produce denser packings—for protocols that try to avoid crystallization as long as possible—is to introduce crystalline inclusions in the packing structure. We provide the values for φ_g and φ_{GCP} obtained so far in Table 3.2. Our data comply well with predictions from the mode-coupling theory,[145]

[139] R. L. Jack and L. Berthier. *Phys. Rev. E*, 85, 021120, 2012.

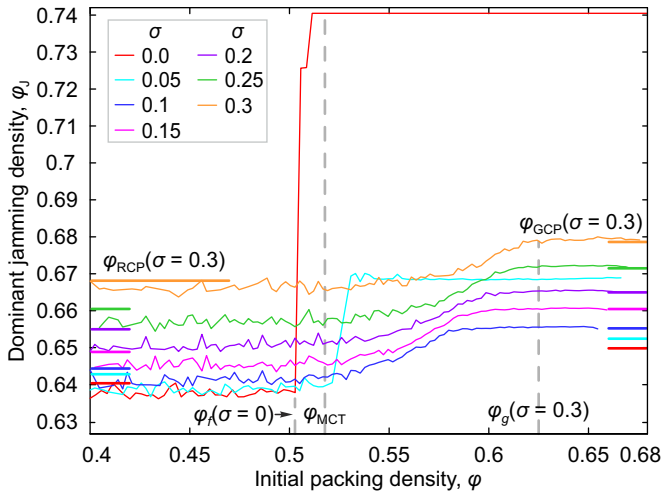

Figure 3.4: Closest jamming density after equilibration φ_J *vs.* initial packing density φ. Colors for the different relative standard deviations σ of the log-normal particle radii distributions are depicted in the legend. All the initial packings were created by proportional decrease of the radii of the densest jammed packings of a corresponding σ (represented as the global maxima of the plots in Fig. 3.2d).

simulations and experimental observations of divergent relaxation times: $\varphi_g = 0.582$ is reported for packings of 10^3 particles with uniform distribution having $\sigma = 0.082$;[144] $\varphi_g = 0.59$ is reported for a binary $50{:}50$ mixture of 10^3 particles with diameter ratio 1.4;[55] $\varphi_g = 0.585$ and 0.586 are reported for packings of 2×10^3 particles with Gaussian distributions of $\sigma = 0.07$ and 0.085, respectively.[33] We display these values in Fig. 3.3 as well. For binary mixtures, σ is computed as relative standard deviation of corresponding discrete probabilities of encountering a specific sphere radius.

We can now call the basins of attraction, the bounding regions, and all the configurations with $\varphi_J \in (\varphi_{\mathrm{RCP}}, \varphi_{\mathrm{GCP}}]$ as glassy, for both monodisperse and polydisperse packings. This definition conforms to the fact that for $\sigma \geq 0.1$ and $\varphi > \varphi_{\mathrm{MCT}}$ glassy bounding regions dominate the available phase space instead of liquid bounding regions. For monodisperse packings it also conforms to the fact that crystalline inclusions appear in jammed packings only for $\varphi > \varphi_{\mathrm{GCP}}$.[13,22,24–26,132] In our previous paper,[146] we referred to the states in closed bounding regions as glassy (following Parisi and Zamponi[2] and Brambilla *et al.*[55]) because for such states there is only one jammed configuration in the achievable phase space and the configurational entropy is zero. This definition is unsuitable in the light of the current results, as the states in closed liquid bounding regions (that dominate the phase space for $\varphi \leq \varphi_{\mathrm{MCT}}$) would be called glassy as well.

3.4.3 Protocol independence

To check if our results are protocol-dependent, we did the following: We (i) took the densest jammed packings obtained in Fig. 3.2 (the FCC crystal for monodisperse packings, the densest partially crystallized packing for $\sigma = 0.05$, and the ideal glass packings for $\sigma \geq 0.1$); (ii) proportionally reduced the radii of the particles in these packings to produce unjammed packings

in the entire range of densities starting from $\varphi = 0.4$ (we call these packings "diluted densest packings", they represent a completely different packing generation protocol); and (iii) repeated the procedure for Fig. 3.2d, *i.e.*, we equilibrated these packings and searched for the closest jammed configurations φ_J for the equilibrated packings. Fig. 3.4 depicts the plot $\varphi_J(\varphi)$ for these diluted densest packings. The horizontal lines to the left and to the right of the figure represent the RCP and GCP limits from Fig. 3.2d.

Monodisperse packings exhibit a well-known freezing transition at $\varphi_f \approx 0.5$ (the value obtained in dedicated studies is ~ 0.494).[2,49,57] Polydisperse packings with $\sigma = 0.05$ exhibit a freezing transition at $\varphi_f \approx 0.52$. For $\sigma \leq 0.05$ and $\varphi > \varphi_f$, the achievable phase space is dominated by the bounding regions of the densest configurations. For $\sigma \leq 0.05$ and $\varphi \leq \varphi_f$, the achievable phase space is dominated by liquid basins of attraction. The plots in Fig. 3.2d for $\sigma \leq 0.05$ differ from Fig. 3.4 for $\varphi \in [\varphi_f, \varphi_m] \cup [\varphi_{\text{off}}, \varphi_{\text{max}}]$. For these φ, the bounding regions for the densest configurations dominate the achievable phase space in Fig. 3.4 but are not achievable from the initial configurations in Fig. 3.2d.

For polydisperse packings with $\sigma \geq 0.1$ and $\varphi \leq \varphi_g$, the plots in Fig. 3.4 are qualitatively and quantitatively similar to the ones in Fig. 3.2d (see the RCP and GCP lines from Fig. 3.2d in Fig. 3.4). It means that the conclusions reached in Section 3.4.2 (Data analysis) are protocol-independent for these packings; the dominant jamming density does not depend on the initial packing configuration, which determines the achievable portion of the phase space. Thus, we may draw our conclusions in Section 3.4.3 for $\sigma \geq 0.1$ and $\varphi \leq \varphi_g$ for the entire available phase space. For $\varphi > \varphi_g$, the plots differ: the dominant jamming density depends on the initial packing configuration. For diluted densest packings with $\sigma \geq 0.1$ and $\varphi > \varphi_g$, the achievable phase space is dominated by the bounding regions of the ideal glass. It is sometimes argued that the available phase space is fully connected for $\varphi \leq \varphi_g$ and splits into disconnected portions at φ_g.[2]

These results comply with the general agreement that the available phase space is ergodic at $\varphi \leq \varphi_g$.[33] For packings that allow crystallization and for which $\varphi_{\text{off}} > \varphi_g$, one may assume that ergodicity breaks at φ_{off}, when the $\varphi_J(\varphi)$ plot becomes protocol-dependent. It was a general assumption in the colloidal literature as well, but recent careful studies of diffusion dynamics show that ergodicity for such packings breaks already at φ_g.[33]

3.4.4 Schematic phase space structure

Finally, we present a schematic image with the phase space structure, where we incorporate all the results obtained so far (Fig. 3.5). We assume that packings that allow crystallization ($\sigma \leq 0.07$) are initially generated in liquid bounding regions for $\varphi \in [\varphi_f, \varphi_{\text{off}}]$ (as it happens in Fig. 3.2d); thus, melting transition and crystallization offset are exhibited for such packings, but not a freezing transition (as it happens in Fig. 3.4). Symbols for different characteristic densities are displayed to the left and below the image. We provide the corresponding values for monodisperse packings to the right and above the image. All the characteristic densities have already been introduced; we only mention that under φ_g for $\sigma < 0.05$ we understand the ideal glass transition densities from extrapolating the $\varphi_g(\sigma)$ plot to $\sigma < 0.05$, as done in Fig.

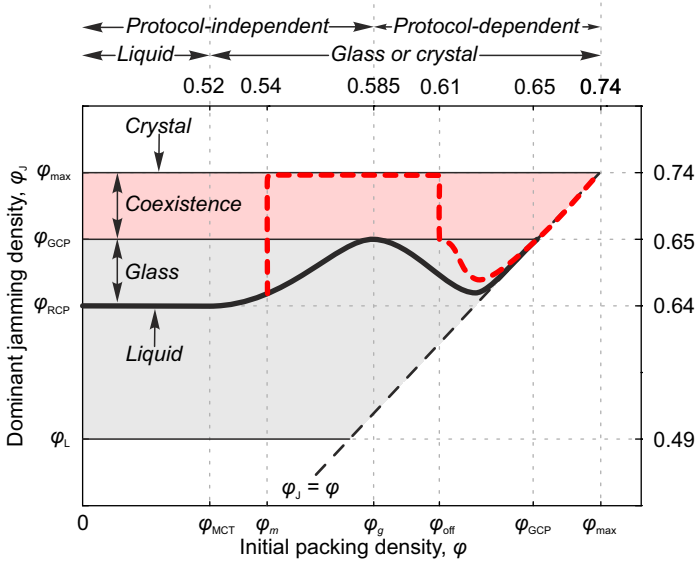

Figure 3.5: Schematic jamming phase diagram for frictionless hard-sphere packings, depicting dominant jamming density φ_J *vs.* initial packing density φ. Opaque areas represent jamming densities that do not dominate the phase space. Red dashed line and red opaque area refer to packings which allow crystallization. φ_L is the lowest jamming density, φ_{RCP} is the random close packing limit (the J-point), φ_{GCP} is the glass close packing limit, φ_{max} is the highest jamming density, φ_{MCT} is the density of transition from liquid to glass, φ_m is the melting transition density (onset of crystallization), φ_g is the ideal glass transition density for packings where crystallization is impossible, and φ_{off} is the density of the offset of crystallization.

3.3 (which corresponds to divergent alpha-relaxation time). If crystallization is impossible, the protocol-dependent (non-ergodic) region for the $\varphi_J(\varphi)$ plot is $\varphi > \varphi_g$ (as depicted at the top of Fig. 3.5). For packings that allow crystallization and for which $\varphi_{\mathrm{off}} > \varphi_g$, we follow Zaccarelli *et al*:[33] and assume that ergodicity and protocol independence break at φ_g as well.

We assume in Fig. 3.5 that in the thermodynamic limit the J-segment $[\varphi_{\mathrm{LT}}, \varphi_{\mathrm{RCP}}]$ converges to a J-point (φ_{RCP});[12] we also assume that the dominant jamming density for any given initial density converges to a point in the thermodynamic limit as well. Opaque areas represent the jamming densities that do not dominate the phase space, but whose basins of attraction are available. Opaque areas are protocol-independent. The red dashed line and the red opaque area refer to packings that allow crystallization.

The procedure that we used to produce Fig. 3.2d can be extended to particles with soft potential. In that case, it is necessary to use the particle number density ρ instead of volume density φ. For each number density ρ and temperature T, one shall sample the phase space according to the usual equilibrium distribution of states in the canonical ensemble. For each sampled configuration, one shall perform the steepest descent in the potential energy landscape (infinitely fast quenching) and track the value of the obtained potential energy minimum U. Presumably, these values will be distributed in one or several narrow intervals around some dominant minima $\tilde{U}(\rho T)$. There may be more than one of them at a given ρ and T if the phase space is not ergodic. Particle interactions are usually pair-wise; typical model potentials for interactions between soft

particles are Gaussian core potential[149,150]and inverse-power potential.[151,152] An example for the rapid quenching of several equilibrated monodisperse two-dimensional packings with Gaussian core potential can be found in Stillinger and Weber.[150] The potential energy of interaction between two particles in inverse-power law systems is $\epsilon(D/r)^n$, where r is the distance between the two particles and ϵ, D, and n are parameters of the potential. Inverse-power law systems have a convenient scaling property. Specifically, it can be shown that all dimensionless excess thermodynamic properties of these systems depend only on a dimensionless reduced number density $\rho_* \equiv \rho D^d(\epsilon/kT)^{d/n}$, where d is the packing dimensionality and k is the Boltzmann constant.[152,153] For polydisperse packings, D depends on a given particle pair, but it can be split into a dimensionless pair-dependent part and a dimensional pair-agnostic part, of which the latter shall be used for calculating ρ_*. Thus, the plot $\tilde{U}(\rho T)$ will be transformed into $\tilde{U}_*(\rho_*)$, where $\tilde{U}_*$ is a dominant dimensionless potential energy minimum. We assume that this plot will resemble Fig. 3.5, only with inverted Y-axis, as far as for hard spheres we defined $\tilde{U} \equiv -\varphi_J$. Previous papers on particles with soft potentials typically focused on the distinction between liquid and crystalline phases.[149,151,152] We believe that finding dominant potential energy minima and building $\tilde{U}(\rho T)$ plots may shed light on other important properties of such systems, including the ideal glass transition and the distinction between liquid and glass phases.

3.4.5 Applicability of liquid equations of state

At the end of this paper, we investigate for which density ranges liquid equations of state are applicable to the hard-sphere packings under study. We compared reduced pressures $p(\varphi)$ in equilibrated packings (*i.e.*, before densification) from Fig. 3.4 (diluted densest packings) with values analytically predicted by equations of state for hard spheres. There are many liquid equations of state for polydisperse packings.[155] We confirm that equations (9)-(13) from Ogarko and Luding[155] produce very similar results, as well as equation (6) from Mansoori *et al*.[156] We use the simplest of these equations of state, the one of Boublík–Carnahan–Starling–Mansoori (eq. (4) in Boublík[154] or eq. (9) in Ogarko and Luding[155]): $p_{\mathrm{CS}}(\varphi) = \frac{1}{1-\varphi} + O_1\frac{3\varphi}{(1-\varphi)^2} + O_2\frac{\varphi^2(3-\varphi)}{(1-\varphi)^3}$ where $O_1 = \frac{\langle r\rangle\langle r^2\rangle}{\langle r^3\rangle}$, $O_2 = \frac{\langle r^2\rangle^3}{\langle r^3\rangle^2}$; $\langle r^i\rangle$ is the ith raw moment of the distribution of particle radii r. We calculated relative differences δ between experimental and theoretically predicted reduced pressures, $\delta = |p(\varphi) - p_{\mathrm{CS}}(\varphi)|\,/p_{\mathrm{CS}}(\varphi)$, and present in Fig. 3.6 the $\delta(\varphi)$ plots for different σ.

Naturally, the reduced pressure in all the equilibrated packings at low densities is very close to the theoretical prediction; pressures differ by no more than 1% ($\delta \leq 0.01$). Pressure in packings that allow crystallization ($\sigma < 0.1$) starts to deviate from theoretical predictions at φ_f. Later on,

[149] F. H. Stillinger. *J. Chem. Phys.*, 65, 3968–3974, 1976.
[150] F. H. Stillinger and T. A. Weber. *Phys. Rev. A*, 25, 978–989, 1982.
[151] S. Prestipino, F. Saija, and P. V. Giaquinta. *J. Chem. Phys.*, 123, 144110, 2005.
[152] C. N. Likos et al. *J. Chem. Phys.*, 126, 224502, 2007.
[153] J. D. Weeks. *Phys. Rev. B*, 24, 1530–1535, 1981.
[155] V. Ogarko and S. Luding. *J. Chem. Phys.*, 136, 124508, 2012.
[156] G. A. Mansoori et al. *J. Chem. Phys.*, 54, 1523–1525, 1971.
[154] T. Boublík. *J. Chem. Phys.*, 53, 471–472, 1970.

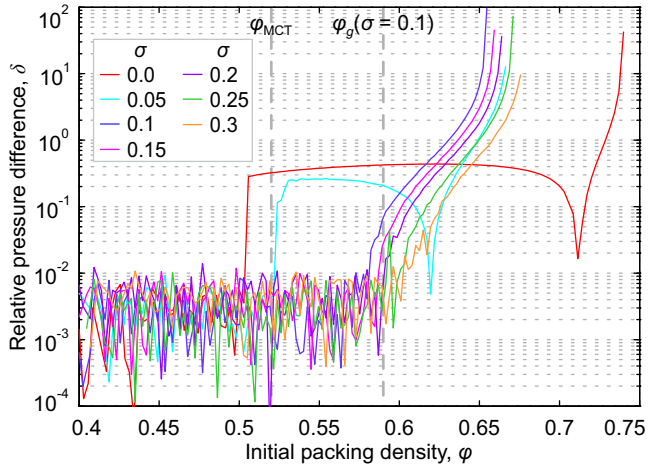

Figure 3.6: Relative difference δ between experimental and theoretically predicted reduced pressures *vs.* initial packing density φ. $\delta = |p(\varphi) - p_{CS}(\varphi)| / p_{CS}(\varphi)$, $p_{CS}(\varphi)$ is the reduced pressure from the Carnahan–Starling equation of state for polydisperse hard spheres.[154,155] Experimental pressures $p(\varphi)$ were measured for equilibrated packings from Section 3.4.3, *cf.* Fig. 3.4. Colors for the different relative standard deviations σ of the log-normal particle radii distributions are depicted in the legend.

we will discuss only packings with $\sigma \geq 0.1$, because crystallization effects are not superimposed on their $\delta(\varphi)$ plots. Surprisingly, theoretical predictions for $p(\varphi)$ for these packings remain valid with the same high accuracy $\delta \leq 0.01$ even for $\varphi > \varphi_{MCT}$, until φ reaches certain values depending on σ (Fig. 3.6). More precisely, $\delta > 0.01$ at $\varphi \approx 0.581$, 0.587, 0.591, 0.596, and 0.602 for $\sigma = 0.1$, 0.15, 0.2, 0.25, and 0.3, respectively. Selecting a different threshold than $\delta = 0.01$ to consider deviations in reduced pressures as high leads to slightly different results. For example, δ is 0.06 at $\varphi \approx 0.588$, 0.596, 0.602, 0.612, 0.622 for $\sigma = 0.1$, 0.15, 0.2, 0.25, and 0.3, respectively (Fig. 3.6). These values of φ are very close to φ_g from Table 3.2 for the corresponding σ. We confirm that the reduced pressure for equilibrated packings from Fig. 3.2c with $\sigma \geq 0.1$ exposes behavior that is qualitatively and quantitatively similar to the one in Fig. 3.6 (data not shown).

3.5 Summary and conclusions

We computer-generated monodisperse and polydisperse frictionless hard-sphere packings of 10^4 particles with log-normal particle diameter distributions in a wide range of densities φ (for monodisperse packings $\varphi = 0.46 - 0.72$). Then we equilibrated these packings and searched for their closest jammed configurations (inherent structures of hard spheres).

We found that the available phase space is dominated at $\varphi \leq 0.52$ by liquid bounding regions with jamming densities $\varphi_J \in [\varphi_{LT}, \varphi_{RCP}]$ ($\varphi_{LT} \approx 0.635$ and $\varphi_{RCP} \approx 0.64$ for monodisperse packings). At $\varphi \approx 0.52$, independent from the particle radii distribution, the structure of the available phase space changes, bounding regions become relatively disjoint (*i.e.*, the fraction of the "wormholes" in bounding surfaces becomes low). The value for this density, also independent from the particle radii distribution, is predicted under certain assumptions by the mode-coupling theory. Thus, we

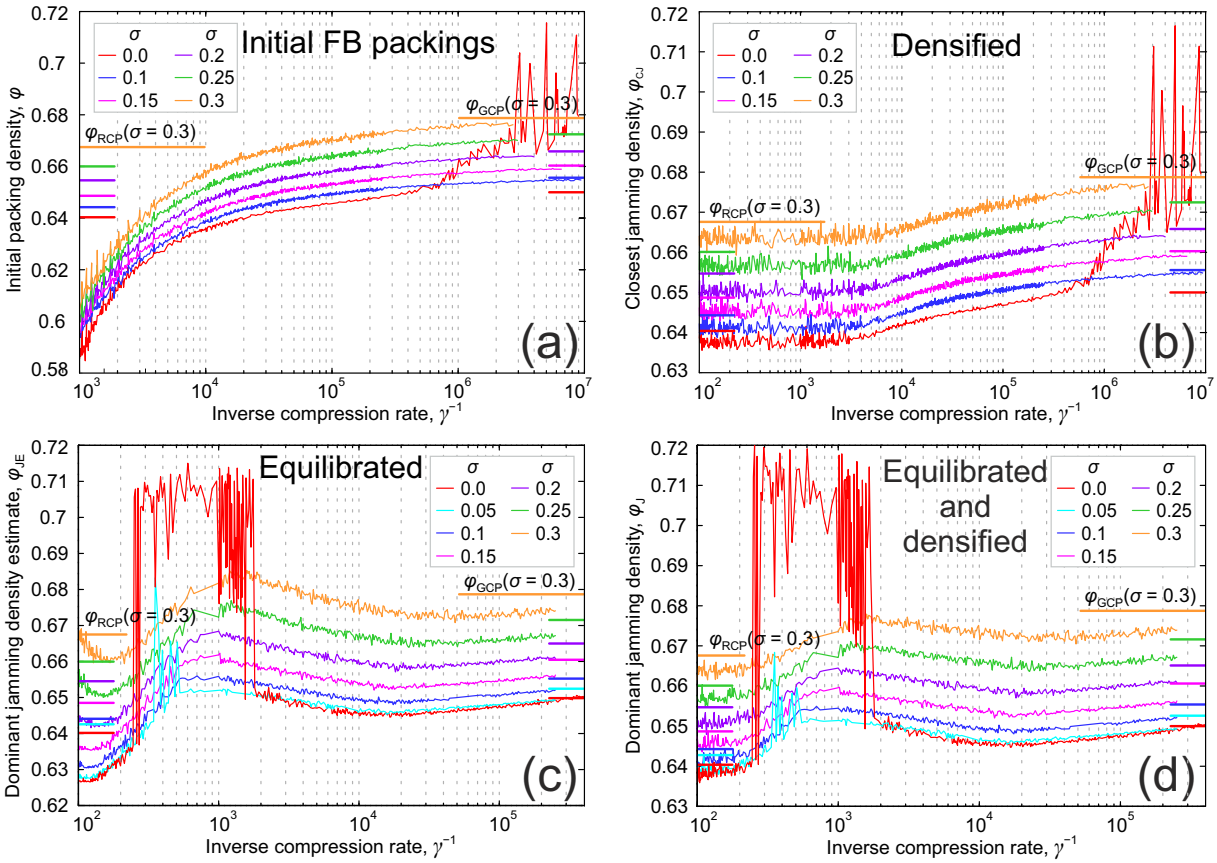

Figure 3.7: (a) Initial packing densities φ *vs.* the inverse compression rate γ^{-1}. (b) Closest jamming densities before equilibration φ_{CJ} *vs.* the inverse compression rate γ^{-1}. (c) Closest jamming density estimates after equilibration φ_{JE} *vs.* the inverse compression rate γ^{-1}. (d) Closest jamming densities after equilibration φ_J *vs.* the inverse compression rate γ^{-1}. All the packings were generated with the force-biased (FB) algorithm. Colours for the different relative standard deviations σ of the log-normal particle radii distributions are depicted in the legend.

refer to this transition density as $\varphi_{\text{MCT}} \approx 0.52$.

For $\varphi > \varphi_{\text{MCT}}$, the dominant jamming densities φ_J increase with φ and the available phase space is dominated by basins of attraction that we call glassy. When φ reaches the ideal glass transition density φ_g, φ_J reaches the ideal glass density (the glass close packing limit) φ_{GCP}, so that the available phase space is dominated at φ_g by the basin of attraction of the ideal glass. φ_g and φ_{GCP} depend on the particle size distribution. For packings with sphere diameter relative standard deviation $\sigma = 0.1$, $\varphi_{\text{GCP}} \approx 0.655$ and $\varphi_g \approx 0.59$. For monodisperse and slightly polydisperse packings, crystallization is superimposed on these processes: it starts at the melting transition density φ_m and ends at the crystallization offset density φ_{off}. For monodisperse packings, $\varphi_m \approx 0.54$ and $\varphi_{\text{off}} \approx 0.61$. If we extrapolate the ideal glass transition densities φ_g for polydisperse packings to $\sigma = 0$ (monodisperse packings), we obtain $\varphi_g \approx 0.585$, in agreement with experiments and simulations on divergent alpha-relaxation time and the jump in compressibility. We verified that the results for packings with $\sigma \geq 0.1$ and $\varphi \leq \varphi_g$ are independent from a packing generation

protocol.

We also discovered that the reduced pressure in equilibrated packings complies with liquid equations of state for hard polydisperse spheres for $\varphi > \varphi_{\mathrm{MCT}}$. Thus, the comparison with liquid equations of state is not sensitive enough to reveal the changes in the structure of the available phase space at φ_{MCT}, which are detected by dominant jamming densities.

3.6 Appendix

3.6.1 Densities *vs.* inverse compression rate

In Fig. 3.7, we provide the same plots as in Fig. 3.2, but built *vs.* the inverse compression rate γ^{-1}, not *vs.* initial packing densities φ (as done in Fig. 3.2b-d). Fig. 3.7b shows the $\varphi_{\mathrm{CJ}}(\gamma^{-1})$ plots that we used to estimate the GCP limits by asymptotic expansion to infinite generation time or zero compression rate. The plots in Fig. 3.7b have a structure predicted by Parisi and Zamponi[2] (Fig. 2a in that paper).

Chapter 4

How to predict the ideal glass transition density in polydisperse hard-sphere packings

Authors:

Vasili Baranau and Ulrich Tallarek*

State of publication:

Published on July 22, 2015 in The Journal of Chemical Physics, Vol. 143.4, pp 044501
DOI: 10.1063/1.4927077

Abstract

The formula for the entropy s of the accessible volume of the phase space for frictionless hard spheres is combined with the Boublík–Mansoori–Carnahan–Starling–Leland (BMCSL) equation of state for polydisperse three-dimensional packings to obtain an analytical expression for s as a function of packing density φ. Polydisperse hard-sphere packings with log-normal, Gaussian, and Pareto particle diameter distributions are generated to estimate their ideal glass transition densities φ_g. The accessible entropy s at φ_g is almost the same for all investigated particle diameter distributions. We denote this entropy as s_g and can predict φ_g for an arbitrary particle diameter distribution through an equation $s(\varphi) = s_g$. If the BMCSL equation of state is used for $s(\varphi)$, then φ_g is found to depend only on the first three moments of a particle diameter distribution.

4.1 Introduction

The nature of the glass transition has been gaining significant attention over the past decades.[2,38,40,157–159] An important concept that emerged from the studies of glass dynamics is that of the ideal glass transition.[2,28,29,33,49,55,144,145] The latter is usually determined by the jump of compressibility or divergent alpha-relaxation time.[2,29,33,49] One of the simplest models that exhibits many interesting and important properties of real atomic, molecular, and colloidal systems, including glassy dynamics, is packings of frictionless hard spheres.[2,3,160] It is generally believed that the phase space of hard spheres becomes non-ergodic at the ideal glass transition density φ_g.[33,144]

In this paper, we derive an expression to predict φ_g for polydisperse packings of frictionless hard spheres. We combine the formula for the excess "liquid" entropy of frictionless hard-sphere packings[61,161] with the Boublík–Mansoori–Carnahan–Starling–Leland (BMCSL) equation of state for polydisperse three-dimensional hard spheres.[154–156] Thus, we obtain an analytical equation for the hard-sphere entropy *vs.* packing density. We assume that the entropy per particle at the ideal glass transition does not depend on the particle diameter distribution if the number of particles is large enough. When the critical value of the entropy per particle at φ_g is known, it is possible to estimate φ_g for packings with arbitrary particle diameter distribution: We need to find a density at which the entropy per particle equals the critical value. The resulting equation implies that φ_g shall depend only on the first three moments of a particle diameter distribution. Recent studies suggest that another characteristic density of frictionless hard-sphere packings, the J-point,[12] also depends only on the first three moments of the particle diameter distributions.[162,163]

The paper is structured as follows. In Section 4.2 (Theory), we derive the formula for the

[2] G. Parisi and F. Zamponi. *Rev. Mod. Phys.*, 82, 789–845, 2010.
[38] C. A. Angell. *J. Phys. Chem. Solids*, 49, 863–871, 1988.
[40] P. G. Debenedetti and F. H. Stillinger. *Nature*, 410, 259–267, 2001.
[157] J. H. Gibbs and E. A. DiMarzio. *J. Chem. Phys.*, 28, 373–383, 1958.
[158] G. Adam and J. H. Gibbs. *J. Chem. Phys.*, 43, 139–146, 1965.
[159] G. L. Hunter and E. R. Weeks. *Rep. Prog. Phys.*, 75, 066501, 2012.
[28] G. Parisi and F. Zamponi. *J. Chem. Phys.*, 123, 144501, 2005.
[29] L. Berthier and T. A. Witten. *Phys. Rev. E*, 80, 021502, 2009.
[33] E. Zaccarelli et al. *Phys. Rev. Lett.*, 103, 135704, 2009.
[49] M. Skoge et al. *Phys. Rev. E*, 74, 041127, 2006.
[55] G. Brambilla et al. *Phys. Rev. Lett.*, 102, 085703, 2009.
[144] G. Pérez-Ángel et al. *Phys. Rev. E*, 83, 060501, 2011.
[145] T. Voigtmann, A. M. Puertas, and M. Fuchs. *Phys. Rev. E*, 70, 061506, 2004.
[3] S. Torquato and F. H. Stillinger. *Rev. Mod. Phys.*, 82, 2633–2672, 2010.
[160] V. Ogarko, N. Rivas, and S. Luding. *J. Chem. Phys.*, 140, 211102, 2014.
[61] D. Asenjo, F. Paillusson, and D. Frenkel. *Phys. Rev. Lett.*, 112, 098002, 2014.
[161] D. Frenkel and A. J. C. Ladd. *J. Chem. Phys.*, 81, 3188–3193, 1984.
[154] T. Boublík. *J. Chem. Phys.*, 53, 471–472, 1970.
[155] V. Ogarko and S. Luding. *J. Chem. Phys.*, 136, 124508, 2012.
[156] G. A. Mansoori et al. *J. Chem. Phys.*, 54, 1523–1525, 1971.
[12] C. S. O'Hern et al. *Phys. Rev. E*, 68, 011306, 2003.
[162] A. Santos et al. *Phys. Rev. E*, 89, 040302, 2014.
[163] K. W. Desmond and E. R. Weeks. *Phys. Rev. E*, 90, 022204, 2014.

entropy *vs.* packing density and the master equation for estimating φ_g. In Section 4.3 (Ideal glass transition densities from simulations), we generate three-dimensional frictionless hard-sphere packings with log-normal, Gaussian, and Pareto diameter distributions and estimate their ideal glass transition densities. In Section 4.4 (Results and discussion), we demonstrate that packing entropy from Section 4.2 at the estimated φ_g does not noticeably depend on the particle diameter distribution. Then, we demonstrate how well our predictions for φ_g compare to the estimates from simulations. Finally, we build a map of the ideal glass transition densities *vs.* the particle diameter standard deviation and skewness, provided that the mean particle diameter is unity.

4.2 Theory

4.2.1 Packing entropy

Each configuration of hard spheres with predefined diameters corresponds to a point in the phase space for these spheres. At any solid volume density $\varphi > 0$, some points in the phase space correspond to configurations with particle intersections and are inaccessible, the others correspond to valid packing configurations and form the accessible part of the phase space. If the accessible phase space is still ergodic at a given density φ, it is possible to explicitly derive its volume V_{acc}.[61,161] If under packing entropy S we understand the logarithm of V_{acc}, $S = \ln(V_{\text{acc}})$, we obtain from Eq. (7) in Asenjo *et al.*[61]

$$S(\varphi) = N \ln(V_{\text{box}}) - N \int_0^{\varphi} \frac{Z(\varphi') - 1}{\varphi'} \, \mathrm{d}\varphi' \, , \tag{4.1}$$

where V_{box} is the volume of the box in which the particles reside, $Z(\varphi)$ is the reduced kinematic pressure (compressibility factor), and N is the number of particles. Here, S is a total entropy, *i.e.*, it includes both configurational and vibrational contributions. It is convenient to renormalize entropies and discard the $N \ln(V_{\text{box}})$ term, as well as to work with entropies per particle, *i.e.*, divide entropy values by N. We refer to this renormalized entropy per particle as s. Formally,

$$s(\varphi) = - \int_0^{\varphi} \frac{Z(\varphi') - 1}{\varphi'} \, \mathrm{d}\varphi' \, . \tag{4.2}$$

4.2.2 Equation of state

The phase space for hard spheres is believed to become non-ergodic at the ideal glass transition density φ_g.[33,164] Thus, Eq. (4.1) is applicable for $\varphi \leq \varphi_g$. A common equation of state utilized for polydisperse hard spheres is the so-called Boublík–Mansoori–Carnahan–Starling–Leland (BMCSL) equation of state.[154–156] Berthier and Witten showed[29] that this equation of state successfully predicts reduced pressure in equilibrated bidisperse hard-sphere packings up to a very

[164] V. Baranau and U. Tallarek. *Soft Matter*, 10, 7838–7848, 2014.

high density 0.597, though different techniques they used predicted φ_g at different densities, from 0.592 to 0.635. In our previous paper,[164] we confirmed that this equation of state predicts pressure in equilibrated hard-sphere packings with log-normal particle diameter distribution for $\varphi \leq \varphi_g$, if the packings do not exhibit spontaneous crystallization. We assume that this equation of state is applicable up to the ideal glass transition for equilibrated packings with any diameter distribution. Thus, we may complement Eq. (4.1) with the specification of the reduced pressure $Z(\varphi)$. When we apply the BMCSL equation of state to packings that exhibit spontaneous crystallization, we imply that crystal-like configurations are excluded from the phase space. As long as we operate only in the range of densities $\varphi \leq \varphi_g$, we do not require any assumptions about the pressure behaviour for $\varphi > \varphi_g$.

We use the following representation of the BMCSL equation of state (Eq. (9) in Ogarko and Luding[155]):

$$Z(\varphi) = \frac{1}{1-\varphi} + O_1 \frac{3\varphi}{(1-\varphi)^2} + O_2 \frac{\varphi^2(3-\varphi)}{(1-\varphi)^3} \ , \tag{4.3}$$

where $O_1 = \frac{\langle r \rangle \langle r^2 \rangle}{\langle r^3 \rangle}$, $O_2 = \frac{\langle r^2 \rangle^3}{\langle r^3 \rangle^2}$, and $\langle r^i \rangle$ is the ith raw moment of particle radii r. Eq. (4.2) then becomes:

$$s(\varphi) = 3O_1 - (O_2 - 1)\ln(1-\varphi) - \frac{(O_2 - 3O_1)\varphi + 3O_1}{(1-\varphi)^2} \ . \tag{4.4}$$

For monodisperse packings, $O_1 = 1$ and $O_2 = 1$.

Below, we use the particle diameter relative standard deviation (polydispersity) σ and the particle diameter skewness γ. Here, $\sigma = \sqrt{\langle \Delta d^2 \rangle}/\langle d \rangle = \sqrt{\langle \Delta r^2 \rangle}/\langle r \rangle$ and $\gamma = \langle \Delta d^3 \rangle / \langle \Delta d^2 \rangle^{3/2} = \langle \Delta r^3 \rangle / \langle \Delta r^2 \rangle^{3/2}$, where d is the particle diameter. The relation between the parameter sets (O_1, O_2) and (σ, γ) is as follows:

$$\sigma^2 = \frac{O_2}{O_1^2} - 1, \gamma = \frac{1}{\sigma^3}\left[\frac{O_2}{O_1^3} - 3\frac{O_2}{O_1^2} + 2\right] \ , \tag{4.5a}$$

$$O_1 = \frac{\sigma^2 + 1}{\gamma\sigma^3 + 3\sigma^2 + 1}, O_2 = \frac{(\sigma^2+1)^3}{(\gamma\sigma^3 + 3\sigma^2 + 1)^2} \ . \tag{4.5b}$$

4.2.3 Equal entropies at the ideal glass transition

We assume that the fraction of the inaccessible phase space at which the phase space becomes non-ergodic does not depend on the particle diameter polydispersity, if the packings contain the same large enough number of particles N. It means that the entropy at the ideal glass transition is the same for all polydispersities at a given large enough N. This assumption will be verified later for computer-generated packings. We refer to the renormalized entropy per particle at the ideal glass transition in the thermodynamic limit as s_g. To predict φ_g for an arbitrary particle size

Table 4.1: Properties of the different particle diameter distributions used in the text.

Distribution	Probability density function	Important moments	Skewness γ *vs.* polydispersity σ
Truncated Gaussian[a]	$f_G(x;\mu_G,\sigma_G) = \\ = C\frac{1}{\sigma_G\sqrt{2\pi}}e^{-\frac{(x-\mu_G)^2}{2\sigma_G^2}}$, $x \geq 0$, $\\ C = 2\left(1-\mathrm{erf}\left(\frac{x-\mu_G}{\sigma_G\sqrt{2}}\right)\right)^{-1}$	$\langle x\rangle \approx \mu_G$, $\\ \langle \Delta x^2\rangle \approx \sigma_G^2$, $\\ \langle \Delta x^3\rangle \approx 0$	$\gamma \approx 0$
Log-normal	$f_{\mathrm{LN}}(x;\mu_{\mathrm{LN}},\sigma_{\mathrm{LN}}) = \\ = \frac{1}{x\sigma_{\mathrm{LN}}\sqrt{2\pi}}e^{-\frac{(\ln(x)-\mu_{\mathrm{LN}})^2}{2\sigma_{\mathrm{LN}}^2}}$, $\\ x > 0$	$\langle x\rangle = e^{\mu_{\mathrm{LN}}+\sigma_{\mathrm{LN}}^2/2}$, $\\ \langle \Delta x^2\rangle = \langle x\rangle^2(e^{\sigma_{\mathrm{LN}}^2}-1)$, $\\ \gamma = (e^{\sigma_{\mathrm{LN}}^2}+2)\sqrt{e^{\sigma_{\mathrm{LN}}^2}-1}$	$\gamma = (\sigma^2+3)\sigma$
Pareto	$f_P(x;x_m,\alpha) = \frac{\alpha x_m^\alpha}{x^{\alpha+1}}$, $\\ x \geq x_m$	$\langle x^i\rangle = \begin{cases} \frac{\alpha x_m^i}{\alpha-i} & \text{if } \alpha > i \\ \infty & \text{if } \alpha \leq i \end{cases}$	$\gamma = \begin{cases} 2\sigma\frac{A+2}{A-2}(A-1) & \text{if } \sigma < \frac{1}{\sqrt{3}} \approx 0.577 \\ \infty & \text{if } \sigma \geq \frac{1}{\sqrt{3}} \approx 0.577 \end{cases}$, $\\$ where $A = \sqrt{1+\frac{1}{\sigma^2}}$

[a] The truncated Gaussian distribution in general has moments different from the usual (untruncated) Gaussian distribution. But the widest distribution $f_G(x;\mu_G,\sigma_G)$ used in our simulations, with $\mu_G = 1$ and $\sigma_G = 0.3$, has $\langle x\rangle \approx 1.0005$ and $\sqrt{\langle \Delta x^2\rangle} \approx 0.2992$. Therefore, in this table we neglect for simplicity corrections to moments stemming from the truncation of values at $x = 0$.

distribution, we need to find such a φ that $s(\varphi) = s_g$. Thus, we arrive at the master equation

$$3O_1 - (O_2 - 1)\ln(1-\varphi) - \frac{(O_2 - 3O_1)\varphi + 3O_1}{(1-\varphi)^2} = s_g \ . \tag{4.6}$$

Instead of s_g, we can parametrize Eq. (4.6) with φ_g of a reference particle diameter distribution. Then, we can compute s_g *via* Eq. (4.4).

4.3 Ideal glass transition densities from simulations

In our previous paper,[164] we estimated the ideal glass transition densities φ_g for particles with log-normal diameter distributions having relative diameter standard deviations σ from 0.05 to 0.3 in steps of 0.05. We repeated the procedure from that paper to determine φ_g for packings with (truncated) Gaussian and Pareto diameter distributions (*cf.* Table 4.1). Gaussian and Pareto distributions also had relative diameter standard deviations σ from 0.05 to 0.3 in steps of 0.05. Now we briefly describe the procedure from that paper.[164]

4.3.1 Definitions

In the following discussion, we rely on the concepts of jamming[3,30,31,77] and inherent structures.[39,54,60] To introduce them, we need two types of packing descriptions. We assume that certain nominal particle diameters are always specified for a packing and that actual particle diameters shall be

[30] A. Donev. *J. Appl. Phys.*, 95, 989–999, 2004.
[31] A. Donev et al. *J. Comput. Phys.*, 197, 139–166, 2004.
[77] A. Donev, F. H. Stillinger, and S. Torquato. *J. Chem. Phys.*, 127, 124509, 2007.
[39] F. H. Stillinger. *Science*, 267, 1935–1939, 1995.
[54] S. Torquato and Y. Jiao. *Phys. Rev. E*, 82, 061302, 2010.
[60] F. H. Stillinger, E. A. DiMarzio, and R. L. Kornegay. *J. Chem. Phys.*, 40, 1564–1576, 1964.

proportional to the nominal ones and are thus determined by the proportionality ratio or by the packing density φ. We also define $\vec{x}$ as a hypervector in the phase space formed by $3(N-1)$ particle coordinates. A packing description needed to define jamming and assumed everywhere outside this subsection specifies both $\vec{x}$ and φ (particle positions and actual diameters); thus, we denote it as $(\vec{x}, \varphi)$. A packing description needed to define inherent structures specifies only particle positions $\vec{x}$ but not the packing density φ (actual particle diameters).

A set of particles $(\vec{x}, \varphi)$ with predefined actual diameters is called jammed, if there exists no combination of particle displacements that avoids particle intersections, except for shifts or rotations of the system as a whole. A packing is called jammed if there is a subset of particles that is jammed. Inherent structures were initially introduced for systems with a soft potential,[39,60] which are described only by $\vec{x}$. For such systems, an inherent structure is by definition a packing configuration $\vec{x}_0$ with a local potential energy minimum in the phase space. For hard-sphere packings, the potential energy $U(\vec{x})$ at a given configuration $\vec{x}$ is replaced by the maximum packing density achievable at this configuration taken with the minus sign, $U(\vec{x}) = -\varphi_{\text{max}}(\vec{x})$. The maximum density $\varphi_{\text{max}}(\vec{x})$ for given particle positions $\vec{x}$ is computed by "inflating" particles so that their diameters remain proportional to the nominal values until at least one pair of particles develops a contact. When we talk about a density of an inherent structure $\vec{x}_0$, we assume $\varphi_{\text{max}}(\vec{x}_0)$. It can be shown that inherent structures correspond to jammed configurations and, vice versa, jammed configurations correspond to inherent structures. For example, let a packing reside in an inherent structure $\vec{x}_0$ and let the particle diameters be maximally possible for these particle positions $\vec{x}_0$ ($\varphi = \varphi_{\text{max}}(\vec{x}_0)$). As far as an inherent structure corresponds to a local density maximum, any infinitesimal change in particle positions from the current configuration $(\vec{x}_0, \varphi_{\text{max}}(\vec{x}_0))$ will result in particle intersections and thus is forbidden. This implies that any inherent structure $\vec{x}_0$ corresponds to a jammed configuration $(\vec{x}_0, \varphi_{\text{max}}(\vec{x}_0))$.

To any configuration $\vec{x}$, we can apply a steepest descent in the potential energy landscape $U(\vec{x})$ (infinitely fast quench, Stillinger quench) and reach a certain inherent structure $\vec{x}_{\text{CJ}}$. In this way, the entire phase space can be split into basins of attraction of inherent structures. Thus, an inherent structure $\vec{x}_{\text{CJ}}$ corresponds to the "closest jammed configuration" $(\vec{x}_{\text{CJ}}, \varphi_{\text{max}}(\vec{x}_{\text{CJ}}))$ for configurations $\vec{x}$ in the basin of attraction of this structure. The density of this configuration $\varphi_{\text{CJ}} = \varphi_{\text{max}}(\vec{x}_{\text{CJ}})$ is thus the "closest jamming density" for configurations $\vec{x}$ in the corresponding basin of attraction. As mentioned in Section 4.2.1, at any given packing density φ certain regions of the phase space will be unavailable. We refer to an intersection of a basin of attraction and the available part of the phase space as a "bounding region". Mathematically precise definitions of inherent structures, basins of attraction, and bounding regions can be found in our previous paper.[146]

At a given packing density φ, bounding regions with a certain jamming density φ_{CJ} will dominate the phase space. We refer to their jammed configurations $(\vec{x}_{\text{CJ}}, \varphi_{\text{max}}(\vec{x}_{\text{CJ}}) = \varphi_{\text{CJ}})$ as "dominant jammed configurations" and denote their jamming density as a "dominant jamming density" φ_{DJ}.[164] If we take an arbitrary packing $(\vec{x}, \varphi)$ at a given density φ and let it equilibrate

[146] V. Baranau and U. Tallarek. *Soft Matter*, 10, 3826–3841, 2014.

(undergo molecular dynamics with zero compression rate), the packing will eventually reach one of the dominant bounding regions, given that the phase space is still ergodic at this density. If the phase space is non-ergodic (formed by disconnected regions), its separate parts will be dominated by different bounding regions. In this case, the closest jamming density of a packing after equilibration will depend on the initial configuration $\vec{x}$.

4.3.2 Simulation procedure

The idea of our method for determination of the ideal glass transition densities φ_g is to generate packings in a wide range of densities φ, equilibrate them, and search for inherent structures of these equilibrated packings. The densities of these inherent structures are the dominant jamming densities φ_{DJ}. By definition, φ_g is a density where the phase space becomes disjoint and non-ergodic. It is believed that the plot φ_{DJ} *vs.* φ for a given particle diameter distribution reaches its maximum at $\varphi = \varphi_g$ if crystallization is suppressed.[2,29,33,49]

Firstly, we computationally generated packings of 10^4 particles in three-dimensional fully-periodic boxes in a wide range of densities (*e.g.*, for Pareto packings with $\sigma = 0.05$, $\varphi = 0.4 - 0.653$) using the force-biased algorithm.[98,99] The lowest contraction rate for the algorithm was 10^{-7}. It ensures that the largest density of the packings is close to the maximum possible density for a given diameter distribution (the glass close packing limit φ_{GCP}).[2]

Secondly, we equilibrated the generated packings, *i.e.*, conducted simulations using the Lubachevsky–Stillinger algorithm[95,135] with zero compression rate until the kinematic pressure became stationary. We equilibrate the packings by performing sets of 2×10^7 collisions with zero compression rate in a loop until the relative difference of reduced pressures between the last two sets is less than 10^{-4}, so that the pressure can be regarded as stationary. More precisely, to measure the pressure during the 2×10^7 collisions, we average pressures for 100 sub-sets of 2×10^5 collisions, which amounts to 20 collisions in a sub-set per particle. We use our own implementation[136] of the Lubachevsky–Stillinger packing generation algorithm to carry out the equilibration.

Thirdly, we searched for the inherent structure densities of the equilibrated packings φ_{DJ} using the modified Lubachevsky–Stillinger algorithm.[136,146,164] The modified algorithm starts from a compression with a high rate ($= 10$) until the non-equilibrium reduced pressure is high enough (10^{12}); then, it reduces the compression rate by a factor of two and runs the simulation again until the pressure is high enough; this loop repeats until the compression rate is below 10^{-4}. The root mean square particle velocity was $\sqrt{3 \cdot 0.2}$. It corresponds to a packing temperature of 0.2, as far as we assigned unity mass to all the particles and set the Boltzmann constant to unity.

[98] J. Mościński et al. *Mol. Simul.*, 3, 201–212, 1989.
[99] A. Bezrukov, M. Bargieł, and D. Stoyan. *Part. Part. Syst. Char.*, 19, 111–118, 2002.
[95] B. D. Lubachevsky and F. H. Stillinger. *J. Stat. Phys.*, 60, 561–583, 1990.
[135] B. D. Lubachevsky. *J. Comput. Phys.*, 94, 255–283, 1991.
[136] V. Baranau https://code.google.com/p/packing-generation/

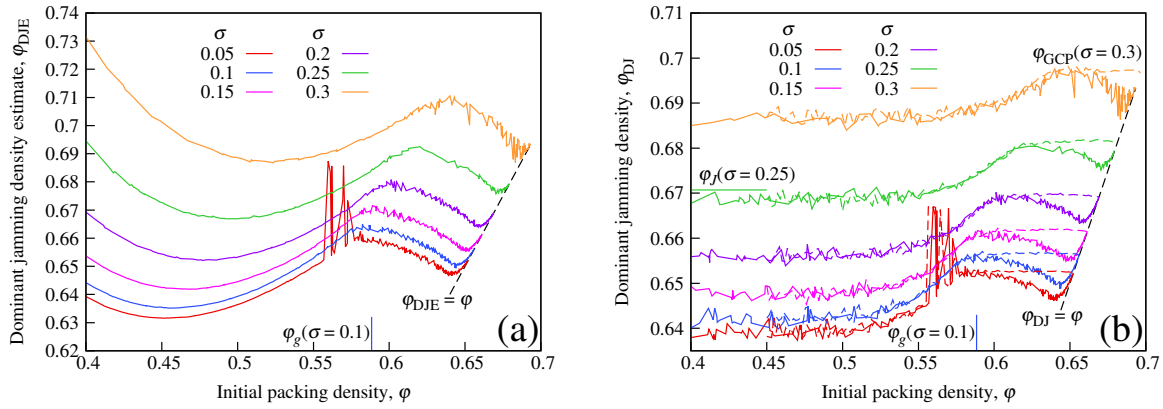

Figure 4.1: Dominant jamming densities for Pareto packings. (a) Estimates of dominant jamming densities through the Salsburg–Wood equation of state. (b) Dominant jamming densities obtained through the modified Lubachevsky–Stillinger algorithm. Particle diameter relative standard deviations σ are provided in the legends. Coloured dashed lines denote dominant jamming densities for diluted densest packings of the corresponding particle diameter distribution.

Similar modifications have been used by other authors before.[20,49,54,138]

It is possible to get estimates of φ_{DJ} (which we will denote as φ_{DJE}) already from equilibrium pressures through the equation of state by Salsburg and Wood,[9,29,49,164] $\varphi_{DJE} = \varphi[1+1/(Z(\varphi)-1)]^3$. This equation is derived under the free-volume approximation, which means that (i) during equilibration particle centers cannot leave the Voronoi cells that correspond to the initial particle positions, and (ii) particles move inside their Voronoi cells independently. Salsburg and Wood[9] derived another functionally similar equation for $\varphi_{DJE}(\varphi)$ under the assumptions that the current bounding region is small enough and closed (*i.e.*, disconnected from other bounding regions). These two sets of assumptions are closely related.[9] We show the estimates φ_{DJE} *vs.* φ for Pareto packings in Fig. 4.1a (*cf.* Fig. 4 in Skoge *et al.*[49]).

Dominant jamming densities φ_{DJ} for Pareto packings are displayed in Fig. 4.1b. We do not show the plots for Gaussian packings because they are qualitatively and quantitatively similar to the plots for the log-normal packings, which can be found in our previous paper.[164] The outburst in the $\varphi_{DJ}(\varphi)$ plot for $\sigma = 0.05$ corresponds to spontaneous partial crystallization.[2,32–34,36,49]

4.3.3 Analysis of dominant jamming densities

In Fig. 4.1, we depict the black dashed lines corresponding to $\varphi_{DJE} = \varphi$ (panel a) and $\varphi_{DJ} = \varphi$ (panel b). The plots for Pareto packings for each polydispersity approach these lines for large values of φ. This happens because at high φ the packings are close to jamming, *i.e.*, the accessible

[20] I. Biazzo et al. *Phys. Rev. Lett.*, 102, 195701, 2009.
[138] Y. Jiao, F. H. Stillinger, and S. Torquato. *J. Appl. Phys.*, 109, 013508, 2011.
[9] Z. W. Salsburg and W. W. Wood. *J. Chem. Phys.*, 37, 798–804, 1962.
[32] E. Sanz et al. *Phys. Rev. Lett.*, 106, 215701, 2011.
[34] C. Valeriani et al. *J. Phys.: Condens. Matter*, 23, 194117, 2011.
[36] L. Filion et al. *J. Chem. Phys.*, 133, 4115, 2010.

parts of the basins of attraction where the packings reside are closed and small. This implies high equilibrium pressure[9] (and thus $\varphi_{\mathrm{DJE}} \approx \varphi$). This also implies that (i) an initial basin of attraction is the only accessible one, and (ii) an initial unjammed packing configuration at φ is close to the jammed configuration of this basin, which is automatically the dominant jammed configuration. Thus, $\varphi_{\mathrm{DJ}} \approx \varphi$.

As mentioned, the plot φ_{DJ} *vs.* φ shall reach its maximum at $\varphi = \varphi_g$ if crystallization is suppressed. The dominant jamming density φ_{DJ} at $\varphi = \varphi_g$ corresponds to a lower boundary of the ideal glass density (the glass close packing limit φ_{GCP}). Additionally, the plateaus in the left part of Fig. 4.1b correspond to the J-segments, which are by definition density intervals where almost all Poisson packings will jam after searching for the closest jamming density (infinitely fast compression).[12,133,147] It is believed that the J-segments converge to their upper boundaries in the thermodynamic limit.[12] These upper boundaries are referred to as J-points φ_J. Fig. 4.1b mostly corresponds to the "many glassy states" model[2,29] and can be mapped to Fig. 7 in Berthier and Witten[29] and Fig. 4a in Parisi and Zamponi.[2] For example, φ_{th}, φ_K, and φ_{GCP} in Fig. 4a in Parisi and Zamponi[2] map to φ_J, φ_g, and φ_{GCP}, respectively, from this paper.

Fig. 4.1a recovers many features of Fig. 4.1b, for example, the local maxima around $\varphi = \varphi_g$, the positions of φ_g, the presence of spontaneous crystallization, and proximity of packings to jamming for $\varphi \to \varphi_{\mathrm{GCP}}$. At the same time, it does not reveal the plateau $\varphi_{\mathrm{DJ}} = \varphi_J$ for low φ, because the preconditions for the equation of state of Salsburg and Wood are not satisfied for such low densities. Thus, Fig. 4.1 shows that the plot $\varphi_{\mathrm{DJE}}(\varphi)$ alone shall be used carefully to analyse the structure of the phase space and should be accompanied by the $\varphi_{\mathrm{DJ}}(\varphi)$ plot. We also point out a principal difference between the plots in Fig. 4.1a and the plots in Fig. 4 in Skoge *et al.*[49] and Figs. 2 and 3 in Ogarko and Luding.[155] These authors track pressures along a single compression and depict jamming density estimates during a single compression. For very slow compressions, these jamming density estimates can be treated as approximations of φ_{DJE}, because a sufficiently slow compression can "equilibrate" the packing before the packing density (and thus the structure of the phase space) is changed significantly.

4.3.4 Diluted densest packings

To demonstrate that the maxima in the $\varphi_{\mathrm{DJ}}(\varphi)$ plots (solid lines, Fig. 4.1b) mark the onset of non-ergodicity, we generated another set of packings and searched for their dominant jamming densities. First, we chose for each σ a reference packing, a packing with φ_{DJ} close to φ_{GCP}. For $\sigma = 0.05 - 0.2$, we took the dominant jammed packing at the maximum initial density (the right-most point in Fig. 4.1b). For $\sigma = 0.25 - 0.3$, we used the dominant jammed packing with maximum jammed density (the highest point in Fig. 4.1b). Then, we scaled the particle positions so that we obtained packings with exactly the same particle diameters but with densities in the range $[0.4,\ \varphi_{\mathrm{GCP}})$. Finally, we determined the dominant jamming densities φ_{DJ} for these scaled packings, as done in Section 4.3.2 above. We refer to these scaled packings as "diluted densest"

[133] M. Pica Ciamarra, M. Nicodemi, and A. Coniglio. *Soft Matter*, 6, 2871–2874, 2010.
[147] R. Ni, M. A. Cohen-Stuart, and M. Dijkstra. *Nat. Commun.*, 4, 2704, 2013.

Table 4.2: Ideal glass transition densities φ_g for the log-normal, Gaussian, and Pareto particle diameter distributions *vs.* different particle diameter relative standard deviations σ.

σ	0.05	0.1	0.15	0.2	0.25	0.3
Log-normal	0.586	0.59	0.595	0.602	0.61	0.622
Gaussian	0.587	0.59	0.594	0.601	0.61	0.617
Pareto	0.586	0.588	0.596	0.604	0.620	0.640

ones. We show the plots φ_{DJ} *vs.* φ for these packings as dashed lines of the corresponding colour in Fig. 4.1b. The $\varphi_{\text{DJ}}(\varphi)$ plots of the force-biased Pareto packings and the diluted densest Pareto packings with the same σ start to deviate approximately at the maxima of the plots for the force-biased packings (solid lines in Fig. 4.1b); the deviation signals the onset of non-ergodicity around the maxima. The diluted densest packings (dashed lines in Fig. 4.1b) also have $\varphi_{\text{DJ}} \approx \varphi_{\text{GCP}}$ for densities φ higher than the positions of the mentioned maxima on the X-axis. The plots for $\varphi_{\text{DJ}}(\varphi)$ for Gaussian packings created with the force-biased algorithm and diluted densest Gaussian packings look qualitatively the same as in Fig. 4.1b.

4.3.5 Determination of the ideal glass transition densities

For Pareto packings, the maxima of the $\varphi_{\text{DJ}}(\varphi)$ plots in Fig. 4.1b are blurred and we could not determine their positions reliably. To estimate φ_g for the Pareto packings, we determined the densities at the onset of the plateaus $\varphi_{\text{DJ}} \approx \varphi_{\text{GCP}}$ in the $\varphi_{\text{DJ}}(\varphi)$ plots for the diluted densest packings in Fig. 4.1b (the dashed lines). More precisely, each dashed line in Fig. 4.1b comprises of three distinct sections: a plateau $\varphi_{\text{DJ}} \approx \varphi_J$ in the left part of the figure, a plateau $\varphi_{\text{DJ}} \approx \varphi_{\text{GCP}}$ in the right part of the figure, and an increase between the two plateaus. Thus, to estimate φ_g for the Pareto packings, we determined the average φ_{DJ} values of the six plateaus $\varphi_{\text{DJ}} \approx \varphi_{\text{GCP}}$ in the right part of Fig. 4.1b. Then, we fitted the increasing parts of each curve between the plateaus with second-order polynomials. Finally, we tracked the points of intersections of these polynomials with the corresponding plateaus $\varphi_{\text{DJ}} \approx \varphi_{\text{GCP}}$. For $\sigma = 0.05$, we excluded points corresponding to spontaneous crystallization. For Gaussian packings, we estimated φ_g by direct detection of the maxima in the $\varphi_{\text{DJ}}(\varphi)$ plots for the force-biased algorithm, as we have done for the log-normal packings.[164] This is possible, because the maxima in the $\varphi_{\text{DJ}}(\varphi)$ plots are pronounced for these particle diameter distributions.

The ideal glass transition densities for the particle size distributions under consideration are presented in Table 4.2. Fig. 4.1b allows to estimate two more characteristic densities of the packings. As mentioned, one can estimate the lower boundary of φ_{GCP} by taking φ_{DJ} at $\varphi = \varphi_g$[164] and φ_J by taking the upper boundary of the plateaus in the left part of the figure. For reference, we present φ_J and φ_{GCP} for the Gaussian and Pareto particle diameter distributions in Table 4.3. The data for the log-normal packings can be found in Table 4 in our previous paper[146] and are included in Table 4.3 for convenience.

Table 4.3: J-point densities φ_J and ideal glass densities φ_{GCP} for the log-normal, Gaussian, and Pareto particle diameter distributions *vs.* different particle diameter relative standard deviations σ.

σ	0.05	0.1	0.15	0.2	0.25	0.3
Log-normal, φ_J	0.642	0.644	0.649	0.654	0.660	0.668
Log-normal, φ_{GCP}	0.653	0.655	0.661	0.665	0.672	0.679
Gaussian, φ_J	0.641	0.645	0.648	0.652	0.657	0.661
Gaussian, φ_{GCP}	0.652	0.656	0.661	0.667	0.671	0.674
Pareto, φ_J	0.642	0.645	0.650	0.659	0.671	0.689
Pareto, φ_{GCP}	0.654	0.658	0.663	0.671	0.680	0.697

4.4 Results and discussion

4.4.1 Ideal glass transition entropies from simulations

We determined entropies per particle at the ideal glass transition $s(\varphi_g)$ for the polydisperse packings under study. Eq. (4.2) was used with two types of pressure: (i) spline-interpolated equilibrium pressure from simulations; and (ii) the BMCSL pressure from Eq. (4.3) (*cf.* Eq. (4.4)). We depict the values of $s(\varphi_g)$ for the log-normal and Pareto packings in Fig. 4.2. Entropies for the Gaussian packings behave very similarly and are omitted for clarity. Fig. 4.2 shows that the entropies at the ideal glass transition do not significantly depend on the particle diameter distribution type and its parameters, which supports the assumption of equal entropies from Section 4.2.3. Fig. 4.2 also shows that the use of the BMCSL equation of state instead of real pressures leads to minute changes in the entropy estimates and thus will have negligible effect on the solution of the equation $s(\varphi) = s_g$. Indeed, let us denote with $Z_{\text{sim}}(\varphi)$ the equilibrium reduced pressure from the simulations and with $Z(\varphi)$, as earlier, the reduced pressure from the BMCSL equation of state, Eq. (4.3). Then, the relative pressure difference $\delta = |Z_{\text{sim}}(\varphi) - Z(\varphi)|/Z_{\text{sim}}(\varphi)$ becomes larger than 10^{-2} not earlier than for $\varphi = \varphi_g - 0.02$ and is never larger than 0.06 at $\varphi = \varphi_g$ for all the packing types under study (*cf.* Fig. 6 in our previous paper[164]).

4.4.2 Comparison of theory and simulations

We chose the value of s_g to minimize the error for the log-normal distribution,[164] *i.e.,* between φ_g from the simulations (Table 4.2) and φ_g from theory (Eq. (4.6)). This led to $s_g = -7.6693$, if the natural logarithm is used for the entropy, and is indicated by the dashed grey line in Fig. 4.2. As mentioned, we can parametrize Eq. (4.6) with φ_g for a specific particle size distribution, producing s_g from Eq. (4.4). We use the monodisperse particle diameter distribution as a reference and denote the corresponding φ_g as φ_g^*. This approach assumes that crystallization is suppressed in monodisperse packings and pressure in these packings is described with the BMCSL equation of state for all $\varphi \leq \varphi_g$. The obtained s_g corresponds to $\varphi_g^* = 0.5861$. We note that a naïve third-order polynomial fit of φ_g from simulations with the log-normal particle diameter distribution and its extrapolation on the monodisperse case gave $\varphi_g^* \approx 0.585$.[164]

We used the value $s_g = -7.6693$ ($\varphi_g^* = 0.5861$) to predict φ_g through Eq. (4.6) for all the packing types under study. The comparison between theoretical predictions and simulation

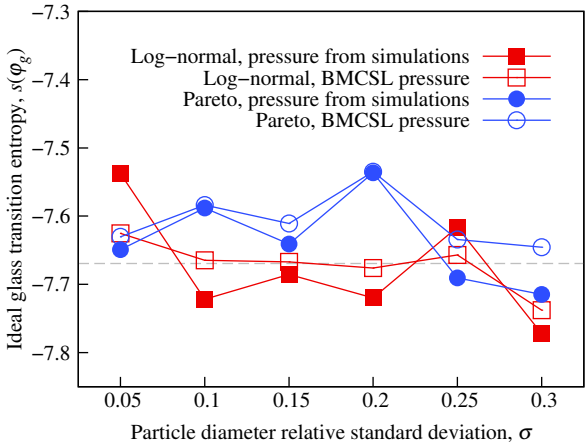

Figure 4.2: Ideal glass transition entropies for the log-normal and Pareto particle diameter distributions (*cf.* Eq. (4.2)). The dashed grey line denotes the value used in Eq. (4.6).

results can be found in Fig. 4.3. The figure shows that Eq. (4.6) can successfully predict the ideal glass transition densities φ_g.

4.4.3 Ideal glass transition density map

According to Eq. (4.6), the ideal glass transition densities shall depend only on the first three raw moments of the particle diameter distributions, if the BMCSL equation of state is used for the compressibility factor. As far as the mean diameter determines the length scale, we can present φ_g as a function of the particle diameter relative standard deviation σ and particle diameter skewness γ. In Fig. 4.4, we present φ_g for different values of these parameters. We also draw the lines that correspond to the log-normal, Gaussian, and Pareto distributions used in this paper. The analytical forms of these lines can be found in Table 4.1. We note here that the results of recent studies suggest that the J-point density φ_J is also determined only by the first three moments of a particle diameter distribution.[162,163]

Ogarko and Luding[155] showed (*cf.* Appendix B of that paper) that for an arbitrary distribution with non-negative support the following property holds: $O_2 \leq O_1$ (more generally, $0 \leq O_1^2 \leq O_2 \leq O_1 \leq 1$). In terms of skewness γ and polydispersity σ, $O_2 \leq O_1$ means that $\gamma \geq \sigma - \frac{1}{\sigma}$, while the other inequalities are always satisfied. The inaccessible values of γ ($\gamma < \sigma - \frac{1}{\sigma}$,) are denoted in Fig. 4.4 with grey colour (shaded lower right corner). The beta and Kumaraswamy distributions, for example, can approach the line $\gamma = \sigma - \frac{1}{\sigma}$ arbitrary close.

Fig. 4.4 shows that distributions with higher skewness shall generally have higher ideal glass transition densities. At the same time, it is not obvious from Fig. 4.4 if there are values of σ and γ that correspond to $\varphi_g < \varphi_g^* = 0.5861$. Nevertheless, it is easy to determine a functional form of O_2 *vs.* O_1 that results in $\varphi_g = \varphi_g^*$: One has to substitute $\varphi_g = \varphi_g^*$ into Eq. (4.6), which will imply a linear dependence of O_2 *vs.* O_1 (omitted here for brevity). It can easily be verified that this critical line will intersect the line $O_2 = O_1$ (boundary of the grey zone in Fig. 4.4) only at $O_1 = 1$.

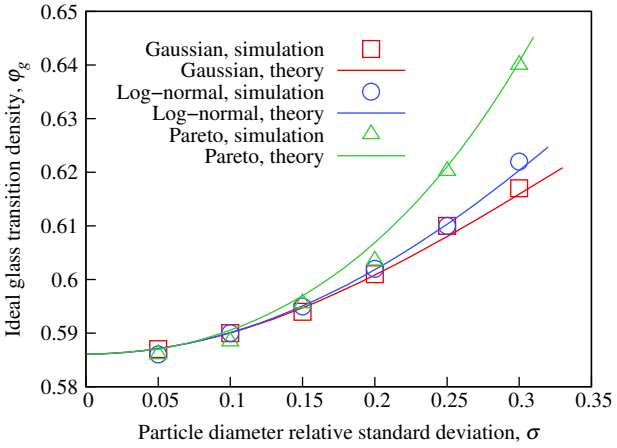

Figure 4.3: Ideal glass transition densities from theory (*cf.* Eq. (4.6)) and simulations (*cf.* Fig. 4.1) for the log-normal, Gaussian, and Pareto particle diameter distributions.

The distribution with $O_1 = O_2 = 1$ is the monodisperse distribution. Thus, the monodisperse distribution possesses the lowest possible ideal glass transition density φ_g according to our model.

As stated in Table 4.1, the skewness of the Pareto distribution diverges and becomes infinite at polydispersity $\sigma \approx 0.577$ (corresponding to the distribution parameter $\alpha = 3$). Infinite skewness implies that both O_1 and O_2 are zero (*cf.* Eq. (4.5b)). It follows from Eq. (4.6) that in this case $\varphi_g = 1 - e^{s_g} = 1 - e^{-7.6} \approx 1$. This result appears unrealistic and may be explained as follows: (i) Assumptions used to derive Eq. (4.6) are not applicable for such distributions; (ii) for such distributions, the ideal glass transition density φ_g is larger than the ideal glass density φ_{GCP}, so φ_g can never be reached and the phase space remains ergodic in the entire range of accessible densities up to φ_{GCP}; (iii) φ_g is indeed close to unity and φ_{GCP} is (as usually) larger than φ_g, which implies that one can actually arrange particles in a packing to cover the entire packing space and reach unity density. There are two more critical values for the Pareto distribution parameter α, *i.e.*, $\alpha = 2$ and $\alpha = 1$, at which the polydispersity and the mean particle diameter, respectively, become infinite. We assume that $\alpha \leq 2$ implies that both O_1 and O_2 can obtain any value in the range $[0, 1]$ depending on the current sample of particle diameters and φ_g can thus attain any value from its possible range. These special cases of the Pareto distribution parameters require separate investigation.

4.5 Summary

In this paper, we combined the formula for the volume of the available phase space of frictionless hard spheres[61,161] with the BMCSL equation of state.[154,155] We thus obtained an analytical equation for the entropy s of frictionless polydisperse three-dimensional hard-sphere packings *vs.* the packing density φ. Through computer simulations, we estimated the ideal glass transition densities φ_g of packings with the log-normal, Gaussian, and Pareto particle diameter distributions. We discovered that the entropy at the estimated ideal glass transition densities does not significantly

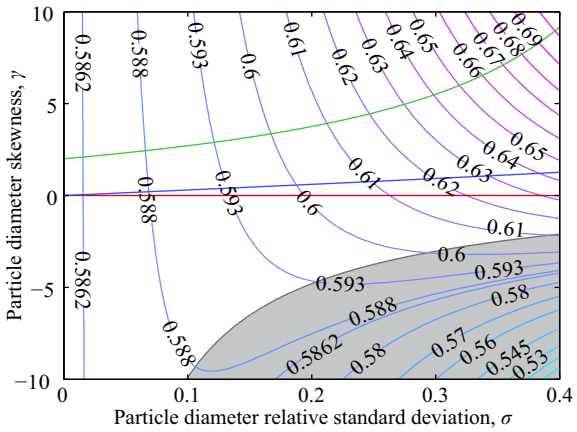

Figure 4.4: Ideal glass transition density map. Red, blue, and green lines correspond to the Gaussian, log-normal, and Pareto particle diameter distributions, respectively.

depend on the particle diameter distribution and presumably equals some characteristic value s_g. Thus, under the assumption of equal entropies at the ideal glass transition, we may predict the ideal glass transition density φ_g for an arbitrary particle diameter distribution by solving the equation $s(\varphi) = s_g$. According to this equation, φ_g shall depend only on the first three raw moments of the particle diameter distribution. We also provided a map of φ_g *vs.* particle diameter relative standard deviation and particle diameter skewness. This map may be used to design particle size distributions with desired values of φ_g. Our results help to understand the nature of the ideal glass transition and predict its properties in more complex atomic, molecular, or colloidal systems.

Chapter 5

Chemical potential and entropy in monodisperse and polydisperse hard-sphere fluids using Widom's particle insertion method and a pore size distribution-based insertion probability

Authors:

Vasili Baranau and Ulrich Tallarek*

State of publication:

Submitted on February 10, 2016 to The Journal of Chemical Physics

Abstract

We estimate the excess chemical potential $\Delta\mu$ and excess entropy per particle Δs of computer-generated, monodisperse and polydisperse, frictionless hard-sphere fluids. For this purpose, we utilize the Widom particle insertion method, which for hard-sphere systems relates $\Delta\mu$ to the probability to successfully (without intersections) insert a particle into a system. This insertion probability is evaluated directly for each configuration of hard spheres by extrapolating to infinity the pore radii (nearest-surface) distribution and integrating its tail. The estimates of $\Delta\mu$ and Δs are compared to (and comply well with) predictions from the Boublík–Mansoori–Carnahan–Starling–Leland equation of state. For polydisperse spheres, we employ log-normal particle radii distributions with polydispersities $\delta = 0.1$, 0.2, and 0.3.

5.1 Introduction

Hard sphere systems are powerful model systems to study colloids, glasses, and granular matter. They are relatively simple but at the same time expose many phenomena characteristic for the

systems above, such as the J-point,[12,133] glass transition,[2,28,29,33,49,55,144,145,160] glass close packing limit,[2] random loose packing limit,[15,16] and others.[1–3,32,34,57] In our group, we also use hard-sphere systems with adjusted volume fraction and microstructural heterogeneity as a model in pore-scale simulations of diffusion, flow, and hydrodynamic dispersion.[6–8] This helps us to establish quantitative relationships between the morphology of microscopically disordered materials and their effective mass transport properties, which poses a considerable challenge in materials science.[165] Introducing polydispersity in hard-sphere systems not only represents more adequately their technical applications,[18] but also allows to better understand the interplay between different exposed phenomena and the physics behind them.[166] For example, monodisperse hard spheres exhibit spontaneous crystallization in a range of particle volume fractions (volume densities) $\varphi = 0.545 - 0.61$,[2,32–34,36,49] which prevents investigation of the glass transition in such systems. Sufficiently polydisperse sphere samples, on the other hand, do not crystallize[33] and allow direct study of the glass transition.

In this paper, we focus on frictionless, colloidal hard-sphere systems, where by definition all configurations without particle intersections are valid and equally probable, in contrast to granular systems, where particles are usually frictional and only mechanically stable configurations are considered valid. One of the relevant areas for investigation of frictionless, colloidal hard spheres was relating thermodynamic properties of these systems to their geometric properties. In the hard-sphere fluid, the excess chemical potential $\Delta\mu$ has been linked[167–169] to the probability

[12] C. S. O'Hern et al. *Phys. Rev. E*, 68, 011306, 2003.
[133] M. Pica Ciamarra, M. Nicodemi, and A. Coniglio. *Soft Matter*, 6, 2871–2874, 2010.
[2] G. Parisi and F. Zamponi. *Rev. Mod. Phys.*, 82, 789–845, 2010.
[28] G. Parisi and F. Zamponi. *J. Chem. Phys.*, 123, 144501, 2005.
[29] L. Berthier and T. A. Witten. *Phys. Rev. E*, 80, 021502, 2009.
[33] E. Zaccarelli et al. *Phys. Rev. Lett.*, 103, 135704, 2009.
[49] M. Skoge et al. *Phys. Rev. E*, 74, 041127, 2006.
[55] G. Brambilla et al. *Phys. Rev. Lett.*, 102, 085703, 2009.
[144] G. Pérez-Ángel et al. *Phys. Rev. E*, 83, 060501, 2011.
[145] T. Voigtmann, A. M. Puertas, and M. Fuchs. *Phys. Rev. E*, 70, 061506, 2004.
[160] V. Ogarko, N. Rivas, and S. Luding. *J. Chem. Phys.*, 140, 211102, 2014.
[15] G. Y. Onoda and E. G. Liniger. *Phys. Rev. Lett.*, 64, 2727–2730, 1990.
[16] M. Jerkins et al. *Phys. Rev. Lett.*, 101, 018301, 2008.
[1] C. Song, P. Wang, and H. A. Makse. *Nature*, 453, 629–632, 2008.
[3] S. Torquato and F. H. Stillinger. *Rev. Mod. Phys.*, 82, 2633–2672, 2010.
[32] E. Sanz et al. *Phys. Rev. Lett.*, 106, 215701, 2011.
[34] C. Valeriani et al. *J. Phys.: Condens. Matter*, 23, 194117, 2011.
[57] W. G. Hoover and F. H. Ree. *J. Chem. Phys.*, 49, 3609–3617, 1968.
[6] S. Khirevich, A. Höltzel, and U. Tallarek. *Commun. Comput. Phys.*, 13, 801–822, 2013.
[7] U. M. Scheven et al. *Phys. Rev. E*, 89, 053023, 2014.
[8] H. Liasneuski et al. *J. Appl. Phys.*, 116, 034904, 2014.
[165] T. Müllner, K. Unger, and U. Tallarek. *New J. Chem.*, accepted, –, 2016.
[18] A. Daneyko et al. *Anal. Chem.*, 83, 3903–3910, 2011.
[166] N. Kumar et al. *Particuology*, 12, 64–79, 2014.
[36] L. Filion et al. *J. Chem. Phys.*, 133, 4115, 2010.
[167] D. J. Adams. *Mol. Phys.*, 28, 1241–1252, 1974.
[168] R. J. Speedy. *J. Chem. Soc., Faraday Trans. 2*, 77, 329–335, 1981.
[169] R. J. Speedy and H. Reiss. *Mol. Phys.*, 72, 999–1014, 1991.

p_{insert} to insert a particle into the equilibrium fluid as $\frac{-\Delta\mu}{kT} = \ln(p_{\text{insert}})$. This equation represents a special case of the more general Widom particle insertion method.[167,170,171]

Measurement of p_{insert} for hard-sphere systems usually involved direct searching for points, where one more particle could be successfully inserted without intersecting originally present particles.[168,169,172] Connected regions of such points are called cavities. Sufficiently dense, finite systems contain no cavities and the method works therefore only for a relatively dilute hard-sphere fluid (*cf.* Fig. 5.2). We discuss the estimation of p_{insert} through cavities and free volumes as well as its limitations further in Section 5.2.5.

A popular tool for the investigation of hard-sphere system geometry is the pore-size (nearest-surface, void size) distribution f_{pore},[83–91] *i.e.*, the distribution of distances from points in the void space of a hard-sphere system to the nearest particle surfaces. By extrapolating this distribution f_{pore} to infinity and estimating the area under its tail we can compute the probability to insert a particle into a current configuration of hard spheres and thus, according to the Widom method, the excess chemical potential and finally the excess entropy.

The aim of this paper is to estimate p_{insert} through f_{pore} in monodisperse and polydisperse hard-sphere systems and to determine $\Delta\mu$ and Δs through the Widom insertion method. We provide a derivation of Widom's method for polydisperse hard spheres here as well, along with an expression for $\Delta\mu$ and Δs through f_{pore}. We validate our predictions for $\Delta\mu$ and Δs against the Boublík–Mansoori–Carnahan–Starling–Leland (BMCSL) equation of state[154–156] and its special case for monodisperse particles, the Carnahan–Starling equation.[173] For the polydisperse case, we employ log-normal particle radii distributions with polydispersities $\delta = \sqrt{\langle \Delta r^2 \rangle}/\langle r \rangle = 0.1$, 0.2, and 0.3. Hard-sphere systems that we use are three-dimensional, periodic in all directions, and consist of 10^4 spheres.

Compared with the estimation of p_{insert} (or $\Delta\mu$) through cavities and free volumes,[168,169,172] estimating p_{insert} through f_{pore} does not require "real" positions for particle insertion to be present in a current configuration. Our method is thus applicable up to the highest possible densities, as long as the extrapolation of f_{pore} is correct. Also, the estimation of p_{insert} through f_{pore} can be easily

[170] B. Widom. *J. Chem. Phys.*, 39, 2808–2812, 1963.
[171] D. Frenkel and B. Smit. *Understanding molecular simulation: From algorithms to applications*. 2nd ed. San Diego: Academic Press, 2002.
[172] S. Sastry et al. *Mol. Phys.*, 95, 289–297, 1998.
[83] S. Torquato, B. Lu, and J. Rubinstein. *Phys. Rev. A*, 41, 2059–2075, 1990.
[84] B. Lu and S. Torquato. *Phys. Rev. A*, 45, 5530–5544, 1992.
[85] S. Torquato. *Phys. Rev. E*, 51, 3170–3182, 1995.
[86] M. Alonso et al. *Chem. Eng. Sci.*, 50, 1983–1988, 1995.
[87] M. Alonso, M. Satoh, and K. Miyanami. *Can. J. Chem. Eng.*, 70, 28–32, 1992.
[88] I. Schenker et al. *Phys. Rev. E*, 80, 021302, 2009.
[89] I. Schenker et al. *Granul. Matter*, 14, 333–340, 2012.
[90] S. Torquato. *Annu. Rev. Mater. Res.*, 32, 77–111, 2002.
[91] D. Stoyan et al. *J. Non-Cryst. Solids*, 357, 1508–1515, 2011.
[154] T. Boublík. *J. Chem. Phys.*, 53, 471–472, 1970.
[155] V. Ogarko and S. Luding. *J. Chem. Phys.*, 136, 124508, 2012.
[156] G. A. Mansoori et al. *J. Chem. Phys.*, 54, 1523–1525, 1971.
[173] N. F. Carnahan and K. E. Starling. *J. Chem. Phys.*, 51, 635–636, 1969.

extended to polydisperse particles and, in principle, to particles of arbitrary shape. As mentioned, sufficiently polydisperse systems do not exhibit spontaneous crystallization (crystal nucleation),[33] contrary to monodisperse spheres, and the absence of crystal nucleation for polydisperse spheres allows to study directly phenomena that are obscured for monodisperse systems, *e.g.*, the ideal glass transition.[2,29] Our method for estimating $\Delta\mu$ through f_{pore} may thus be helpful in future studies of polydisperse fluids approaching the ideal glass transition.

We presented the procedure for fitting f_{pore} in monodisperse systems in Ref.[132] and employ it in the present work for both monodisperse and polydisperse particles. The validation of this procedure for monodisperse systems can be found in Ref.[132], the validation for polydisperse systems follows below (*cf.* Fig. 5.2). With certain assumptions about the structure of the phase space, we also related in Ref.[132] p_{insert} to ΔS (excess entropy of all the particles in the system) as $\ln(p_{\text{insert}}) = \Delta S$. We abandon this relation in the present work in favor of the Widom method, because the latter is a better established technique known to comply with equations of state.[172] The present work is thus different from Ref.[132] in regard to the application of Widom's method and the use of polydisperse particles.

5.2 Theory

In this section, we present equations required for the transitions from excess chemical potential $\Delta\mu$ to insertion probability p_{insert} and from p_{insert} to the pore-size distribution f_{pore}. We also present equations for expressing Δs through $\Delta\mu$ and the equations for validating our results against predictions from the equations of state.

Sections 5.2.1 and 5.2.2 present all the thermodynamic relations necessary for our discussion, *i.e.*, relations (i) between p_{insert} and $\Delta\mu$ and (ii) between $\Delta\mu$, Δs, and reduced pressure. The derivation for the polydisperse case can be found in Appendix 5.5. Section 5.2.3 presents equations of state that we utilize to obtain analytical expressions for Δs *vs.* φ and $\Delta\mu$ *vs.* φ and to validate our results from the Widom method. Section 5.2.4 shows how to estimate p_{insert} through f_{pore}. Finally, Section 5.2.5 discusses an alternative method of estimating p_{insert} through cavities and free volumes.

We use standard symbols p, V, U, T, S, μ, and N for kinematic pressure, volume, internal energy, temperature, entropy, chemical potential, and number of particles, respectively (in the canonical ensemble); k, T, and h denote the Boltzmann constant, temperature, and Planck length, respectively. We also use the reduced pressure $Z = pV/NkT$.[173,174] For the ideal gas, $Z^\circ = 1$. Excess quantities are denoted with Δ. We measure the excess entropy per particle Δs in units of the Boltzmann constant: $\Delta s = \frac{\Delta S}{kN}$. For hard spheres, both Z and Δs as well as $\frac{\Delta\mu}{kT}$ depend only on the solid volume fraction φ.

[132] V. Baranau et al. *Soft Matter*, 9, 3361–3372, 2013.
[174] N. F. Carnahan and K. E. Starling. *J. Chem. Phys.*, 53, 600–603, 1970.

5.2.1 Monodisperse hard spheres

In this subsection, we present equations that are needed for the monodisperse hard-sphere fluid. The derivations for most of them can be found in corresponding references and we do not repeat them here for clarity. More general derivations for polydisperse hard-sphere systems are presented in Appendix 5.5.

We start with the Widom particle insertion method for the estimation of μ.[167,170,171] For a system of N particles with arbitrary potential it reads

$$-\frac{\Delta\mu}{kT} = \ln\left[\left\langle \exp\left(-\frac{\Psi_N}{kT}\right)\right\rangle\right], \tag{5.1}$$

where averaging is performed by trying to uniformly insert the Nth particle into an equilibrium system of $N-1$ particles and Ψ_N is the potential energy of interaction of the Nth particle with all the remaining $N-1$ particles.

For hard spheres, Ψ_N is either zero or infinity and $\langle\exp(-\Psi_N/kT)\rangle$ is just the probability to correctly insert a hard sphere into an equilibrated system of $N-1$ spheres. The Widom method for hard spheres therefore reads[167–169]

$$-\frac{\Delta\mu}{kT} = \ln(p_{\text{insert}}). \tag{5.2}$$

We present the method for estimating p_{insert} in Section 5.2.4. To validate our estimation, we need the equation that expresses $\Delta\mu$ through Z and Δs:[167,169,174]

$$\frac{-\Delta\mu}{kT} = \ln(p_{\text{insert}}) = \Delta s - Z + 1. \tag{5.3}$$

Δs and Z are obtained from the equation of state in Section 5.2.3.

We also want to express the excess entropy solely through insertion probabilities and then compare it with the excess entropy from the equation of state. We briefly derive an expression of Δs purely through $\Delta\mu$. We introduce the partition function of the hard-sphere system Z_N and utilize the fundamental theorem of calculus for $\Delta\ln Z_N$ given that V and T are constant: $\Delta\ln Z_N = \Delta\ln Z_{N_0} + \int_{N_0}^{N}\left(\frac{\partial\Delta\ln Z_N}{\partial N}\right)_{T,V}\mathrm{d}N'$. The total entropy S can be expressed through $A = U - TS$, where by definition the Helmholtz free energy is $A = -kT\ln Z_N$. As far as all configurations in the hard-sphere fluid without particle intersections possess zero potential energy, the average internal energy is $U = U^\circ = \frac{3}{2}NkT$ or $\Delta U = 0$. It leads to $\Delta S = k\Delta\ln Z_N$ or $\Delta\ln Z_N = N\Delta s$. By utilizing $\frac{\partial\Delta\ln Z_N}{\partial N} = \frac{-\Delta\mu}{kT}$ (which follows from the definition of the chemical potential, $-\frac{\mu}{kT} = \frac{\partial}{\partial N}(\ln Z_N)$) we get $N\Delta s = N_0\Delta s_0 + \int_{N_0}^{N}\frac{-\Delta\mu}{kT}\mathrm{d}N'$. After switching from N to φ using $\varphi = NV_{\text{sp}}/V$,

where V_{sp} is sphere volume, we obtain

$$\Delta s = \frac{\varphi_0}{\varphi}\Delta s_0 + \frac{1}{\varphi}\int_{\varphi_0}^{\varphi}\frac{-\Delta\mu}{kT}\mathrm{d}\varphi' = \frac{\varphi_0}{\varphi}\Delta s_0 + \frac{1}{\varphi}\int_{\varphi_0}^{\varphi}\ln(p_{\text{insert}})\mathrm{d}\varphi'. \tag{5.4}$$

5.2.2 Polydisperse hard spheres

We repeat here the equations from Section 5.2.1 extended to polydisperse systems. The derivation of these equations can be found in Appendix 5.5.

The Widom method reads

$$-\frac{\Delta\mu_i}{kT} = \ln(p_{\text{insert},i}), \tag{5.5}$$

where $\Delta\mu_i$ and $p_{\text{insert},i}$ are the excess chemical potential and insertion probability for a particle of the ith species. In our case, particle species is defined by particle radius, though the same equation would apply for particles of arbitrary shape—the species would then be defined by the current shape and orientation.

The link between Δs, Z, and $\Delta\mu$ becomes

$$\left\langle\frac{-\Delta\mu}{kT}\right\rangle_R = \langle\ln(p_{\text{insert}})\rangle_R = \Delta s - Z + 1, \tag{5.6}$$

where $\langle x\rangle_R$ refers to the number-average of x over the particle radii distribution. The expression of Δs through $\Delta\mu$ is

$$\Delta s = \frac{\varphi_0}{\varphi}\Delta s_0 + \frac{1}{\varphi}\int_{\varphi_0}^{\varphi}\left\langle\frac{-\Delta\mu}{kT}\right\rangle_R\mathrm{d}\varphi' = \frac{\varphi_0}{\varphi}\Delta s_0 + \frac{1}{\varphi}\int_{\varphi_0}^{\varphi}\langle\ln(p_{\text{insert}})\rangle_R\mathrm{d}\varphi'. \tag{5.7}$$

When the particle radii distribution $f_R(r)$ is continuous, the averages are computed as

$$\langle\Delta\mu\rangle_R = \int_0^\infty \Delta\mu_r f_R(r)\mathrm{d}r,\ \langle\ln(p_{\text{insert}})\rangle_R = \int_0^\infty \ln(p_{\text{insert,r}})f_R(r)\mathrm{d}r, \tag{5.8}$$

where $p_{\text{insert,r}}$ is the probability to insert a particle of radius r into a hard-sphere configuration.

5.2.3 Equations of state

For validation, we need expressions of Δs *vs.* φ and of Z *vs.* φ. There are many equations of state $Z(\varphi)$ available for hard spheres. One of the most popular ones, which works also for polydisperse spheres, is the BMCSL equation[154–156,175] (or simply the Carnahan–Starling equation

[175] M. Maiti, A. Lakshminarayanan, and S. Sastry. *Eur. Phys. J. E*, 36, 1–13, 2013.

for monodisperse spheres[173]). We use the following representation of the BMCSL equation of state (Eq. (9) in Ogarko and Luding[155]):

$$Z(\varphi) = \frac{1}{1-\varphi} + O_1 \frac{3\varphi}{(1-\varphi)^2} + O_2 \frac{\varphi^2(3-\varphi)}{(1-\varphi)^3}, \tag{5.9}$$

where $O_1 = \frac{\langle r\rangle\langle r^2\rangle}{\langle r^3\rangle}$, $O_2 = \frac{\langle r^2\rangle^3}{\langle r^3\rangle^2}$, and $\langle r^i\rangle$ is the ith raw moment of particle radii r. For monodisperse spheres, $O_1 = 1$ and $O_2 = 1$. Validation of the BMCSL equation of state can be found in Refs.[29,164,175]

To derive an expression of Δs *vs.* φ, one has to utilize the following equation, which can be obtained through thermodynamic integration:[61,161,167,174] $\Delta s = -\int_0^{\varphi} \frac{Z(\varphi')-1}{\varphi'}\,\mathrm{d}\varphi'$. When we substitute here Eq. (5.9), we get[176]

$$\Delta s(\varphi) = 3O_1 - (O_2 - 1)\ln(1-\varphi) - \frac{(O_2 - 3O_1)\varphi + 3O_1}{(1-\varphi)^2}. \tag{5.10}$$

5.2.4 How to estimate insertion probability for hard-sphere systems

We estimate p_{insert} (in monodisperse systems) or $p_{\text{insert},r}$ (in polydisperse systems) by the following procedure. Firstly, we randomly generate a large number (10^7) of points with uniform spatial distribution in a system of hard spheres. Secondly, we calculate the distances to the nearest particle surfaces r_1 for every generated point: if the distance to the nearest particle center is r_c and the nearest particle radius is r_0, $r_1 = r_c - r_0$. Thirdly, we estimate the probability density function of these distances $f_{\text{pore}}(r_1)$. Then it is possible to calculate p_{insert} or $p_{\text{insert},r}$. If particle radius in the monodisperse case is R, we write

$$p_{\text{insert}} = \int_R^{\infty} f_{\text{pore}}(r_1)\mathrm{d}r_1, \; p_{\text{insert},r} = \int_r^{\infty} f_{\text{pore}}(r_1)\mathrm{d}r_1. \tag{5.11}$$

The distribution $f_{\text{pore}}(r_1)$ is described in many papers as the pore-size (nearest surface, void size) distribution.[83–91] $f_{\text{pore}}(r_1)$ can also be calculated through the Euclidean distance transform,[177–179] *i.e.*, an operator that maps for each point in the void space the distance to the closest solid point.

In finite systems, the integrals in Eq. (5.11) cannot be measured directly through the observed values of $f_{\text{pore}}(r_1)$, because we never observe infinitely large cavities. Moreover, for most hard sphere configurations discussed in this paper (denser than $\varphi \sim 0.5$, *cf.* Fig. 5.2) the max-

[164] V. Baranau and U. Tallarek. *Soft Matter*, 10, 7838–7848, 2014.
[61] D. Asenjo, F. Paillusson, and D. Frenkel. *Phys. Rev. Lett.*, 112, 098002, 2014.
[161] D. Frenkel and A. J. C. Ladd. *J. Chem. Phys.*, 81, 3188–3193, 1984.
[176] V. Baranau and U. Tallarek. *J. Chem. Phys.*, 143, 044501, 2015.
[177] C. R. Maurer, R. S. Qi, and V. Raghavan. *IEEE Trans. Pattern Anal. Mach. Intell.*, 25, 265–270, 2003.
[178] R. Fabbri et al. *ACM Comput. Surv.*, 40, 2:1–2:44, 2008.
[179] Y. Lucet. *Image Vis. Comput.*, 27, 37–44, 2009.

imum value for r_1 (the radius of the inserted "virtual" particle) is below the average particle radius, which implies that actually none of the values of $f_{\text{pore}}(r_1)$ needed for integration can be directly observed at high φ and that there are no cavities in hard-sphere systems. That is why we need to fit $f_{\text{pore}}(r_1)$ and extrapolate it to infinity.

As in our previous work[132] we follow Schenker *et al.*[88] and fit $f_{\text{pore}}(r_1)$ with a truncated Gaussian distribution:

$$f_{\text{pore}}(r_1) = C_p \frac{1}{\sigma_p\sqrt{2\pi}} \exp\left(-\frac{(r_1-\mu_p)^2}{2\sigma_p^2}\right),\ r_1 \geq 0. \tag{5.12}$$

Theoretical results[83–85] predict that $f_{\text{pore}}(r_1)$ is of the form $A\exp(ar_1^3+br_1^2+cr_1+d)$, of which Eq. (5.12) is a special case. The validity of the function in Eq. (5.12) was already demonstrated for monodisperse systems in our previous paper[132] (see Fig. 2 in that reference). Tests for polydisperse systems are provided later in Section 5.3.4 (Fig. 5.2).

The normalization constant C_p in Eq. (5.12) corresponds to the fact that the probability for a randomly inserted point to appear in the interparticle void space is $1-\varphi$. This constant can be computed using the requirement $\int_0^\infty f_{\text{pore}}(r_1)\mathrm{d}r_1 = 1-\varphi$.

Fits of f_{pore} for both monodisperse and polydisperse systems were performed by least-square fitting of the measured $\ln(f_{\text{pore}}(r_1))$ with the second-order polynomial for $r_1 \geq 0.1$ (given that the average particle diameter is unity). An alternative is to use the maximum likelihood method for the truncated Gaussian distribution,[114] but we found that least-square fits give slightly better estimates for p_{insert} and $p_{\text{insert},r}$, because they favor values with large r_1, and we are specifically interested in the extrapolation of f_{pore} from large r_1 to infinity.

By combining Eqs. (5.2), (5.11), and (5.12), we get for monodisperse systems

$$\frac{-\Delta\mu}{kT} = \ln(p_{\text{insert}}) = \ln\left(\frac{C_p}{2}\left[1-\operatorname{erf}\left\{\frac{R-\mu_p}{\sigma_p\sqrt{2}}\right\}\right]\right). \tag{5.13}$$

As follows from Eqs. (5.8), (5.11), and (5.12), the corresponding equation for polydisperse systems reads

$$\begin{aligned}\left\langle\frac{-\Delta\mu}{kT}\right\rangle_R &= \langle\ln(p_{\text{insert}})\rangle_R = \int_0^\infty \ln\left(\int_r^\infty f_{\text{pore}}(r_1)\mathrm{d}r_1\right) f_R(r)\mathrm{d}r \\ &= \int_0^\infty \ln\left(\frac{C_p}{2}\left[1-\operatorname{erf}\left\{\frac{r-\mu_p}{\sigma_p\sqrt{2}}\right\}\right]\right) f_R(r)\mathrm{d}r.\end{aligned} \tag{5.14}$$

[114] A. C. Cohen. *Ann. Math. Stat.*, 21, 557–569, 1950.

5.2.5 Cavities and free volumes

At the end of this section, we compare our approach with the estimation of $\frac{-\Delta\mu}{kT} = \ln(p_{\text{insert}})$ through cavity[168,169,175,180–185] and free volume[172,175,182,184,186] statistics.

The insertion probability p_{insert} can be estimated through cavities.[168,169] A cavity is a connected region in a hard-sphere system, for which each point can be the center of an inserted particle so that the inserted particle does not intersect particles originally present in the system. If V_0 is the total volume of cavities, $\langle v_c \rangle$ the average cavity volume, and N_c the number of cavities in a system, then

$$p_{\text{insert}} = V_0/V = \langle v_c \rangle N_c/V. \tag{5.15}$$

This result can be reformulated in terms of free volumes.[168,172,187] In this context, the free volume of a particular sphere in a system is a set of points, for which the sphere can be continuously displaced without intersecting other spheres (with fixed positions) in the system. This "geometric" free volume shall not be confused with a "thermodynamic" free volume[9,51–53] (*cf.* Section 6 in Ref.[169]). By noticing that a cavity is free volume of a sphere that can be added to a system, several relations between cavity geometry and free volume geometry can be derived.[172] For example, if $\langle v_f \rangle$, $\langle s_f \rangle$, and $\langle s_c \rangle$ are the average free volume of particles in a system, the average surface of free volumes of particles in a system, and the average surface of cavities in a system, respectively, we can write

$$\langle v_f^{-1} \rangle = \langle v_c \rangle^{-1}, \langle s_f/v_f \rangle = \langle s_c \rangle / \langle v_c \rangle. \tag{5.16}$$

To complete the discussion of cavities and free volumes, we note that reduced pressure Z can also be expressed in terms of free volumes and cavities:[168,172,175,182,186,187]

$$Z = \frac{pV}{NkT} = 1 + \frac{R}{D}\frac{\langle s_c \rangle}{\langle v_c \rangle} = 1 + \frac{R}{D}\left\langle \frac{s_f}{v_f} \right\rangle, \tag{5.17}$$

where R is the particle radius and D is the system dimensionality (3 in our case). This equation is also a special case of a more general equation that can be derived for an arbitrary pair potential through the Widom insertion method.[167,170]

[180] R. K. Bowles and R. J. Speedy. *Mol. Phys.*, 83, 113–125, 1994.
[181] S. Sastry et al. *Phys. Rev. E*, 56, 5524–5532, 1997.
[182] P. G. Debenedetti and T. M. Truskett. *Fluid Phase Equilib.*, 158-160, 549–556, 1999.
[183] A. Vishnyakov, P. G. Debenedetti, and A. V. Neimark. *Phys. Rev. E*, 62, 538–544, 2000.
[184] P. G. Debenedetti et al. *Adv. Chem. Eng.*, 28, 21–79, 2001.
[185] M. Mézard et al. *J. Stat. Mech.*, 2011, P03002, 2011.
[186] M. Maiti and S. Sastry. *J. Chem. Phys.*, 141, 044510, 2014.
[187] W. G. Hoover, W. T. Ashurst, and R. Grover. *J. Chem. Phys.*, 57, 1259–1262, 1972.
[9] Z. W. Salsburg and W. W. Wood. *J. Chem. Phys.*, 37, 798–804, 1962.
[51] J. G. Kirkwood. *J. Chem. Phys.*, 18, 380–382, 1950.
[52] R. J. Buehler et al. *J. Chem. Phys.*, 19, 61–71, 1951.
[53] W. W. Wood. *J. Chem. Phys.*, 20, 1334–1334, 1952.

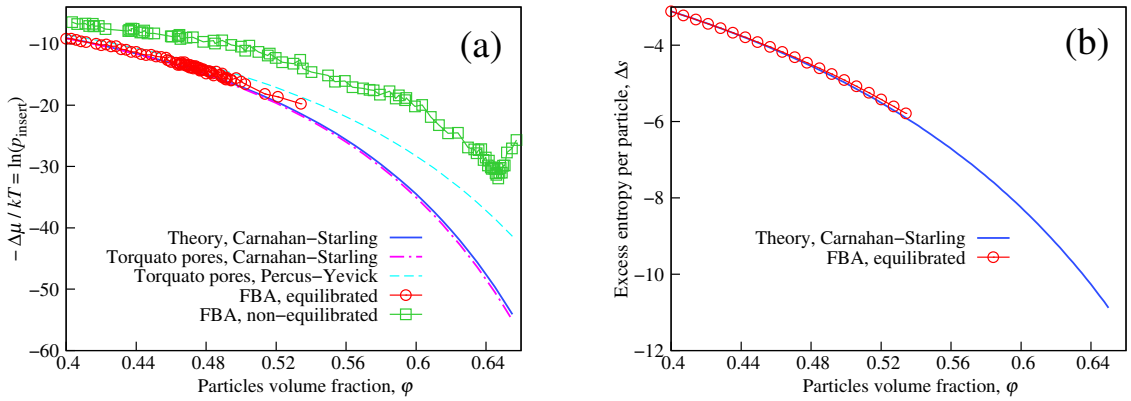

Figure 5.1: Validation of the chemical potential and entropy estimates for monodisperse hard-sphere systems. (a) Comparison of $-\Delta\mu/kT$ from theory with obtained estimates. "Theory, Carnahan–Starling", blue solid line: theoretical prediction (Eq. (5.3)) when the Carnahan–Starling equation of state is supplied (Eqs. (5.9) and (5.10)). "FBA equilibrated", red circles: Widom's estimates ($-\Delta\mu/kT = \ln(p_{\text{insert}})$) when the pore-size distribution (Eq. (5.13)) from equilibrated FBA configurations is supplied. "Torquato pores, Carnahan-Starling", magenta dashed-dotted line: Widom's estimates when the pore-size distribution predicted by Torquato *et al.*[83] for the Carnahan–Starling equation of state is supplied. "Torquato pores, Percus–Yevick", cyan dashed line: Widom's estimates when the pore-size distribution predicted by Torquato *et al.*[83] for the Percus–Yevick equation of state is supplied. "FBA non-equilibrated", green squares: Widom's estimates when the pore-size distribution (Eq. (5.13)) from non-equilibrated FBA configurations is supplied. (b) Comparison of the excess entropy per particle Δs from theory with estimates. "Theory, Carnahan-Starling", blue line: thermodynamic integration with the Carnahan–Starling equation of state (Eq. (5.10)). "FBA, equilibrated", red circles: integration of the chemical potential (Eq. (5.4)); the chemical potential is taken from Widom's estimates for the equilibrated FBA configurations (red circles in panel (a)).

As mentioned, even in moderately dense hard-sphere systems with $\varphi \approx 0.5$ cavities cannot be observed directly. It is not problematic for the estimation of pressure through Eq. (5.17), because cavity statistics can be completely replaced with free volume statistics (the term $\langle s_f/v_f\rangle$). The excess chemical potential, though, is expressed through free volumes by combining Eqs. (5.2), (5.15), and (5.16) as

$$\frac{-\Delta\mu}{kT} = \ln\left(\frac{N_c\langle v_c\rangle}{V}\right) = \ln\left(\frac{N_c}{V\langle v_f^{-1}\rangle}\right). \tag{5.18}$$

The last relation implies that the number of cavities in a hard-sphere system is still needed to estimate p_{insert} or $\Delta\mu$ even after switching to the average free volume. Thus, this method can be applied only to relatively dilute arrangements of hard spheres.

5.3 Results and discussion

5.3.1 Overview

In this section, we compare $\frac{-\Delta\mu}{kT}$ and Δs from theoretical predictions with values obtained through the pore-size distribution $f_{\text{pore}}(r_1)$ in computer-generated monodisperse and polydisperse hard-sphere systems. Theoretical excess chemical potentials are taken from Eqs. (5.3) and

(5.6), after the BMCSL equation of state is supplied (Eqs. (5.9) and (5.10)). The theoretical excess entropy is taken from Eq. (5.10). Estimates of the excess chemical potential through the Widom method and pore-size distribution are computed according to Eqs. (5.13) and (5.14) for monodisperse and polydisperse spheres, respectively. Estimates of the excess entropy through the Widom method are computed according to Eqs. (5.4) and (5.7) for monodisperse and polydisperse cases, respectively.

5.3.2 Preparation of hard-sphere configurations

All hard-sphere configurations that we use are three-dimensional, with periodic boundaries in all directions, and consist of 10^4 particles. Polydisperse spheres have log-normal particle radii distribution with three values of polydispersity, $\delta = \sqrt{\langle \Delta r^2 \rangle}/\langle r \rangle = 0.1$, 0.2, and 0.3. Widom's method assumes that the hard spheres are equilibrated. We already studied the properties of equilibrated monodisperse and log-normal systems in our previous papers[164,176] and we use a subset of the systems from Ref.[164] here.

The equilibration procedure requires some initial hard sphere arrangements to be supplied as input. The generation of initial non-equilibrated configurations as well as their equilibration are explained in Ref.[164] We used two sets of initial configurations in that work. The first set was generated by the force-biased algorithm (FBA).[98,99,132] The second set was prepared by taking the densest obtained FBA configurations and scaling particle diameters to reach desired densities. These configurations were referred to as "diluted densest" configurations. In the present manuscript, we use monodisperse equilibrated FBA configurations, monodisperse non-equilibrated FBA configurations, and polydisperse equilibrated "diluted densest" configurations.

Equilibration in Ref.[164] was realized by performing event-driven molecular dynamics simulations[92,135,188] starting at initial configurations from above. Technically, this was the Lubachevsky–Stillinger algorithm[95,135] running with zero compression rate until kinematic pressure became stationary. We equilibrated systems by performing sets of $2 \cdot 10^7$ collisions with zero compression rate in a loop until the relative difference of reduced pressures between the last two sets was less than 10^{-4}, so that pressure can be regarded as stationary. More precisely, to measure pressure during the $2 \cdot 10^7$ collisions, we averaged pressures for 100 sub-sets of $2 \cdot 10^5$ collisions, which amounts to 20 collisions in a sub-set per particle.

5.3.3 Monodisperse hard spheres

We now compare $\frac{-\Delta\mu}{kT}$ and Δs from theoretical predictions with values obtained through the pore-size distribution in monodisperse systems.

[98] J. Mościński et al. *Mol. Simul.*, 3, 201–212, 1989.
[99] A. Bezrukov, M. Bargieł, and D. Stoyan. *Part. Part. Syst. Char.*, 19, 111–118, 2002.
[92] A. Donev, S. Torquato, and F. H. Stillinger. *J. Comput. Phys.*, 202, 765–793, 2005.
[135] B. D. Lubachevsky. *J. Comput. Phys.*, 94, 255–283, 1991.
[188] S. Miller and S. Luding. *J. Comput. Phys.*, 193, 306–316, 2004.
[95] B. D. Lubachevsky and F. H. Stillinger. *J. Stat. Phys.*, 60, 561–583, 1990.

For that purpose, we used configurations with solid volume fraction $\varphi = 0.4 - 0.54$. We cannot use $\varphi > 0.545$ for two reasons: (i) for $\varphi = 0.545 - 0.61$ monodisperse systems exhibit spontaneous crystallization during equilibration,[2,32–34,36,49] (ii) for $\varphi > 0.61$ the phase space presumably is non-ergodic.[2,33,37,144,164] For spontaneously crystallized systems, the pore-size distributions are not sufficiently Gaussian and we are not aware of analytical equations of state in this region (though one can, in principle, use reduced pressure from simulations). We have to exclude configurations with $\varphi > 0.61$ as well, because the phase space for hard spheres, even if crystallization is suppressed, becomes non-ergodic according to some estimates at $\varphi \approx 0.585$.[33,37,144] This density is termed the ideal glass transition density φ_g.[2,28,29,33,49,55,144,145] We also recovered $\varphi_g = 0.585$ in our previous simulations with equilibration.[164,176] For monodisperse spheres, we estimated φ_g by analyzing sufficiently polydisperse systems, which do not exhibit spontaneous crystallization, and extrapolating their φ_g to the monodisperse case.

We note that the determination of φ_g remains a matter of debate. For example, different techniques are reported to yield estimates of φ_g from 0.614 to 0.635 for a bidisperse $50 : 50$ (by number) system with particle radii ratio of 1.4.[29,55] Similarly, it has been suggested that the "offset" of crystallization for monodisperse spheres at $\varphi \approx 0.61$ corresponds to φ_g.[56] Recent careful simulations indicate that these are indeed unrelated phenomena and that the phase space becomes non-ergodic at φ lower than 0.61.[32–34] Because of difficulties with determination of φ_g it is possible that we only estimated lower bounds on φ_g in Ref.[164], in which case our equilibration protocol was not capable of equilibrating configurations between the estimated φ_g and the "true" φ_g. In this case the Widom method and equilibrium thermodynamics are also not applicable to such systems.

We present the comparison of $\frac{-\Delta\mu}{kT}$ from Eqs. (5.3) and (5.13) in Fig. 5.1a. For demonstration, we also present $\frac{-\Delta\mu}{kT}$ for the non-equilibrated FBA configurations used as input for equilibration. Each point on the two FBA lines in Fig. 5.1a corresponds to a single configuration. We see that $\frac{-\Delta\mu}{kT}$ from Eqs. (5.3) and (5.13) demonstrate excellent agreement for the equilibrated FBA configurations. As expected, the non-equilibrium configurations have pore-size distributions different from the equilibrated systems and their excess chemical potentials are not complying with the theoretical predictions.

We also provide in Fig. 5.1a the estimates for $\frac{-\Delta\mu}{kT} = \ln\left(\int_R^\infty f_{\text{pore}}(r_1)\mathrm{d}r_1\right)$ based on the theoretical prediction for $f_{\text{pore}}(r_1)$ by Torquato *et al.*[83] The form of $f_{\text{pore}}(r_1)$ depends on the assumed equation of state. We present for comparison the results obtained after supplying the Carnahan-Starling equation of state (*cf.* Eq. (4.33) in Ref.[83]) and the Percus–Yevick equation of state (*cf.* Eq. (4.27) in Ref.[83]). The result for the Carnahan-Starling equation of state comes very close to the analytical computation with Eqs. (5.3), (5.9), and (5.10) which supports the premise that $\ln(f_{\text{pore}}(r_1))$ shall be a polynomial of at most third order.

We mention here that the computation through free volumes according to Eq. (5.18) (*cf.* Fig. 9 in Sastry *et al.*[172]) produces comparably accurate results (in the range $\varphi < 0.494$ presented

[37] R. J. Speedy. *Mol. Phys.*, 95, 169–178, 1998.
[56] W. van Megen and S. M. Underwood. *Phys. Rev. E*, 49, 4206–4220, 1994.

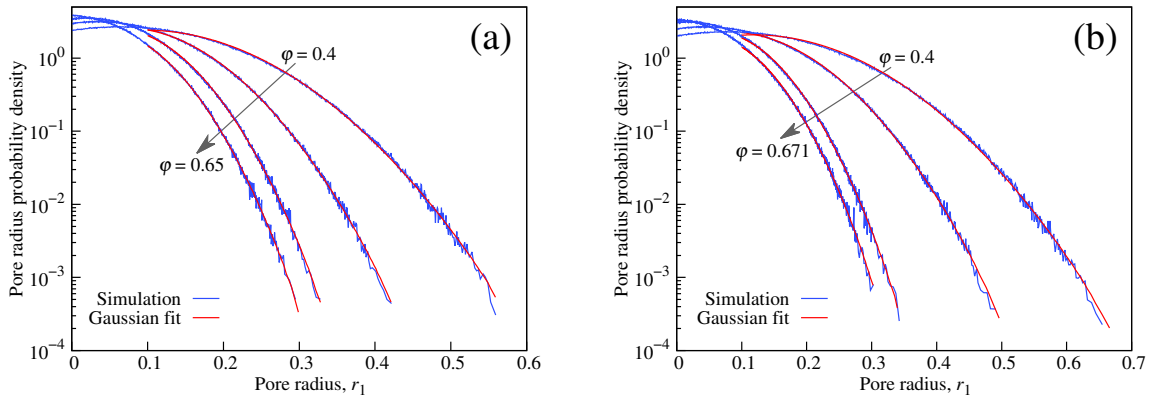

Figure 5.2: Pore-size distributions for polydisperse hard spheres (blue) and their Gaussian fits (red). Particle radii have log-normal distribution, average particle diameter is normalized to unity. (a) Polydispersity $\delta = \sqrt{\langle \Delta r^2 \rangle}/\langle r \rangle = 0.1$. Solid volume fractions φ along the arrow are 0.4, 0.5, 0.58, and 0.65. (b) Polydispersity $\delta = 0.3$. Solid volume fractions φ along the arrow are 0.4, 0.5, 0.615, and 0.671.

in Ref.[172]). But, as explained, this technique is not extendable to high densities.

Fig. 5.1b demonstrates theoretical excess entropies Δs from Eq. (5.10) and excess entropy estimates from integrating chemical potential (Eq. (5.4)), when chemical potential estimates for the equilibrated FBA configurations from Fig. 5.1a are supplied. We use Δs_0 from the BMCSL equation of state (Eq. (5.10)) at $\varphi_0 = 0.4$. Again, the agreement is very good. We note though that the agreement between $\frac{-\Delta\mu}{kT}$ in Fig. 5.1a can be viewed as more convincing, since it does not involve any artificial matching of curves, whereas in Fig. 5.1b we impose equality for Δs at $\varphi = \varphi_0$ implicitly.

5.3.4 Polydisperse hard spheres

In this section, we provide validation for polydisperse hard spheres. We use equilibrated "diluted densest" sphere configurations with log-normal particle radii distribution

$$f_R(r) = f_{\text{LN}}(r; \mu_{\text{LN}}, \sigma_{\text{LN}}) = \frac{1}{r\sigma_{\text{LN}}\sqrt{2\pi}} \exp\left[-\frac{(\ln(r) - \mu_{\text{LN}})^2}{2\sigma_{\text{LN}}^2}\right]. \tag{5.19}$$

We can rewrite Eq. (5.14) to account for the log-normal particle radii distribution:

$$\left\langle \frac{-\Delta\mu}{kT} \right\rangle_R = \langle \ln(p_{\text{insert}}) \rangle_R = \int_0^\infty \ln\left(\frac{C_p}{2}\left[1 - \text{erf}\left\{\frac{r - \mu_p}{\sigma_p\sqrt{2}}\right\}\right]\right) f_{\text{LN}}(r; \mu_{\text{LN}}, \sigma_{\text{LN}}) \text{d}r. \tag{5.20}$$

We use three polydispersities $\delta = \sqrt{\langle \Delta r^2 \rangle}/\langle r \rangle$, $\delta = 0.1$, 0.2, and 0.3. It is known that hard spheres with $\delta > 0.08$ do not exhibit spontaneous crystallization,[33] so the smallest δ chosen, $\delta = 0.1$, is high enough in that regard.

First, we demonstrate in Fig. 5.2 how the pore-size distributions of the equilibrated polydis-

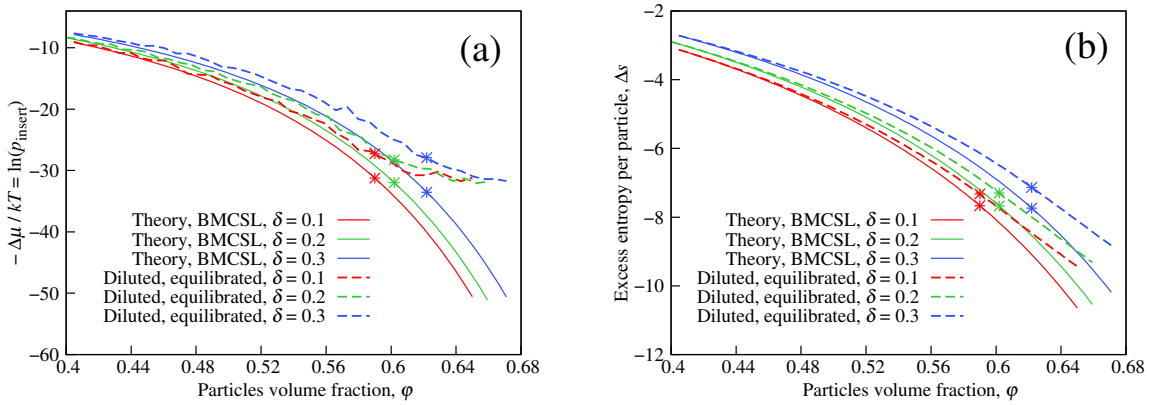

Figure 5.3: Validation of the chemical potential and entropy estimates for polydisperse systems with log-normal sphere radii distributions and polydispersities δ. (a) Comparison of $\langle -\Delta\mu/kT \rangle_R$ from theory with obtained estimates. "Theory, BMCSL", solid lines: theoretical prediction (Eq. (5.6)) when the Boublík–Mansoori–Carnahan–Starling–Leland equation of state is supplied (Eqs. (5.9) and (5.10)). "Diluted, equilibrated", dashed lines: Widom's estimates ($\langle -\Delta\mu/kT \rangle_R = \langle \ln(p_{\text{insert}}) \rangle_R$) when the pore-size distributions (Eq. (5.20)) from equilibrated "diluted densest" configurations are supplied. (b) Comparison of the excess entropy per particle Δs from theory with estimates. "Theory, BMCSL", solid lines: thermodynamic integration with the BMCSL equation of state (Eq. (5.10)). "Diluted, equilibrated", dashed lines: integration of the chemical potential (Eq. (5.7)); the chemical potential is taken from Widom's estimates for the equilibrated "diluted densest" configurations (dashed lines in panel (a)). Stars of the corresponding colours denote our estimates of the ideal glass transition densities φ_g.

perse hard spheres comply with Gaussian fits. The figure shows that in the entire range of studied densities the tails of the pore-size distributions conform exceptionally well to the Gaussian form for all studied polydispersities, $\delta \leq 0.3$. As mentioned, a similar comparison for non-equilibrated monodisperse spheres can be found in Fig. 2 of Ref.[132]

The results of the validation for $\langle -\Delta\mu/kT \rangle_R = \langle \ln(p_{\text{insert}}) \rangle_R$ and Δs are presented in Fig. 5.3. Panel (a) compares $\langle \ln(p_{\text{insert}}) \rangle_R$ from Eq. (5.20)—dashed lines—with the analytical result from Eq. (5.6) (when Eqs. (5.9) and (5.10) are supplied)—solid lines. Panel (b) compares Δs from Eq. (5.7) (when Eq. (5.20) is supplied)—dashed lines—with Δs from Eq. (5.10)—solid lines. In panel (b), we use Δs_0 from the BMCSL equation of state at $\varphi_0 = 0.4$. The dashed lines in Fig. 5.3a connect individual points, each representing a single sphere configuration. Configurations for all polydispersities δ were prepared at solid volume fraction steps $\Delta\varphi \approx 0.007$.

As for the monodisperse spheres, it is believed that at a certain volume fraction φ, referred to as the ideal glass transition density φ_g, the phase space for a given particle size distribution presumably becomes non-ergodic[2,33] and the equation of state, as well as the Widom insertion method and thermodynamic relations, are not expected to be applicable. The stars in both panels of Fig. 5.3 denote our estimates of φ_g for the respective polydispersity δ.[164]

The comparison of the BMCSL equation of state for log-normal "diluted densest" configurations with stationary pressures from simulations can be found in Fig. 6 of our previous paper.[164] The equilibrium reduced pressure that we observed started to deviate from Eq. (5.9) at our estimates of φ_g. It proves that the BMCSL equation of state is applicable at least up to our estimates

of φ_g . Other validations of the BMCSL equation for polydisperse systems produce quantitatively similar results.[29,175] There are extensions of the BMCSL equation to higher densities,[189] which are parametrized by the final jamming density of a current metastable branch at which the hard-sphere system resides, but in this paper we decided to restrain ourselves from discussing equations of state for $\varphi > \varphi_g$ given controversial interpretations of this density region.

As mentioned, the employed estimates of φ_g may be lower bounds of the "real" ideal glass transition densities and our equilibration procedure was not sufficient at the densities in-between. In this case the Widom method and equilibrium thermodynamics are also not applicable to densities higher than the estimated φ_g.

The results from the Widom method compare well with the analytical results at $\varphi < \varphi_g$, especially for low densities. Similar to Fig. 5.1, Fig. 5.3a can be seen as more convincing than Fig. 5.3b, because we do not enforce a matching of curves at any density, which we do implicitly in Fig. 5.3b by selecting an initial φ_0 for integration.

5.4 Summary

We have applied the Widom insertion method to systems of monodisperse and polydisperse hard spheres to express the excess chemical potential through the probabilities to insert a particle into an equilibrated configuration. We used random, computer-generated, monodisperse and polydisperse, three-dimensional configurations with periodic boundary conditions. Polydisperse spheres had log-normal radii distributions with polydispersities $\delta = 10\%$, 20%, and 30%. We estimated particle insertion probabilities by fitting pore-size distributions, extrapolating them to infinity, and measuring the area under their tails. In such systems, it is also possible to estimate the excess entropy per particle Δs as a functional of only the excess chemical potential, so that we were able to express Δs through the pore-size distribution.

We compared estimated excess chemical potentials and entropies to theoretical predictions that can be derived from equations of state for the hard-sphere fluid. We used configurations with solid volume fraction $\varphi > 0.4$ and supplied the Boublík-Mansoori–Carnahan–Starling–Leland (BMCSL) equation of state into theoretical relations for chemical potential and entropy.

Both the estimated excess chemical potential and the estimated excess entropy comply well with theoretical predictions in the range of φ where equilibrium pressure in the hard-sphere systems is described by the BMCSL equation of state. In monodisperse systems, the BMCSL equation of state (which becomes the Carnahan–Starling equation of state) applies up to the melting transition at $\varphi = 0.545$. In sufficiently polydisperse systems, the BMCSL equation of state applies to higher densities, in our case at least up to $\varphi = 0.59$ for $\delta = 0.1$ and up to $\varphi = 0.622$ for $\delta = 0.3$. This happens because spontaneous crystallization is suppressed in these systems. In our simulations, pressure after equilibration departs from the BMCSL equation of state at densities that coincide with our estimates for the ideal glass transition, where the phase space presumably becomes non-ergodic and equilibrium statistical physics is inapplicable.

[189] P. Paricaud. *J. Chem. Phys.*, 143, 044507, 2015.

In an accompanying paper,[190] we extended the combined approach from the current work for estimating Δs through p_{insert} and p_{insert} through f_{pore} to granular packings of frictional particles, where only mechanically stable configurations are considered valid. Methodology presented in the current manuscript is used to estimate the Edwards entropy[44,47,61,62] through the particle insertion probability.

Acknowledgements

We thank the John von Neumann Institute for Computing (NIC) and the Jülich Supercomputing Center (JSC), Forschungszentrum Jülich (FZJ, Jülich, Germany), for the allocation of a special CPU-time grant (NIC project number: 10261, JSC project ID: HMR10).

5.5 Appendix

Here we briefly derive the equations from Section 5.2.2. This section can also serve in understanding the equations for monodisperse particles.

5.5.1 Widom's method

We assume at first a finite number of species (*i.e.*, possible particle radii) M, with N_i being the number of particles of the ith species, $\sum_i N_i = N$. The partition function of a fluid of N indistinguishable particles of mass m is

$$Z_N = \left(\frac{2\pi mkT}{h^2}\right)^{3N/2} Q_N, \tag{5.21}$$

where Q_N is the configurational integral

$$Q_N = \frac{1}{\prod_j N_j!} \int_V \dots \int_V \exp\left(-\frac{U_N}{kT}\right) \mathrm{d}\vec{r}_1 \dots \mathrm{d}\vec{r}_N. \tag{5.22}$$

Here, U_N is the potential energy of interaction of all the N particles.

By definition, the chemical potential for a species is

$$-\frac{\mu_i}{kT} = \frac{\partial}{\partial N_i}(\ln Z_N) = \frac{3}{2}\ln\left(\frac{2\pi mkT}{h^2}\right) + \frac{\partial \ln(Q_N)}{\partial N_i}. \tag{5.23}$$

We notice that

$$\frac{\partial \ln(Q_N)}{\partial N_i} = \ln \frac{Q_{N+1,i}}{Q_N}, \tag{5.24}$$

[190] V. Baranau et al. *Soft Matter*, 12, 3991–4006, 2016.
[44] S. F. Edwards and R. B. S. Oakeshott. *Physica A*, 157, 1080–1090, 1989.
[47] D. Bi et al. *Annu. Rev. Condens. Matter Phys.*, 6, 63–83, 2015.
[62] R. K. Bowles and S. S. Ashwin. *Phys. Rev. E*, 83, 031302, 2011.

where $Q_{N+1,i}$ is the configurational integral of a system after adding one more particle of type i.

The Widom method proceeds with the evaluation of $Q_{N+1,i}$ through Q_N and $\Psi_{N+1,i}$—the potential energy of interaction of the $N+1$th particle with the initial N particles:

$$\begin{aligned} Q_{N+1,i} =& \frac{1}{(N_i+1)\prod_j N_j!} \int\limits_V \dots \int\limits_V \exp\left(-\frac{\Psi_{N+1,i}}{kT}\right) \exp\left(-\frac{U_N}{kT}\right) \mathrm{d}\vec{r}_1 \dots \mathrm{d}\vec{r}_{N+1} \\ =& Q_N \frac{1}{N_i+1} \int\limits_V \dots \int\limits_V \exp\left(-\frac{\Psi_{N+1,i}}{kT}\right) \frac{\exp\left(-\frac{U_N}{kT}\right)}{Q_N \prod_j N_j!} \mathrm{d}\vec{r}_1 \dots \mathrm{d}\vec{r}_{N+1} \\ =& Q_N \frac{V}{N_i+1} \left\langle \exp\left(-\frac{\Psi_{N+1,i}}{kT}\right) \right\rangle_{\mathrm{PS}}. \end{aligned} \tag{5.25}$$

Here, averaging (over the "phase space") assumes that we take all the spatial configurations of N particles with their corresponding weight in the canonical ensemble $\frac{\exp\left(-\frac{U_N}{kT}\right)}{Q_N \prod_j N_j!} = \frac{\exp\left(-\frac{U_N}{kT}\right)}{\int\limits_V \dots \int\limits_V \exp\left(-\frac{U_N}{kT}\right) \mathrm{d}\vec{r}_1 \dots \mathrm{d}\vec{r}_N}$ and try to insert the $N+1$th particle into the system uniformly.

Thus,

$$-\frac{\mu_i}{kT} = \frac{3}{2} \ln\left(\frac{2\pi mkT}{h^2}\right) + \ln\left(\frac{V}{N_i}\right) + \ln\left(\left\langle \exp\left(-\frac{\Psi_{N+1,i}}{kT}\right) \right\rangle_{\mathrm{PS}}\right). \tag{5.26}$$

We replaced N_i+1 with N_i, which is valid for large enough N. For the ideal gas with the same species composition, we immediately get

$$-\frac{\mu_i^\circ}{kT} = \frac{3}{2} \ln\left(\frac{2\pi mkT}{h^2}\right) + \ln\left(\frac{V}{N_i}\right). \tag{5.27}$$

We could continue our discussion operating with absolute quantities, like μ_i in Eq. (5.26), but we notice that for hard spheres thermodynamic properties like μ_i in Eq. (5.26) contain $\frac{N_i}{V}$ (number density), which can take any value for a fixed volume density φ, depending on the choice of sphere radii. To get rid of this term, we switch to excess quantities. The excess chemical potential $\Delta\mu_i = \mu_i - \mu_i^\circ$ is

$$-\frac{\Delta\mu_i}{kT} = \ln\left(\left\langle \exp\left(-\frac{\Psi_{N+1,i}}{kT}\right) \right\rangle_{\mathrm{PS}}\right). \tag{5.28}$$

Next, we assume that an equilibrium system of N particles can represent the entire configurational space.[168,187] Therefore, we can estimate $\langle \exp(-\Psi_{N+1,i}/kT) \rangle_{\mathrm{PS}}$ by inserting a particle into only a single equilibrated configuration of N particles:

$$\left\langle \exp\left(-\frac{\Psi_{N+1,i}}{kT}\right) \right\rangle_{\mathrm{PS}} = \left\langle \exp\left(-\frac{\Psi_{N+1,i}}{kT}\right) \right\rangle, \tag{5.29}$$

where averaging at the right-hand side is performed by trying to insert the $N+1$th particle uniformly into an equilibrated configuration. We thus arrive at

$$-\frac{\Delta\mu_i}{kT} = \ln\left[\left\langle \exp\left(-\frac{\Psi_{N+1,i}}{kT}\right)\right\rangle\right]. \tag{5.30}$$

For hard spheres, both $\Psi_{N+1,i}$ and U_N are either zero or infinity, and thus $Q_N\prod_j N_j! = \int_V ... \int_V e^{-\frac{U_N}{kT}} \mathrm{d}\vec{r}_1 ... \mathrm{d}\vec{r}_N$ is just the volume in the phase space of correct configurations of N particles (the ones without intersections), while $\langle \exp(-\Psi_{N+1,i}/kT)\rangle_{\mathrm{PS}}$ is the average probability of correctly inserting a particle into a configuration of N spheres,[167] where averaging is performed over all correct configurations of N hard spheres. We shall take only correct configurations of N particles for averaging, because incorrect ones will have zero weight due to $U_N = \infty$ in Eq. (5.25). If we omit averaging and switch to equilibrated (valid) configurations, like in Eq. (5.29), we write

$$\left\langle \exp\left(-\frac{\Psi_{N+1,i}}{kT}\right)\right\rangle = p_{\mathrm{insert},i}, \tag{5.31}$$

where "insert, i" refers to insertion of the particle of type i into the equilibrated hard-sphere fluid. We finally get

$$-\frac{\Delta\mu_i}{kT} = \ln(p_{\mathrm{insert},i}). \tag{5.32}$$

5.5.2 Entropy through pressure and chemical potential

To derive Eq. (5.6) (or Eq. (5.3) in the monodisperse case), we start by writing the expression for the Gibbs free energy G in the (equilibrated) hard-sphere system:[174]

$$G = A + pV = U - TS + pV = \sum_i \mu_i N_i. \tag{5.33}$$

Eq. (5.33) in excess quantities becomes

$$\Delta U - T\Delta S + V\Delta p = \sum_i \Delta\mu_i N_i. \tag{5.34}$$

After dividing Eq. (5.34) by NkT, utilizing $\Delta U = 0$ and $Z^\circ = 1$, we obtain Eq. (5.6)

$$\left\langle \frac{-\Delta\mu}{kT}\right\rangle_R = \langle \ln(p_{\mathrm{insert}})\rangle_R = \Delta s - Z + 1, \tag{5.35}$$

where $\langle x\rangle_R$ refers to the number-average of x over particle species (in our case, particle radii), $\langle x\rangle_R = \sum_i x_i N_i/N$.

5.5.3 Entropy through chemical potential

To derive Eq. (5.7), we shall express changes in $\Delta \ln Z_N$ through the integral over particle groups of size L ($1 \ll L \ll N$), so that each group is large enough to capture particle statistics accurately. If groups are indexed by a variable q and L_i is the number of particles of type i in the group, we write $\Delta \ln Z_N - \Delta \ln Z_{N_0} = \int_q \sum_{i=1}^{M} L_i \left(\frac{\partial \Delta \ln Z_N}{\partial N_i} \right)_{T,V} \mathrm{d}q' = \int_q \sum_{i=1}^{M} L_i \left(\frac{-\Delta \mu_i}{kT} \right)_{T,V} \mathrm{d}q' = \int_q L \left\langle \frac{-\Delta \mu}{kT} \right\rangle_R \mathrm{d}q' = \int_N \left\langle \frac{-\Delta \mu}{kT} \right\rangle_R \mathrm{d}N'$. Then, by following the steps from Section 5.2.1, we arrive at

$$\Delta s = \frac{\varphi_0}{\varphi} \Delta s_0 + \frac{1}{\varphi} \int_{\varphi_0}^{\varphi} \left\langle \frac{-\Delta \mu}{kT} \right\rangle_R \mathrm{d}\varphi' = \frac{\varphi_0}{\varphi} \Delta s_0 + \frac{1}{\varphi} \int_{\varphi_0}^{\varphi} \langle \ln(p_{\text{insert}}) \rangle_R \mathrm{d}\varphi'. \tag{5.36}$$

When we switch to continuous distributions, then all the averages over particle radii are computed with respect to a continuous particle radii distribution $f_R(r)$, as done in Eq. (5.8).

We notice here one further advantage of switching to excess quantities. The absolute average chemical potential $\langle \mu \rangle_R$ contains a term $\sum_i \frac{N_i}{N} \ln \left(\frac{V}{N_i} \right)$ (*cf.* Eq. (5.26)), which can be transformed into $\ln \left(\frac{V}{N} \right) - \sum_i \frac{N_i}{N} \ln \left(\frac{N_i}{N} \right) = \ln \left(\frac{V}{N} \right) + s_R$, where s_R is the information entropy of the particle radii distribution. After switching to continuous distributions, this quantity diverges. In information theory, it is common to work with differential entropies when dealing with continuous distributions. As we switch to excess thermodynamic entropy, we do not have to resolve divergent s_R and employ differential entropies, because the entire term s_R cancels and becomes absorbed by polydisperse ideal gas quantities.

Chapter 6

Upper bound on the Edwards entropy in frictional monodisperse hard-sphere packings

Authors:

Vasili Baranau, Song-Chuan Zhao, Mario Scheel, Ulrich Tallarek* and Matthias Schröter*

State of publication:

Accepted on March 14, 2016 in Soft Matter
DOI: 10.1039/C6SM00567E

Abstract

We extend the Widom particle insertion method [B. Widom, *J. Chem. Phys.*, 1963, **39**, 2808–2812] to determine an upper bound s_{ub} on the Edwards entropy in frictional hard-sphere packings. s_{ub} corresponds to the logarithm of the number of mechanically stable configurations for a given volume fraction and boundary conditions. To accomplish this, we extend the method for estimating the particle insertion probability through the pore-size distribution in frictionless packings [V. Baranau *et al., Soft Matter*, 2013, **9**, 3361–3372] to the case of frictional particles. We use computer-generated and experimentally obtained three-dimensional sphere packings with volume fractions φ in the range 0.551 to 0.65. We find that s_{ub} has a maximum in the vicinity of the Random Loose Packing Limit $\varphi_{\mathrm{RLP}} = 0.55$ and decreases then monotonically with increasing φ to reach a minimum at $\varphi = 0.65$. Further on, s_{ub} does not distinguish between real mechanical stability and packings in close proximity to mechanical stable configurations. The probability to find a given number of contacts for a particle inserted in a large enough pore does not depend on φ, but it decreases strongly with the contact number.

6.1 A statistical mechanics approach to granular media

While granular materials are ubiquitous in our daily live, we still lack a comprehensive theory describing their behaviour. The underlying problem stems from their mesoscopic size (typically

several hundred micrometers). In consequence, granular systems are *athermal*, *i.e*. thermal fluctuations are orders of magnitudes smaller than the potential energy of the particles in a gravitational field. Also, they are *dissipative* as collisions and sliding contacts excite internal degrees of freedom which irreversibly convert the kinetic energy of the particles into heat. Finally, all contacts between particles are *frictional*, *i.e*. the contact forces between particles have tangential components.

Still, if granular materials are dilute, which means that their volume fraction φ is smaller than a few percent, their dynamics can be well described by an appropriately extended kinetic theory, which has by now reached the maturity level of text books.[191]

But the question, if dense systems with $\varphi \geq 0.55$ can also be described with the toolkit of statistical mechanics is still open to debate. One of the first suggestions that this might be the case was made by Sam Edwards and coworkers in two seminal papers.[44,192] They suggested that due to the dissipative nature of granular systems the role of the conserved quantity should be played by the volume of the system. Assuming that there exists some type of dynamics which samples all *mechanically stable states* of the system equiprobably, they defined a *configurational entropy* S which is proportional to the logarithm of the number of mechanically stable states at a given volume V. Finally, they introduce a configurational temperature X, named compactivity, in analogy to classical statistical mechanics as $1/X = \partial S(V)/\partial V$.

The following almost three decades have seen an increasing number of work building on

[191] N. V. Brilliantov and T. Pöschel. *Kinetic theory of granular gases*. Oxford: Oxford University Press, 2004.
[44] S. F. Edwards and R. B. S. Oakeshott. *Physica A*, 157, 1080–1090, 1989.
[192] A. Mehta and S. F. Edwards. *Physica A*, 157, 1091–1100, 1989.

these ideas.[1,23,45,61,63–66,68–74,79,94,193–211] Specifically, it has been realized that for each spatial configuration of frictional hard spheres there can be a multitude of contact force configurations, which all fulfill the same boundary stress conditions.[202] This leads to a second temperature-like variable named angoricity $\hat{\alpha}$.[45,64,66] Moreover, there exists a number of open questions regarding the feasibility of such an approach. For example there exist four different approaches how to built a "thermometer" to determine compactivity and angoricity from experimental data.[23,64,66,73,74,193,197,201,203,207] It turns out that only two of them agree quantitatively while the other two have problems to account for certain aspects of loose packings.[63] Other open questions include the existence of a zeroth law for X and $\hat{\alpha}$[66] and the possibility or even necessity of an equiprobable sampling protocol.[61,68–70,204,209] For recent reviews on this field see Refs.[46,47]

[1] C. Song, P. Wang, and H. A. Makse. *Nature*, 453, 629–632, 2008.
[23] T. Aste and T. Di Matteo. *Eur. Phys. J. B*, 64, 511–517, 2008.
[45] S. F. Edwards. *Physica A*, 353, 114–118, 2005.
[61] D. Asenjo, F. Paillusson, and D. Frenkel. *Phys. Rev. Lett.*, 112, 098002, 2014.
[63] S. Zhao and M. Schröter. *Soft Matter*, 10, 4208–4216, 2014.
[64] S. Henkes, C. S. O'Hern, and B. Chakraborty. *Phys. Rev. Lett.*, 99, 038002, 2007.
[65] S. Henkes and B. Chakraborty. *Phys. Rev. E*, 79, 061301, 2009.
[66] J. G. Puckett and K. E. Daniels. *Phys. Rev. Lett.*, 110, 058001, 2013.
[68] G. Gao et al. *Phys. Rev. E*, 80, 061304, 2009.
[69] N. Xu, D. Frenkel, and A. J. Liu. *Phys. Rev. Lett.*, 106, 245502, 2011.
[70] S. S. Ashwin et al. *Phys. Rev. E*, 85, 061307, 2012.
[71] R. Monasson and O. Pouliquen. *Physica A*, 236, 395–410, 1997.
[72] R. K. Bowles and S. S. Ashwin. *Phys. Rev. E*, 83, 031302, 2011.
[73] C. Briscoe et al. *Phys. Rev. Lett.*, 101, 188001, 2008.
[74] S. McNamara et al. *Phys. Rev. E*, 80, 031301, 2009.
[79] R. Blumenfeld and S. F. Edwards. *Phys. Rev. Lett.*, 90, 114303, 2003.
[94] K. Wang et al. *Phys. Rev. E*, 86, 011305, 2012.
[193] E. R. Nowak et al. *Phys. Rev. E*, 57, 1971–1982, 1998.
[194] H. A. Makse and J. Kurchan. *Nature*, 415, 614–617, 2002.
[195] M. Nicodemi, A. F., and A. Coniglio. *EPL*, 60, 684–690, 2002.
[196] H. A. Makse, J. Brujić, and S. F. Edwards. "Statistical mechanics of jammed matter" in: *The Physics of Granular Media* ed. by Haye Hinrichsen and Dietrich E. Wolf. Weinheim: Wiley-VCH, 2004.
[197] M. Schröter, D. I. Goldman, and H. L. Swinney. *Phys. Rev. E*, 71, 030301, 2005.
[198] P. T. Metzger and C. M. Donahue. *Phys. Rev. Lett.*, 94, 148001, 2005.
[199] M. Pica Ciamarra, A. Coniglio, and M. Nicodemi. *Phys. Rev. Lett.*, 97, 158001, 2006.
[200] F. Lechenault et al. *J. Stat. Mech.*, 2006, P07009–P07009, 2006.
[201] P. Ribiére et al. *Eur. Phys. J. E*, 22, 249–253, 2007.
[202] B. P. Tighe et al. *Soft Matter*, 6, 2908–2917, 2010.
[203] L. A. Pugnaloni et al. *Pap. Phys.*, 3, 030004, 2011.
[204] F. Paillusson and D. Frenkel. *Phys. Rev. Lett.*, 109, 208001, 2012.
[205] S. Zhao et al. *EPL*, 97, 34004, 2012.
[206] M. Schröter and K. E. Daniels. *arXiv e-prints*, arXiv:1501.02155, 2012.
[207] R. Blumenfeld, J. F. Jordan, and S. F. Edwards. *Phys. Rev. Lett.*, 109, 238001, 2012.
[208] I. G. Tejada. *Eur. Phys. J. E*, 37, 1–8, 2014.
[209] F. Paillusson. *Phys. Rev. E*, 91, 012204, 2015.
[210] Y. Wu and S. Teitel. *Phys. Rev. E*, 91, 022207, 2015.
[211] V. Becker and K. Kassner. *arXiv e-prints*, arXiv:1506.03288, 2015.
[46] M. Pica Ciamarra et al. *Soft Matter*, 8, 9731–9737, 2012.
[47] D. Bi et al. *Annu. Rev. Condens. Matter Phys.*, 6, 63–83, 2015.

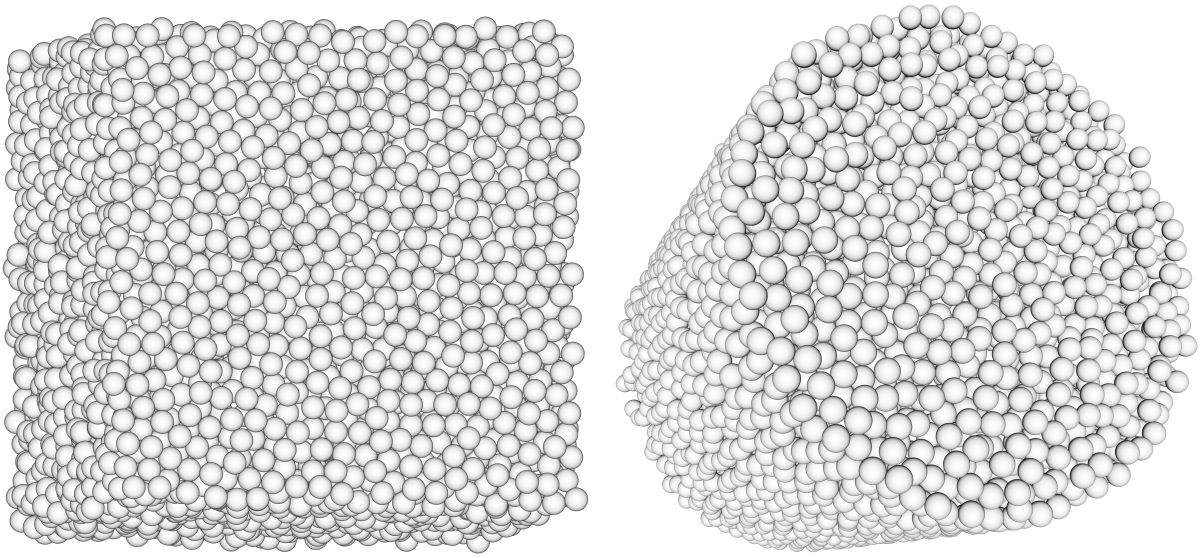

Figure 6.1: Example of a computer-generated and a reconstructed packing. Left: Computer-generated Lubachevsky–Stillinger packing at the density $\varphi = 0.65$. Right: Reconstructed fluidized bed packing (flow rate $Q = 167$ µl/s) with the density $\varphi = 0.5784$ in the bulk region.

6.1.1 Defining mechanically stability

A core idea of Edwards' approach is to consider only mechanically stable packings. For an experimentalist on earth such packings are the most generic state of granular matter: Due to gravity and the dissipative nature of contacts and collisions, eventually all grains in a not permanently driven sample will come to a complete rest. And the resulting packings will have a small but finite bulk and shear modulus as they have to withstand the anisotropic pressure p created by gravity. This pressure can only be reduced to zero by microgravity[212] or embedding the particles in a density matched fluid.[16]

Comparing with thermal hard sphere model systems, such as colloids, the condition of mechanical stability reduces significantly the number of valid configurations in the phase space. While the former only require non-overlap between all particles, the latter additionally require that the particles have a least in average Z_{iso} contacts, to exhibit a finite shear and bulk modulus. This isostatic contact number Z_{iso} can be computed by equating the number n_{dof} of degrees of freedom each particle possesses with the number of constraints fixed by its contacts $n_{\text{dof}} = m\frac{Z_{\text{iso}}}{2}$. The factor two in the number of constraints $mZ_{\text{iso}}/2$ follows from the fact that each contact is shared by two particles; the multitude m of blocked forces depends on the dimension, the shape of the contact area and the friction coefficient μ. For spheres in three dimensions $m = 1$ in the frictionless case (each contact blocks only one normal force) and $m = 3$ for frictional contacts (one normal and two tangential forces). n_{dof} does also depend on μ: for $\mu = 0$ we only need to

[212] P. Yu et al. *Granul. Matter*, 16, 165–173, 2014.
[16] M. Jerkins et al. *Phys. Rev. Lett.*, 101, 018301, 2008.

consider the three translations, for $\mu > 0$ additionally the three rotations become relevant. This calculation is strictly valid only for infinite friction. For a more detailed discussion see Ref.[213]

This results in $Z_{\text{iso}} = 4$ for frictional spheres (granular matter) and $Z_{\text{iso}} = 6$ for frictionless spheres (such as foams and emulsions). One consequence of the lower Z_{iso} for frictional spheres is that most granular packings are hyperstatic ($Z > Z_{\text{iso}}$) as shown in simulations and experiments.[214–218]

The intuitive connection between Z and φ seems obvious: the more dilute the packing, the fewer contacts should there be on average. However, for frictional hard spheres, where Z is controlled by the packing geometry and not compression, there exists presently only a mean field theory.[1] The predicted $Z(\varphi)$ is in good agreement with experiments[218,219] and the ansatz has recently been expanded to more shapes,[220,221] however only for the frictionless case.

6.1.2 The range of mechanically stable packings

As the Edwards entropy is only defined for mechanically stable, yet amorphous states, we are interested here in the upper and lower bound of φ between which these packings exist in the thermodynamic limit. A counter example are the "tunnelled crystals" described in Ref.[137] Here the number of configurations does not grow exponentially with the number of particles in the system. Which means that in the thermodynamic limit their entropy is zero.

The upper boundary is often referred to as the *Random Close Packing* (RCP). Although both its exact value of φ and its physical interpretation are still a matter of debate[14,21,142] there is a growing consensus that $\varphi \approx 0.65$ corresponds to the onset of crystallization in monodisperse sphere packings.[13,21,24–26,75,126,222] An alternative, more precise name would be the *Glass Close Packing* (GCP) limit as it is the highest achievable density for packings with suppressed crystallization,

[213] M. van Hecke. *J. Phys.: Condens. Matter*, 22, 033101, 2010.
[214] L. E. Silbert et al. *Phys. Rev. E*, 65, 031304, 2002.
[215] H. P. Zhang and H. A. Makse. *Phys. Rev. E*, 72, 011301, 2005.
[216] K. Shundyak, M. van Hecke, and W. van Saarloos. *Phys. Rev. E*, 75, 010301, 2007.
[217] S. Henkes, M. van Hecke, and W. van Saarloos. *EPL*, 90, 14003, 2010.
[218] F. M. Schaller et al. *Phys. Rev. Lett.*, 114, 158001, 2015.
[219] T. Aste, M. Saadatfar, and T. J. Senden. *J. Stat. Mech.*, 2006, P07010, 2006.
[220] A. Baule et al. *Nat. Commun.*, 4, 2194, 2013.
[221] A. Baule and H. A. Makse. *Soft Matter*, 10, 4423–4429, 2014.
[137] S. Torquato and F. H. Stillinger. *J. Appl. Phys.*, 102, 093511, 2007.
[14] S. Torquato, T. M. Truskett, and P. G. Debenedetti. *Phys. Rev. Lett.*, 84, 2064–2067, 2000.
[21] A. V. Anikeenko and N. N. Medvedev. *Phys. Rev. Lett.*, 98, 235504, 2007.
[142] R. D. Kamien and A. J. Liu. *Phys. Rev. Lett.*, 99, 155501, 2007.
[13] S. C. Kapfer et al. *Phys. Rev. E*, 85, 030301, 2012.
[24] B. A. Klumov, S. A. Khrapak, and G. E. Morfill. *Phys. Rev. B*, 83, 184105, 2011.
[25] M. Bargieł and E. M. Tory. *Adv. Powder Technol.*, 12, 533–557, 2001.
[26] K. Lochmann et al. *Eur. Phys. J. B*, 53, 67–76, 2006.
[75] Y. Jin and H. A. Makse. *Physica A*, 389, 5362–5379, 2010.
[126] C. Radin. *J. Stat. Phys.*, 131, 567–573, 2008.
[222] N. Francois et al. *Phys. Rev. Lett.*, 111, 148001, 2013.

which is the ideal glass density for monodisperse spheres.[2,132,146,164] The onset of crystallization at GCP has to be distinguished from the spontaneous crystallization occurring in equilibrating thermal systems such as colloids at $\varphi \approx 0.494 - 0.61$.[2,32–34,36,49,57,148] The latter is driven by the entropy increase due to newly gained vibrational degrees of freedom which implies that these hard sphere crystals are not mechanically stable. In contrast, in the crystallization happening above the GCP limit all particles are completely arrested by their contacts with their neighbors. Because the contact number at GCP is larger or equal to 6 and therefore above Z_{iso} of both the frictionless and the frictional cases, this upper boundary is unaffected by μ.

The lower bound on the mechanical stability of granular, frictional packings is commonly referred to as the *Random Loose Packing* (RLP). It does depend on pressure[15,16] and the friction coefficient:[16,223] the higher μ the smaller is φ_{RLP}. For experimentally relevant values of $\mu \approx 0.5$ and vanishing pressure φ_{RLP} approaches 0.55.[1,15,16,111,223–225] While the existence of an RLP is an experimental fact, the physics behind this threshold is still an open question. However, numerical studies[216,217] of the μ dependence of Z_{iso} lead to the conjecture that at least in the zero pressure limit RLP does correspond to the isostatic point.

In summary, the configurational entropy of sphere packings can only be nonzero for volume fractions between the Random Loose Packing limit (depends on friction, but for most materials $\varphi \approx 0.55$) and the Glass Close Packing limit (independent of friction, $\varphi \approx 0.65$).

6.1.3 Measuring the configurational entropy

Except for simplified model systems[71,72] the configurational entropy can not be directly computed from first principles. And a direct enumeration of the distinct mechanical states can only achieved for systems composed of a relatively small number (less than 20) of frictionless disks.[67–70]

Under certain additional assumptions, $S(\varphi)$ can be computed from the volume fluctuations of a repeatedly driven granular packing.[63,73,74] However, the results obtained this way do not agree: while in Ref.[63,73] $S(\varphi)$ decreases monotonously from RLP to RCP, in Ref.[74] an intermediate

[2] G. Parisi and F. Zamponi. *Rev. Mod. Phys.*, 82, 789–845, 2010.
[132] V. Baranau et al. *Soft Matter*, 9, 3361–3372, 2013.
[146] V. Baranau and U. Tallarek. *Soft Matter*, 10, 3826–3841, 2014.
[164] V. Baranau and U. Tallarek. *Soft Matter*, 10, 7838–7848, 2014.
[32] E. Sanz et al. *Phys. Rev. Lett.*, 106, 215701, 2011.
[33] E. Zaccarelli et al. *Phys. Rev. Lett.*, 103, 135704, 2009.
[34] C. Valeriani et al. *J. Phys.: Condens. Matter*, 23, 194117, 2011.
[36] L. Filion et al. *J. Chem. Phys.*, 133, 4115, 2010.
[49] M. Skoge et al. *Phys. Rev. E*, 74, 041127, 2006.
[57] W. G. Hoover and F. H. Ree. *J. Chem. Phys.*, 49, 3609–3617, 1968.
[148] P. N. Pusey et al. *Phil. Trans. R. Soc. A*, 367, 4993–5011, 2009.
[15] G. Y. Onoda and E. G. Liniger. *Phys. Rev. Lett.*, 64, 2727–2730, 1990.
[223] G. R. Farrell, K. M. Martini, and N. Menon. *Soft Matter*, 6, 2925–2930, 2010.
[111] L. E. Silbert. *Soft Matter*, 6, 2918–2924, 2010.
[224] J. M. Valverde and A. Castellanos. *EPL*, 75, 985, 2006.
[225] G. W. Delaney, J. E. Hilton, and P. W. Cleary. *Phys. Rev. E*, 83, 051305, 2011.
[67] M. Pica Ciamarra and A. Coniglio. *Phys. Rev. Lett.*, 101, 128001, 2008.

Table 6.1: Properties of numerical (first three rows) and experimental (last row) packing preparation protocols used in the paper.

Protocol	Mechanical stability	Friction	Gravity	Periodic b.c.	No. of particles	No. of packings	Density range
Lubachevsky–Stillinger	Approximately stable	−	−	+	10^4	71	$0.560 - 0.650$
Makse	Stable	+	−	+	10^4	13	$0.551 - 0.637$
Diluted	Unstable	−	−	+	10^4	36	$0.550 - 0.650$
Fluidized bed	Stable	+	+	−	$1903 - 2053$[a]	503	$0.570 - 0.592$

[a] In the bulk region.

maximum of $S(\varphi)$ was reported.

Finally, S can be determined for soft frictionless disks by dividing the total accessible phase space volume by that of an average basin of attraction.[61,69,70,226] Due to its limitation to frictionless systems these results have however been limited to the rather narrow range of volume fractions around GCP.

6.1.4 Outline

In this paper, we present a method to compute an upper bound on the Edwards entropy of frictional hard-sphere packings. This method is an extension of the Widom particle insertion method,[167,170,171] which for frictionless hard spheres links the excess chemical potential of a packing to the probability of particle insertion in this packing. For this paper, we need the probability of inserting a particle into a mechanically stable packing so that the inserted particle is mechanically stable itself. To determine this probability, we extend a method for estimating the particle insertion probability in frictionless packings[132] onto the case of frictional packings.

The paper is structured as follows: In Section 6.2 we discuss the preparation protocols utilized for creating the packings used in the paper, Section 6.3 introduces the method to estimate the Edwards entropy of the packings, and in Section 6.4 we present and discuss our results. Finally, Section 6.5 concludes our paper and the appendix 6.6 provides additional experimental details.

6.2 Packing preparation

In this section, we describe the computational protocols and experimental methods used to create mechanically stable packings of spheres. Additionally, we introduce a method for the numerical generation of mechanically unstable packings, which are used for comparison. A summary of the different preparation protocols can be found in Table 6.1, two example packings are depicted in

[226] S. Martiniani et al. *Phys. Rev. E*, 93, 012906, 2016.
[167] D. J. Adams. *Mol. Phys.*, 28, 1241–1252, 1974.
[170] B. Widom. *J. Chem. Phys.*, 39, 2808–2812, 1963.
[171] D. Frenkel and B. Smit. *Understanding molecular simulation: From algorithms to applications*. 2nd ed. San Diego: Academic Press, 2002.

Fig. 6.1.

6.2.1 Lubachevsky–Stillinger packings

The Lubachevsky–Stillinger (LS) algorithm[95,135] simulates Newtonian dynamics and elastic collisions of hard spheres in a vacuum with zero gravity, while at the same time the spheres grow (or, equivalently, the box is contracted). The algorithm terminates when the non-equilibrium reduced pressure (compressibility factor)[49,156] reaches a certain threshold (10^{12}). After termination, the final configuration of the particles, *i.e*. their coordinates and radii are stored as one packing. The volume fraction of this packing can be controlled by the compression rate of the box; for low enough compression rates the packings become crystalline.

The packings generated by the LS algorithm contain 10^4 monodisperse frictionless spheres, residing in a cubic box with periodic boundary conditions. Using the code by Skoge *et al*.[49] we created packings in a density range $\varphi = [0.565 - 0.65]$, corresponding to compression rates between 0.2 to 4.6×10^{-4}. Some of the packings with $\varphi > 0.6$ were already used in Figs. 3 and 4 of Baranau *et al*.[132]

Mechanical stability of the resulting packings is not automatically enforced by the Lubachevsky–Stillinger algorithm. An infinite equilibrium pressure would be equivalent to mechanical stability even for frictionless particles,[9] but (i) the pressure that is tracked during the algorithm operation is inherently non-equilibrium and (ii) the dynamics is stopped at a finite pressure threshold where the particles are still moving.

However, as our analysis below will show the properties of these packing are close to the properties of fully arrested packings. This can also seen by expanding all particles with a single linear strain step of 10^{-4} and counting particle intersections as contacts.[1] The average contact number Z determined in such a way is larger than the isostatic, frictional limit of 4 in all our simulations. This is not a generic feature of numerically produced packings and other protocols produce packings with $\varphi < 0.65$ only with $Z \approx 0$.[132]

6.2.2 Makse packings

The next set of packings corresponds to the mechanically stable packings used in the the paper by Briscoe *et al*.[73], which can be downloaded from Ref.[227] This protocol takes Lubachevsky–Stillinger packings and stabilizes them with a discrete element method (*cf.* Section VI from Supplementary material in Ref.[1]). During the operation of the discrete element method, the particles are enhanced with Hertzian normal forces and tangential friction. Like the Lubachevsky–Stillinger

[95] B. D. Lubachevsky and F. H. Stillinger. *J. Stat. Phys.*, 60, 561–583, 1990.
[135] B. D. Lubachevsky. *J. Comput. Phys.*, 94, 255–283, 1991.
[156] G. A. Mansoori et al. *J. Chem. Phys.*, 54, 1523–1525, 1971.
[9] Z. W. Salsburg and W. W. Wood. *J. Chem. Phys.*, 37, 798–804, 1962.
[227] H. Makse *Software and Data | Hernan Makse*
http://www-levich.engr.ccny.cuny.edu/webpage/hmakse/software-and-data/

Table 6.2: Experimental parameters for the fluidized bed packings. The column "Number of particles" refers to the analyzed bulk region.

Flow rate, Q	Flow duration	Resolution	No. of particles	No. of packings	Average bulk density, φ	Density range
250 µl/s	10 s	12 µm/voxel	$1909 - 1962$	263	0.574	$0.570 - 0.579$
167 µl/s	10 s	12 µm/voxel	$1903 - 1968$	173	0.575	$0.571 - 0.580$
150 µl/s	15 s	18 µm/voxel	2053[a]	67	0.588	$0.581 - 0.592$

[a] For this set of packings, we were slightly varying the radius of the bulk region to ensure an equal amount of spheres in the latter.

packings, these packings are three-dimensional and reside in cubic boxes with periodic boundary conditions in all directions.

The lowest value of $\varphi = 0.5513$ for Makse packings was reached by Briscoe *et al*. for spheres with a friction coefficient of $\mu = 10^4$. To avoid mixing of packings created with different parameters, we use in this paper only the subset of their packings created with this value of μ.

6.2.3 Fluidized bed packings

This experimental dataset addresses the question of mechanical stability by preparing loose packings of glass spheres which are (a) completely at rest and (b) stable under a finite pressure, *i.e*. their own weight.

The sample consists of 14000 monodisperse quartz glass spheres with a diameter of 351 ± 0.5 µm from Sandoz Fils S.A. Individual packings are created by fluidizing the particles with flow pulses of water in a fluidized bed.[197] Then X-ray tomographies of the samples were obtained at the European synchrotron radiation facility (ESRF) in Grenoble at beamline ID15A. The high X-ray flux allowed us to take a full tomogram with up to 1500 projections in less than 20 seconds in the monochromatic X-ray beam. This enabled us to gather several hundred tomograms (*cf.* Table 6.2), each representing a separate packing configuration.

The fluidized bed consists of a cylindrical tube with an inner diameter of 8 mm or 22.7 particle diameters. The inner surface of the tube was roughened manually to prevent crystallization near the boundary. During preparation, the bed is expanded by a short water pulse (10 or 15 s), then it sediments for 10 seconds. After sedimentation, while the bed is in a stationary state, a tomogram is taken. Then the cycle "water pulse–sedimentation–reconstruction" is repeated.

The fluidization parameters used in three different experiments are listed in Table 6.2. We will subsequently refer to the three experiments according to their flow rate Q, *i.e*. Q_250, Q_167, and Q_150. Table 6.2 lists also the average φ of all packings, as well as the φ interval in each set. The fluidized bed volume fraction was measured by uniformly generating 10^7 points in the bulk regions and counting the number of points that were inside the particles. In agreement with previous work[197] we find that lower flow rates create denser packings. By comparing successive tomograms, we validated that even the lowest Q used in the experiments was sufficient to create a new packing configuration with each pulse. To ensure that beds are not disturbed by the rotation during the tomography scans, we took two tomograms without issuing a water pulse

in-between. The resulting difference in particle positions is smaller than our overall accuracy of approximately 0.1 voxel.

The sphere positions were first detected as the centers of mass of the binarized images; this estimate was then improved by finding the cross correlation maximum with a set of grey-scale template shifted in 0.1 voxel steps along all axes. This method proved itself superior to an interpolation from a set of cross correlations based on a voxel-distance grid. Together with the good monodispersity of the quartz spheres this method results in the, to our knowledge, best published accuracy of experimental particle positions. This claim is made quantitative in appendix 6.6.1, where we demonstrate the first peak of the pair correlation function.

We restrict our subsequent analysis to the bulk regions of the fluidized bed packings, *i.e.* we analyse only particles whose centers are at least 2 mm (respectively, 5.6 particle diameters) away from the cylinder boundary. In addition, we exclude a layer of two particle diameters at the top and bottom of every reconstructed packing.

We find that we still have to exclude 34% of the packings from our analysis because their pore-size distributions show features which both differ from theoretical predictions and are not seen in any of the computer-generated packings. We attribute these unexpected features to image processing artefacts which distort the positions of a small number of spheres. Details on how experiments with untypical pore-size distribution are identified can be found in Appendix 6.6.2.

6.2.4 Diluted packings

This type of packings is intended to illustrate the effect of missing mechanical stability. They are created by first taking a reference Lubachevsky–Stillinger packing at a density $\varphi = 0.65$. Then, particle positions and box size are proportionally scaled to obtain densities in a desired range $\varphi = 0.55 - 0.65$. The resulting packings have contact numbers Z equal to zero and are therefore not mechanically stable.

6.3 Computing an upper bound on the Edwards entropy

6.3.1 Theoretical approach

In this subsection, we discuss our modified version of the Widom particle insertion method[167,170,171] which allows us to compute an upper bound on the Edwards entropy per particle. The main idea here is that we enforce the condition of mechanical stability by (a) starting from packings which already posses this property and (b) by inserting particles in such a way that they will have enough contacts to be mechanically stable themselves.

Edwards entropy

Ignoring the contact forces, each packing configuration of N monodisperse spheres can be represented as a point in a $3N$-dimensional packing phase space (3 coordinates per particle center). If the side lengths of the packing box are L_x, L_y, and L_z, the total phase space volume equals

$V_{\text{tot}} = (L_x L_y L_z)^N$.

Packing preparation protocols can be described in two equivalent ways: either the volume of the box is decreased, or the particle diameter is increased. The former is more equivalent to experimental methods where fixed-size particles "settle" from an expanded state into a final volume. The latter is normally used in numerical protocols.

We will assume in the following discussion monodisperse packings that are prepared by increasing the particle diameters: Starting from an arbitrary low density configuration in the phase space, the protocol changes the particle positions (moving the configurational point in the phase space) and at the same time increases the particle diameter until they reach a configuration that is mechanically stable for a given friction coefficient. These ideas can be generalized to polydispers packings by assigning a nominal diameter to each particle before multiplying with the growth factor.

Then configurations with the same final particle diameter can be grouped into equivalence classes if these configurations can be obtained from one another by (i) continuous symmetry operations (translational or—in case of cylindrical or spherical boundaries—rotational symmetries);[9] (ii) rattler displacements.

Thus, the entire phase space can be divided into (protocol-dependent) countable[226] basins of attraction of equivalence classes of mechanically stable configurations with different particle volume fractions (densities). For frictionless particles, basins of attraction can be produced, among other protocols, by "Stillinger quenches" (quenches that try to increase particle diameters as fast as possible).[39,150]

In order to investigate the "number of mechanically stable states" at a given particle diameter D or equivalently volume fraction φ, we need to operate with the density of states. It will be more convenient to investigate the number of states in a small interval of final particle diameters D.

If N is the number of particles, V is the box volume, Ω_i is the volume of the phase space of a basin of attraction, and D_i is its final particle diameter, we can write the total volume of the basins of attraction with $D_i \in [D; D + \mathrm{d}D)$ as

$$\Omega(N, V, D, \mathrm{d}D) = \sum_{D_i \in [D; D+\mathrm{d}D)} \Omega_i(N, V) \tag{6.1}$$

and the probability to encounter a state i in the interval of final diameters $[D; D + \mathrm{d}D)$ as

$$p_i(N, V, D, \mathrm{d}D) = \frac{\Omega_i(N, V)}{\Omega(N, V, D, \mathrm{d}D)}, \; D_i \in [D; D + \mathrm{d}D). \tag{6.2}$$

[39] F. H. Stillinger. *Science*, 267, 1935–1939, 1995.
[150] F. H. Stillinger and T. A. Weber. *Phys. Rev. A*, 25, 978–989, 1982.

Thus, we can write the entropy of mechanically stable states with $D_i \in [D; D + \mathrm{d}D)$:

$$S(N, V, D, \mathrm{d}D) = \ln\left(\frac{1}{N!}\right) - \sum_{D_i \in [D; D+\mathrm{d}D)} p_i \ln(p_i), \tag{6.3}$$

where $\frac{1}{N!}$ accounts for indistinguishability of particles.[61,226]

If we assume equiprobability of stable states,[47,61] *i.e.* the equality of all Ω_i, the Edwards entropy becomes $S = \ln(C/N!)$ where $C(N, V, D, \mathrm{d}D)$ is the number of mechanically stable configurations with $D_i \in [D; D + \mathrm{d}D)$.

Switching back to a more experimental view we assume now that the final particle diameter is equal to the initial one but the box is rescaled to match the final density. This leads to a range of accepted box linear dimensions $[L, L + h)$ instead of a range for accepted particle diameters, where h can be termed a "granular Planck length".

$$S(N, V, D, h) = \ln\left[\frac{1}{N!} C(N, V, D, h)\right]. \tag{6.4}$$

It will be convenient for the discussion below to allow particle centers to move inside the Planck volumes of size h^3. *I.e.* the entire phase space will be split into hypercubes of volume h^{3N} and a hypercube is considered mechanically stable if it contains at least one mechanically stable configuration. The number of mechanically stable hypercubes will be equal to $C(N, V, D, h)$ for a sufficiently small h (if h is too big, one hypercube may contain several mechanically stable configurations). Again, hypercubes shall be merged into equivalence classes. From now on D and h are considered fixed and we omit them from the list of parameters.

We can also define a probability to sample a correct (mechanically stable) configuration among all possible configurations as

$$p_{\text{correct}}(N, V) = C(N, V) h^{3N} / V^N. \tag{6.5}$$

Then the Edwards entropy can be expressed as $S = \ln\left[\frac{1}{N!} p_{\text{correct}} (V/h^3)^N\right]$.

Widom's insertion method

To estimate $C(N, V)$, we adapt the Widom particle insertion method[167,170,171] to granular systems. Let us keep the volume of a packing V fixed, but add one more particle to the packing of N particles which is in the configuration X_i, where $i = 1..C(N, V)$. We can then define K_i as the number of possible positions in a packing to insert the $N + 1$th particle in this packing so that (a) there is no overlap with already present particles and (b) the additional particle is itself in a mechanically stable position. This second condition is equal to the requirement that the $N + 1$th particle has in average at least the isostatic number of contacts with its neighbors.

The number of all correct configurations $C(N+1,V)$ can thus be estimated as

$$C(N+1,V) \geq K_1 + K_2 + ... + K_{C(N,V)} = C(N,V)\langle K\rangle, \tag{6.6}$$

where the average is over all correct configurations for the (N,V) system. The inequality stems from the fact that some unstable configurations of N particles can become stable if we add the $N+1$th particle, and we miss them. In Section 6.4.4 we give an estimate for the prevalence of such configurations.

We can now introduce the average insertion probability (into an already stable packing):

$$\langle p_{\text{insert}}\rangle = \frac{\langle K\rangle}{V/h^3} = \frac{\langle K\rangle h^3}{V}. \tag{6.7}$$

Eq. (6.6) is then transformed into

$$C(N+1,V) \geq C(N,V)\frac{V}{h^3}\langle p_{\text{insert}}\rangle. \tag{6.8}$$

By combining Eqs. (6.4) and (6.8) we obtain

$$S(N+1,V) \geq S(N,V) + \ln\left[\frac{V}{Nh^3}\langle p_{\text{insert}}\rangle\right]. \tag{6.9}$$

By combining Eqs. (6.8) and (6.5), we could also derive an equivalent expression for $p_{\text{correct}}(N,V)$:

$$p_{\text{correct}}(N+1,V) \geq p_{\text{correct}}(N,V)\langle p_{\text{insert}}\rangle. \tag{6.10}$$

We immediately derive from Eq. (6.9)

$$S(N_2,V) \geq S(N_1,V) + \int_{N_1}^{N_2} \ln\left[\frac{V}{Nh^3}\langle p_{\text{insert}}\rangle\right] \mathrm{d}N. \tag{6.11}$$

We will later use N_2, the larger N, as a reference point, so we express $S(N_1,V)$ through $S(N_2,V)$ and also make substitutions $N_1 \to N$ and $N_2 \to N_0$:

$$S(N,V) \leq S(N_0,V) + \int_{N_0}^{N} \ln\left[\frac{V}{N'h^3}\langle p_{\text{insert}}\rangle\right] \mathrm{d}N'. \tag{6.12}$$

An important step in the Widom method is to assume that the $\langle p_{\text{insert}}\rangle$ can be represented by

p_{insert} from a single system:

$$\langle p_{\text{insert}} \rangle = p_{\text{insert}}. \tag{6.13}$$

A sufficient condition for Eq. (6.13) in classical systems is that an examined single packing is in equilibrium. But the discussion above does not necessarily require packings to be equilibrated and does not imply ergodicity. The only requirement is that packings produced by a given protocol at given (N, V) possess similar properties and are in this sense "typical", so that we can apply Eq. (6.13). The replacement of $\langle p_{\text{insert}} \rangle$ with p_{insert} is often used implicitly, e.g. in Eq. (3) in Ref.[168] and Eq. (4) in Ref.[187]

It will be more natural to switch in Eq. (6.12) to the entropy per particle, $s = S/N$. This quantity shall depend only on the particle volume fraction φ and h. We also replace N with φ in the integration in Eq. (6.12) through $\varphi = NV_{\text{sp}}/V$, where V_{sp} is the sphere volume. We thus arrive at the master equation (where we use the subscript "ub" to denote the upper bound)

$$\begin{aligned} s_{\text{ub}}(\varphi) =& \frac{\varphi_0}{\varphi} s_0(\varphi_0) + \frac{\varphi - \varphi_0}{\varphi} \left[\ln\left(\frac{V_{\text{sp}}}{h^3} \right) + 1 \right] \\ & - \frac{\varphi \ln(\varphi) - \varphi_0 \ln(\varphi_0)}{\varphi} + \frac{1}{\varphi} \int_{\varphi_0}^{\varphi} \ln(p_{\text{insert}}) \mathrm{d}\varphi'. \end{aligned} \tag{6.14}$$

A natural choice for φ_0 in Eq. (6.14) is the point where s_0 is zero: The entire term $\frac{\varphi_0}{\varphi} s_0(\varphi_0)$ will then vanish. As discussed in the introduction, the highest possible value of φ for packings with suppressed crystallization is the Glass Close Packing limit φ_{GCP}. At this endpoint of the amorphous branch of the hard sphere phase diagram[142] there will be only one densest configuration (up to particle permutations, symmetry operations, and possibly up to rattler displacement). All configurations equivalent up to continuous symmetry operations, such as translations, and rattler displacements, are already combined by design into equivalence classes. The number of discrete symmetry operations is the same for any N, it is 48 for a fully periodic cubic box (symmetry order of the octahedral symmetry O_h).[228] The density φ_{GCP} can be expressed through the box size L_{GCP} with $\varphi_{\text{GCP}} = N \frac{\pi D^3}{6} \frac{1}{L_{\text{GCP}}^3}$. If we select h so that the last interval of box volumes $(L_{\text{GCP}} - h, L_{\text{GCP}}]$ in Eq. (6.4) contains only the GCP configuration, then we can compute s_0 as $s_0 = \ln(48N!/N!)/N = 48/N$. Which in the thermodynamic limit will go to zero. We note that this selection of the reference point leaves h hidden in s_{ub} (*cf.* Eq. (6.4)), and the value of h is essentially unknown.

Remarks on Widom's method

Eq. (6.8) represents the essence of the Widom particle insertion method[167,170,171] for granular matter and is equivalent to Eq. (1) in Ref.[170] or Eq. (5) in Ref.[167] These equations are derived for

[168] R. J. Speedy. *J. Chem. Soc., Faraday Trans. 2*, 77, 329–335, 1981.
[187] W. G. Hoover, W. T. Ashurst, and R. Grover. *J. Chem. Phys.*, 57, 1259–1262, 1972.
[228] D. M. Bishop. *Group theory and chemistry*. Revised ed. New York: Dover Publications, 1993.

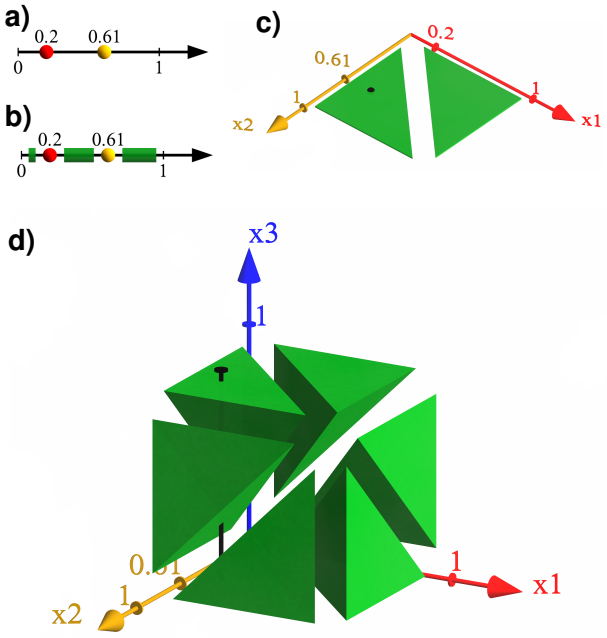

Figure 6.2: Visualization of the Widom method (Eq. (6.15)) using a one-dimensional hard-sphere system, and ignoring the condition of mechanical stability. **Panel a)** shows a specific two-particle system in a one-dimensional box extending from 0 to 1. **Panel c)** displays the available phase space $p_{\text{correct}}(2, V)$, for arbitrary positions of the two particles, as a green area. The specific system of panel a) is here indicated as a black dot. **Panel b)** visualizes in green the available space for the insertion of a third particle in this specific system without overlap with the first two particles. The green area in **panel d)** shows the available phase space of the generic three-particle system. Panel b) coresponds to an one-dimensional hyperslice of this phase space, it is indicated by the black vertical line. The Widom insertion method now corresponds to the statement that one can compute $p_{\text{correct}}(3, V)$ (the fraction of the green volume in 3D in panel d)) by multiplying $p_{\text{correct}}(2, V)$ (the fractiton of green area in panel c)) with p_{insert} (the fraction of the green length in panel b)).

classical thermodynamic systems with arbitrary potential. Eq. (2.2) in Ref.[169] is the expression of the same idea, but specifically for the hard-sphere fluid.

A more detailed mathematical discussion of the Widom method can be found in our accompanying paper.[229] We validate there our procedure[132] for estimating p_{insert} for the hard-sphere fluid. The same procedure, extended for granular systems, is presented in the next section.

For classical systems, all the equations in the previous section are exact. For such systems one also measures the volume of valid configurations, not their number. The phase space for classical systems contains additional kinetic degrees of freedom, but switching to excess quantities eliminates them from equations. Thus, it is more common to express Eq. (6.10) through the excess chemical potential $\Delta\mu$, $\Delta\mu/kT = -\ln(\langle p_{\text{insert}}\rangle)$.[167–170] Eq. (6.14) looks even simpler in excess quantities, $\Delta s = \Delta s_0\varphi_0/\varphi + \varphi^{-1}\int_{\varphi_0}^{\varphi}\ln(p_{\text{insert}})\mathrm{d}\varphi'$. We validate this form of equation in the accompanying paper.[229] Eq. (6.10) requires minimal changes to switch to classical systems, we

[169] R. J. Speedy and H. Reiss. *Mol. Phys.*, 72, 999–1014, 1991.
[229] V. Baranau and U. Tallarek. *J. Chem. Phys.*, 144, 214503, 2016.

only have to replace inequality with equality:

$$p_{\text{correct}}(N+1,V) = p_{\text{correct}}(N,V)\langle p_{\text{insert}}\rangle. \tag{6.15}$$

We illustrate Eq. (6.15) in Fig. 6.2 for the case of a one-dimensional hard-sphere fluid with $N = 2$ (*i.e.* ignoring the requirement of mechanical stability). In this case the $N+1$ phase space is only three-dimensional and can therefore be still visualized.

Both s and s_0 in Eq. (6.14) contain h (*cf.* Eq. (6.4)). Thus, the presence of additional h^3 there, as well as of V_{sp}, can be daunting. We note though that V_{sp} and h^3 in Eq. (6.14) are also both hidden in p_{insert} and are cancelled out. The presence of h^3 follows directly from Eq. (6.7). To understand the dependence of p_{insert} on V_{sp}, we notice that K from Eq. (6.7) shall be extensive, *i.e.* $K = N\alpha(\varphi)$, and thus $p_{\text{insert}} = \varphi\alpha(\varphi)\frac{h^3}{V_{\text{sp}}} = \varphi\alpha(\varphi)\frac{h^3}{\pi D^3/6}$, where D is particle diameter. We will discuss the implications

$$p_{\text{insert}} \sim h^3 (\text{if } h \to 0),\ p_{\text{insert}} \sim D^{-3} \tag{6.16}$$

during the estimation of p_{insert} below. We believe it is easier to use p_{insert} instead of α, but V_{sp} and h^3 in Eq. (6.14) shall be exactly the ones used for estimation of p_{insert}.

In classical systems the Widom insertion method is normally used in conjunction with the canonical ensemble.[167,170,171] This is in principle also possible for the granular case: The ratio $C(N,V)/h$ from Eq. (6.4) represents the density of states, which can also be written as $\sum_i \delta(V_i - V)$,[44,47] where the summation of delta-functions is over all mechanically stable states. Switching to the canonical ensemble would remove the delta-functions and the unknown hidden h from Eq. (6.14). In the canonical ensemble the partition function Z_N looks like $Z_N = \sum_i \exp[-V_i/\chi]$, where χ is the compactivity. Here the compactivity controls the average volume that the small subsystem gains when it is generated (along with a large "bath" of particles) with a certain packing preparation protocol. However, as the correct method to measure compactivities is still an active area of research,[63] we abstain here from switching to the canonical ensemble.

We also mention that for particles with soft shells, when mechanically stable states are defined by local elastic energy minima and shells are wide enough to avoid zero energy plateaus at any relevant φ, entropy can be defined as the number of states at every φ even in the micro-canonical ensemble.[61,226] It would also remove the delta-functions and unknown hidden h from Eq. (6.14). We do not consider such particles in this paper.

How to estimate the insertion probability p_{insert}

The insertion probability is measured by randomly placing a large number of points inside the packing and then determining for each point the distances to the surfaces of several nearest particles (*cf.* Fig. 6.3). This way we measure for each random point a set of r_z, which denote the distance from the point to the zth closest particle surface (the range of z is discussed below).

The idea is now to estimate the correct insertion probability of a "virtual" particle with a given number of contacts by giving conditions on these distances. We assume two particles to

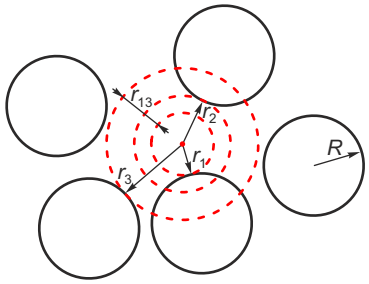

Figure 6.3: Schematic illustration of distances from a random point to the closest particle surfaces in two dimensions.

be in contact if the closest distance between their surfaces does not exceed some small arbitrary constant δ. To insert a virtual particle with an arbitrary radius r_0 having $\geq z$ contacts, we require two conditions: (a) the particle has to fit in, *i.e.* $r_1 = r_0$, (b) it has to touch at least z particles, *i.e.* $r_z \leq r_1 + \delta$.

The last condition will be easier to discuss if we operate with relative distances $r_{1z} = r_z - r_1$ for $z > 1$ (*cf.* Fig. 6.3). By inserting a large number of virtual particles we then measure the probability density functions for the distributions of r_1 and r_{1z}, which we denote as $f(r_1)$ and $g_{1z}(r_1, r_{1z})$, respectively (note that g_{1z} depends on r_1 as well). $f(r_1)$ is described in many papers as pore-size distribution.[83–91] We also operate with the conditional probability density $g_{1z}(r_{1z} \mid r_1)$ to find a given value r_{1z} when the distance to the first closest sphere is r_1: $g_{1z}(r_{1z} \mid r_1) = g_{1z}(r_1, r_{1z})/f(r_1)$. We denote the corresponding cumulative distributions as $G_{1z}(r_1, r_{1z})$ and $G_{1z}(r_{1z} \mid r_1)$.

The probability density $h_z(r_0)$ to insert a particle with radius r_0 and at least z contacts can be computed using the two conditions named above as

$$\begin{aligned} h_z(r_0)\mathrm{d}r_0 =& \Pr\{r_1 \in [r_0, r_0 + \mathrm{d}r_0), r_{1z} \in [0, \delta)\} \\ =& f(r_0)\mathrm{d}r_0 \times \Pr\{r_{1z} \in [0, \delta) \mid r_1 = r_0\}. \end{aligned} \tag{6.17}$$

Here, by definition,

$$\Pr\{r_{1z} \in [0, \delta) \mid r_1 = r_0\} = G_{1z}(\delta \mid r_0). \tag{6.18}$$

$G_{1z}(\delta \mid r_0)$ can be interpreted as "zero distance probability", *i.e.* the probability to have at least z

[83] S. Torquato, B. Lu, and J. Rubinstein. *Phys. Rev. A*, 41, 2059–2075, 1990.
[84] B. Lu and S. Torquato. *Phys. Rev. A*, 45, 5530–5544, 1992.
[85] S. Torquato. *Phys. Rev. E*, 51, 3170–3182, 1995.
[86] M. Alonso et al. *Chem. Eng. Sci.*, 50, 1983–1988, 1995.
[87] M. Alonso, M. Satoh, and K. Miyanami. *Can. J. Chem. Eng.*, 70, 28–32, 1992.
[88] I. Schenker et al. *Phys. Rev. E*, 80, 021302, 2009.
[89] I. Schenker et al. *Granul. Matter*, 14, 333–340, 2012.
[90] S. Torquato. *Annu. Rev. Mater. Res.*, 32, 77–111, 2002.
[91] D. Stoyan et al. *J. Non-Cryst. Solids*, 357, 1508–1515, 2011.

contacts for a pore with radius r_0. By combining Eqs. (6.17) and (6.18), we obtain

$$h_z(r_0) = f(r_0) \cdot G_{1z}(\delta \mid r_0). \tag{6.19}$$

If R is the radius of "real" particles, then $h_z(R)\mathrm{d}R$ is the probability for an inserted particle to have at least z contacts and the radius in the range $[R, R + \mathrm{d}R)$.

To enforce mechanical stability for inserted virtual particles, we have to choose a relevant z. The two immediate choices are $z = 3$ and $z = 4$. It is known that 4 is the minimal possible average coordination number in mechanically stable packings (realized in packings with infinite friction). Contact number distribution is never a "delta-function"[1], so non-rattler particles with three contacts are inevitable, though not every configuration of three contacts will be mechanically stable. We will denote the correct minimal z as z_{min}, but will discuss the choice between $z_{\text{min}} = 3$[70,113,230] and $z_{\text{min}} = 4$[19,59] in the Results section 6.4.

At this point, we can estimate the probability p_{insert} from Eq. (6.14) to correctly insert a particle in a packing:

$$p_{\text{insert}} = \mathrm{d}R \cdot f(R) \cdot G_{1z_{\text{min}}}(\delta \mid R). \tag{6.20}$$

The distributions $f(R)$ and $G_{1z}(\delta \mid R)$ depend all implicitly on the volume fraction φ and thus determine the dependence of p_{insert} on φ.

Scaling of p_{insert} with h and D

Because we define mechanically stable configurations up to Planck volumes h^{3N}, particle centers are allowed to move inside their Planck volumes h^3 without invalidating the condition of mechanical stability of configurations. It implies that both $\mathrm{d}R$ and δ shall be equal to the Planck length assumed in Eq. (6.14). In the following we will use $h = 2 \times 10^{-7}$:

$$\mathrm{d}R = \delta = h = 2 \times 10^{-7}. \tag{6.21}$$

Eq. (6.16) implies that p_{insert} scales as h^3 and D^{-3}. Because h is present as $\mathrm{d}R$ in Eq. (6.20) explicitly, $G_{1z_{\text{min}}}(h \mid R)$ shall conform to

$$G_{1z_{\text{min}}}(h \mid R) \sim h^2 \text{ (if } h \to 0). \tag{6.22}$$

We will use this restriction in Section 6.4.1. To examine scaling of Eq. (6.20) with D, we shall express $f(R)$ and $G_{1z_{\text{min}}}(\delta \mid R)$ through dimensionless distributions $f^\circ(\frac{R}{D})$ and $G^\circ_{1z_{\text{min}}}(\frac{\delta}{D} \mid \frac{R}{D})$, respectively. From the elementary probability theory it follows that $f(r_1)\mathrm{d}r_1 = f^\circ(\frac{r_1}{D})\mathrm{d}\frac{r_1}{D}$ and thus $f(r_1) = f^\circ(\frac{r_1}{D})\frac{1}{D}$. Through rewriting $g_{1z}(r_1, r_{1z})$ in the same way (applied to both arguments)

[113] C. B. O'Donovan and M. E. Möbius. *Phys. Rev. E*, 84, 020302, 2011.
[230] C. F. Schreck et al. *Phys. Rev. Lett.*, 107, 078301, 2011.
[19] M. Clusel et al. *Nature*, 460, 611–615, 2009.
[59] L. Berthier, H. Jacquin, and F. Zamponi. *Phys. Rev. E*, 84, 051103, 2011.

and dividing by $f(R)$, we can write $g_{1z}(r_{1z} \mid r_1)\mathrm{d}r_{1z} = g^{\circ}_{1z}(\frac{r_{1z}}{D} \mid \frac{r_1}{D})\mathrm{d}\frac{r_{1z}}{D}$. Thus, $G_{1z}(h \mid r_1) = \int_0^h g_{1z}(r_{1z} \mid r_1)\mathrm{d}r_{1z} = \int_0^{h/D} g^{\circ}_{1z}(\frac{r_{1z}}{D} \mid \frac{r_1}{D})\mathrm{d}\frac{r_{1z}}{D}$. Notice that we had to change the limits of integration. It means that whenever we require that $G_{1z}(h \mid r_1) \sim h^2$ (*i.e.* $G_{1z}(h \mid r_1) = A(D)h^2$), it implies that $G_{1z}(h \mid r_1) \sim \left[\frac{h}{D}\right]^2$ (*i.e.* $G_{1z}(h \mid r_1) = B\left[\frac{h}{D}\right]^2$). Thus, $p_{\text{insert}} = f^{\circ}(\frac{r_1}{D})\frac{h}{D}B\left[\frac{h}{D}\right]^2$, and scaling with both h and D is correct, if Eq. (6.22) indeed holds as expected. We will imply $D = 1a.u.$ everywhere below.

6.3.2 Overview of data analysis steps

In finite size packings, such as our experiments and simulations, neither $f(R)$ nor $G_{1z_{\text{min}}}(h \mid R)$ can be measured directly. The maximum observed value for r_1 (radius of inserted particle) is $\sim 0.4R$. Moreover, the minimum values of $r_{1z_{\text{min}}}$ (and generally of all r_{1z}) are much larger than h even for $r_1 < 0.4R$. To fix this issue, we fit the obtained values of $f(r_1)$ and extrapolate $r_1 \to R$. Additionally, we need to fit $G_{1z}(r_{1z} \mid r_1)$ for $z = z_{\text{min}}$ and extrapolate $r_{1z} \to h$ and $r_1 \to R$. To make our results more general, we will present a method applicable for all z from 3 at least to 11.

The entire procedure to estimate the upper bound of the Edwards entropy according to Eq. (6.14) contains therefore the following steps:

1. We uniformly generate 10^7 random points in all packings. For each point, we measure distances to the closest particles, with indices z from 3 to 11 (though in principle we will need only $z = z_{\text{min}}$).
2. We fit $f(r_1)$ and extrapolate it to $r_1 = R$ (*cf.* the next section for the fitting procedures).
3. We distribute values of r_1 into bins. Initially we use 100 bins of equal size, then merge some of them to ensure that the minimum number of points in each bin is 80. For each bin (*i.e.* for each r_1), we fit $g_{1z}(r_{1z} \mid r_1)$ as a function of r_{1z}. Then we extrapolate it to $r_{1z} = 0$, and estimate $G_{1z}(h \mid r_1)$.
4. For each value of z, we fit $G_{1z}(h \mid r_1)$ as a function of r_1 and extrapolate it to $r_1 = R$.
5. Finally, we insert $f(R)$ and $G_{1z_{\text{min}}}(h \mid R)$ into Eq. (6.20) to obtain p_{insert} at each φ and insert p_{insert} into Eq. (6.14) to obtain the upper bound of the Edwards entropy per particle s_{ub}.

6.3.3 Details of the fitting and extrapolation steps

In this subsection we will justify our choice of fit functions used for the extrapolation steps. In order to demonstrate better statistics we present in the figures in this section the combined distributions $g_{1z}(r_{1z} \mid r_1)$ from 39 fluidized bed packings with $\varphi = 0.587 \pm 0.003$.

Fitting $f(r_1)$ and extrapolating it to $r_1 = R$

As in our previous work[132] we followed Schenker *et al.*[88] and fitted $f(r_1)$ with the truncated Gaussian distribution:[114]

$$f(r_1) = C\frac{1}{\sigma\sqrt{2\pi}}\exp\left(-\frac{(r_1-\mu)^2}{2\sigma^2}\right), r_1 \geq 0. \tag{6.23}$$

Theoretical results[83–85] predict that $f(r_1)$ is of the form $A\exp(ar_1^3+br_1^2+cr_1+d)$, of which Eq. (6.23) is a special case. The validity of the function from Eq. (6.23) was already demonstrated in our previous paper[132] (see Fig. 2 in that reference).

The normalization constant C in Eq. (6.23) corresponds to the fact that the probability for a pore to appear in the interparticle void space is $1-\varphi$. It can be computed using $\int_0^\infty f(r_1)\mathrm{d}r = 1-\varphi$. Fits were performed with the maximum likelihood method for a truncated Gaussian distribution.[114]

Fitting $g_{1z}(r_{1z} \mid r_1)$ and extrapolating it to $r_{1z} = 0$

We found that the two-parameter probability distribution known as the Nakagami distribution[231] provides the best fits for all the distributions $g_{1z}(r_{1z} \mid r_1)$ computed in experiments and simulations ($z = 3..11$). The Nakagami probability density function $f_x(x; m, \Omega)$ is defined as

$$f_x(x; m, \Omega) = \frac{2m^m}{\Gamma(m)\Omega^m}x^{2m-1}\exp\left(-\frac{m}{\Omega}x^2\right). \tag{6.24}$$

It is a two-parameter distribution, which is defined for $x \in [0, +\infty)$. At $x = 0$, it grows as x^{2m-1}. At large x, it decays as $\exp(-x^2)$. Examples of the distribution $g_{1z}(r_{1z} \mid r_1)$ as a function of r_{1z} for contact numbers $z = 3, 4, 7,$ and 8 and their fits with the Nakagami distribution are presented in Fig. 6.4.

As there is no first-principle based theory supporting our choice of the Nakagami distribution, we have tried to fit other distributions with support $x \in [0, +\infty)$ and $f_x \to 0$ at $x \to 0$. The result is that one-parameter distributions do not have enough degrees of freedom to fit all the different $g_{1z}(r_{1z} \mid r_1)$ curves, while three-parameter distributions are too flexible and fits are not robust. Among the examined two-parameter distributions, the gamma and Rice distributions possess shapes similar to the observed $g_{1z}(r_{1z} \mid r_1)$, but the quality of fit is inferior to the Nakagami distribution. For example, the gamma distribution decays at large x with $\exp(-x)$ which is too slow.

From the parameters m and Ω from the Nakagami fit we compute the zero distance probability $G_{1z}(h \mid r_1)$, which is the cumulative density function of the Nakagami distribution F_x at

[114] A. C. Cohen. *Ann. Math. Stat.*, 21, 557–569, 1950.

[231] M. Nakagami. "The m-distribution–a general formula of intensity distribution of rapid fading" in: *Statistical Methods in Radio Wave Propagation* ed. by W. C. Hoffman. Oxford: Pergamon Press, 1960.

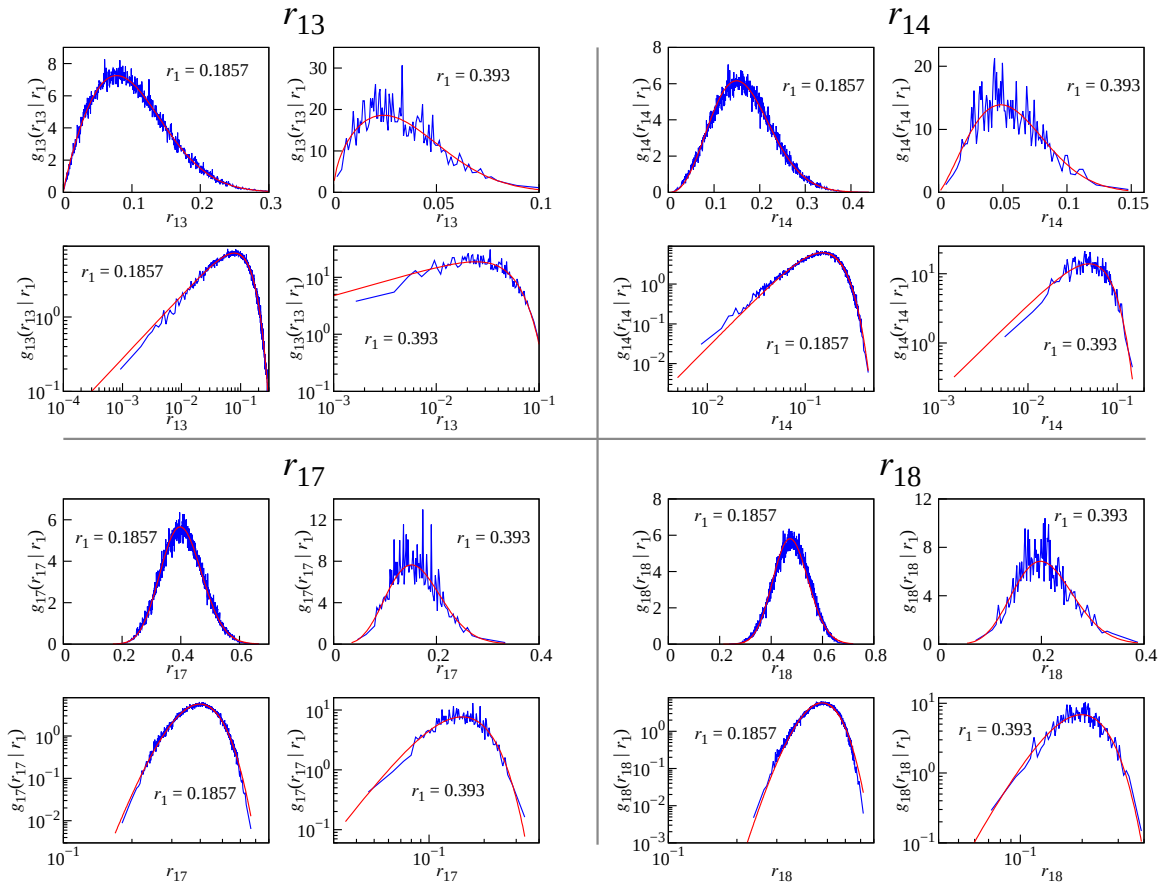

Figure 6.4: The experimentally obtained $g_{1z}(r_{1z} \mid r_1)$ (blue lines) are well fit with Nakagami distributions (red lines). The data represent 39 combined fluidized bed packings (Q_150) with an average φ of 0.585. Distributions for r_{13}, r_{14}, r_{17}, and r_{18} (respectively $z = 3$, 4, 7, and 8) are displayed. Each fit is shown twice, in a linear (top) and in a log-log scale (bottom). The particle diameter is normalized to unity.

$x = h$. The latter has the following analytical expression

$$F_x(x; m, \Omega) = P(m, \frac{m}{\Omega}x^2) \stackrel{\text{def}}{=} \gamma(m, \frac{m}{\Omega}x^2)/\Gamma(m). \tag{6.25}$$

Here, $P(s, x)$ is the regularized incomplete gamma function, $\gamma(s, x) = \int_0^x t^{s-1}e^{-t}\mathrm{d}t$ is the lower incomplete gamma function, and $\Gamma(m)$ is the gamma function. Thus, we can express $G_{1z}(h \mid r_1)$ as

$$G_{1z}(h \mid r_1) = \gamma(m, \frac{m}{\Omega}h^2)/\Gamma(m). \tag{6.26}$$

Fitting $G_{1z}(h \mid r_1)$ and extrapolating it to $r_1 = R$

The last step is to extrapolate the zero distance probability $G_{1z}(h \mid r_1)$ to $r_1 = R$. Fig 6.5 shows $G_{1z}(h \mid r_1)$ for the contact numbers 3 and 8 as blue lines. In the absence of a theoretically-derived

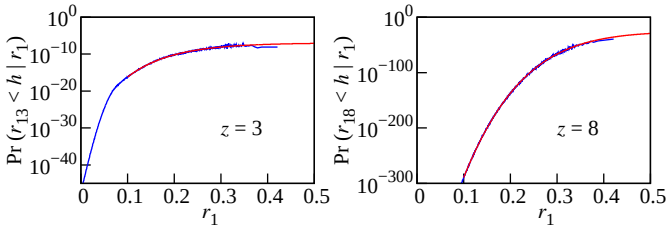

Figure 6.5: Extrapolating the zero distance probability $G_{1z}(h \mid r_1)$ (blue lines) using Eq. (6.27) (red lines). $G_{1z}(h \mid r_1) \equiv \Pr(r_{1z} < h \mid r_1)$ is the probability that a pore with radius r_1 will have exactly z contacts with real particles in a shell of width h. The data represent 39 combined fluidized bed packings (Q_150) with an average φ of 0.585. The particle diameter is normalized to unity, the extrapolation is therefore to $r_1 = 0.5$.

fit function we use a heuristically motivated least-squares fit of the form:

$$\ln\left[G_{1z}(h \mid r_1)\right] = d - \exp[ar_1^2 + br_1 + c] \tag{6.27}$$

for all points with $r_1 \geq 0.1$, which is the lowest boundary for which the fit is still applicable for all coordination numbers z. Corresponding fits are depicted as the red lines in Fig. 6.5.

We confirm that the estimates of p_{insert} do not change qualitatively if $G_{1z_{\text{min}}}(h \mid R)$ is determined by averaging the three $G_{1z_{\text{min}}}(h \mid r_1)$ values with the highest available r_1.

6.4 Results and discussion

6.4.1 Scaling of zero-distance probabilities $G_{1z}(h \mid R)$ with h

Eq. (6.22) requires that $G_{1z_{\text{min}}}(h \mid R) \sim h^2$ for sufficiently small h. It follows from the form of the Nakagami distribution (Eq. (6.24)) that for small x the cumulative Nakagami distribution $F_x(x; m, \Omega)$ scales as x^{2m}. For a given protocol, m is a function of z, φ, and r_1. Thus, Eq. (6.22) implies that $m_{z_{\text{min}}}(r_1 = R) = 1$ at all φ (the Nakagami distribution is then transformed into the Rayleigh distribution).

To test the behaviour of m_z, we build $m_z(r_1)$ from the Nakagami fits for the combined $g_{1z}(r_{1z} \mid r_1)$ distributions for the 39 Q_150 packings used in Section 6.3.3 (with $\varphi = 0.587 \pm 0.003$). The results are presented in the left panel of Fig. 6.6.

As before, to estimate $m_z(R)$ we have to extrapolate r_1 to R. For $z \leq 6$, the $m_z(r_1)$ plots visually reach asymptotes for the largest values of r_1 for all the packings that we used. Thus, to estimate $m_z(R)$ we simply take an average of the last three values of $m_z(r_1)$. The plots $m_z(R)$ vs. φ for the Makse packings are presented in the right panel of Fig. 6.6.

The values with $z \leq 8$ show no systematic dependence on φ in Fig. 6.6. Thus, we can compute their averages. The estimates $\langle m_z(R)\rangle_\varphi$ for the Makse packings are ($z = 3..11$): 0.792, 1.238, 1.761, 2.424, 3.185, 4.128, 5.883, 8.412, and 11.923. The values with $z > 6$ are very crude estimates.

Both $m_3(R)$ and $m_4(R)$ are around unity, which is in line with the requirement $m_{z_{\text{min}}} = 1$.

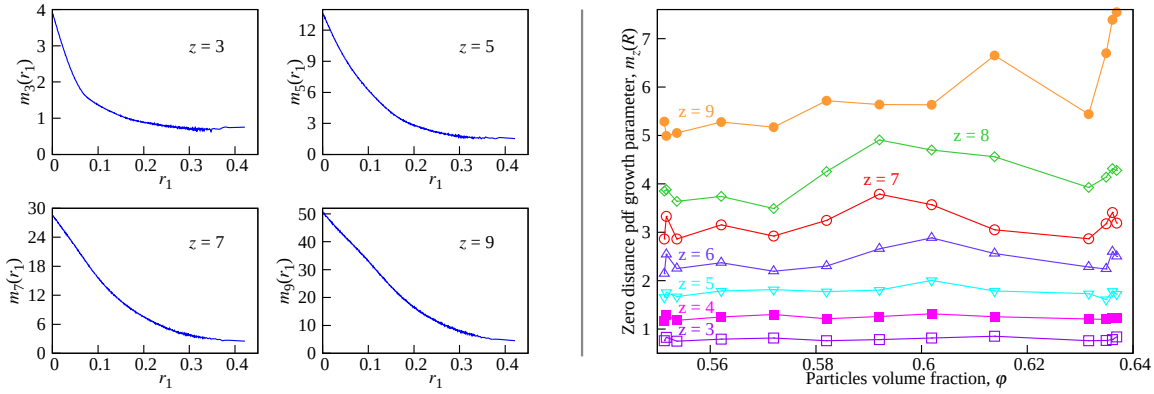

Figure 6.6: Left: Nakagami growth parameter m vs. the pore radius r_1 for different contact numbers z. The data represent 39 combined fluidized bed packings (Q_150) with an average φ of 0.585. We extrapolate $m_z(r_1)$ to the particle radius $r_1 = R = 0.5$ by averaging the three right-most points of each plot. Right: Asymptotic Nakagami growth parameters $m_z(r_1 = R)$ vs. the particles volume fraction φ for different contact numbers z. Presented are the data from the Makse packings.

None of them is equal to unity though. One possible explanation is that our estimates for $m_4(R)$ are still too high and the plot $m_4(r_1)$ continues to decrease with r_1 (like plots $m_z(r_1)$ do, *cf.* Fig. 6.6), so that it eventually reaches the value $m_4(r_1) = 1$ at $r_1 = R$. This effect will be incorporated into the extrapolation of $G_{1z}(h \mid r_1)$ with $r_1 \to R$ (*cf.* Fig. 6.5), if this extrapolation is correct. At the same time, $m_3(R)$ does not seem to reach the value 1. Thus, we will prefer $z_{\min} = 4$ to $z_{\min} = 3$.

The proximity of $m_3(R)$ and $m_4(R)$ to unity and their independence from φ, as expected from general scaling considerations, demonstrate the validity of our approach and the correctness of fits, though we never incorporated these requirements during the fitting procedure.

6.4.2 Zero-distance probabilities $G_{1z}(h \mid R)$

Fig. 6.7 shows that the zero distance probabilities $G_{1z}(h \mid R)$ have no systematic dependence on φ for $z \geq 3$. The data shown here represent the Makse packings, but the Lubachevsky–Stillinger packings behave qualitativly similar. This result corresponds to the statement that the local structure of large pores in a packing remains unchanged over the entire density range of random monodisperse packings.

Because the values of $G_{1z}(h \mid R)$ do not change systematically with φ, we can compute an average $\langle G_{1z}(h \mid R) \rangle_\varphi$ by averaging over the whole volume fraction range. The corresponding results for all the protocols are shown in Fig. 6.8. For the fluidized bed packings, we combined the data for all the values of flow rate Q prior to averaging.

Differences between the protocols become only apparent for $z > 5$. Among the numerical protocols, the Makse packings have the highest zero distance probabilities, followed by the Lubachevsky–Stillinger packings. Zero distance probabilities for the diluted packings are significantly

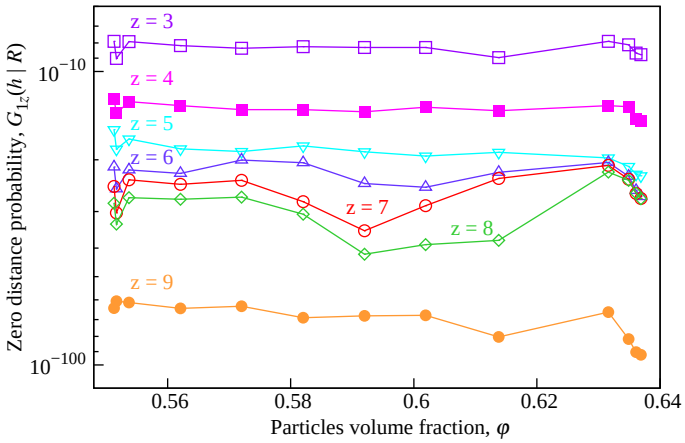

Figure 6.7: The zero-distance probabilities $G_{1z}(h \mid R)$ for the different contact numbers z show no systematic dependence on the volume fraction φ. Presented are the data from the Makse packings.

lower, especially for $z > 7$. This sequence corresponds to the "degree of mechanical stability" of the packings: the Makse packings are mechanically stable, the Lubachevsky–Stillinger packings are close to being stable, while the diluted packings have large interparticle gaps by design. Fluidized bed packings demonstrate even higher "degree of mechanical stability" than the Makse packings for $z > 9$, but there is a crossover in the order of lines between $z = 8$ and $z = 9$. Fig. 6.8 demonstrates that $G_{1z}(h \mid R)$ might therefore be an interesting tool to quantify the proximity to mechanical stability.

6.4.3 Insertion probabilities p_{insert}

Fig. 6.9 shows the results for p_{insert} computed with $z_{\text{min}} = 4$. We have excluded here the diluted packings, because their average coordination number is zero.

Two main results are visible in Fig. 6.9. First, within error bars the Makse, LS, and fluidized bed packing agree quantitatively in their p_{insert}, without any fit parameter. Interestingly, the agreement between the only approximately stable LS and fully stable fluidized bed packings is better than with the also fully mechanically stable Makse packings. We will come back to this point in Section 6.4.4. Second, p_{insert} exhibits a maximum at RLP and decays then monotonously with increasing φ.

6.4.4 Upper bound on the Edwards entropy per particle

With $p_{\text{insert}}(\varphi)$ at hand, we can compute the estimates of the Edwards entropy per particle s_{ub} according to Eq. (6.14). As discussed in Section 6.3.1.2, we asssume here that s_0 becomes zero at the Glass Close Packing limit $\varphi_{\text{GCP}} = 0.65$. Because the Makse packings are only defined up to a maximum φ of 0.637 and because the $p_{\text{insert}}(\varphi)$ of the Lubachevsky–Stillinger packings agrees better with the experimental data in Fig. 6.9, we will use the Lubachevsky–Stillinger

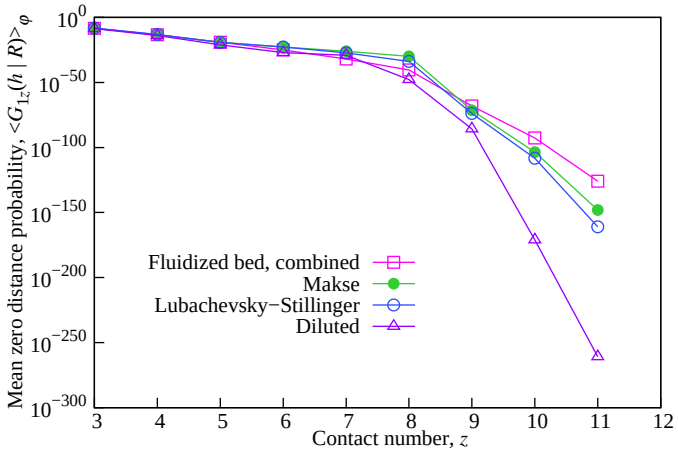

Figure 6.8: Zero-distance probabilities $\langle G_{1z}(h \mid R)\rangle_\varphi$ averaged over the whole range of volume fractions.

packings to compute the upper bound on the Edwards entropy displayed in Fig. 6.10. At least in the range $0.570 < \varphi < 0.592$, s_{ub} can also be computed form the fluidized bed data, using a corresponding Lubachevsky–Stillinger value of s at $\varphi_0 = 0.592$ as a reference value s_0 in Eq. (6.14). This results is also shown in Fig. 6.10; it is within our accuracy indistguishable from the Lubachevsky–Stillinger derived values.

The values of s_{ub} exhibit a maximum at RLP and decay monotonously with increasing φ. This behaviour supports previous numerical[1,133] and experimental[63] analyses. It also agrees with the idea that s drops sharply to zero (in the canonical ensemble) for φ below RLP.

More generally, this method to compute s_{ub} will allow for the first time to test the different protocols that have been suggested to measure the configurational temperature X.[23,63,64,66,73,74,193,197,201,203,207] Moreover, our approach should be extendable to bidisperse systems, which will allow to test the idea that segregation in dense bidisperse systems is controlled by configurational entropy.[195,206,232–235]

The origin of the difference between $s(\varphi)$ and $s_{\text{ub}}(\varphi)$ are configurations which gain stability only due to insertion of an additional particle. To account for such configurations, we can formally rewrite Eq. (6.6) as:

$$C(N+1,V) = C(N,V)\langle K\rangle\alpha(N,V), \tag{6.28}$$

where the a priori unknown function $\alpha(N,V)$ measures how many configurations of the (N,V) ensemble will become stable only after adding one more particle. This implies $\alpha(N,V) \geq 1$ with $\alpha(N,V) = 1$ only in the case that there are no "fluid" configurations which will develop a finite

[133] M. Pica Ciamarra, M. Nicodemi, and A. Coniglio. *Soft Matter*, 6, 2871–2874, 2010.
[232] Y. Srebro and D. Levine. *Phys. Rev. E*, 68, 061301, 2003.
[233] A. Coniglio, A. Fierro, and M. Nicodemi. *Physica D*, 193, 292–302, 2004.
[234] M. Tarzia et al. *Phys. Rev. Lett.*, 95, 078001, 2005.
[235] T. Finger, M. Schröter, and R. Stannarius. *New J. Phys.*, 17, 093023, 2015.

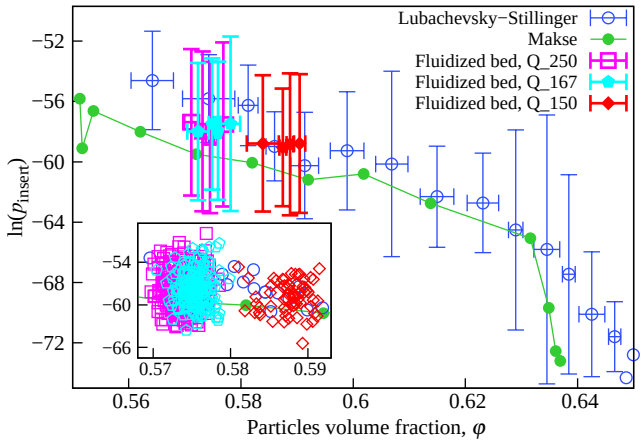

Figure 6.9: All the estimates of $p_{\text{insert}}(\varphi)$ decrease monotonously with the volume fraction φ. Results are computed using Eq. (6.20) with $z_{\text{min}} = 4$. LS and fluidized bed data points were binned in the main plot. Vertical error bars represent 95% prediction intervals in bins, horizontal error bars represent minimum and maximum densities in bins. Data were grouped to ensure 5, 66, 43, and 17 packings in the bins for the LS, Q_250, Q_167, and Q_150 lines, respectively. The inset shows all the individual experiments.

yield stress if a single particle is inserted.

If we keep the definition for the average insertion probability *into an already stable packing* (Eq. (6.7)) the same, Eq. (6.12) will then be replaced by:

$$S(N,V) = S(N_0,V) + \int_{N_0}^{N} \ln\left[\frac{V}{N'h^3}\langle p_{\text{insert}}\rangle\right] \mathrm{d}N' + \int_{N_0}^{N} \ln(\alpha)\mathrm{d}N', \tag{6.29}$$

which corresponds to the statement that

$$S_{\text{ub}}(\varphi) - S(\varphi) = -\int_{N_0}^{N} \ln(\alpha)\mathrm{d}N'. \tag{6.30}$$

Because $\alpha \geq 1$ and $N < N_0$, this difference will always be positive and it will increase with decreasing φ, *i.e.* it will be maximum at the RLP limit.

A qualitative estimate for α might be obtained by investigating the case of removing a particle from the packing under consideration. The likelihood that any of the neighbors of this particle becomes unstable will decrease with increasing distance to isostaticity, $z - z_{\text{iso}}$. Which corresponds to the statement that packings close to RLP are the most “fragile”. By analogy, configuration close to RLP should therefore also be the most likely to gain mechanical stability by adding another particle. Thus, we conclude that α will be maximum at the RLP limit. This argument should also allow to measure α numerically and therefore turn the upper bound into a direct estimate of the Edwards entropy. To do so one needs to measure the probability that removing a single particles

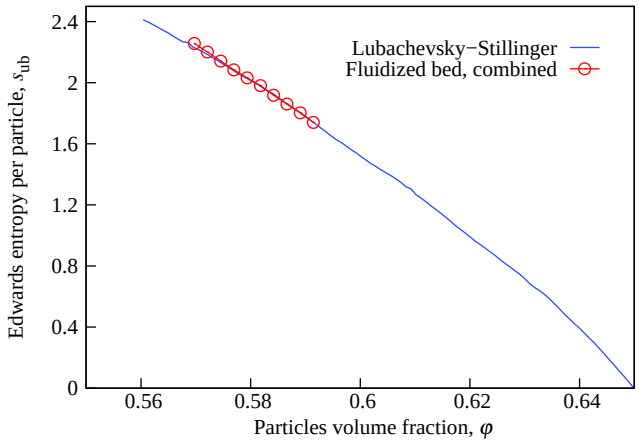

Figure 6.10: The upper bounds on the Edwards entropy per particle $s_{ub}(\varphi)$ decrease monotonously with the volume fraction φ. Results are computed using Eq. (6.14) with $z_{min} = 4$, p_{insert} is taken from Fig. 6.9.

from a given mechanically stable packings will make it lose its stability.

Our analysis does not consider the effects of a finite boundary pressure and by design we have no access to the degeneracy that hyperstatic packings have in the phase space spanned by the contact forces. However, all our packings were comprised from hard particles so that particle positions and contact forces decouple. The numerical packings do so by design, and the fluidized bed experiments were done under a constant pressure small enough that the glass spheres can be considered as perfectly hard: the pressure between two glass spheres at the bottom of a 1 m high column will deform them by approximately 10 nm, which is an orders of magnitude smaller than the vertical surface roughness of typical glass spheres.[236] And the grain column in our fluidized bed experiment was only 0.03 m high.

However, the value of RLP, measured with glass spheres, does depend on pressure.[16] This means that at least close to the isostatic point also s will show some pressure dependence. This effect originates in the reduced degeneracy in the contact force space; the closer to isostaticity a packing is, the fewer configurations will exist to fulfil certain pressure boundary conditions. An analysis of loose packing created at different pressure levels should provide interesting insights.

Finally, we would like to point out that a generalization of our method to other particles shapes, such as ellipsoids or Platonic bodies, seems feasible.

6.5 Summary

In this paper, we present a method to compute an upper bound on the Edwards entropy per particle of a three-dimensional, mechanically stable hard-sphere packings in a microcanonical ensemble. We modify the Widom insertion method to be applicable for granular systems and also extend our method to estimate particle insertion probabilities for hard-sphere systems using

[236] S. Utermann et al. *Phys. Rev. E*, 84, 031306, 2011.

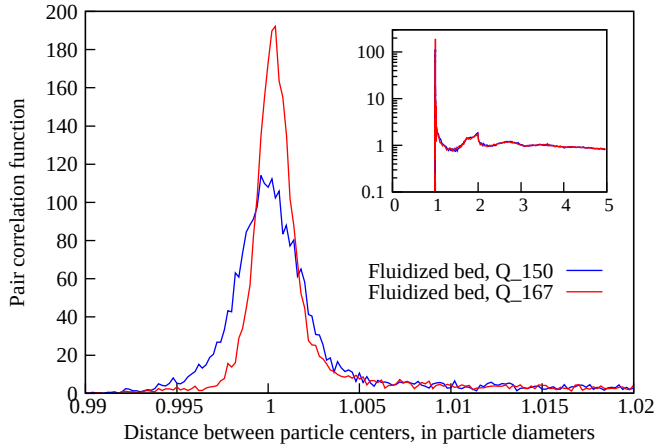

Figure 6.11: Pair correlation function for fluidized bed packings. The inset shows the data in a semi-log scale. The bin width is $2 \times 10^{-4} D$ in the main figure and $2 \times 10^{-2} D$ in the inset, except for the points inside the $0.99 - 1.02\ D$ interval, where we use the bins from the main plot. D is the particle diameter.

their pore-size distribution to account for the requirement of mechanical stability of the packing. Then we supply these insertion probabilities into the master equation from the Widom method.

We apply this procedure to experimentally obtained and computer-generated packings covering the volume fraction range from 0.551 to $\varphi_{\mathrm{GCP}} \approx 0.65$ (the Glass Close Packing density, according to some estimates). The experimental packings are created with flow pulses in a water-fluidized bed, the numerical packings are prepared with the Lubachevsky–Stillinger algorithm. One subset, taken from the publication of Briscoe *et al.*[73], adds an additional discrete element simulation step to obtain fully jammed configurations.

Starting from a minimum at the Glass Close Packing density the upper bound on the Edwards entropy grows monotonically with decreasing volume fraction to reach a maximum around the Random Loose Packing density $\varphi_{\mathrm{RLP}} \approx 0.55$. Because there are by definition no mechanically stable packings below Random Loose Packing, the Edwards entropy shall drop there to zero (in the canonical ensemble).

Additionally, we find that the local structure around pores large enough to fit in another particle does not depend on the volume fraction. This volume fraction independence was quantified by computing the probabilities of the inserted particles to have a given number of contacts.

Acknowledgements

We thank Sibylle Nägle for creating Fig. 6.2 and Udo Krafft and Wolf Keiderling for building the fluidized bed setup. X-ray tomographies were performed on the ID15A beamline at the European Synchrotron Radiation Facility (ESRF), Grenoble, France. Computational resources were provided by FZJ (Forschungszentrum Jülich, Germany). We are grateful to the John von Neumann Institute for Computing (NIC) and the Jülich Supercomputing Center (JSC) for the allocation of a special CPU-time grant (NIC project number: 8214, JSC project ID: HMR10). The French National Research Agency (ANR) is acknowledged for support via EQUIPEX grant

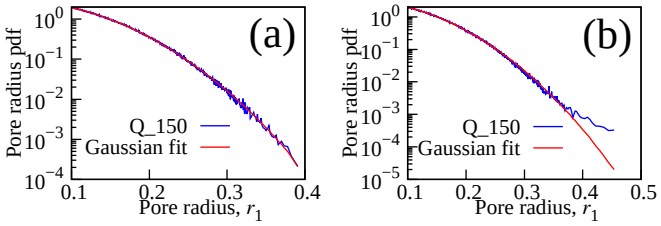

Figure 6.12: Experimentally obtained pore radii probability density functions (blue lines) and their fits with Gaussian distributions (red lines) for two reconstructed packings: (a) accepted packing; (b) rejected packing. The particle diameter is normalized to unity.

ANR-11-EQPX-0031 (project NanoimagesX).

6.6 Appendix

6.6.1 Pair correlation functions for the fluidized bed packings

The monodispersity of the particles and the high quality of the particle detection of the fluidized bed experiments is demonstrated by the pair correlation functions shown in Fig. 6.11. The data corresponds to individual fluidized bed packings where we have discarded a layer of one diameter thickness along the cylinder walls. While the absolute height of the first peak, which corresponds to particles in contact, depends on the bin size, its width is a testimonial to the quality of the data.

6.6.2 Selecting fluidized bed packings

Approximately 34% of the fluidized bed packings were discarded due to the atypical pore-size distributions. Fig. 6.12 show two examples. The experiment in panel (b) behaves atypically as the tail deviates from the expected Gaussian curve (Eq. (6.23)) towards higher probability densities. Such a behaviour was neither observed in the computer-generated Makse, Lubachevsky–Stillinger, and diluted packings. Nor was it observed for the force-biased and Jodrey–Tory packings studied in our previous paper[132] and by Schenker *et al.*[88] Thus, we assume that this atypical behaviour stems from reconstruction artefacts and discard such packings from the calculation of entropies.

Fig. 6.12 demonstrates also that the pore-size distribution may serve as an additional indicator of packing reconstruction quality, besides the pair-correlation function discussed in Section 6.6.1.

Summary and conclusions

In this thesis we investigated properties of three-dimensional hard-sphere packings. The first five chapters were devoted to frictionless packings, the last chapter deals with frictional packings. All of the chapters utilize computer-generated packings of 10^4 particles residing in cubic boxes with periodic boundary conditions. The last chapter also incorporates the results for experimentally reconstructed packings residing in cylindrical tubes. For computer packing generation, we used the Lubachevsky–Stillinger, Jodrey–Tory, and force-biased algorithms. The last chapter also includes Lubachevsky–Stillinger packings, additionally stabilized with the discrete element method. Chapters 1 and 6 deal with monodisperse packings, chapters 2-4 investigate also polydisperse packings. Chapters 2 and 3 utilize the log-normal particle diameter distribution, chapter 4 includes results also for the Pareto and Gaussian particle diameter distributions. Each chapter corresponds to a published or submitted paper.

- In Chapter 1, we introduce a method to estimate the particle insertion probability for frictionless hard-sphere packings through the pore-size distribution. Under certain assumptions, we link this insertion probability to the total (fluid) entropy of such packings. We calculate insertion probabilities for monodisperse packings in a wide range of volume fractions (densities) $\varphi = 0.6 - 0.7$. We demonstrate the onset of crystallization for monodisperse packings at the volume fraction (density) $\varphi \approx 0.65$. We also demonstrate that this value is different from the J-point ($\varphi_J \approx 0.64$ for monodisperse packings). We interpret the value $\varphi \approx 0.65$ as the Glass Close Packing (GCP) limit (the ideal glass density).
- In Chapter 2, we (i) computationally generate polydisperse packings with the log-normal radii distribution and (ii) search for their closest jammed configurations (do the infinitely fast quench, Stillnger quench). We confirm our assumption that $\varphi \approx 0.64$ and $\varphi \approx 0.65$ in the monodisperse case and corresponding densities in polydisperse cases shall be interpreted as the J-point and the GCP limit, respectively. We demonstrate that frictionless random jammed packings can be produced in the entire range between these two limits, which explains why the density of the random-close packing (RCP) is estimated in different papers at different values. Linking $\varphi \approx 0.65$ in the monodisperse to the GCP limit case also explains the onset of crystallization at this density observed in many papers. We advocate that the RCP phenomenon shall thus be regarded as two different phenomena.
- In Chapter 3, we (i) computationally generate polydisperse packings with the log-normal radii distribution, (ii) equilibrate them, and (iii) do Stillnger quenches. This procedure allows us to investigate the structure of the phase space for polydisperse packings. It also confirms our interpretation of $\varphi \approx 0.64$ and $\varphi \approx 0.65$ in the monodisperse case and corresponding densities in polydisperse cases as the J-point and the GCP limit, respectively.

The estimates of these limits from Chapter 2 are also confirmed. Additionally, this procedure allows to estimate the ideal glass transition densities (producing $\varphi_g \approx 0.585$ for monodisperse packings).

- In Chapter 4, we repeat the protocol from Chapter 3 for particles with the Pareto and Gaussian diameter distributions. We notice that if the Boublík–Mansoori–Carnahan–Starling–Leland (BMCSL) equation of state is used, the excess entropy per particle s can be computed analytically for an arbitrary particle size distribution and density φ (if $\varphi \leq \varphi_g$). We demonstrate that the excess entropies of the log-normal, Pareto, and Gaussian packings are approximately the same at the estimated values of φ_g and assume that they equal some characteristic value s_g. Thus, we propose a method to estimate the ideal glass transition density for an arbitrary particle size distribution: we need to find such a density where the fluid entropy for this distribution equals the characteristic value from above, $s(\varphi) = s_g$.
- In Chapter 5, we improve the connection between the insertion probability and entropy from the first chapter by utilizing a more advanced Widom particle insertion method, which links the insertion probability to the excess chemical potential. The excess entropy can in turn be computed through the excess chemical potential. We extend the estimation of the insertion probability through the pore-size distribution and of the excess chemical potential and entropy through the insertion probability onto the case of polydisperse packings. We demonstrate that the excess chemical potential and excess entropy comply with predictions from the Boublík–Mansoori–Carnahan–Starling–Leland equation of state.
- In Chapter 6, we extend the methods for the insertion probability estimation through the pore-size distribution (Chapter 1) and for the entropy estimation through the insertion probability (Chapter 5) onto the case of frictional particles and estimate the upper bound of the Edwards entropy for frictional monodisperse packings. We demonstrate that the upper bound of the Edwards entropy decreases monotonously for monodisperse packings from the Random Loose Packing limit ($\varphi_{\text{RLP}} \approx 0.55$) to the Glass Close Packing limit ($\varphi_{\text{GCP}} \approx 0.65$).

Overall, this study extends the understanding of glass transition, jamming, and the Edwards entropy behavior in the system of hard spheres. Our results can help understand these phenomena in more complex atomic, molecular, and colloidal systems.

Bibliography

[1] C. SONG, P. WANG, and H. A. MAKSE. "A phase diagram for jammed matter". *Nature* 453, 629–632, 2008. DOI: 10.1038/nature06981 (see pp. 1, 2, 4, 5, 9, 14–16, 19, 26, 29, 38, 49, 53, 66, 100, 121, 123, 124, 126, 136, 143)

[2] G. PARISI and F. ZAMPONI. "Mean-field theory of hard sphere glasses and jamming". *Reviews of Modern Physics* 82, 789–845, 2010. DOI: 10.1103/RevModPhys.82.789 (see pp. 1, 3–9, 15, 16, 26, 28, 31, 33, 34, 38, 39, 42, 43, 47, 48, 55, 61, 66, 67, 74–78, 83, 86, 91–93, 100, 102, 110, 112, 124)

[3] S. TORQUATO and F. H. STILLINGER. "Jammed hard-particle packings: From Kepler to Bernal and beyond". *Reviews of Modern Physics* 82, 2633–2672, 2010. DOI: 10.1103/RevModPhys.82.2633 (see pp. 1, 3, 5, 6, 16, 27, 38, 39, 69, 86, 89, 100)

[4] T. C. HALES. "A proof of the Kepler conjecture". *Annals of Mathematics* 162, 1065–1185, 2005. (see p. 1)

[5] T. C. HALES, M. ADAMS, G. BAUER, D. TAT DANG, J. HARRISON, T. LE HOANG, C. KALISZYK, V. MAGRON, S. MCLAUGHLIN, T. TAT NGUYEN, T. QUANG NGUYEN, T. NIPKOW, S. OBUA, J. PLESO, J. RUTE, A. SOLOVYEV, A. HOAI THI TA, T. N. TRAN, D. THI TRIEU, J. URBAN, K. KHAC VU, and R. ZUMKELLER. "A formal proof of the Kepler conjecture". *arXiv e-prints* 1501, arXiv:1501.02155, 2015. (see p. 1)

[6] S. KHIREVICH, A. HÖLTZEL, and U. TALLAREK. "Validation of pore-scale simulations of hydrodynamic dispersion in random sphere packings". *Communications in Computational Physics* 13, 801–822, 2013. DOI: 10.4208/cicp.361011.260112s (see pp. 1, 27, 38, 55, 66, 100)

[7] U. M. SCHEVEN, S. KHIREVICH, A. DANEYKO, and U. TALLAREK. "Longitudinal and transverse dispersion in flow through random packings of spheres: A quantitative comparison of experiments, simulations, and models". *Physical Review E* 89, 053023, 2014. DOI: 10.1103/PhysRevE.89.053023 (see pp. 1, 100)

[8] H. LIASNEUSKI, D. HLUSHKOU, S. KHIREVICH, A. HÖLTZEL, U. TALLAREK, and S. TORQUATO. "Impact of microstructure on the effective diffusivity in random packings of hard spheres". *Journal of Applied Physics* 116, 034904, 2014. DOI: 10.1063/1.4889821 (see pp. 1, 100)

[9] Z. W. SALSBURG and W. W. WOOD. "Equation of state of classical hard spheres at high density". *The Journal of Chemical Physics* 37, 798–804, 1962. DOI: 10.1063/1.1733163 (see pp. 1, 5, 6, 16, 30, 31, 38, 39, 41, 43, 58, 59, 61, 68, 71, 92, 93, 107, 126, 129)

[10] J. D. BERNAL and J. MASON. "Packing of spheres: Co-ordination of randomly packed spheres". *Nature* 188, 910–911, 1960. DOI: 10.1038/188910a0 (see pp. 1, 15, 29, 38, 53, 54, 66)

[11] G. D. SCOTT and D. M. KILGOUR. "The density of random close packing of spheres". *Journal of Physics D: Applied Physics* 2, 863–866, 1969. DOI: 10.1088/0022-3727/2/6/311 (see pp. 2, 15, 29, 38, 66)

[12] C. S. O'HERN, L. E. SILBERT, A. J. LIU, and S. R. NAGEL. "Jamming at zero temperature and zero applied stress: The epitome of disorder". *Physical Review E* 68, 011306, 2003. DOI: 10.1103/

PhysRevE.68.011306 (see pp. 2, 3, 8, 9, 15, 16, 18, 29, 32, 38, 39, 45, 51, 53, 54, 66, 69, 73, 79, 86, 93, 100)

[13] S. C. KAPFER, W. MICKEL, K. MECKE, and G. E. SCHRÖDER-TURK. "Jammed spheres: Minkowski tensors reveal onset of local crystallinity". *Physical Review E* 85, 030301, 2012. DOI: 10.1103/PhysRevE.85.030301 (see pp. 2, 3, 14, 29, 38, 49, 51, 54, 66, 74–77, 123)

[14] S. TORQUATO, T. M. TRUSKETT, and P. G. DEBENEDETTI. "Is random close packing of spheres well defined?" *Physical Review Letters* 84, 2064–2067, 2000. DOI: 10.1103/PhysRevLett.84.2064 (see pp. 2, 16, 33, 38, 69, 123)

[15] G. Y. ONODA and E. G. LINIGER. "Random loose packings of uniform spheres and the dilatancy onset". *Physical Review Letters* 64, 2727–2730, 1990. DOI: 10.1103/PhysRevLett.64.2727 (see pp. 2, 4, 100, 124)

[16] M. JERKINS, M. SCHRÖTER, H. L. SWINNEY, T. J. SENDEN, M. SAADATFAR, and T. ASTE. "Onset of mechanical stability in random packings of frictional spheres". *Physical Review Letters* 101, 018301, 2008. DOI: 10.1103/PhysRevLett.101.018301 (see pp. 2, 4, 53, 100, 122, 124, 145)

[17] J. C. GIDDINGS. *Dynamics of chromatography: Principles and theory*. New York: Marcel Dekker, 1965. (see p. 2)

[18] A. DANEYKO, A. HÖLTZEL, S. KHIREVICH, and U. TALLAREK. "Influence of the particle size distribution on hydraulic permeability and eddy dispersion in bulk packings". *Analytical Chemistry* 83, 3903–3910, 2011. DOI: 10.1021/ac200424p (see pp. 2, 100)

[19] M. CLUSEL, E. I. CORWIN, A. O. N. SIEMENS, and J. BRUJIĆ. "A 'granocentric' model for random packing of jammed emulsions". *Nature* 460, 611–615, 2009. DOI: 10.1038/nature08158 (see pp. 2, 55, 136)

[20] I. BIAZZO, F. CALTAGIRONE, G. PARISI, and F. ZAMPONI. "Theory of amorphous packings of binary mixtures of hard spheres". *Physical Review Letters* 102, 195701, 2009. DOI: 10.1103/PhysRevLett.102.195701 (see pp. 2, 16, 44, 92)

[21] A. V. ANIKEENKO and N. N. MEDVEDEV. "Polytetrahedral nature of the dense disordered packings of hard spheres". *Physical Review Letters* 98, 235504, 2007. DOI: 10.1103/PhysRevLett.98.235504 (see pp. 3, 14, 29, 38, 49, 51, 54, 66, 74–76, 123)

[22] A. V. ANIKEENKO, N. N. MEDVEDEV, and T. ASTE. "Structural and entropic insights into the nature of the random-close-packing limit". *Physical Review E* 77, 031101, 2008. DOI: 10.1103/PhysRevE.77.031101 (see pp. 3, 14, 17, 19, 26, 29, 33, 38, 39, 49, 51, 54, 66, 69, 74–77)

[23] T. ASTE and T. DI MATTEO. "Structural transitions in granular packs: statistical mechanics and statistical geometry investigations". *European Physical Journal B: Condensed Matter and Complex Systems* 64, 511–517, 2008. DOI: 10.1140/epjb/e2008-00224-8 (see pp. 3, 14, 26, 29, 38, 49, 51, 54, 66, 74–76, 121, 143)

[24] B. A. KLUMOV, S. A. KHRAPAK, and G. E. MORFILL. "Structural properties of dense hard sphere packings". *Physical Review B* 83, 184105, 2011. DOI: 10.1103/PhysRevB.83.184105 (see pp. 3, 14, 29, 38, 49, 51, 54, 66, 74–77, 123)

[25] M. BARGIEŁ and E. M. TORY. "Packing fraction and measures of disorder of ultradense irregular packings of equal spheres. II. Transition from dense random packing". *Advanced Powder Technology* 12, 533–557, 2001. DOI: 10.1163/15685520152756660 (see pp. 3, 14, 17, 29, 38, 49, 51, 54, 66, 74–77, 123)

[26] K. LOCHMANN, A. ANIKEENKO, A. ELSNER, N. MEDVEDEV, and D. STOYAN. "Statistical verification of crystallization in hard sphere packings under densification". *European Physical Journal B: Condensed Matter and Complex Systems* 53, 67–76, 2006. DOI: 10.1140/epjb/e2006-00348-9 (see pp. 3, 17, 27, 38, 49, 51, 54, 66, 74–77, 123)

[27] B. A. KLUMOV, Y. JIN, and H. A. MAKSE. "Structural properties of dense hard sphere packings". *Journal of Physical Chemistry B* 118, 10761–10766, 2014. DOI: 10.1021/jp504537n (see p. 3)

[28] G. PARISI and F. ZAMPONI. "The ideal glass transition of hard spheres". *The Journal of Chemical Physics* 123, 144501, 2005. DOI: 10.1063/1.2041507 (see pp. 3, 8, 86, 100, 110)

[29] L. BERTHIER and T. A. WITTEN. "Glass transition of dense fluids of hard and compressible spheres". *Physical Review E* 80, 021502, 2009. DOI: 10.1103/PhysRevE.80.021502 (see pp. 3, 4, 7–9, 66, 67, 76, 86, 87, 91–93, 100, 102, 105, 110, 113)

[30] A. DONEV. "Jamming in hard sphere and disk packings". *Journal of Applied Physics* 95, 989–999, 2004. DOI: 10.1063/1.1633647 (see pp. 3, 16, 38, 69, 89)

[31] A. DONEV, S. TORQUATO, F. H. STILLINGER, and R. CONNELLY. "A linear programming algorithm to test for jamming in hard-sphere packings". *Journal of Computational Physics* 197, 139–166, 2004. DOI: 10.1016/j.jcp.2003.11.022 (see pp. 3, 16, 31, 38, 69, 89)

[32] E. SANZ, C. VALERIANI, E. ZACCARELLI, W. C. K. POON, P. N. PUSEY, and M. E. CATES. "Crystallization mechanism of hard sphere glasses". *Physical Review Letters* 106, 215701, 2011. DOI: 10.1103/PhysRevLett.106.215701 (see pp. 3, 7, 66, 74, 92, 100, 110, 124)

[33] E. ZACCARELLI, C. VALERIANI, E. SANZ, W. C. K. POON, M. E. CATES, and P. N. PUSEY. "Crystallization of hard-sphere glasses". *Physical Review Letters* 103, 135704, 2009. DOI: 10.1103/PhysRevLett.103.135704 (see pp. 3, 7, 39, 66, 74–79, 86, 87, 91, 92, 100, 102, 110–112, 124)

[34] C. VALERIANI, E. SANZ, E. ZACCARELLI, W. C. K. POON, M. E. CATES, and P. N. PUSEY. "Crystallization and aging in hard-sphere glasses". *Journal of Physics: Condensed Matter* 23, 194117, 2011. DOI: 10.1088/0953-8984/23/19/194117 (see pp. 3, 7, 66, 74, 92, 100, 110, 124)

[35] P. CHAUDHURI, L. BERTHIER, and S. SASTRY. "Jamming transitions in amorphous packings of frictionless spheres occur over a continuous range of volume fractions". *Physical Review Letters* 104, 165701, 2010. DOI: 10.1103/PhysRevLett.104.165701 (see pp. 3, 16, 18, 28, 39, 54, 66)

[36] L. FILION, M. HERMES, R. NI, and M. DIJKSTRA. "Crystal nucleation of hard spheres using molecular dynamics, umbrella sampling, and forward flux sampling: A comparison of simulation techniques". *The Journal of Chemical Physics* 133, 4115, 2010. DOI: 10.1063/1.3506838; (see pp. 4, 66, 74, 92, 100, 110, 124)

[37] R. J. SPEEDY. "The hard sphere glass transition". *Molecular Physics* 95, 169–178, 1998. DOI: 10.1080/00268979809483148 (see pp. 4, 6, 8, 110)

[38] C. A. ANGELL. "Perspective on the glass transition". *Journal of Physics and Chemistry of Solids* 49, 863–871, 1988. DOI: 10.1016/0022-3697(88)90002-9 (see pp. 4, 6, 86)

[39] F. H. STILLINGER. "A topographic view of supercooled liquids and glass formation". *Science* 267, 1935–1939, 1995. DOI: 10.1126/science.267.5206.1935 (see pp. 4, 6, 39, 41, 67, 69, 89, 90, 129)

[40] P. G. DEBENEDETTI and F. H. STILLINGER. "Supercooled liquids and the glass transition". *Nature* 410, 259–267, 2001. DOI: 10.1038/35065704 (see pp. 4, 6, 86)

[41] V. LUBCHENKO and P. G. WOLYNES. "Theory of structural glasses and supercooled liquids". *Annual Review of Physical Chemistry* 58, 235–266, 2007. DOI: 10.1146/annurev.physchem.58.032806.104653 (see pp. 4, 6)

[42] A. CAVAGNA. "Supercooled liquids for pedestrians". *Physics Reports* 476, 51–124, 2009. DOI: 10.1016/j.physrep.2009.03.003 (see pp. 4, 6, 7)

[43] L. BERTHIER and G. BIROLI. "Theoretical perspective on the glass transition and amorphous materials". *Reviews of Modern Physics* 83, 587–645, 2011. DOI: 10.1103/RevModPhys.83.587 (see pp. 4, 6, 7, 67)

[44] S. F. EDWARDS and R. B. S. OAKESHOTT. "Theory of powders". *Physica A: Statistical and Theoretical Physics* 157, 1080–1090, 1989. DOI: 10.1016/0378-4371(89)90034-4 (see pp. 4, 9, 10, 14, 15, 19, 20, 114, 120, 134)

[45] S. F. EDWARDS. "The full canonical ensemble of a granular system". *Physica A: Statistical and Theoretical Physics* 353, 114–118, 2005. DOI: 10.1016/j.physa.2005.01.045 (see pp. 4, 10, 121)

[46] M. PICA CIAMARRA, P. RICHARD, M. SCHRÖTER, and B. P. TIGHE. "Statistical mechanics for static granular media: open questions". *Soft Matter* 8, 9731–9737, 2012. DOI: 10.1039/C2SM06898B (see pp. 4, 10, 53, 70, 121)

[47] D. BI, S. HENKES, K. E. DANIELS, and B. CHAKRABORTY. "The statistical physics of athermal materials". *Annual Review of Condensed Matter Physics* 6, 63–83, 2015. DOI: 10.1146/annurev-conmatphys-031214-014336 (see pp. 4, 9, 10, 114, 121, 130, 134)

[48] P. WANG, C. SONG, Y. JIN, and H. A. MAKSE. "Jamming II: Edwards' statistical mechanics of random packings of hard spheres". *Physica A: Statistical and Theoretical Physics* 390, 427–455, 2011. DOI: 10.1016/j.physa.2010.10.017 (see pp. 4, 5, 9, 10, 14, 16, 19, 39)

[49] M. SKOGE, A. DONEV, F. H. STILLINGER, and S. TORQUATO. "Packing hyperspheres in high-dimensional Euclidean spaces". *Physical Review E* 74, 041127, 2006. DOI: 10.1103/PhysRevE.74.041127 (see pp. 5, 6, 16, 25, 29–31, 44, 49, 66, 71, 74, 76, 78, 86, 91–93, 100, 110, 124, 126)

[50] F. H. STILLINGER and Z. W. SALSBURG. "Limiting polytope geometry for rigid rods, disks, and spheres". *Journal of Statistical Physics* 1, 179–225, 1969. DOI: 10.1007/BF01007250 (see pp. 5, 6)

[51] J. G. KIRKWOOD. "Critique of the free volume theory of the liquid state". *The Journal of Chemical Physics* 18, 380–382, 1950. DOI: 10.1063/1.1747635 (see pp. 6, 107)

[52] R. J. BUEHLER, R. H. WENTORF JR., J. O. HIRSCHFELDER, and C. F. CURTISS. "The free volume for rigid sphere molecules". *The Journal of Chemical Physics* 19, 61–71, 1951. DOI: 10.1063/1.1747991 (see pp. 6, 107)

[53] W. W. WOOD. "Note on the free volume equation of state for hard spheres". *The Journal of Chemical Physics* 20, 1334–1334, 1952. DOI: 10.1063/1.1700747 (see pp. 6, 107)

[54] S. TORQUATO and Y. JIAO. "Robust algorithm to generate a diverse class of dense disordered and ordered sphere packings via linear programming". *Physical Review E* 82, 061302, 2010. DOI: 10.1103/PhysRevE.82.061302 (see pp. 6, 42, 44, 47, 53, 67, 69, 70, 89, 92)

[55] G. BRAMBILLA, D. EL MASRI, M. PIERNO, L. BERTHIER, L. CIPELLETTI, G. PETEKIDIS, and A. B. SCHOFIELD. "Probing the equilibrium dynamics of colloidal hard spheres above the mode-coupling glass transition". *Physical Review Letters* 102, 085703, 2009. DOI: 10.1103/PhysRevLett.102.085703 (see pp. 7, 66, 76, 77, 86, 100, 110)

[56] W. VAN MEGEN and S. M. UNDERWOOD. "Glass transition in colloidal hard spheres: Measurement and mode-coupling-theory analysis of the coherent intermediate scattering function". *Physical Review E* 49, 4206–4220, 1994. DOI: 10.1103/PhysRevE.49.4206 (see pp. 7, 74, 110)

[57] W. G. HOOVER and F. H. REE. "Melting transition and communal entropy for hard spheres". *The Journal of Chemical Physics* 49, 3609–3617, 1968. DOI: 10.1063/1.1670641 (see pp. 7, 66, 74, 78, 100, 124)

[58] D. FRENKEL. "Order through disorder: Entropy-driven phase transitions" in: *Complex Fluids* ed. by LUIS GARRIDO. Springer Berlin Heidelberg, 1993. (see p. 7)

[59] L. BERTHIER, H. JACQUIN, and F. ZAMPONI. "Microscopic theory of the jamming transition of harmonic spheres". *Physical Review E* 84, 051103, 2011. DOI: 10.1103/PhysRevE.84.051103 (see pp. 8, 136)

[60] F. H. STILLINGER, E. A. DIMARZIO, and R. L. KORNEGAY. "Systematic approach to explanation of the rigid disk phase transition". *The Journal of Chemical Physics* 40, 1564–1576, 1964. DOI: 10.1063/1.1725362 (see pp. 8, 42, 67, 69, 89, 90)

[61] D. ASENJO, F. PAILLUSSON, and D. FRENKEL. "Numerical calculation of granular entropy". *Physical Review Letters* 112, 098002, 2014. DOI: 10.1103/PhysRevLett.112.098002 (see pp. 9, 10, 86, 87, 97, 105, 114, 121, 125, 130, 134)

[62] R. K. BOWLES and S. S. ASHWIN. "Edwards entropy and compactivity in a model of granular matter". *Physical Review E* 83, 031302, 2011. DOI: 10.1103/PhysRevE.83.031302 (see pp. 10, 114)

[63] S. ZHAO and M. SCHRÖTER. "Measuring the configurational temperature of a binary disc packing". *Soft Matter* 10, 4208–4216, 2014. DOI: 10.1039/C3SM53176G (see pp. 10, 121, 124, 134, 143)

[64] S. HENKES, C. S. O'HERN, and B. CHAKRABORTY. "Entropy and temperature of a static granular assembly: An ab initio approach". *Physical Review Letters* 99, 038002, 2007. DOI: 10.1103/PhysRevLett.99.038002 (see pp. 10, 14, 121, 143)

[65] S. HENKES and B. CHAKRABORTY. "Statistical mechanics framework for static granular matter". *Physical Review E* 79, 061301, 2009. DOI: 10.1103/PhysRevE.79.061301 (see pp. 10, 121)

[66] J. G. PUCKETT and K. E. DANIELS. "Equilibrating temperaturelike variables in jammed granular subsystems". *Physical Review Letters* 110, 058001, 2013. DOI: 10.1103/PhysRevLett.110.058001 (see pp. 10, 121, 143)

[67] M. PICA CIAMARRA and A. CONIGLIO. "Random very loose packings". *Physical Review Letters* 101, 128001, 2008. DOI: 10.1103/PhysRevLett.101.128001 (see pp. 10, 53, 70, 124)

[68] G. GAO, J. BLAWZDZIEWICZ, C. S. O'HERN, and M. SHATTUCK. "Experimental demonstration of nonuniform frequency distributions of granular packings". *Physical Review E* 80, 061304, 2009. DOI: 10.1103/PhysRevE.80.061304 (see pp. 10, 121, 124)

[69] N. XU, D. FRENKEL, and A. J. LIU. "Direct Determination of the Size of Basins of Attraction of Jammed Solids". *Physical Review Letters* 106, 245502, 2011. DOI: 10.1103/PhysRevLett.106.245502 (see pp. 10, 19, 121, 124, 125)

[70] S. S. ASHWIN, J. BLAWZDZIEWICZ, C. S. O'HERN, and M. D. SHATTUCK. "Calculations of the structure of basin volumes for mechanically stable packings". *Physical Review E* 85, 061307, 2012. DOI: 10.1103/PhysRevE.85.061307 (see pp. 10, 19, 121, 124, 125, 136)

[71] R. MONASSON and O. POULIQUEN. "Entropy of particle packings: An illustration on a toy model". *Physica A: Statistical and Theoretical Physics* 236, 395–410, 1997. DOI: 10.1016/S0378-4371(96)00369-X (see pp. 10, 121, 124)

[72] R. K. BOWLES and S. S. ASHWIN. "Edwards entropy and compactivity in a model of granular matter". *Physical Review E* 83, 031302, 2011. DOI: 10.1103/PhysRevE.83.031302 (see pp. 10, 121, 124)

[73] C. BRISCOE, C. SONG, P. WANG, and H. A. MAKSE. "Entropy of jammed matter". *Physical Review Letters* 101, 188001, 2008. DOI: 10.1103/PhysRevLett.101.188001 (see pp. 10, 14, 19, 121, 124, 126, 143, 146)

[74] S. MCNAMARA, P. RICHARD, S. K. DE RICHTER, G. LE CAER, and R. DELANNAY. "Measurement of granular entropy". *Physical Review E* 80, 031301, 2009. DOI: 10.1103/PhysRevE.80.031301 (see pp. 10, 121, 124, 143)

[75] Y. JIN and H. A. MAKSE. "A first-order phase transition defines the random close packing of hard spheres". *Physica A: Statistical and Theoretical Physics* 389, 5362–5379, 2010. DOI: 10.1016/j.physa.2010.08.010 (see pp. 14, 15, 17, 26–29, 38, 53, 54, 66, 123)

[76] C. BRISCOE, C. SONG, P. WANG, and H. A. MAKSE. "Jamming III: Characterizing randomness via the entropy of jammed matter". *Physica A: Statistical and Theoretical Physics* 389, 3978–3999, 2010. DOI: 10.1016/j.physa.2010.05.054 (see pp. 14, 19, 29, 32)

[77] A. DONEV, F. H. STILLINGER, and S. TORQUATO. "Configurational entropy of binary hard-disk glasses: Nonexistence of an ideal glass transition". *The Journal of Chemical Physics* 127, 124509, 2007. DOI: 10.1063/1.2775928 (see pp. 14, 31, 89)

[78] V. S. KUMAR and V. KUMARAN. "Voronoi cell volume distribution and configurational entropy of hard-spheres". *The Journal of Chemical Physics* 123, 114501, 2005. DOI: 10.1063/1.2011390 (see p. 14)

[79] R. BLUMENFELD and S. F. EDWARDS. "Granular entropy: Explicit calculations for planar assemblies". *Physical Review Letters* 90, 114303, 2003. DOI: 10.1103/PhysRevLett.90.114303 (see pp. 14, 121)

[80] T. ASTE and T. DI MATTEO. "Emergence of Gamma distributions in granular materials and packing models". *Physical Review E* 77, 021309, 2008. DOI: 10.1103/PhysRevE.77.021309 (see pp. 14, 15, 19, 20, 26)

[81] S. S. ASHWIN and R. K. BOWLES. "Complete jamming landscape of confined hard discs". *Physical Review Letters* 102, 235701, 2009. DOI: 10.1103/PhysRevLett.102.235701 (see p. 14)

[82] P. GIAQUINTA and G. GIUNTA. "About entropy and correlations in a fluid of hard spheres". *Physica A: Statistical and Theoretical Physics* 187, 145–158, 1992. DOI: 10.1016/0378-4371(92)90415-M (see p. 14)

[83] S. TORQUATO, B. LU, and J. RUBINSTEIN. "Nearest-neighbor distribution functions in many-body systems". *Physical Review A* 41, 2059–2075, 1990. DOI: 10.1103/PhysRevA.41.2059 (see pp. 14, 21, 27, 101, 105, 106, 108, 110, 135, 138)

[84] B. LU and S. TORQUATO. "Nearest-surface distribution functions for polydispersed particle systems". *Physical Review A* 45, 5530–5544, 1992. DOI: 10.1103/PhysRevA.45.5530 (see pp. 14, 21, 27, 101, 105, 106, 135, 138)

[85] S. TORQUATO. "Nearest-neighbor statistics for packings of hard spheres and disks". *Physical Review E* 51, 3170–3182, 1995. DOI: 10.1103/PhysRevE.51.3170 (see pp. 14, 21, 27, 101, 105, 106, 135, 138)

[86] M. ALONSO, E. SAINZ, F. LOPEZ, and K. SHINOHARA. "Void-size probability distribution in random packings of equal-sized spheres". *Chemical Engineering Science* 50, 1983–1988, 1995. DOI: 10.1016/0009-2509(95)00061-9 (see pp. 14, 21, 101, 105, 135)

[87] M. ALONSO, M. SATOH, and K. MIYANAMI. "Void-size distribution in two-dimensional random packings of equal-sized disks". *The Canadian Journal of Chemical Engineering* 70, 28–32, 1992. DOI: 10.1002/cjce.5450700105 (see pp. 14, 21, 101, 105, 135)

[88] I. SCHENKER, F. T. FILSER, L. J. GAUCKLER, T. ASTE, and H. J. HERRMANN. "Quantification of the heterogeneity of particle packings". *Physical Review E* 80, 021302, 2009. DOI: 10.1103/PhysRevE.80.021302 (see pp. 14, 15, 19, 21, 22, 27, 101, 105, 106, 135, 138, 147)

[89] I. SCHENKER, F. FILSER, M. HÜTTER, and L. GAUCKLER. "The influence of the degree of heterogeneity on the elastic properties of random sphere packings". *Granular Matter* 14, 333–340, 2012. DOI: 10.1007/s10035-012-0316-5 (see pp. 14, 21, 27, 101, 105, 135)

[90] S. TORQUATO. "Statistical description of microstructures". *Annual Review of Materials Research* 32, 77–111, 2002. DOI: 10.1146/annurev.matsci.32.110101.155324 (see pp. 14, 21, 101, 105, 135)

[91] D. STOYAN, A. WAGNER, H. HERMANN, and A. ELSNER. "Statistical characterization of the pore space of random systems of hard spheres". *Journal of Non-Crystalline Solids* 357, 1508–1515, 2011. DOI: 10.1016/j.jnoncrysol.2010.12.033 (see pp. 14, 21, 101, 105, 135)

[92] A. DONEV, S. TORQUATO, and F. H. STILLINGER. "Neighbor list collision-driven molecular dynamics simulation for nonspherical hard particles." *Journal of Computational Physics* 202, 765–793, 2005. DOI: 10.1016/j.jcp.2004.08.025 (see pp. 14, 16, 19, 109)

[93] A. V. KYRYLYUK, M. A. VAN DE HAAR, L. ROSSI, A. WOUTERSE, and A. P. PHILIPSE. "Isochoric ideality in jammed random packings of non-spherical granular matter". *Soft Matter* 7, 1671–1674, 2011. DOI: 10.1039/c0sm00754d (see pp. 14, 19)

[94] K. WANG, C. SONG, P. WANG, and H. A. MAKSE. "Edwards thermodynamics of the jamming transition for frictionless packings: Ergodicity test and role of angoricity and compactivity". *Physical Review E* 86, 011305, 2012. DOI: 10.1103/PhysRevE.86.011305 (see pp. 15, 19, 20, 121)

[95] B. D. LUBACHEVSKY and F. H. STILLINGER. "Geometric properties of random disk packings". *Journal of Statistical Physics* 60, 561–583, 1990. DOI: 10.1007/BF01025983 (see pp. 15, 16, 25, 40, 71, 91, 109, 126)

[96] W. S. JODREY and E. M. TORY. "Computer simulation of close random packing of equal spheres". *Physical Review A* 32, 2347–2351, 1985. DOI: 10.1103/PhysRevA.32.2347 (see pp. 15, 16, 18, 70)

[97] M. BARGIEŁ and J. MOŚCIŃSKI. "C-language program for the irregular close packing of hard spheres". *Computer Physics Communications* 64, 183–192, 1991. DOI: 10.1016/0010-4655(91)90060-X (see pp. 15, 16, 70)

[98] J. MOŚCIŃSKI, M. BARGIEŁ, Z. A. RYCERZ, and P. W. M. JACOBS. "The force-biased algorithm for the irregular close packing of equal hard spheres". *Molecular Simulation* 3, 201–212, 1989. DOI: 10.1080/08927028908031373 (see pp. 15, 17, 40, 70, 91, 109)

[99] A. BEZRUKOV, M. BARGIEŁ, and D. STOYAN. "Statistical analysis of simulated random packings of spheres". *Particle & Particle Systems Characterization* 19, 111–118, 2002. DOI: 10.1002/1521-4117(200205)19:2<111::AID-PPSC111>3.0.CO;2-M (see pp. 15, 17, 18, 40, 70, 91, 109)

[100] J. D. BERNAL. "Geometry of the structure of monatomic liquids". *Nature* 185, 68–70, 1960. DOI: 10.1038/185068a0 (see pp. 15, 29)

[101] C. S. O'HERN, S. A. LANGER, A. J. LIU, and S. R. NAGEL. "Random packings of frictionless particles". *Physical Review Letters* 88, 075507, 2002. DOI: 10.1103/PhysRevLett.88.075507 (see pp. 15, 16, 18, 29, 39)

[102] N. XU, J. BLAWZDZIEWICZ, and C. S. O'HERN. "Random close packing revisited: Ways to pack frictionless disks". *Physical Review E* 71, 061306, 2005. DOI: 10.1103/PhysRevE.71.061306 (see pp. 15, 16, 18, 29, 31, 39)

[103] G. GAO, J. BŁAWZDZIEWICZ, and C. S. O'HERN. "Frequency distribution of mechanically stable disk packings". *Physical Review E* 74, 061304, 2006. DOI: 10.1103/PhysRevE.74.061304 (see p. 15)

[104] C. F. SCHRECK, C. S. O'HERN, and L. E. SILBERT. "Tuning jammed frictionless disk packings from isostatic to hyperstatic". *Physical Review E* 84, 011305, 2011. DOI: 10.1103/PhysRevE.84.011305 (see p. 15)

[105] S. ALEXANDER. "Amorphous solids: their structure, lattice dynamics and elasticity". *Physics Reports* 296, 65–236, 1998. DOI: 10.1016/S0370-1573(97)00069-0 (see p. 16)

[106] N. XU and E. S. C. CHING. "Effects of particle-size ratio on jamming of binary mixtures at zero temperature". *Soft Matter* 6, 2944–2948, 2010. DOI: 10.1039/b926696h (see pp. 16, 18, 39)

[107] H. A. MAKSE, D. L. JOHNSON, and L. M. SCHWARTZ. "Packing of compressible granular materials". *Physical Review Letters* 84, 4160–4163, 2000. DOI: 10.1103/PhysRevLett.84.4160 (see pp. 16, 39)

[108] P. WANG, C. SONG, Y. JIN, K. WANG, and H. A. MAKSE. "Distribution of volumes and coordination numbers in jammed matter: mesoscopic ensemble". *Journal of Statistical Mechanics: Theory and Experiment*, P12005, 2010. DOI: 10.1088/1742-5468/2010/12/P12005 (see pp. 16, 27, 39)

[109] C. F. MOUKARZEL. "Isostatic phase transition and instability in stiff granular materials". *Physical Review Letters* 81, 1634–1637, 1998. DOI: 10.1103/PhysRevLett.81.1634 (see p. 16)

[110] A. DONEV, S. TORQUATO, and F. H. STILLINGER. "Pair correlation function characteristics of nearly jammed disordered and ordered hard-sphere packings". *Physical Review E* 71, 011105, 2005. DOI: 10.1103/PhysRevE.71.011105 (see pp. 16, 25, 27, 39)

[111] L. E. SILBERT. "Jamming of frictional spheres and random loose packing". *Soft Matter* 6, 2918–2924, 2010. DOI: 10.1039/c001973a (see pp. 16, 124)

[112] A. MEHTA. "Spatial, dynamical and spatiotemporal heterogeneities in granular media". *Soft Matter* 6, 2875–2883, 2010. DOI: 10.1039/b926809j (see p. 16)

[113] C. B. O'DONOVAN and M. E. MÖBIUS. "Spatial correlations in polydisperse, frictionless, two-dimensional packings". *Physical Review E* 84, 020302, 2011. DOI: 10.1103/PhysRevE.84.020302 (see pp. 16, 25, 136)

[114] A. C. COHEN. "Estimating the mean and variance of normal populations from singly truncated and doubly truncated samples". *The Annals of Mathematical Statistics* 21, 557–569, 1950. (see pp. 22, 106, 138)

[115] M. ABRAMOWITZ and I. A. STEGUN. *Handbook of mathematical functions: With formulas, graphs, and mathematical tables*. New York: Dover Publications, 1965. (see p. 23)

[116] G. GAO, J. BLAWZDZIEWICZ, C. S. O'HERN, and M. D. SHATTUCK. "Experimental demonstration of nonuniform frequency distributions of granular packings". *Physical Review E* 80, 061304, 2009. DOI: 10.1103/PhysRevE.80.061304 (see p. 25)

[117] S. KHIREVICH, A. DANEYKO, A. HÖLTZEL, A. SEIDEL-MORGENSTERN, and U. TALLAREK. "Statistical analysis of packed beds, the origin of short-range disorder, and its impact on eddy dispersion". *Journal of Chromatography A* 1217, 4713–4722, 2010. DOI: 10.1016/j.chroma.2010.05.019 (see pp. 26, 27, 49)

[118] P. J. STEINHARDT, D. R. NELSON, and M. RONCHETTI. "Bond-orientational order in liquids and glasses". *Physical Review B* 28, 784–805, 1983. DOI: 10.1103/PhysRevB.28.784 (see pp. 26, 49)

[119] K. LOCHMANN, L. OGER, and D. STOYAN. "Statistical analysis of random sphere packings with variable radius distribution". *Solid State Sciences* 8, 1397–1413, 2006. DOI: 10.1016/j.solidstatesciences.2006.07.011 (see pp. 27, 55)

[120] G. W. DELANEY, T. D. MATTEO, and T. ASTE. "Combining tomographic imaging and DEM simulations to investigate the structure of experimental sphere packings". *Soft Matter* 6, 2992–3006, 2010. DOI: 10.1039/B927490A (see p. 27)

[121] S. KHIREVICH, A. HÖLTZEL, A. DANEYKO, A. SEIDEL-MORGENSTERN, and U. TALLAREK. "Structure–transport correlation for the diffusive tortuosity of bulk, monodisperse, random sphere packings". *Journal of Chromatography A* 1218, 6489–6497, 2011. DOI: 10.1016/j.chroma.2011.07.066 (see pp. 27, 66)

[122] D. HLUSHKOU, S. KHIREVICH, V. APANASOVICH, A. SEIDEL-MORGENSTERN, and U. TALLAREK. "Pore-scale dispersion in electrokinetic flow through a random sphere packing". *Analytical Chemistry* 79, 113–121, 2007. DOI: 10.1021/ac061168r (see p. 27)

[123] A. DANEYKO, S. KHIREVICH, A. HÖLTZEL, A. SEIDEL-MORGENSTERN, and U. TALLAREK. "From random sphere packings to regular pillar arrays: Effect of the macroscopic confinement on hydrodynamic dispersion". *Journal of Chromatography A* 1218, 8231–8248, 2011. DOI: 10.1016/j.chroma.2011.09.039 (see p. 27)

[124] V. BURYACHENKO, N. PAGANO, R. KIM, and J. SPOWART. "Quantitative description and numerical simulation of random microstructures of composites and their effective elastic moduli". *International Journal of Solids and Structures* 40, 47–72, 2003. DOI: 10.1016/S0020-7683(02)00462-6 (see p. 27)

[125] S. KHIREVICH, A. HÖLTZEL, A. SEIDEL-MORGENSTERN, and U. TALLAREK. "Geometrical and topological measures for hydrodynamic dispersion in confined sphere packings at low column-to-particle diameter ratios". *Journal of Chromatography A* 1262, 77–91, 2012. DOI: 10.1016/j.chroma.2012.08.086 (see pp. 27, 49)

[126] C. RADIN. "Random close packing of granular matter". *Journal of Statistical Physics* 131, 567–573, 2008. DOI: 10.1007/s10955-008-9523-1 (see pp. 28, 123)

[127] T. ASTE, M. SAADATFAR, and T. J. SENDEN. "Geometrical structure of disordered sphere packings". *Physical Review E* 71, 061302, 2005. DOI: 10.1103/PhysRevE.71.061302 (see p. 28)

[128] T. ASTE and A. CONIGLIO. "Cell theory for liquid solids and glasses: From local packing configurations to global complex behaviors". *EPL (Europhysics Letters)* 67, 165–171, 2004. DOI: 10.1209/epl/i2003-10284-x (see pp. 29, 34, 38, 49, 51, 54, 66, 74–76)

[129] M. HERMES and M. DIJKSTRA. "Jamming of polydisperse hard spheres: The effect of kinetic arrest". *EPL (Europhysics Letters)* 89, 38005, 2010. DOI: 10.1209/0295-5075/89/38005 (see pp. 31, 34)

[130] A. ZINCHENKO. "Algorithm for random close packing of spheres with periodic boundary conditions". *Journal of Computational Physics* 114, 298–307, 1994. DOI: 10.1006/jcph.1994.1168 (see pp. 38, 60, 66)

[131] J. G. BERRYMAN. "Random close packing of hard spheres and disks". *Physical Review A* 27, 1053–1061, 1983. DOI: 10.1103/PhysRevA.27.1053 (see pp. 38, 53, 54, 66)

[132] V. BARANAU, D. HLUSHKOU, S. KHIREVICH, and U. TALLAREK. "Pore-size entropy of random hard-sphere packings". *Soft Matter* 9, 3361–3372, 2013. DOI: 10.1039/C3SM27374A (see pp. 38, 39, 43, 48, 49, 51, 54, 66, 69, 71, 74–77, 102, 106, 109, 112, 124–126, 133, 138, 147)

[133] M. PICA CIAMARRA, M. NICODEMI, and A. CONIGLIO. "Recent results on the jamming phase diagram". *Soft Matter* 6, 2871–2874, 2010. DOI: 10.1039/b926810c (see pp. 38, 45, 51, 53, 69, 73, 93, 100, 143)

[134] M. C. VARGAS and G. PÉREZ-ÁNGEL. "Crystallization time scales for polydisperse hard-sphere fluids". *Physical Review E* 87, 042313, 2013. DOI: 10.1103/PhysRevE.87.042313 (see pp. 39, 71)

[135] B. D. LUBACHEVSKY. "How to simulate billiards and similar systems". *Journal of Computational Physics* 94, 255–283, 1991. DOI: 10.1016/0021-9991(91)90222-7 (see pp. 40, 71, 91, 109, 126)

[136] V. BARANAU https://code.google.com/p/packing-generation/ (see pp. 41, 44, 71, 91)

[137] S. TORQUATO and F. H. STILLINGER. "Toward the jamming threshold of sphere packings: Tunneled crystals". *Journal of Applied Physics* 102, 093511, 2007. DOI: 10.1063/1.2802184 (see pp. 41, 53, 68, 70, 123)

[138] Y. JIAO, F. H. STILLINGER, and S. TORQUATO. "Nonuniversality of density and disorder in jammed sphere packings". *Journal of Applied Physics* 109, 013508, 2011. DOI: 10.1063/1.3524489 (see pp. 44, 53, 70, 92)

[139] R. L. JACK and L. BERTHIER. "Random pinning in glassy spin models with plaquette interactions". *Physical Review E* 85, 021120, 2012. DOI: 10.1103/PhysRevE.85.021120 (see pp. 49, 76)

[140] R. S. FARR and R. D. GROOT. "Close packing density of polydisperse hard spheres". *The Journal of Chemical Physics* 131, 244104, 2009. DOI: 10.1063/1.3276799 (see p. 52)

[141] G. E. SCHRÖDER-TURK, W. MICKEL, M. SCHRÖTER, G. W. DELANEY, M. SAADATFAR, T. J. SENDEN, K. MECKE, and T. ASTE. "Disordered spherical bead packs are anisotropic". *EPL (Europhysics Letters)* 90, 34001, 2010. DOI: 10.1209/0295-5075/90/34001 (see p. 53)

[142] R. D. KAMIEN and A. J. LIU. "Why is random close packing reproducible?" *Physical Review Letters* 99, 155501, 2007. DOI: 10.1103/PhysRevLett.99.155501 (see pp. 54, 123, 132)

[143] K. A. NEWHALL, I. JORJADZE, E. VANDEN-EIJNDEN, and J. BRUJIĆ. "A statistical mechanics framework captures the packing of monodisperse particles". *Soft Matter* 7, 11518–11525, 2011. DOI: 10.1039/c1sm06243c (see p. 55)

[144] G. PÉREZ-ÁNGEL, L. E. SÁNCHEZ-DÍAZ, P. E. RAMÍREZ-GONZÁLEZ, R. JUÁREZ-MALDONADO, A. VIZCARRA-RENDÓN, and M. MEDINA-NOYOLA. "Equilibration of concentrated hard-sphere fluids". *Physical Review E* 83, 060501, 2011. DOI: 10.1103/PhysRevE.83.060501 (see pp. 66, 76, 77, 86, 100, 110)

[145] T. VOIGTMANN, A. M. PUERTAS, and M. FUCHS. "Tagged-particle dynamics in a hard-sphere system: Mode-coupling theory analysis". *Physical Review E* 70, 061506, 2004. DOI: 10.1103/PhysRevE.70.061506 (see pp. 66, 75, 76, 86, 100, 110)

[146] V. BARANAU and U. TALLAREK. "Random-close packing limits for monodisperse and polydisperse hard spheres". *Soft Matter* 10, 3826–3841, 2014. DOI: 10.1039/C3SM52959B (see pp. 66, 68, 69, 72, 74–77, 90, 91, 94, 124)

[147] R. NI, M. A. COHEN-STUART, and M. DIJKSTRA. "Pushing the glass transition towards random close packing using self-propelled hard spheres". *Nature Communications* 4, 2704, 2013. DOI: 10.1038/ncomms3704 (see pp. 69, 93)

[148] P. N. PUSEY, E. ZACCARELLI, C. VALERIANI, E. SANZ, W. C. K. POON, and M. E. CATES. "Hard spheres: crystallization and glass formation". *Philosophical Transactions of the Royal Society A: Mathematical, Physical & Engineering Sciences* 367, 4993–5011, 2009. DOI: 10.1098/rsta.2009.0181 (see pp. 74, 124)

[149] F. H. STILLINGER. "Phase transitions in the Gaussian core system". *The Journal of Chemical Physics* 65, 3968–3974, 1976. DOI: 10.1063/1.432891 (see p. 80)

[150] F. H. STILLINGER and T. A. WEBER. "Hidden structure in liquids". *Physical Review A* 25, 978–989, 1982. DOI: 10.1103/PhysRevA.25.978 (see pp. 80, 129)

[151] S. PRESTIPINO, F. SAIJA, and P. V. GIAQUINTA. "Phase diagram of softly repulsive systems: The Gaussian and inverse-power-law potentials". *The Journal of Chemical Physics* 123, 144110, 2005. DOI: 10.1063/1.2064639 (see p. 80)

[152] C. N. LIKOS, B. M. MLADEK, D. GOTTWALD, and G. KAHL. "Why do ultrasoft repulsive particles cluster and crystallize? Analytical results from density-functional theory". *The Journal of Chemical Physics* 126, 224502, 2007. DOI: 10.1063/1.2738064 (see p. 80)

[153] J. D. WEEKS. "Volume change on melting for systems with inverse-power-law interactions". *Physical Review B* 24, 1530–1535, 1981. DOI: 10.1103/PhysRevB.24.1530 (see p. 80)

[154] T. BOUBLÍK. "Hard-sphere equation of state". *The Journal of Chemical Physics* 53, 471–472, 1970. DOI: 10.1063/1.1673824 (see pp. 80, 81, 86, 87, 97, 101, 104)

[155] V. OGARKO and S. LUDING. "Equation of state and jamming density for equivalent bi- and polydisperse, smooth, hard sphere systems". *The Journal of Chemical Physics* 136, 124508, 2012. DOI: 10.1063/1.3694030 (see pp. 80, 81, 86–88, 93, 96, 97, 101, 104, 105)

[156] G. A. MANSOORI, N. F. CARNAHAN, K. E. STARLING, and T. W. LELAND. "Equilibrium thermodynamic properties of the mixture of hard spheres". *The Journal of Chemical Physics* 54, 1523–1525, 1971. DOI: 10.1063/1.1675048 (see pp. 80, 86, 87, 101, 104, 126)

[157] J. H. GIBBS and E. A. DIMARZIO. "Nature of the Glass Transition and the Glassy State". *The Journal of Chemical Physics* 28, 373–383, 1958. DOI: 10.1063/1.1744141 (see p. 86)

[158] G. ADAM and J. H. GIBBS. "On the temperature dependence of cooperative relaxation properties in glass-forming liquids". *The Journal of Chemical Physics* 43, 139–146, 1965. DOI: 10.1063/1.1696442 (see p. 86)

[159] G. L. HUNTER and E. R. WEEKS. "The physics of the colloidal glass transition". *Reports on Progress in Physics* 75, 066501, 2012. DOI: 10.1088/0034-4885/75/6/066501 (see p. 86)

[160] V. OGARKO, N. RIVAS, and S. LUDING. "Communication: Structure characterization of hard sphere packings in amorphous and crystalline states". *The Journal of Chemical Physics* 140, 211102, 2014. DOI: 10.1063/1.4880236 (see pp. 86, 100)

[161] D. FRENKEL and A. J. C. LADD. "New Monte Carlo method to compute the free energy of arbitrary solids. Application to the fcc and hcp phases of hard spheres". *The Journal of Chemical Physics* 81, 3188–3193, 1984. DOI: 10.1063/1.448024 (see pp. 86, 87, 97, 105)

[162] A. SANTOS, S. B. YUSTE, M. LÓPEZ DE HARO, G. ODRIOZOLA, and V. OGARKO. "Simple effective rule to estimate the jamming packing fraction of polydisperse hard spheres". *Physical Review E* 89, 040302, 2014. DOI: 10.1103/PhysRevE.89.040302 (see pp. 86, 96)

[163] K. W. DESMOND and E. R. WEEKS. "Influence of particle size distribution on random close packing of spheres". *Physical Review E* 90, 022204, 2014. DOI: 10.1103/PhysRevE.90.022204 (see pp. 86, 96)

[164] V. BARANAU and U. TALLAREK. "On the jamming phase diagram for frictionless hard-sphere packings". *Soft Matter* 10, 7838–7848, 2014. DOI: 10.1039/C4SM01439A (see pp. 87–92, 94, 95, 105, 109, 110, 112, 124)

[165] T. MÜLLNER, K. UNGER, and U. TALLAREK. "Characterization of microscopic disorder in reconstructed porous materials and assessment of mass transport-relevant structural descriptors". *New Journal of Chemistry* accepted, –, 2016. DOI: 10.1039/c5nj03346b (see p. 100)

[166] N. KUMAR, O. I. IMOLE, V. MAGNANIMO, and S. LUDING. "Effects of polydispersity on the micro–macro behavior of granular assemblies under different deformation paths". *Particuology* 12, 64–79, 2014. DOI: 10.1016/j.partic.2013.07.011 (see p. 100)

[167] D. J. ADAMS. "Chemical potential of hard-sphere fluids by Monte Carlo methods". *Molecular Physics* 28, 1241–1252, 1974. DOI: 10.1080/00268977400102551 (see pp. 100, 101, 103, 105, 107, 116, 125, 128, 130, 132–134)

[168] R. J. SPEEDY. "Cavities and free volume in hard-disc and hard-sphere systems". *Journal of the Chemical Society, Faraday Transactions 2: Molecular and Chemical Physics* 77, 329–335, 1981. DOI: 10.1039/F29817700329 (see pp. 100, 101, 103, 107, 115, 132, 133)

[169] R. J. SPEEDY and H. REISS. "Cavities in the hard sphere fluid and crystal and the equation of state". *Molecular Physics* 72, 999–1014, 1991. DOI: 10.1080/00268979100100741 (see pp. 100, 101, 103, 107, 133)

[170] B. WIDOM. "Some topics in the theory of fluids". *The Journal of Chemical Physics* 39, 2808–2812, 1963. DOI: 10.1063/1.1734110 (see pp. 101, 103, 107, 125, 128, 130, 132–134)

[171] D. FRENKEL and B. SMIT. *Understanding molecular simulation: From algorithms to applications*. 2nd ed. San Diego: Academic Press, 2002. (see pp. 101, 103, 125, 128, 130, 132, 134)

[172] S. SASTRY, T. M. TRUSKETT, P. G. DEBENEDETTI, S. TORQUATO, and F. H. STILLINGER. "Free volume in the hard sphere liquid". *Molecular Physics* 95, 289–297, 1998. DOI: 10.1080/00268979809483161 (see pp. 101, 102, 107, 110, 111)

[173] N. F. CARNAHAN and K. E. STARLING. "Equation of state for nonattracting rigid spheres". *The Journal of Chemical Physics* 51, 635–636, 1969. DOI: 10.1063/1.1672048 (see pp. 101, 102, 105)

[174] N. F. CARNAHAN and K. E. STARLING. "Thermodynamic properties of a rigid-sphere fluid". *The Journal of Chemical Physics* 53, 600–603, 1970. DOI: 10.1063/1.1674033 (see pp. 102, 103, 105, 116)

[175] M. MAITI, A. LAKSHMINARAYANAN, and S. SASTRY. "Characterization of void space in polydisperse sphere packings: Applications to hard-sphere packings and to protein structure analysis". *European Physical Journal E: Soft Matter and Biological Physics* 36, 1–13, 2013. DOI: 10.1140/epje/i2013-13005-4 (see pp. 104, 105, 107, 113)

[176] V. BARANAU and U. TALLAREK. "How to predict the ideal glass transition density in polydisperse hard-sphere packings". *The Journal of Chemical Physics* 143, 044501, 2015. DOI: 10.1063/1.4927077 (see pp. 105, 109, 110)

[177] C. R. MAURER, R. S. QI, and V. RAGHAVAN. "A linear time algorithm for computing exact Euclidean distance transforms of binary images in arbitrary dimensions". *IEEE Transactions on Pattern Analysis and Machine Intelligence* 25, 265–270, 2003. DOI: 10.1109/TPAMI.2003.1177156 (see p. 105)

[178] R. FABBRI, L. D. F. COSTA, J. C. TORELLI, and O. M. BRUNO. "2D Euclidean distance transform algorithms: A comparative survey". *ACM Computing Surveys* 40, 2:1–2:44, 2008. DOI: 10.1145/1322432.1322434 (see p. 105)

[179] Y. LUCET. "New sequential exact Euclidean distance transform algorithms based on convex analysis". *Image and Vision Computing* 27, 37–44, 2009. DOI: 10.1016/j.imavis.2006.10.011 (see p. 105)

[180] R. K. BOWLES and R. J. SPEEDY. "Cavities in the hard sphere crystal and fluid". *Molecular Physics* 83, 113–125, 1994. DOI: 10.1080/00268979400101111 (see p. 107)

[181] S. SASTRY, D. S. CORTI, P. G. DEBENEDETTI, and F. H. STILLINGER. "Statistical geometry of particle packings. I. Algorithm for exact determination of connectivity, volume, and surface areas of void space in monodisperse and polydisperse sphere packings". *Physical Review E* 56, 5524–5532, 1997. DOI: 10.1103/PhysRevE.56.5524 (see p. 107)

[182] P. G. DEBENEDETTI and T. M. TRUSKETT. "The statistical geometry of voids in liquids". *Fluid Phase Equilibria* 158-160, 549–556, 1999. DOI: 10.1016/S0378-3812(99)00135-1 (see p. 107)

[183] A. VISHNYAKOV, P. G. DEBENEDETTI, and A. V. NEIMARK. "Statistical geometry of cavities in a metastable confined fluid". *Physical Review E* 62, 538–544, 2000. DOI: 10.1103/PhysRevE.62.538 (see p. 107)

[184] P. G. DEBENEDETTI, T. M. TRUSKETT, C. P. LEWIS, and F. H. STILLINGER. "Theory of supercooled liquids and glasses: Energy landscape and statistical geometry perspectives". *Advances in Chemical Engineering* 28, 21–79, 2001. DOI: 10.1016/S0065-2377(01)28003-X (see p. 107)

[185] M. MÉZARD, G. PARISI, M. TARZIA, and F. ZAMPONI. "On the solution of a 'solvable' model of an ideal glass of hard spheres displaying a jamming transition". *Journal of Statistical Mechanics: Theory and Experiment* 2011, P03002, 2011. DOI: 10.1088/1742-5468/2011/03/P03002 (see p. 107)

[186] M. MAITI and S. SASTRY. "Free volume distribution of nearly jammed hard sphere packings". *The Journal of Chemical Physics* 141, 044510, 2014. DOI: 10.1063/1.4891358 (see p. 107)

[187] W. G. HOOVER, W. T. ASHURST, and R. GROVER. "Exact dynamical basis for a fluctuating cell model". *The Journal of Chemical Physics* 57, 1259–1262, 1972. DOI: 10.1063/1.1678384 (see pp. 107, 115, 132)

[188] S. MILLER and S. LUDING. "Event-driven molecular dynamics in parallel". *Journal of Computational Physics* 193, 306–316, 2004. DOI: 10.1016/j.jcp.2003.08.009 (see p. 109)

[189] P. PARICAUD. "Extension of the BMCSL equation of state for hard spheres to the metastable disordered region: Application to the SAFT approach". *The Journal of Chemical Physics* 143, 044507, 2015. DOI: 10.1063/1.4927148 (see p. 113)

[190] V. BARANAU, S.-C. ZHAO, M. SCHEEL, U. TALLAREK, and M. SCHRÖTER. "Upper bound on the Edwards entropy in frictional monodisperse hard-sphere packings". *Soft Matter* 12, 3991–4006, 2016. DOI: 10.1039/C6SM00567E (see p. 114)

[191] N. V. BRILLIANTOV and T. PÖSCHEL. *Kinetic theory of granular gases*. Oxford: Oxford University Press, 2004. (see p. 120)

[192] A. MEHTA and S. F. EDWARDS. "Statistical mechanics of powder mixtures". *Physica A: Statistical and Theoretical Physics* 157, 1091–1100, 1989. DOI: 10.1016/0378-4371(89)90035-6 (see p. 120)

[193] E. R. NOWAK, J. B. KNIGHT, E. BEN-NAIM, H. M. JAEGER, and S. R. NAGEL. "Density fluctuations in vibrated granular materials". *Physical Review E* 57, 1971–1982, 1998. (see pp. 121, 143)

[194] H. A. MAKSE and J. KURCHAN. "Testing the thermodynamic approach to granular matter with a numerical model of a decisive experiment". *Nature* 415, 614–617, 2002. DOI: 10.1038/415614a (see p. 121)

[195] M. NICODEMI, A. F., and A. CONIGLIO. "Segregation in hard-sphere mixtures under gravity. An extension of Edwards approach with two thermodynamical parameters". *EPL (Europhysics Letters)* 60, 684–690, 2002. DOI: 10.1209/epl/i2002-00363-0 (see pp. 121, 143)

[196] H. A. MAKSE, J. BRUJIĆ, and S. F. EDWARDS. "Statistical mechanics of jammed matter" in: *The Physics of Granular Media* ed. by HAYE HINRICHSEN and DIETRICH E. WOLF. Weinheim: Wiley-VCH, 2004. (see p. 121)

[197] M. SCHRÖTER, D. I. GOLDMAN, and H. L. SWINNEY. "Stationary state volume fluctuations in a granular medium". *Physical Review E* 71, 030301, 2005. DOI: 10.1103/PhysRevE.71.030301 (see pp. 121, 127, 143)

[198] P. T. METZGER and C. M. DONAHUE. "Elegance of disordered granular packings: A validation of Edward's hypothesis". *Physical Review Letters* 94, 148001, 2005. DOI: 10.1103/PhysRevLett.94.148001 (see p. 121)

[199] M. PICA CIAMARRA, A. CONIGLIO, and M. NICODEMI. "Thermodynamics and statistical mechanics of dense granular media". *Physical Review Letters* 97, 158001, 2006. DOI: 10.1103/PhysRevLett.97.158001 (see p. 121)

[200] F. LECHENAULT, F. DA CRUZ, O. DAUCHOT, and E. BERTIN. "Free volume distributions and compactivity measurement in a bidimensional granular packing". *Journal of Statistical Mechanics: Theory and Experiment* 2006, P07009–P07009, 2006. DOI: 10.1088/1742-5468/2006/07/P07009 (see p. 121)

[201] P. RIBIÉRE, P. RICHARD, P. PHILIPPE, D. BIDEAU, and R. DELANNAY. "On the existence of stationary states during granular compaction". *European Physical Journal E: Soft Matter and Biological Physics* 22, 249–253, 2007. DOI: 10.1140/epje/e2007-00017-x (see pp. 121, 143)

[202] B. P. TIGHE, J. H. SNOEIJER, T. J. H. VLUGT, and M. VAN HECKE. "The force network ensemble for granular packings". *Soft Matter* 6, 2908–2917, 2010. DOI: 10.1039/B926592A (see p. 121)

[203] L. A. PUGNALONI, J. DAMAS, I. ZURIGUEL, and D. MAZA. "Master curves for the stress tensor invariants in stationary states of static granular beds. Implications for the thermodynamic phase space". *Papers in Physics* 3, 030004, 2011. DOI: 10.4279/pip.030004 (see pp. 121, 143)

[204] F. PAILLUSSON and D. FRENKEL. "Probing ergodicity in granular matter". *Physical Review Letters* 109, 208001, 2012. DOI: 10.1103/PhysRevLett.109.208001 (see p. 121)

[205] S. ZHAO, S. SIDLE, H. L. SWINNEY, and M. SCHRÖTER. "Correlation between Voronoi volumes in disc packings". *EPL (Europhysics Letters)* 97, 34004, 2012. DOI: 10.1209/0295-5075/97/34004 (see p. 121)

[206] M. SCHRÖTER and K. E. DANIELS. "Granular segregation in dense systems: the role of statistical mechanics and entropy". *arXiv e-prints*, arXiv:1501.02155, 2012. (see pp. 121, 143)

[207] R. BLUMENFELD, J. F. JORDAN, and S. F. EDWARDS. "Interdependence of the volume and stress ensembles and equipartition in statistical mechanics of granular systems". *Physical Review Letters* 109, 238001, 2012. DOI: 10.1103/PhysRevLett.109.238001 (see pp. 121, 143)

[208] I. G. TEJADA. "Ensemble theory for slightly deformable granular matter". *European Physical Journal E: Soft Matter and Biological Physics* 37, 1–8, 2014. DOI: 10.1140/epje/i2014-14081-6 (see p. 121)

[209] F. PAILLUSSON. "Devising a protocol-related statistical mechanics framework for granular materials". *Physical Review E* 91, 012204, 2015. DOI: 10.1103/PhysRevE.91.012204 (see p. 121)

[210] Y. WU and S. TEITEL. "Statistics of conserved quantities in mechanically stable packings of frictionless disks above jamming". *Physical Review E* 91, 022207, 2015. DOI: 10.1103/PhysRevE.91.022207 (see p. 121)

[211] V. BECKER and K. KASSNER. "Simulations support protocol independency of the granular temperature". *arXiv e-prints*, arXiv:1506.03288, 2015. (see p. 121)

[212] P. YU, S. FRANK-RICHTER, A. BÖRNGEN, and M. SPERL. "Monitoring three-dimensional packings in microgravity". *Granular Matter* 16, 165–173, 2014. DOI: 10.1007/s10035-013-0479-8 (see p. 122)

[213] M. VAN HECKE. "Jamming of soft particles: geometry, mechanics, scaling and isostaticity". *Journal of Physics: Condensed Matter* 22, 033101, 2010. DOI: 10.1088/0953-8984/22/3/033101 (see p. 123)

[214] L. E. SILBERT, D. ERTAŞ, G. S. GREST, T. C. HALSEY, and D. LEVINE. "Geometry of frictionless and frictional sphere packings". *Physical Review E* 65, 031304, 2002. DOI: 10.1103/PhysRevE.65.031304 (see p. 123)

[215] H. P. ZHANG and H. A. MAKSE. "Jamming transition in emulsions and granular materials". *Physical Review E* 72, 011301, 2005. DOI: 10.1103/PhysRevE.72.011301 (see p. 123)

[216] K. SHUNDYAK, M. VAN HECKE, and W. VAN SAARLOOS. "Force mobilization and generalized isostaticity in jammed packings of frictional grains". *Physical Review E* 75, 010301, 2007. DOI: 10.1103/PhysRevE.75.010301 (see pp. 123, 124)

[217] S. HENKES, M. VAN HECKE, and W. VAN SAARLOOS. "Critical jamming of frictional grains in the generalized isostaticity picture". *EPL (Europhysics Letters)* 90, 14003, 2010. DOI: 10.1209/0295-5075/90/14003 (see pp. 123, 124)

[218] F. M. SCHALLER, M. NEUDECKER, M. SAADATFAR, G. W. DELANEY, G. E. SCHRÖDER-TURK, and M. SCHRÖTER. "Local origin of global contact numbers in frictional ellipsoid packings". *Physical Review Letters* 114, 158001, 2015. DOI: 10.1103/PhysRevLett.114.158001 (see p. 123)

[219] T. ASTE, M. SAADATFAR, and T. J. SENDEN. "Local and global relations between the number of contacts and density in monodisperse sphere packs". *Journal of Statistical Mechanics: Theory and Experiment* 2006, P07010, 2006. DOI: 10.1088/1742-5468/2006/07/P07010 (see p. 123)

[220] A. BAULE, R. MARI, L. BO, L. PORTAL, and H. A. MAKSE. "Mean-field theory of random close packings of axisymmetric particles". *Nature Communications* 4, 2194, 2013. DOI: 10.1038/ncomms3194 (see p. 123)

[221] A. BAULE and H. A. MAKSE. "Fundamental challenges in packing problems: from spherical to non-spherical particles". *Soft Matter* 10, 4423–4429, 2014. DOI: 10.1039/C3SM52783B (see p. 123)

[222] N. FRANCOIS, M. SAADATFAR, R. CRUIKSHANK, and A. SHEPPARD. "Geometrical frustration in amorphous and partially crystallized packings of spheres". *Physical Review Letters* 111, 148001, 2013. DOI: 10.1103/PhysRevLett.111.148001 (see p. 123)

[223] G. R. FARRELL, K. M. MARTINI, and N. MENON. "Loose packings of frictional spheres". *Soft Matter* 6, 2925–2930, 2010. DOI: 10.1039/C0SM00038H (see p. 124)

[224] J. M. VALVERDE and A. CASTELLANOS. "Random loose packing of cohesive granular materials". *EPL (Europhysics Letters)* 75, 985, 2006. DOI: 10.1209/epl/i2006-10208-4 (see p. 124)

[225] G. W. DELANEY, J. E. HILTON, and P. W. CLEARY. "Defining random loose packing for nonspherical grains". *Physical Review E* 83, 051305, 2011. DOI: 10.1103/PhysRevE.83.051305 (see p. 124)

[226] S. MARTINIANI, K. J. SCHRENK, J. D. STEVENSON, D. J. WALES, and D. FRENKEL. "Turning intractable counting into sampling: Computing the configurational entropy of three-dimensional jammed packings". *Physical Review E* 93, 012906, 2016. DOI: 10.1103/PhysRevE.93.012906 (see pp. 125, 129, 130, 134)

[227] H. MAKSE *Software and Data | Hernan Makse* http://www-levich.engr.ccny.cuny.edu/webpage/hmakse/software-and-data/ (see p. 126)

[228] D. M. BISHOP. *Group theory and chemistry*. Revised ed. New York: Dover Publications, 1993. (see p. 132)

[229] V. BARANAU and U. TALLAREK. "Chemical potential and entropy in monodisperse and polydisperse hard-sphere fluids using Widom's particle insertion method and a pore size distribution-based insertion probability". *The Journal of Chemical Physics* 144, 214503, 2016. DOI: 10.1063/1.4953079 (see p. 133)

[230] C. F. SCHRECK, T. BERTRAND, C. S. O'HERN, and M. D. SHATTUCK. "Repulsive contact interactions make jammed particulate systems inherently nonharmonic". *Physical Review Letters* 107, 078301, 2011. DOI: 10.1103/PhysRevLett.107.078301 (see p. 136)

[231] M. NAKAGAMI. "The m-distribution–a general formula of intensity distribution of rapid fading" in: *Statistical Methods in Radio Wave Propagation* ed. by W. C. HOFFMAN. Oxford: Pergamon Press, 1960. (see p. 138)

[232] Y. SREBRO and D. LEVINE. "Role of friction in compaction and segregation of granular materials". *Physical Review E* 68, 061301, 2003. DOI: 10.1103/PhysRevE.68.061301 (see p. 143)

[233] A. CONIGLIO, A. FIERRO, and M. NICODEMI. "Stationary probability distribution in granular media". *Physica D* 193, 292–302, 2004. DOI: 10.1016/j.physd.2004.01.042 (see p. 143)

[234] M. TARZIA, A. FIERRO, M. NICODEMI, M. PICA CIAMARRA, and A. CONIGLIO. "Size segregation in granular media induced by phase transition". *Physical Review Letters* 95, 078001, 2005. DOI: 10.1103/PhysRevLett.95.078001 (see p. 143)

[235] T. FINGER, M. SCHRÖTER, and R. STANNARIUS. "The mechanism of long-term coarsening of granular mixtures in rotating drums". *New Journal of Physics* 17, 093023, 2015. DOI: 10.1088/1367-2630/17/9/093023 (see p. 143)

[236] S. UTERMANN, P. AURIN, M. BENDEROTH, C. FISCHER, and M. SCHRÖTER. "Tailoring the frictional properties of granular media". *Physical Review E* 84, 031306, 2011. DOI: 10.1103/PhysRevE.84.031306 (see p. 145)